AD-A043 605 CIVIL ENGINEERING LAB (NAVY) PORT HUENEME CALIF F/G 6/2
A FINITE ELEMENT HEAD INJURY MODEL. VOLUME I. THEORY, DEVELOPME--ETC(U)
JUL 77 T A SHUGAR

UNCLASSIFIED CEL-TR-854-1 NL

1 OF 3
AD A043605

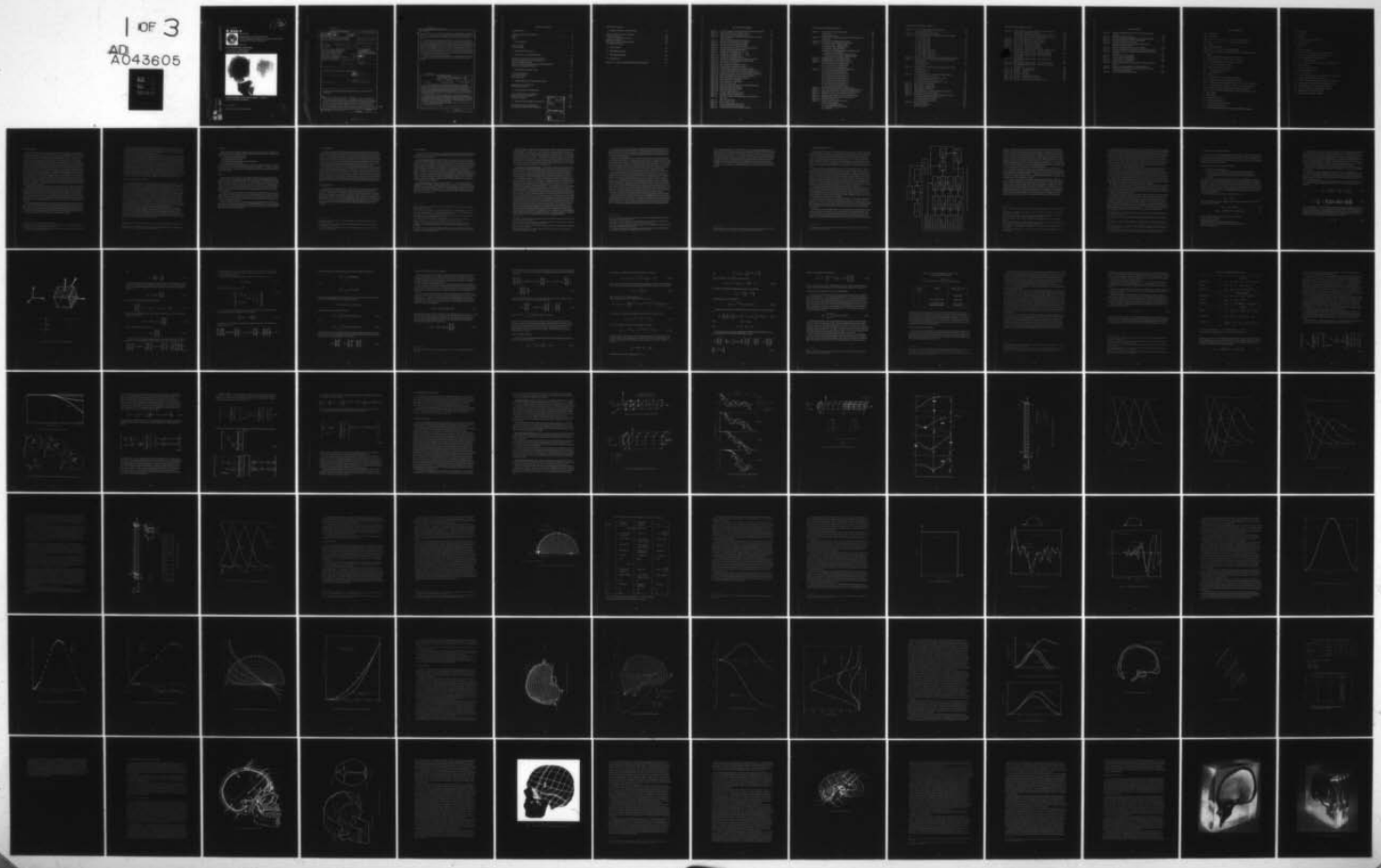

Technical Report

R 854-1

Sponsored by

DEPARTMENT OF TRANSPORTATION,
NAVAL AEROSPACE MEDICAL RESEARCH LABORATORY,
and OFFICE OF NAVAL RESEARCH

July 1977

CIVIL ENGINEERING LABORATORY
Naval Construction Battalion Center
Port Hueneme, California 93043

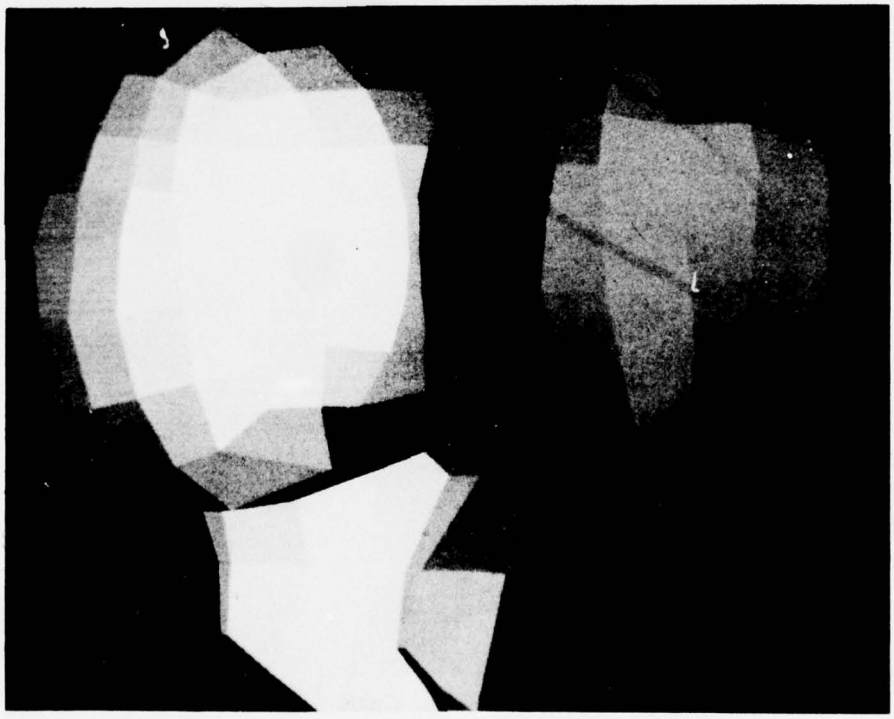

A FINITE ELEMENT HEAD INJURY MODEL – Volume I: Theory, Development, and Results

by T. A. Shugar

Unclassified

SECURITY CLASSIFICATION OF THIS PAGE (When Data Entered)

REPORT DOCUMENTATION PAGE		READ INSTRUCTIONS BEFORE COMPLETING FORM
1. REPORT NUMBER CEL-TR-854	2. GOVT ACCESSION NO. DN 244152	3. RECIPIENT'S CATALOG NUMBER
4. TITLE (and Subtitle) A FINITE ELEMENT HEAD INJURY MODEL. Volume I. Theory, Development, and Results		5. TYPE OF REPORT & PERIOD COVERED Final; June 1973 – June 1977 6. PERFORMING ORG. REPORT NUMBER
7. AUTHOR(s) T. A. Shugar		8. CONTRACT OR GRANT NUMBER(s)
9. PERFORMING ORGANIZATION NAME AND ADDRESS CIVIL ENGINEERING LABORATORY Naval Construction Battalion Center Port Hueneme, California 93043		10. PROGRAM ELEMENT, PROJECT, TASK AREA & WORK UNIT NUMBERS DOT-HS-289-3-550-1A ONR-61153N, RR023-03-01; NAMRL N00203-75-WR-00142
11. CONTROLLING OFFICE NAME AND ADDRESS Department of Transportation, Naval Aerospace Medical Research Laboratory, and Office of Naval Research		12. REPORT DATE July 1977 13. NUMBER OF PAGES 195
14. MONITORING AGENCY NAME & ADDRESS(if different from Controlling Office)		15. SECURITY CLASS. (of this report) Unclassified 15a. DECLASSIFICATION/DOWNGRADING SCHEDULE

16. DISTRIBUTION STATEMENT (of this Report)

Approved for public release; distribution unlimited.

RR023p3

17. DISTRIBUTION STATEMENT (of the abstract entered in Block 20, if different from Report)

RR023p3p1

18. SUPPLEMENTARY NOTES

19. KEY WORDS (Continue on reverse side if necessary and identify by block number)

Biomechanics, structural models, head injury prediction, impact, dynamics, transients, finite element.

20. ABSTRACT (Continue on reverse side if necessary and identify by block number)

The results of a head injury model development program are presented, including a description of the resulting model's features and its capabilities for simulating direct and indirect impact forces. The model's validity is discussed in terms of level of confidence and verification. Skull bone response and brain response are presented for a variety of dynamic simulations. Over 75 dynamic and static computer runs have been executed in its development. The basic features of the model are described, including recognizable skull geometry, linear

continued

DD FORM 1 JAN 73 1473 EDITION OF 1 NOV 65 IS OBSOLETE

Unclassified

SECURITY CLASSIFICATION OF THIS PAGE (When Data Entered)

391 111.

20. Continued

elastic and linear visco-elastic behavior, and a capability for specifying arbitrary impact loads and boundary conditions. A special modification of the isoparametric element is shown to be particularly suited to simulation of the dynamic response of nearly incompressible brain matter.

A preprocessor enables automatic mesh generation of a skull model consistent with a prescribed set of geometrical data supplied by the user. Either complete three-dimensional skulls or skulls symmetrical with respect to the midsagittal plane can be specified in the mesh generation process. Additionally, scale factors can be prescribed which modify existing skull meshes and achieve parametric control on size and shape. A postprocessor facilitates the reduction of the large amount of data that is typical of a head impact simulation. The scope and limitations imposed by the assumption of linearity are discussed. The results demonstrate that while some minor changes appear indicated, the model predictions yield useful insight into the mechanical causes of skull and brain injury.

Volume I of this report also contains Appendix A, a clinical description of head injury. Volume II contains Appendixes B through G covering the computer programs for skull modeling.

Library Card

Civil Engineering Laboratory
A FINITE ELEMENT HEAD INJURY MODEL – VOLUME I:
Theory, Development, and Results (Final) by T. A. Shugar
TR-854 – I 195 pp illus July 1977 Unclassified

1. Biomechanics 2. Head injury predictions I. DOT-HS-289-3-550

The results of a head injury model development program are presented, including a description of the resulting model's features and its capabilities for simulating direct and indirect impact forces. Level of confidence and verification of the model is discussed. Skull bone and brain responses are presented for a variety of dynamic simulations. Basic features of the model are described, including recognizable skull geometry, linear elastic and linear visco-elastic behavior, and capability for specifying arbitrary impact loads and boundary conditions. A special modification of the isoparametric element is particularly suited to simulation of the dynamic response of nearly incompressible brain matter.

A preprocessor enables automatic mesh generation of a skull model with geometrical data supplied by the user. Either complete three-dimensional skulls or skulls symmetrical with respect to the midsagittal plane can be specified for mesh generation. Additionally, scale factors can modify existing skull meshes and achieve parametric control on size and shape. A postprocessor can reduce the large amount of data typical of a head impact simulation. The model predictions yield useful insight into the mechanical causes of skull and brain injury.

Volume I includes a clinical description of head injury (Appendix A); Volume II contains the computer programs for skull modeling.

TABLE OF CONTENTS

CONTENTS (Continued)

LIST OF ILLUSTRATIONS

LIST OF ILLUSTRATIONS (Continued)

LIST OF ILLUSTRATIONS (Continued)

LIST OF ILLUSTRATIONS (Continued)

LIST OF TABLES

LIST OF SYMBOLS

W_I internal work

W_E external work

$\{\epsilon\}$ $\epsilon_{xx}, \epsilon_{yy}, \epsilon_{zz}, 2\epsilon_{xy}, 2\epsilon_{xz}, 2\epsilon_{yz}$ strain vector and components

$\{\sigma\}$ $\sigma_{xx}, \sigma_{yy}, \sigma_{zz}, \sigma_{xy}, \sigma_{xz}, \sigma_{yz}$ stress vector and components

V volume

$\{d\}$ displacement vector

$\{f\}$ $f_{xi}\ f_{yi}\ f_{zi}$ body force vector and components

$\{\bar{P}\}$ $\bar{P}_{xi}\ \bar{P}_{yi}\ \bar{P}_{zi}$ prescribed external surface traction vector and components

S surface

u_i i^{th} node displacement component in the x direction

v_i i^{th} node displacement component in the y direction

w_i i^{th} node displacement component in the z direction

$[B]$ element strain-displacement matrix

n superscript, refers to the n^{th} element

$[m]^n$ mass matrix for the n^{th} element

$[N]$ shape function matrix

N_i shape function

ξ, η, ζ local reference system coordinates (curvilinear)

X, Y, Z global reference system coordinates (Cartesian)

U, V, W global displacement components in the X, Y, Z direction, respectively

u, v, w local displacement components in the X, Y, Z direction, respectively

$[D]$ linear elastic material property matrix relating stress and strain

$[D(t-\tau)]$ linear viscoelastic material property matrix relating stress and strain

λ Lamé constant

G shear modulus

$\dot{(\ )}$ first time derivative of ( )

$\ddot{(\ )}$ second time derivative of ( )

β, δ coefficients for Newmark operator

θ coefficient for Wilson operator

ρ, α polar modulus and polar phase for operator stability determination

K bulk modulus

ν Poisson's ratio

$|J|$ Jacobian

$[k]^n$ stiffness matrix for the n^{th} element

$[\rho]$ mass density matrix

Δt time interval

t time

τ dummy time variable

$[k(t-\tau)]^n$ stiffness matrix for the n^{th} viscoelastic element

u displacement for a single-degree-of-freedom system

m mass for a single degree of freedom system

$E(t + \Delta t - \tau)$ relaxation modulus

$f(t + \Delta t)$ forcing function for a single degree of freedom system

λ_i relaxation times

nv number of viscoelastic terms

nq number of quadrature terms

E_0, E_i relaxation moduli

W_i natural circular frequency for a single degree of freedom system

Δu change in displacement u during Δt interval

$[k_i]^n$ n^{th} viscoelastic element stiffness matrix for the i^{th} term

H_i weighting factors defined in Gaussian quadrature process

$K_{i,i}$ global stiffness matrix coefficient on the diagonal

$\overline{F}_i$ prescribed impact force at the i^{th} degree of freedom

U_i displacement at i^{th} degree of freedom

m_i lumped mass at i^{th} degree of freedom

INTRODUCTION

Evaluation of head injury received from direct blows is necessary for development of adequate protection systems for the head. The need for biomechanical models that predict head injury has been expressed by both the engineering and the medical community: e.g., to aid safety specialists in developing protection standards for vehicle occupants; to aid engineers in choosing military aircraft and other vehicle designs for crew and occupant safety; to improve the capability of neurosurgeons in managing brain trauma. Irrespective of its professional application, clinical-pathological-mechanical correlation of head injury is what is sought. Statistics compiled by the National Safety Council reveal that the vehicle accident is a major cause of death in this country. Recent reductions in maximum speed limit and construction of safer roads in this country are improving upon the highway death rate and at the same time are making the crashworthiness design of automobiles more feasible than in the past. Fatalities went from 56,000 in 1973 to 46,000 in 1975[1]. It has been estimated[1] that in 1975 the Interstate Highway System saved 4,400 lives. Relative reduction in fatalities was twice as great on those roads affected by the speed limit reduction to 55 mph as on those roads which were not affected[2]. The goal should be to make all crashes survivable. With regard to transportation in aircraft, both commercial and military, the goal cannot be so optimistic, but improvements in the crashworthiness design of aircraft are definitely justifiable and warranted.

Statistical studies of injury during aircraft crashes have shed some light on the incidence of head injury. Two difficult questions have to be asked of the data: "Were the crashes in question survivable?" and, "In fatal instances, could death be attributed to head injury?" A survivable crash has been defined as one in which the forces transmitted to the occupant through his seat, restraint system, or surrounding components do not exceed human tolerance[3]. Though it is the best we have, this definition is only preliminary because it includes the phrase "human tolerance." Certainly one of the goals of head injury research, as exemplified by the model studies discussed herein, is to determine the levels of human tolerance to impact.

Some statistics regarding injuries in rotary wing aircraft crashes are germane; reference 3 reports on 2,546 helicopter accidents studied. It was determined at the outset that 93% of these crashes were survivable. Then it was computed that 40% of the total number of fatalities occurred in the survivable group (this amounted to 439 deaths that should not have occurred). It was further determined that 23% of the preventable deaths were due to head injury alone and that 29% of the 2,699 survivors sustained head injuries.

---

[1] National Safety Council Accident facts. Chicago, Illinois, 1976.

[2] National Highway and Transportation Safety Agency. NHTSA DOT-HS-801715: Effect of the fuel shortage on travel and highway safety, by E. C. Cerrelli. Washington, D.C., Aug 1975.

[3] S. P. Desjardins. "Vehicle crashworthiness," Numerical and Computer Methods in Structural Mechanics, ed. S. J. Fenves, et al. New York, Academic Press, 1973, pp 557-584.

Impact energy associated with fixed wing aircraft crashes is generally expected to be higher than that associated with rotary wing aircraft crashes. For that reason, the percentage of survivable crashes in fixed wing aircraft accidents is expected to be less, but crashworthiness of these aircraft must be improved as well.

The head receives basically two kinds of dynamic loads: (1) a direct impact involving hard, localized, contact-impact forces applied directly to some portion of the skull and (2) an indirect impact involving forces transmitted from the neck to the base of the skull, possibly with additional nonlocalized, soft contacts to the head. The first type commonly involves the impact of heads with windshields, instrument panels, sidewalls, and seat backs. The second occurs when the occupant's restraint system (seat belts, air bags, etc.) prevents his reaching surrounding structures. Space for occupants is always at a premium; therefore, it is not always feasible to remove structural components from the occupants' strike zone[4]. The only alternative is to design the occupants' immediate environment so that if contact occurs the effect is minimized. Energy-absorbing structures and sometime protective helmets are essential components of crashworthiness design. Their effectiveness should be evaluated in conjunction with a head injury model[5], along with other surrogates of the head.

Approaches to Head Injury Prediction

The prediction of head injury can be approached in many ways; various injury or severity indices that offer attractive expedient solutions have been proposed. These are usually based on data derived from experiments with cadavers and human volunteers. This data naturally possess limitations. Often little agreement exists among these methods of injury prediction because each method choosen fits the experimental data with a different curve, but the primary objection to these methods is that they, by definition, must either simplify many variable relationships or fail. As a result parameters are often contrived that have no fundamental basis for measurement, but which are critical to the accuracy of the method. Results, therefore, vary, depending upon how these parameters are measured or estimated.

In any approach to head injury prediction, the final usefullness of the derived injury prediction data depends on how conveniently it can be synthesized and formatted for assimilation. Primarily because of the computer, this convenience requirement does not preclude a more rigorous approach to obtaining useful injury prediction information which accounts for the many engineering variable relationships present in the problem. Further, if the more rigorous approach is successful, more is obtained than an estimate of injury hazard; it also provides insight into the clinical-pathological-mechanical causes of head injury. This is why many investigators have chosen mathematical modeling as an approach to head injury prediction. It is a more instructive approach and can result in a useful and convenient data base of head-injury prediction.

---

[4]Army Air Mobility Research and Development Laboratory. TR 71-22: Crash survival design guide. Fort Eustis, Va, Oct 1971.

[5]K. J. Saczalski, et al. "A critical assessment of the use of non-human responding surrogates for safety system evaluation," in Proceedings of the Twentieth Stapp Car Crash Conference, SAE, 1976.

Objective

This research was to develop a computer program, based on the laws of mechanics, for simulating structural deformation response and for predicting impact injury throughout the head. The model was intended for use in:

(1) understanding injury mechanisms
(2) defining tolerance envelopes
(3) predicting dynamic responses to specific accidents
(4) conducting sensitivity analyses

The specific objective was to compute the time histories of displacement, strain, and stress throughout the skull-brain system induced by arbitrary head impacts. Further, a similar primate model was to be constructed for correlating the response to that measured in animal impact experiments.

Scope

Requirements of the head-injury model (HIM) included three-dimensional skull-brain geometry simulation, taking full advantage of symmetry about the midsagittal plane in the generation of the geometrical construction. Neck-related injury was not included, though arbitrary boundary conditions at the base of the skull could be specified to approximate the influence of the neck on the skull-brain response in any simulation. Thus, the model pertained to closed brain injury and skull fracture exclusive of any mitigating neck influence. Arbitrary initial conditions in the form of either initial displacements or initial velocities could be specified.

A major part of the investigation was the computation of impact forces existing at the interface between the skull model and arbitrary simulated targets. The variation in contact forces and areas over which the forces act (contact area) were sought as a function of time. Non-linear geometry and constitutive behavior were to be included in the contact problem as well as in the skull/brain model.

This research represents 3 years of study under contract DOT-HS-289-3-550IA for the Department of Transportation, Work Request N0020375WR00142 for the Naval Aerospace Medical Research Laboratory Detachment, New Orleans, and Work Request N0001476WR-60083 for the Office of Naval Research.

1. BACKGROUND

The relatively high incidence of head injuries occurring in automobile and survivable aircraft crashes, combined with the potential seriousness of these injuries, has been responsible for the preponderant concentration of biomechanics research in head impact. Experimental research has sought to generate data in support of head-injury model development. Engineers who construct models must be cognizant of these experimental results. Basically, models must be capable of (1) accepting as input the mechanical properties of the head, (2) including both experimentally and statistically observed mechanisms of injury, and (3) simulating live primate impact tests and correlating the resulting measured data.

Many attempts have been made to develop biomechanical models for predicting mechanical phenomena responsible for head trauma. Head injury studies can be divided into two classes: primarily experimental and primarily theoretical. Experimental studies utilize anthropomorphic dummies, cadavers, animals, etc., and require expensive and time-consuming research programs. On the other hand, theoretical studies utilize the laws of mechanics to predict mechanical responses of the head and can provide an efficient tool for investigating head injury phenomena. Fundametally, only two kinds of mathematical approaches—analytical and numerical—have been demonstrated in head injury modeling; both are deterministic.

Analytical Models

The analytical models appeared first. Examples of these models are one-dimensional fluid-filled, rigid containers[6] and two-dimensional, axisymmetric, fluid-filled, elastic spheres[7,8]. Their solutions were usually in the form of truncated infinite series, and assistance from the computer was required to obtain data. These models have provided useful insight into pressures and pressure wave propagations within a continuum of contained compressible fluid. However, they are necessarily limited to analytically simple modeling parameters; for example, they can neither simulate recognizable skull geometry nor loading histories and boundary conditions for head impacts typical of those presented in vehicle accidents.

---

[6] T. Hayashi. "Study of intracranial pressure caused by head impact," Journal, Faculty of Engineering, University of Tokyo, 1969, pp 30-59.

[7] A. E. Engin and Y. King Liu. "Axisymmetric response of a fluid-filled spherical shell in free vibrations," Journal of Biomechanics, vol. 3, no. 1, Jan 1970.

[8] Y. C. Lee and S. H. Advani. "Transient response of a sphere to torsional loading - a head injury model. Math," Biosciences, vol. 6, 1970, pp 473-486.

Numerical Models

The belief expressed herein is that only the numerical models have the potential for providing all three of the necessary and basic ingredients stated above and thus offer greater potential for reliable prediction.

Finite Difference Method. The finite difference technique falls within this category; but, in spite of some noteworthy efforts, this technique has demonstrated little potential beyond axisymmetric simulation. Reference 9 describes a one-dimensional finite difference model in which the importance of including the various layers of different cranial materials and their influence on dissipation of energy as stress waves travers the layers was investigated. This particular work was then extended to a two-dimensional, axisymmetric sphere[10]; others, too, have discretized axisymmetric fluid-filled shells with spherical[11] and elliptical[12] shapes. Geometrical zoning in the finite difference technique is potentially very flexible, but further extensions to three-dimensional head injury models are difficult to envision. For short load durations typical of wave propagation regimes, however, the finite difference methods are attractive, especially when nonlinear behavior and axisymmetric skull configurations are considered.

Finite Element Method. The finite element method[13,14], on the other hand, is an established three-dimensional modeling technique and is, therefore, eminently suited for modeling the general head impact. Therefore, the following review will mention only those efforts based upon the finite element method. A more thorough examination is made in Reference 15. Excellent reviews of head injury models based upon alternative approaches can be found in Reference 16.

---

[9] Naval Air Development Center. Report No. NADC-CS-7113: Impact analysis of the skull-brain system, by Stephen L. Gordon. Warminster, Pa, Dec 1971.

[10] Interim Report No. NADC 73065-40: Analysis of head impact, by Stephen L. Gordon. Warminster, Pa, Apr 1973.

[11] J. V. Benedict, F. H. Harris, and D. U. von Rosenberg. "An analytical investigation of the cavitation hypothesis of brain damage," Journal of Basic Engineering, vol. 92, Sep 1970, pp 597-603.

[12] Anthony James Crispino. A dynamic analysis of elastic model of the human head, M. S. thesis, Department of Mechanical Engineering, University of Washington. Seattle, Wash, 1972.

[13] O. C. Zienkiewicz. The finite element method in engineering science. London, England, McGraw-Hill, 1971.

[14] Richard H. Gallagher. Finite element analysis: Fundamentals. Englewood Cliffs, N.J., 1975.

[15] Shugar, T. A., "Simulating and Modeling the Human Head's Response to Impact," Aircraft Crashworthiness, Eds K. Saczalski, G. T. Singley III, W. D. Pilkey, and R. Huston, University Press of Virginia, Charlottsville, 1975, pp 213-234.

[16] A. I. King and C. C. Chou. "Mathematical modeling, simulation and experimental testing of biomechanical system crash response," paper presented at Eleventh Annual Meeting, American Institute of Aeronautics and Astronautics, Washington, D.C., Feb 1975. (AIAA paper no. 75-272)

The first suggestion that finite element techniques could be advantageous in head injury modeling appeard one decade ago[17], but feasibility of a three-dimensional model at that time is doubtful. Axisymmetric computer codes were available, however, and could have easily been applied toward solving the fluid-filled, spherical shell problem. The method was not applied until some years later[18]. This application was significant because it attempted to deal with actual skull geometry, and, in doing so, a primary advantage of the finite element technique in head injury modeling was demonstrated for the first time. The analysis was limited to an empty skull and static loading but did conclude that the sandwich nature of cranial bone should be modeled as a layered structure.

Axisymmetric Finite Element Model. An axisymmetric finite element model was constructed to demonstrate the effectiveness of the method as a potential head injury investigatory technique[19]. Spherical configurations were assumed to be useful head injury models; and, if the finite element model correlated well with experimental data obtained from an instrumented spherical aluminum shell, the model was assumed to be reliable. Computed strains were about 20% higher than measured strains on the aluminum surface.

A subsequent attempt at axisymmetric, finite element modeling of the skull was conducted with more success[20]. The axisymmetric configuration was more justifiable when the analysis of protective helmets was undertaken. Rotational symmetry is a convenient and reasonably accurate configuration for evaluating a variety of helmet parameters, even though the head itself is not rotationally symmetric. Furthermore, when a two-dimensional analysis can accomplish the objective sufficiently, it is to be preferred over a fully three-dimensional analysis. Findings regarding helmets will not be discussed in this report, but such work does offer some significant points regarding head injury modeling with the finite element method. An inviscid fluid was reported as being employed for brain material characterization during analyses with one axisymmetric code. A second computer code capable of specifying linear viscoelastic properties, but which apparently could not also specify the fluidity alluded to earlier, was employed in the simulation of an empty spherical shell. The consitutive relation for the shell was an exponentially decaying relaxation modulus developed experimentally from impact load data on bone samples. The experimental data from which the relaxation modulus was derived were characterized by load durations in the microsecond range and were applicable to impact loads with durations of approximately 50 μsec and less. Rather good correlation was shown in a comparison of computed and measured data for the axisymmetric configuration. The axisymmetric trest setup displayed support conditions which were rotationally symmetric. The spherical aluminum shells were covered with a nested set of spherical shell caps which simulated the helmets.

---

[17] W. Goldsmith. "The physical processes producing head injury," in Proceedings of the Head Injury Conference, Lippincott, Philadelphia, Pa, 1966, pp 350-382.

[18] Office of Naval Research. Technical Report No. 8: Elastic analysis of a skull, by C. H. Hardy and P. V. Marcal. Washington, D.C., Nov 1971. (Contract No. N00014-67-A-0191-0007)

[19] V. H. Kenner and W. Goldsmith. "Dynamic loading of a fluid-filled spherical shell," International Journal of Mechanical Sciences, vol. 14, 1972, pp 557-568.

[20] T. B. Khali, W. Goldsmith, and J. L. Sackman. "Impact on a model head-helmet system," International Journal of Mechanical Sciences, vol. 16, 1974, pp 609-625.

It is significant to note that when the axisymmetric finite element results were compared with experimental data obtained from a cadaver head fitted with a helmet, the correlation deteriorated. The reasons stated were that the boundary condition or geometry of the cadaver experiments were not faithfully duplicated and that correct material behavior was not sufficiently simulated.

Spherical and ellipsoidal models were constructed in a more recent two-dimensional finite element analysis study[21] to devise a better model—one that would reveal the etiology of head injury due to impact. The ellipsoidal model seemed to be a slight improvement over the spherical model; nevertheless, the results were stated to be inconclusive. The computed intracranial response was based on a viscoelastic core material, which was specified in the form of a Voight solid for the shear moduli; the bulk moduli were specified as elastic constants. An uncertainty was expressed concerning the viscous component constant.

Another interesting feature of this finite element study was the manner in which the temporal integration of the system equations of motion was carried out. The iterative method is not commonly employed in the mainstream of dynamic finite element analysis. It holds some promise for large nonlinear systems, but currently suffers from two objections[22]. First, convergence to required accuracy has been found to be slow for general applications, making them inferior to direct integration methods. Second, it is impossible to repeat solutions for a different set of loading conditions without once again sustaining the cost of the iterative integration process. The result is that the iterative method can be more expensive than the more common direct integration methods for linear systems. The study does, once again, demonstrate the utility of the finite element method in head injury; in this case the effects of geometry and duration of impact were easily examined. Also of importance is the choice of a computer code that allows for viscoelastic behavior.

A three-dimensional finite element model of the brain applicable to prescribed translational acceleration of the skull symmetrical about the midsagittal plane was constructed[23]. A rigid skull was assumed and, therefore, was applicable to brain injury in those cases where skull deformation does not contribute to the injury. Obviously the model cannot directly relate to skull fracture. More recently the model has been extended to account for rotation[24]. This work demonstrates the detail which can be achieved in simulating geometry.

---

[21] H. S. Chan. "Mathematical model for closed head impact," in *Proceedings of the Eighteenth Stapp Car Crash Conference*, Ann Arbor, Mich, Dec 1974, pp 557-578.

[22] Ernst Schrem. "Computer implementation of the finite-element procedure," Numerical and Computer Methods in Structural Mechanics, ed. S. J. Fenves, et al. New York, Academic Press, 1973, pp 79-117.

[23] C. C. Ward. A dynamic finite element model of the human brain, Ph. D. thesis, Department of Engineering, University of California at Los Angeles. Los Angeles, Calif, 1974.

[24] C. C. Ward and R. B. Thompson. "The development of a detailed finite element brain model," in Proceedings of the Nineteenth Stapp Car Crash Conference, San Diego, Calif, Nov 1975. pp 641-670.

Various intracranial structures were discretized in an extremely painstaking fashion. Foremost among them were the falx and tentorium membranes that divide the cranial vault into separate cavities. In this work a Poisson's ratio of 0.48 and a Young's modulus of 10 psi were specified for brain material. At first glance, these numbers appear insignificantly different from published values but in fact, result in a bulk modulus of approximately 80 psi. This value represented a compressible brain material characterization whose resistance to volumetric change was over three orders of magnitude less than the reported value of 305,000 psi[25]. No provisions were made for the inclusion of viscoelastic material characterization. A modal analysis or eigenvalue approach was employed to solve the equations of motion.

---

[25]West Virginia University, Biomechanics Laboratories, Department of T and AM. Head injury model construction program data compilation and review. Morgantown, W. Va., Jun 1971. (Contract No. PH-43-67-1137)

2. ORGANIZATIONAL PLAN

The problem of developing a head injury model is of a complexity different from that usually encountered by engineers. A cautious and deliberate approach was therefore taken. Several research groups were ultimately involved in the development of the head injury model. To facilitate a discussion of their participation a schematic diagram of the head injury model development program is presented in Figure 2-1. The sponsoring agencies—NHTSA, NAMRL and ONR*—gave CEL overall responsibility for carrying out the various research tasks, each of which is designated with a box and located within the dashed line. These tasks were either performed in-house, or a subcontract was let to an outside research group.

Simulation of the cranial anatomy as closely as possible was first necessary. This requirement superseded all other requirements in the model development because it distinguished this head injury model effort from all previous efforts. However, reasonable limits exist for geometrical simulation in any model development. A subcontract was thus initiated to delineate those areas of the skull/brain anatomy clinically known to have a higher frequency of involvement with head trauma. More attention was to be given those areas during the process of discretization. Clinical descriptions of head injury mechanisms were obtained so that, where possible, the model could be constructed to accommodate such mechanisms. The Los Angeles County/University of Southern California (LAC/USC) Medical Center furnished this information; their report is included as Appendix A.

Developing a three-dimensional discretization proved to be a difficult task and required more effort than originally expected. Manual discretizing of the skull continuum was initially attempted in an effort to be extremely responsive to geometrical detail. However, measuring difficulties and uncontrollable element aspect ratios prevented success. Instead, automated procedures proved to be the optimal method, although some accuracy may have been compromised in the simulation of geometry.

The skull/brain module was to be actually the end product of the discretization process and entails more than the automatic mesh generation scheme. For example, it includes parametric control on size and shape of the skull being discretized, a mesh checking scheme, mass distribution computation capability (skull inertia tensor), and several default options, all of which attempt to facilitate the user in his effort to construct a three-dimensional discretization.

The deliberateness of the approach was perhaps nowhere else more apparent than in the construction of successive models. The development of one-dimensional (actually a prismatic assemblage of three-dimensional elements) models and the gradual increase in the complexity of two-dimensional, axisymmetric and plane strain models instead of concentrating on a three-dimensional model from the start, was the intent of the successive model

---

*National Highway Traffic Safety Administration, Naval Aerospace Medical Research Laboratory Detachment, Michoud Station, and the Office of Naval Research.

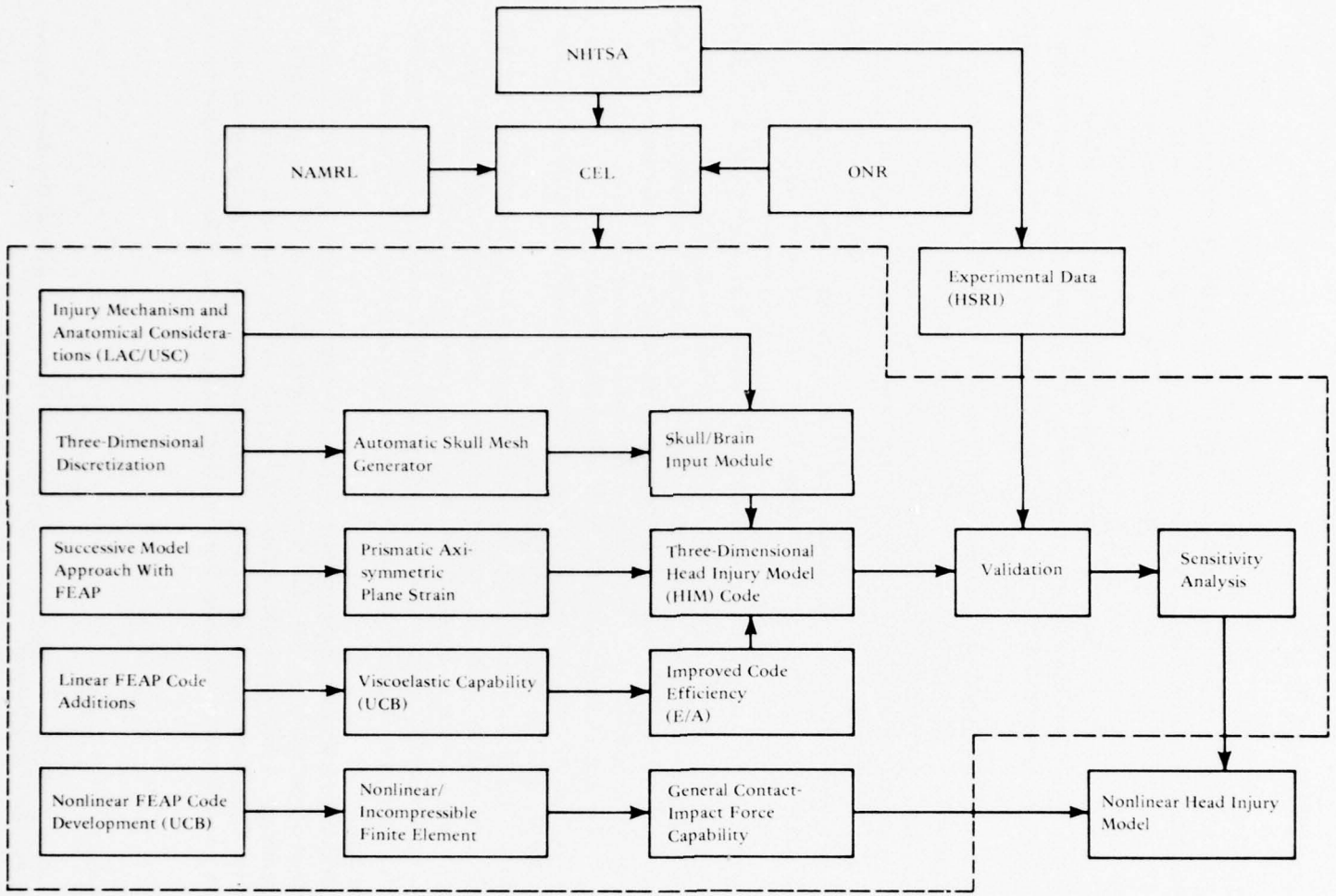

Figure 2-1. Schematic Diagram of Head Injury Model Development Program.

approach. In spite of their obvious spatial differences the models were closely related numerically, and because of this the successive model approach is especially effective in an orderly development of the final three-dimensional model. A relatively new, general purpose, finite element analysis program (FEAP)[26], developed at the University of California at Berkeley (UCB), was employed in the successive model approach. In the process, each model was composed of elements from the same family of isoparametric finite element formulations, and each was integrated in the time domain by the same method; i.e., the same implicit integration operator was employed throughout the development. Therefore, information and experience gained from exercising the preliminary models were ultimately applicable to the numerical behavior of the three-dimensional model.

It was recognized early that the basic FEAP code would have to be modified in two areas to facilitate development of the three-dimensional head injury model. A linear viscoelastic capability was thought to be highly desirable in view of the large volume of literature on viscoelastic properties of biomaterial[27-32]. A subcontract was let to the University of California to incorporate into the code the capability of prescribing linear viscoelastic mechanical properties for the skull/brain materials.

It was also recognized that a finite element head injury model would be relatively expensive to operate parametrically. Computer costs associated with dynamic, three-dimensional models of any kind are known to be high; but, add to that, construction of a model where geometrical detail is of high priority and costs are pushed even higher. To effect modifications which would improve the FEAP code's efficiency, a subcontract was let to Engineering/Analysis (E/A) Corporation of Redondo Beach, California. A summary of the modifications is presented in Appendix B (Volume II). E/A also provided a bandwidth minimizer program which optimally reorders the nodal point numbering system for any skull/brain discretization prior to its use as input data for the head injury model code.

---

[26] University of California, Department of Civil Engineering, Finite element analysis program, by R. L. Taylor. Berkeley, Calif.

[27] J. W. Pugh, et al. "Elastic and viscoelastic properties of trabecular bone: dependence on structure," Journal of Biomechanics, vol 6, no. 5, sep 1973.

[28] Y. C. Fung. "Stress-strain-history relations of soft tissues in simple elongation," Biomechanics, ed. Y. C. Fung, N. Perrone, and M. Anliker. Englewood Cliffs, NJ, Prentice-Hall, 1972. pp 181-208.

[29] R. C. Tennyson, R. Ewert, and V. Niranjan. "Dynamic viscoelastic response of bone," Experimental Mechanics, Nov 1972.

[30] H. C. Wang and A. S. Wineman. "A mathematical model for the determination of viscoelastic behavior of brain in vivo - I Oscillatory response," Journal of Biomechanics, vol 5, 1972. pp 431-446.

[31] X. T. Truong. "Visco-elastic propagation of longitudinal waves in skeletal muscle," Journal of Biomechanics, vol 5, 1972. pp 1-10.

[32] J. E. Galford and J. H. McElhaney. "A viscoelastic study of scalp, brain, and dura," Journal of Biomechanics, vol 3, 1970. pp 211-221.

A comprehensive program of head injury model validation was developed in consonance with NHTSA. CEL, though not involved directly with the experimental work itself, helped establish the validation test plan requirements for experimental data so that the kinds of experimental tests conducted could also be simulated. NHTSA contracted with the Highway Safety Research Institute (HSRI), University of Michigan, to design and conduct experimental tests, the data from which would constitute the primary means for verifying the accuracy of the head injury model. The types of experimental tests included (1) static load deflection measurements of dry rhesus monkey skulls, (2) dynamic tests with strain gages affixed to the same skulls, and (3) impact tests on anesthesized rhesus monkeys instrumented with both strain gages and pressure transducers.

After completion of the validation effort a sensitivity analysis or parameter study was conducted wherein a series of dynamic simulations were made using the displacement boundary conditions at the base of the skull as the parameters. Among the many alternative parameter studies that could have been conducted, this particular study was found to be more useful because the head injury model does not possess a neck discretization and, therefore, cannot simulate directly the influence of the neck on the base of the skull during impact. However, by investigating the sensitivity of the skull bone structural response and the intracranial pressure response to changes in the prescribed displacement boundary condition at the skull base, the limits of the neck's influence can be established.

To satisfy the requirement for a nonlinear head injury model the linear FEAP code had to be extended to the nonlinear regime. Though some provision was made for nonlinear behavior in the original code it was decided to proceed with a linear model development and to subcontract the nonlinear code development. This work was eventually accomplished by the original FEAP code author at UCB.

Two additional requirements of the head injury model were associated with the nonlinear development. A nearly incompressible, nonlinear finite element had to be added to the element library to model the intracranial contents. Also, a general contact/impact force computation capability needed to be developed to predict accurately the stress histories existing at the interface between the skull and an arbitrary target. Individually or collectively, these requirements suggested a basic research project, as contrasted with the linear model development, and as such were ultimately handled separately by subcontract to UCB. Much progress was reported in a series of documents [33-37], and the final code implementation of the developed theoretical concept has been completed in two dimensions.

---

[33] Civil Engineering Laboratory. CR75.007 Finite element formulation and solution of contract-impact problems in continuum mechanics, by T. J. R. Hughes, R. L. Taylor and J. L. Sackman. University of California, Berkeley, Calif, May 1974. (SESM Report No. 74-8)

[34] CR75.008 Finite element formulation and solution of contact-impact problems in continuum mechanics - Part II, by T. J. R. Hughes, R. L. Taylor, and J. L. Sackman. University of California, Berkeley, Calif, Jan 1975. (SESM Report No. 75-3)

[35] CR77.001 Finite element formulation and solution of contact-impact problems in continuum mechanics - Part III, by T. J. R. Hughes, R. L. Taylor, and J. L. Sackman. University of California, Berkeley, Calif, Jul 1975. (SESM Report No. 75-7)

[36] Civil Engineering Laboratory. CR77.002 Finite element formulation and solution of contact-impact problems in continuum mechanics, Part IV by T. J. R. Hughes, R. L. Taylor, J. R. Sackman, and W. Kanoknukulchai. University of California, Berkeley, Calif, 1976.

[37] T. J. R. Hughes, et al. "Finite element formulation and solution of a class of contact-impact problems in continuum mechanics," paper presented at Third Conference, Structural Mechanics Reactor Technology, London, 1975.

3. THEORETICAL CONSIDERATIONS

In this section the governing matrix equations of motion for dynamic linear viscoelasticity are developed beginning with the theorem of virtual work. Then, before their solution is described, two separate discussions are given which describe: first, how the HIM code deals efficiently with viscoelastic history vectors, and second, how the nearly incompressible property of brain material is handled.

Principle of Virtual Work and Equations of Motion

The principle of virtual work states:

> If a structure is in "equilibrium" under a set of external forces and if the structure is given a virtual displacement consistent with the constraints of the structure, then the external work done is equal to the internal virtual work done.

The word equilibrium is placed in quotes because it can refer to either static or dynamic equilibrium. Strictly speaking, with the latter form we are dealing with not the original principle of virtual work, but with D'Alemberts' extension of the original version which includes the inertial forces. The principle of virtual work applies to viscoelastic constitutive relations as well as linear elastic constitutive relations. In this presentation the inertial terms and the constitutive relations are included in generalized form for completeness because the head injury model possesses dynamic capabilities and both linear elastic and linear viscoelastic materials capability.

The virtual work principle may be expressed for a body as

$$\delta W_I - \delta W_E = 0 \tag{3-1}$$

where δW_I and δW_E are the internal and external virtual work expressions, respectively. They are defined as follows

$$\delta W_I = \int_V \delta\{\epsilon\}^T \{\sigma\} dV \tag{3-2}$$

$$\delta W_E = \int_V \delta\{d\}^T \{f\} dV + \int_S \delta\{d\}^T \{\bar{p}\} dS \tag{3-3}$$

where $\{\epsilon\}$ and $\{\sigma\}$ are the strain and stress vectors, respectively
V is the volume of the body
$\{d\}$ the displacement vector
$\{f\}$ is the body force vector containing the inertia forces
$\{\bar{p}\}$ the external surface traction vector prescribed over the surface S
$\delta(\,)$ the first variation of $(\,)$.

At this point it is convenient to discretize Equation 3-1 in developing the finite element formulation. However, this can be done in either of two ways. The first is to discretize Equation 3-1 exactly as it is; i.e., pertaining to the whole body. An alternative way is to rewrite Equation 3-1 for a single finite element and presume, for the time being, that the body's virtual work can be expressed legitimately as a summation of all elements of the virtual work contribution from each element. The latter approach is convenient in this case because it takes full advantage of the finite element method's ability to account for the prescription of different constitutive relations within the skull/brain continuum.

The basic finite element chosen in constructing the head injury model is the eight-node, isoparametric element and is shown in Figure 3-1 together with its assumed linear displacement function.

The X-Y-Z axes form an inertially fixed reference system. The displacements u, v, and w are defined with respect to this system. The ξ-η-ζ axes define the local element coordinate system. The displacements within an element and on its boundaries are functions of the local coordinates in the form of shape functions N_i and the nodal point displacements at the corners u_i, v_i, and w_i.

A general definition of strain is given by Green's strain tensor for which ϵ_x and ϵ_{xy} are two examples of the six independent components of $\{\epsilon\}$. These two components are defined as

$$\epsilon_{xx} = \frac{\partial u}{\partial x} + \frac{1}{2}\left[\left(\frac{\partial u}{\partial x}\right)^2 + \left(\frac{\partial v}{\partial x}\right)^2 + \left(\frac{\partial w}{\partial x}\right)^2\right] \tag{3-4}$$

and

$$\epsilon_{xy} = \frac{1}{2}\left\{\frac{\partial u}{\partial y} + \frac{\partial v}{\partial x} + \left[\left(\frac{\partial u}{\partial x}\right)\left(\frac{\partial u}{\partial y}\right) + \left(\frac{\partial v}{\partial x}\right)\left(\frac{\partial v}{\partial y}\right) + \left(\frac{\partial w}{\partial x}\right)\left(\frac{\partial w}{\partial y}\right)\right]\right\} \tag{3-5}$$

For a linear analysis, it is assumed that the strains are small and their products (second-order terms) may be neglected. To this small strain assumption is added a small displacement assumption. Practically, this means that the geometry of the elements remain basically unchanged during the loading process and that first order, infinitesimal, linear strain approximations can be used. In this way Equations 3-4 and 3-5 reduce to

$$\epsilon_{xx} \doteq \frac{\partial u}{\partial x} \tag{3-6}$$

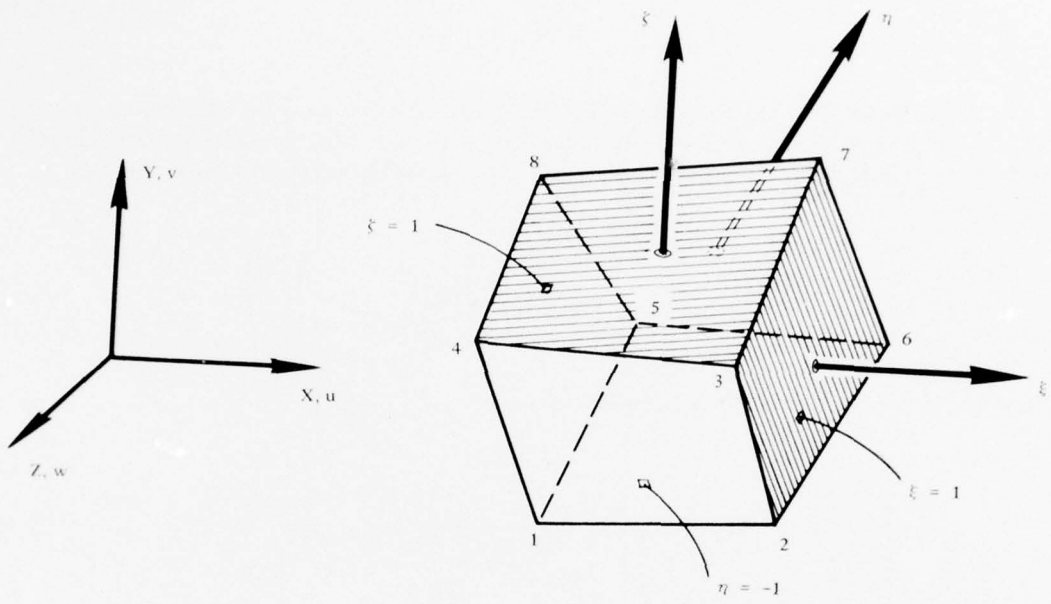

$$u(\xi,\eta,\zeta) = \sum_{i=1}^{8} N_i u_i$$

$$v(\xi,\eta,\zeta) = \sum_{i=1}^{8} N_i v_i$$

$$w(\xi,\eta,\zeta) = \sum_{i=1}^{8} N_i w_i$$

$$N_i = \frac{1}{8}(1+\xi_o)(1+\eta_o)(1+\zeta_o)$$

$$\xi_o = \xi\xi_i$$

$$\eta_o = \eta\eta_i$$

$$\zeta_o = \zeta\zeta_i$$

Figure 3-1. Isoparametric Element and Shape Function.

and

$$\epsilon_{xy} \doteq \frac{1}{2}\left(\frac{\partial u}{\partial y} + \frac{\partial v}{\partial x}\right) \tag{3-7}$$

Because the displacement components are functions of the local coordinates, the partial differentiation indicated must be carried out using the chain rule. The differentiation will result in a strain-displacement matrix [B] whose components are functions of the local coordinates; i.e.,

$$\{\epsilon\} = [B(\xi,\eta,\zeta)] \begin{Bmatrix} u_i \\ v_i \\ w_i \end{Bmatrix} \tag{3-8}$$

where the generalized nodal point displacements are

$$\begin{Bmatrix} u_i \\ v_i \\ w_i \end{Bmatrix} = \left\lfloor u_1\ u_2 \ldots u_8 \middle|\ v_1\ v_2 \ldots v_8 \middle|\ w_1\ w_2 \ldots w_8 \right\rfloor^T \tag{3-9}$$

We may now express the body force vector for the element in terms of the corresponding generalized acceleration as

$$\{f\} = -[\rho]\{\ddot{d}\} = -[\rho][N] \begin{Bmatrix} \ddot{u}_i \\ \ddot{v}_i \\ \ddot{w}_i \end{Bmatrix} \tag{3-10}$$

and the external traction force vector as

$$\{\bar{p}\} = \begin{Bmatrix} \bar{p}_{xi} \\ \bar{p}_{yi} \\ \bar{p}_{zi} \end{Bmatrix} \tag{3-11}$$

Equation 3-1, the virtual work equation, may now be written using the generalized displacement and the strain-displacement relationship for the eight-node element as follows

$$\int_V \begin{Bmatrix} \delta u_i \\ \delta v_i \\ \delta w_i \end{Bmatrix}^T [B]^T \{\sigma\} dV + \int_V \begin{Bmatrix} \delta u_i \\ \delta v_i \\ \delta w_i \end{Bmatrix}^T [N]^T [\rho][N] \begin{Bmatrix} \ddot{u}_i \\ \ddot{v}_i \\ \ddot{w}_i \end{Bmatrix} dV - \int_S \begin{Bmatrix} \delta u_i \\ \delta v_i \\ \delta w_i \end{Bmatrix}^T \begin{Bmatrix} \bar{p}_{xi} \\ \bar{p}_{yi} \\ \bar{p}_{zi} \end{Bmatrix} dS = 0 \tag{3-12}$$

where the superscript n refers to the volume or surface area of the n^{th} element of the body.

At this point we can either specify a linear elastic or linear viscoelastic relationship between stress $\{\sigma\}$ and strain $\{\epsilon\}$.

The linear elastic constitutive relationship between stress and strain is given by

$$\{\sigma\} = [D]\ \{\epsilon\} \tag{3-13}$$

where $\{\sigma\} = \left[\sigma_{xx}\sigma_{yy}\sigma_{zz}\sigma_{xy}\sigma_{xz}\sigma_{yz}\right]^T$

$$[D] \equiv \begin{bmatrix} (\lambda + 2G) & \lambda & \lambda & 0 & 0 & 0 \\ & (\lambda + 2G) & \lambda & 0 & 0 & 0 \\ & & (\lambda + 2G) & 0 & 0 & 0 \\ & & & 2G & 0 & 0 \\ & \text{symmetric} & & & 2G & 0 \\ & & & & & 2G \end{bmatrix} \tag{3-14}$$

The Lamé constant λ and the shear modulus G can be expressed in terms of the more common bulk modulus K and Poisson's ratio ν as follows

$$\lambda = \frac{3\,K\,\nu}{1+\nu} \text{ and } G = \frac{3\,K(1-2\nu)}{2(1+\nu)} \tag{3-15}$$

If Equation 3-13 is substituted into Equation 3-12 and the arbitrary virtual displacements factored out, we have

$$\begin{Bmatrix} \delta u_i \\ \delta v_i \\ \delta w_i \end{Bmatrix}^T \left(\int_V [B]^T [D] [B] \begin{Bmatrix} u_i \\ v_i \\ w_i \end{Bmatrix} dV + \int_V [N]^T [\rho] [N] \begin{Bmatrix} \ddot{u}_i \\ \ddot{v}_i \\ \ddot{w}_i \end{Bmatrix} dV - \int_S [N]^T \begin{Bmatrix} \bar{p}_{xi} \\ \bar{p}_{yi} \\ \bar{p}_{zi} \end{Bmatrix} dS \right) = 0 \tag{3-13}$$

The stiffness matrix $[k]^n$ and mass matrix $[m]^n$ of the n^{th} element are defined as

$$[k]^n = \int_{V_n} [B]^T [D] [B] \, dV$$

and

$$[m]^n = \int_{V_n} [N]^T [\rho] [N] \, dV$$

Carrying out the integration in local coordinate space we first make use of the relationship between elemental volumes in the two coordinate systems

$$dV = dX \, dY \, dZ = \left| J \right| d\xi \, d\eta \, d\zeta$$

and rewrite the stiffness and mass matrices as

$$[k]^n = \int_{-1}^{1} \int_{-1}^{1} \int_{-1}^{1} [B]^T [D] [B] \left| J \right| d\xi \, d\eta \, d\zeta \tag{3-14}$$

and

$$[m]^n = \int_{-1}^{1} \int_{-1}^{1} \int_{-1}^{1} [N]^T [\rho] [N] \left| J \right| d\xi \, d\eta \, d\zeta \tag{3-15}$$

For Equation 3-13 to be satisfied for arbitrary virtual nodal displacements the expression in parentheses must vanish. Invoking this condition yields the equation of motion for element n which can be written using Equations 3-14 and 3-15 as

$$[m]^n \begin{Bmatrix} \ddot{u}_i \\ \ddot{v}_i \\ \ddot{w}_i \end{Bmatrix}^n + [k]^n \begin{Bmatrix} u_i \\ v_i \\ w_i \end{Bmatrix}^n = \begin{Bmatrix} f_{xi} \\ f_{yi} \\ f_{zi} \end{Bmatrix}^n \tag{3-16}$$

Equations of Motion for Linear Viscoelasticity

If instead of Equation 3-13 we specify a linear viscoelastic relationship between stress and strain, considerably more complications will result, but the complexites can be surmounted by approximate means. The result is that the head injury model code can approximate the time-dependent relationship between stress and strain exhibited by biological materials when such a mechanism is justified.

Since considerable attention has been devoted to the viscoelastic nature of biological materials, it would be expected that a head injury model must possess the ability to account for viscoelastic materials. What follows is a detailed description of how viscoelastic material characterization is implemented into the equations of motion. This work is largely due to Taylor [38].

Viscoelastic materials are often called "memory" materials; that is, the current state of stress in the material is determined not only by the current deformation, but also by all past deformation states. Moreover, the memory exhibits a fading phenomenon in that past deformation states influence the current stress state to a lesser degree than do more recent deformation states. These characteristics are reflected in the constitutive model for viscoelasticity by the Stieltjes integral; i.e.,

$$\{\sigma(t)\} = \int_0^t [D(t-\tau)] \frac{\partial}{\partial \tau} \{\epsilon(\tau)\} d\tau \tag{3-17}$$

where $\{\sigma(t)\}$ is the stress vector at current time t, $\{\epsilon(\tau)\}$ is the strain vector for $0 \leq \tau \leq t$, and $[D(t-\tau)]$ is the constitutive matrix composed of two independent relaxation functions for isotropic materials. This constitutive model may now be combined with the eight-node finite element by substituting into Equation 3-17 the corresponding strain-displacement relations given in Equation 3-8. Thus we have

$$\{\sigma(t)\} = \int_0^t [D(t-\tau)] [B] \frac{\partial}{\partial \tau} \begin{Bmatrix} u_i \\ v_i \\ w_i \end{Bmatrix} d\tau \tag{3-18}$$

---

[38] R. L. Taylor. "An approximate method for thermovisco-elastic stress analysis," Nuclear Engineering and Design, vol. 4, 1966, p. 21.

Proceeding as before, this expression for $\{\sigma(t)\}$ is substituted into the virtual work equation for an element n (Equation 3-12); with the virtual displacements factored out, the following is obtained

$$\begin{Bmatrix} \delta u_i \\ \delta v_i \\ \delta w_i \end{Bmatrix}^T \left(\int_V \int_0^t [B]^T [D(t-\tau)] [B] \frac{\partial}{\partial \tau} \begin{Bmatrix} u_i \\ v_i \\ w_i \end{Bmatrix} d\tau \, dV + \int_V [N]^T [\rho] [N] \begin{Bmatrix} \ddot{u}_i \\ \ddot{v}_i \\ \ddot{w}_i \end{Bmatrix} dV \right.$$

$$\left. - \int_S [N]^T \begin{Bmatrix} \bar{p}_{xi} \\ \bar{p}_{yi} \\ \bar{p}_{zi} \end{Bmatrix} dS \right) = 0 \qquad (3\text{-}19)$$

Again invoking the arbitrariness of the virtual displacements in the above equation we can write the equation of motion for a viscoelastic element as

$$[m]^n \begin{Bmatrix} \ddot{u}_i \\ \ddot{v}_i \\ \ddot{w}_i \end{Bmatrix}^n + \int_0^t [k(t-\tau)]^n \frac{\partial}{\partial \tau} \begin{Bmatrix} u_i \\ v_i \\ w_i \end{Bmatrix}^n d\tau = \begin{Bmatrix} f_{xi} \\ f_{yi} \\ f_{zi} \end{Bmatrix}^n \qquad (3\text{-}20)$$

where $[k(t-\tau)]^n = \int_{-1}^{1} \int_{-1}^{1} \int_{-1}^{1} [B]^T [D(t-\tau)] [B] \, |J| \, d\xi \, d\eta \, d\zeta$

and $[m]^n$ is as defined in Equation 3-15. Hence, to solve the general linear viscoelastic problem (Equation 3-20) utilizing the finite element method requires the solution of simultaneous linear integral equations. Without further restriction the numerical solution of integral equations of this form requires extensive effort. The following section shows a method whereby effort can be greatly reduced without undue restriction on the class of problems that can be solved.

Solution of Integral Equations

Consider a typical integral equation governing the motion of a single-degree-of-freedom system with viscoelastic behavior

$$m\ddot{u} + \int_{-\infty}^{t+\triangle t} E(t+\triangle t-\tau) \frac{\partial u}{\partial \tau} \, d\tau = f(t+\triangle t) \qquad (3\text{-}21)$$

If the body is in equilibrium until time zero, Equation 3-21 becomes

$$m\ddot{u} + E(t+\triangle t)\,u(o) + \int_o^{t+\triangle t} E(t+\triangle t-\tau)\,\frac{\partial u}{\partial \tau}\,d\tau = f(t+\triangle t) \qquad (3\text{-}22)$$

If the relaxation modulus for the material is characterized by a Prony series, a simplification to the solution by step forward time integration will be shown to result. Therefore, write

$$E(t) = E_o + \sum_{i=1}^{nv} E_i e^{-t/\lambda_i} \qquad (3\text{-}23)$$

where nv is the number of terms in the series.
Substituting Equation 3-23 into Equation 3-22 we can write

$$m\ddot{u} + E_o u(t+\triangle t) + \sum_{i=1}^{nv}\left[E_i e^{-(t+\triangle t)/\lambda_i} + E_i e^{-(t+\triangle t)/\lambda_i}\int_o^{t+\triangle t} e^{\tau/\lambda_i}\,\frac{\partial u}{\partial \tau}\,d\tau\right] = f(t+\triangle t) \qquad (3\text{-}24)$$

This equation is simplified by defining the last term on the left-hand side as I; i.e.,

$$I_i(t+\triangle t) = E_i e^{-(t+\triangle t)/\lambda_i}\int_o^{t+\triangle t} e^{t/\lambda_i}\,\frac{\partial u}{\partial \tau}\,d\tau \qquad (3\text{-}25)$$

and can be expanded for subsequent computational advantage as

$$I_i(t+\triangle t) = e^{-\triangle t/\lambda_i} I_i(t) + E_i e^{-(t+\triangle t)/\lambda_i}\int_t^{t+\triangle t} e^{\tau/\lambda_i}\,\frac{\partial u}{\partial \tau}\,d\tau \qquad (3\text{-}25a)$$

Equation 3-25a is a recursive equation for step-forward integration of Equation 3-24, provided the integral on the right-hand side of Equation 3-25a can be solved numerically. To do this it is assumed that the displacement u varies linearly over each time increment. In this way

$$\frac{\partial u}{\partial \tau} = \frac{u(t+\triangle t) - u(t)}{\triangle t} = \frac{\triangle u(t)}{\triangle t}$$

is treated as a constant over the interval $t<\tau<t+\triangle t$,

and $$\int_{t}^{t+\triangle t} e^{\tau/\lambda_i}\, d\tau = \lambda_i \left[e^{(t+\triangle t)/\lambda_i} - e^{t/\lambda_i} \right]$$

Thus, the integral I_i; can be written in recursive form as

$$I_i(t+\triangle t) = e^{-\triangle t/\lambda_i} I_i(t) + E_i \lambda_i \frac{\triangle u(t)}{\triangle t}(1 - e^{\triangle t/\lambda_i}) \qquad (3\text{-}25b)$$

One further computational simplification is made for I_i by defining

$$h_i(\triangle t) = \frac{E_i \lambda_i}{\triangle t}\left(1 - e^{\triangle t/\lambda_i}\right)$$

and rewriting the recursive formula as

$$I_i(t+\triangle t) = e^{-\triangle t/\lambda_i} I_i(t) + h_i(\triangle t)\ \triangle u(t) \qquad (3\text{-}25c)$$

Making use of Equation 3-25c, the equation of motion (Equation 3-24) can be written as

$$m\ddot{u} + \left[E_o + \sum_{i=1}^{nv} h_i(\triangle t) \right] \triangle u(t) = f(t+\triangle t) - E_o\, u(t) - \sum_{i=1}^{n} e^{-\triangle t/\lambda_i} I_i(t) \qquad (3\text{-}26)$$

where $$I_i(o) = E_i\, u(o)$$

and $$u(t+\triangle t) = u(t) + \triangle u(t)$$

The fomulation given above for a single-degree-of-freedom system holds also for a system of equations for any viscoelastic finite element. That is

$$[m]^n \begin{Bmatrix} \ddot{u}_i \\ \ddot{v}_i \\ \ddot{w}_i \end{Bmatrix}^n + \left([k_o] + \sum_{i=1}^{nv} [k_i(\triangle t)] \right)^n \begin{Bmatrix} \triangle u \\ \triangle v \\ \triangle w \end{Bmatrix}^n = \begin{Bmatrix} f_{xi} \\ f_{yi} \\ f_{zi} \end{Bmatrix}^n - [k]^n \begin{Bmatrix} u(t) \\ u(t) \\ w(t) \end{Bmatrix}^n$$

$$- \left\{ \sum_{i=1}^{nv} e^{-\triangle t/\lambda_i} I_i(t) \right\} \qquad (3\text{-}27)$$

where history integrals are now defined by

$$\{I_i(t+\triangle t)\} = \left\{ \sum_{i=1}^{nv} e^{-\triangle t/\lambda_i} I_i(t) \right\} + [k_i(\triangle t)] \begin{Bmatrix} \triangle u(t) \\ \triangle v(t) \\ \triangle w(t) \end{Bmatrix} \tag{3-28}$$

and $[k_o]$ and $[k_i]$ are viscoelastic element stiffness matrices. They are defined in the same manner as element stiffness matrices for elastic materials (see Equations 3-14 and 3-20).

Normal and Reduced Integration of Element Stiffness Matrix

For some time it has been known that in the application of finite element methods for nearly incompressible ($\nu \cong 0.5$) or incompressible materials ($\nu = 0.5$), numerical problems will be encountered with the usual displacement theory. To discuss how such materials are dealt with in the ordinary displacement formulation of finite element analysis it is necessary to discuss the method of evaluating the integrals defining the element stiffness matrices shown in Equations 3-14 or 3-20. The procedure is equally applicable to elastic or viscoelastic materials. In actual practice the integration over the element volume is carried out numerically using the method of Gaussian quadrature. The numerical form of Equation 3-14 for an element n becomes

$$[k]^n = \sum_{j=1}^{nq} \sum_{j=1}^{nq} \sum_{j=1}^{nq} H_i [B]^T [D] [B] |J| \tag{3-29}$$

In this triple summation, terms on the right-hand side are evaluated at specific points within the element known as Gauss points. The H_i are weighting factors and their values are shown in Table 3-1. Ordinarily for eight-node, isoparametric elements, such as those employed for the skull bone in this investigation, two-term (nq = 2) quadrature is employed. This implies eight Gaussian points. The eight Gauss points include two each on the plus and minus sides of the three local coordinate axes (see Figure 3-1). However, evaluating the element stiffness matrix for nearly incompressible materials is another matter.

Fried [39] has provided mathematical insight into why the normal two-term quadrature would be incorrect for nearly incompressible materials. He shows that a reduced integration must be used for those terms involving the Lamé constant in Equation 3-29. With the eight-node isoparametric element, the correct reduced integration is one-point Gaussian

---

[39] I. Fried. "Finite element analysis of incompressible material by residual energy balancing," International Journal of Solids-Structures, vol. 10, 1974, pp 993-1002.

Table 3-1. Abscissae and Weight Coefficients of the Gaussian Quadrature Formula

$$\int_{-1}^{1}\int_{-1}^{1}\int_{-1}^{1} f(\epsilon,\eta,\zeta)d\epsilon\, d\eta\, d\zeta = \sum_{j=1}^{nq}\sum_{j=1}^{nq}\sum_{j=1}^{nq} H_{iii} f(a_{1j}\, a_{2j}\, a_{3j})$$

Number of Terms, nq	Abscissae, ±a	Weight Coefficients, H
1	0	2.0000 0000
2	0.57735 02691 89626	1.0000 0000
3	0.77459 66692 41482 0.00000 00000 00000	0.555 555 555 0.888 888 888

quadrature at the element centroid. Naylor [40] has also demonstrated the necessity of reduced integration in several finite element analyses of nearly incompressible materials. This is the basic technique employed for brain material by Shugar and Katona [41] in the HIM code. Though it can be employed either way, the HIM code currently specifies reduced integration for terms involving both λ and G in Equation 3-29. No instability due to energy-less shear modes has been observed when using reduced integration involving all terms and when the elements are enclosed or confined.

Solution of the Equations of Motion

In this section an account is given of the method by which the HIM code integrates the dynamic equations of motion for the skull/brain system when either direct or indirect impact loadings are specified. The method is termed a step-by-step or direct integration technique and is suited to large systems of equations such as those which would emanate from a three-dimensional discretization of the head.

---

[40] D. J. Naylor. "Stresses in nearly incompressible materials by finite elements with application to the calculation of excess pore pressures," International Journal for Numerical Methods in Engineering, vol. 8, 1974, pp 443-460.

[41] T. A. Shugar and M. G. Katona. "Development of finite element head injury model," Journal of Engineering Mechanics Division, ASCE, vol. 101, EM3, Jun 1975, pp 223-239.

In the realm of dynamic finite element computer codes, much has been written concerning the most advantageous method of numerically integrating the equations of motion. The objective in this investigation was to canvass the available integration techniques and evaluate them in the context of criteria developed for large three-dimensional finite element models. An early selection of an operator was desirable so that it could be employed throughout the successive model development and its behavior under various conditions could be scrutinized for better understanding of its strengths and deficiencies.

The criteria for selecting a solution scheme are much the same for all finite element codes[42] : the nature of the problem to be solved, particularly the size of the problem and the load-time characteristics.

The first step is to choose between a modal superposition approach or a direct integration technique. The former approach is not feasible for large problems unless only a few of the lower modes are desired, which implies that the loading is sluggish and only excites the lower modes[43,44]. In the case of the head injury model the problem is very large. Within the realm of direct impact loading, short load durations are the rule rather than the exception and one can reasonably expect to encounter the wide spectrum of frequencies. Thus, the loading can excite substantially a number of the higher modes. Furthermore, the mode superposition approach presumes linearity. Therefore, because the system is large, because the loads will possess short durations, and because an extension to nonlinear behavior is envisioned, the modal superposition approach was discarded in favor of a direct integration technique. This decision also related to the selection of a finite element computer code for modeling the head. A modal analysis capability was not considered relevant in the code selection process.

The choice is then reduced to that of either an implicit or an explicit integration technique. The explicit method has the advantage of being extremely fast computationally for each time step because no triangularization is involved. However, the time step size is restricted by the Courant stability criterion. That is, the time step must be less than the smallest sonic travel time across any element. Unless some means is provided within the code to control the time step size during execution, the user runs the risk of an unstable solution. For codes dealing with large three-dimensional discretizations intended for repeated use in parametric studies, the possibility of instability is to be avoided. Even with

---

[42] R. S. Dunham, R. E. Nickell, and D. C. Stickler. "Integration operators for transient structural response," Computers and Structures, vol 2, no. 1/2, Feb 1972. pp 1-16.

[43] R. W. Clough and J. Penzien. Dynamics of structures. New York, McGraw-Hill Book Company, 1975. p. 271.

[44] R. D. Cook. Concepts and applications of finite element analysis. New York, John Wiley and Sons, Inc., 1974. pp 252-253.

permissible time steps an exorbitant number would be required to span typical load durations. These considerations, which are primarily practical in nature, reduce the selection to one of the implicit integration operator techniques. Some of these techniques are unconditionally stable and provide control over computer costs by allowing a choice of time step size independent of the Courant stability criterion.

Among the implicit schemes, the Newmark ($\gamma = 1/2, \beta = 1/4$) operator[45], the Wilson averaging operator[46], and the Houbolt operator[47] are more prevalent. The accuracy of these methods was studied to decide which would be more suitable for the head injury model.

Inherent in all implicit schemes is the tendency to artificially attenuate the response and to artificially elongate the period and shift the phase of the response during integration of the equations of motion.

Response attenuation for each operator was investigated with a simple 1-degree-of-freedom linear oscillator. This procedure was first used to study stability of finite difference solutions[48] and has been used contemporaneously by others[49] in evaluating the relative merits of integration operators. Only a heuristic account of the evaluation procedure is presented in this paper. More complete information is contained in the references cited.

The free response of a single-degree-of-freedom linear oscillator is governed by the differential equation of motion

$$\ddot{u} + \omega^2 u = 0 \qquad (3\text{-}30)$$

where u is the displacement and ω is the natural circular frequency. The procedure begins by substituting the integration operator expressions presented in Table 3-2 into Equation 3-30 at time t_{n+1}. In this way a numerical form of the equation (also shown in Table 3-2) for each operator is derived, and it will be necessary to find the expression for a typical

---

[45] Nathan M. Newmark. "A method of computation for structural dynamics," Journal of the Engineering Mechanics Division, ASCE, EM3, Jul 1959.

[46] University of California. SESM Report 68-1: A computer program for the dynamic stress analysis of underground structures, by E. L. Wilson. Berkeley, Calif, Jan 1968.

[47] John C. Houbolt. "A recurrence matrix solution for the dynamic response of elastic aircraft," Journal of Aero Science, vol. 17, 1950, p. 540.

[48] P. D. Lax and R. D. Richtmeyer. "Survey of the stability of linear finite difference equations," Communications on Pure and Applied Mathematics, vol. 9, no. 2, May 1956.

[49] Robert E. Nickell. "On the stability of approximation operators in problems of structural dynamics," International Journal of Solids and Structures, vol. 7, 1971, pp 301-319.

Table 3-2. Integration Operator Description

	Newmark[a]
Displacement	$u_{n+1} = u_n + \dot{u}_n \triangle t + (0.5 - \beta)\ddot{u}_n \triangle t^2 + \beta \ddot{u}_{n+1} \triangle t^2$
Velocity	$\dot{u}_{n+1} = \dot{u}_n + (1 - \gamma)\ddot{u}_n \triangle t + \gamma \ddot{u}_{n+1} \triangle t$
Equation 1	$\ddot{u}_{n+1} + -q[u_n + \dot{u}_n \triangle t + (0.5 - \beta)\ddot{u}_n \triangle t^2] = 0$
	Wilson Averaging[b]
Displacement	$u_{n+1} = u_n + \dot{u}_n \triangle t + (\ddot{u}_{n+1} + 2\ddot{u}_n) \triangle t^2/6$
Velocity	$\dot{u}_{n+1} = \dot{u}_n + (\ddot{u}_{n+1} + \ddot{u}_n) \triangle t/2$
Equation 1	$\ddot{u}_{n+1} + [1 - (3+q\theta \triangle t)/3\theta]\ddot{u}_n - (\theta \triangle t \dot{u}_n + u_n) q/\theta = 0$
	Houbolt
Velocity	$\dot{u}_{n+1} = \frac{1}{6 \triangle t}(11u_{n+1} - 18u_n + 9u_{n-1} - 2u_{n-2})$
Acceleration	$\ddot{u}_{n+1} = \frac{1}{\triangle t^2}(2u_{n+1} - 5u_n + 4u_{n-1} - u_{n-2})$
Equation 1	$\frac{1}{\triangle t^2}(2u_{n+1} - 5u_n + 4u_{n-1} - u_{n-2}) + \omega^2 u_{n+1} = 0$

[a] For the Newmark operator, $q = \omega^2/(1+\omega^2 \triangle t^2 \beta)$ where $\beta = 1/4$, $\gamma = 1/2$

[b] For the Wilson Averaging operator, $q = 6\omega^2/[6+(\omega\theta \triangle t)^2]$ where $\theta = 2$

response u_{n+1} for each. After the particular operator under evaluation has been introduced, the resulting numerical equation of motion is then cast into a difference equation of motion by using difference approximations to the derivatives. The oscillating component of the solution (in polar form) of this difference equation is,

$$u_{n+1} = \rho^{n+1}\left[A_1 e^{i\alpha(n+1)} + A_2 e^{-i\alpha(n+1)}\right] \tag{3-31}$$

The terms ρ and α are the polar modulus and polar phase, respectively, and the constants A_1 and A_2 are determined from initial conditions.

From Equation 3-31 it is seen that the response will grow without limit and therefore be unstable if $\rho > 1$. However, if $\rho < 1$ the response will be attenuated continuously. Each of the operators will yield a different function for the modulus ρ in terms of a parameter ϕ which in turn is the product of frequency ω and time step size Δt. Although attenuation occurs for $\rho < 1$, this condition is preferable to instability and is the requirement for a stable integration operator. The results of this investigation are presented in Figure 3-2, where the moduli ρ are plotted as a function of ϕ. It is seen that all three operators are unconditionally stable; i.e., $\rho < 1$ for any time step size Δt. Further, it is seen that the Newmark operator possesses no attenuation and, on that basis, is the choice among the three operators investigated. This conclusion is corroborated in Reference 42 which states further that the Newmark operator is also a good choice for nonlinear applications.

Other considerations could be important criteria, depending on the investigator's objectives. For example, computer time (number of numerical operations) is important although it is believed that the three operators studied are economically equal. Furthermore, an evaluation based on a single-degree-of-freedom system may be inconclusive inasmuch as subsequent application of the operator is with highly complex systems. To the writer's knowledge there are no reliable evaluation techniques which account for system complexity. The Newmark operator ($\beta = 1/4$, $\gamma = 1/2$) will evidence numerical damping in systems more complex than one-degree-of-freedom (i.e., general systems).

Instead of the entire complex system of the skull, the mathematical focus here will be on the integration of the equations associated with two typical arbitrary mass points (or nodes) within the global system, as shown in Figure 3-3. From this, the salient features of the solution process can be illustrated without direct reference to the remainder of the system.

DIRECT IMPACT — The governing equations of motion for arbitrary mass points i and i+1 at time step S+1 when subjected to specified direct impact forces $\bar{F}(\tau)$ are

$$\begin{bmatrix} m_i & \\ & m_{i+1} \end{bmatrix} \begin{Bmatrix} \ddot{U}_i \\ \ddot{U}_{i+1} \end{Bmatrix}^{(S+1)} + \begin{bmatrix} K_{i,i} & K_{i,i+1} \\ K_{i+1,i+1} & K_{i+1,i+2} \\ \text{symmetric} & \end{bmatrix} \begin{Bmatrix} U_i \\ U_{i+1} \end{Bmatrix}^{(S+1)} = \begin{Bmatrix} \bar{F}_i \\ \bar{F}_{i+1} \end{Bmatrix}^{(S+1)} \tag{3-32}$$

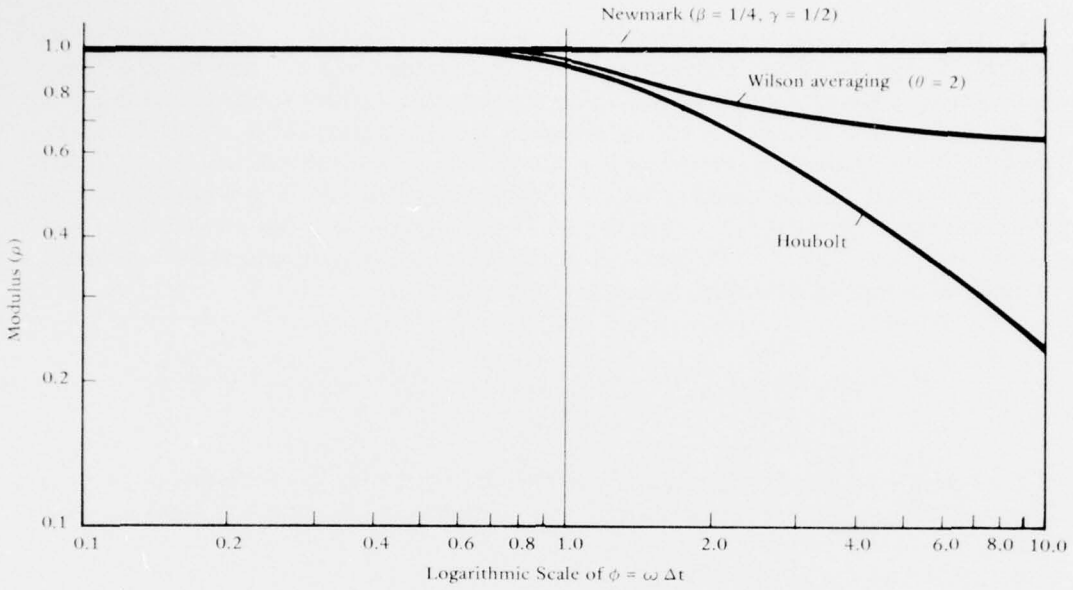

Figure 3-2. Results of Numerical Damping Evaluation.

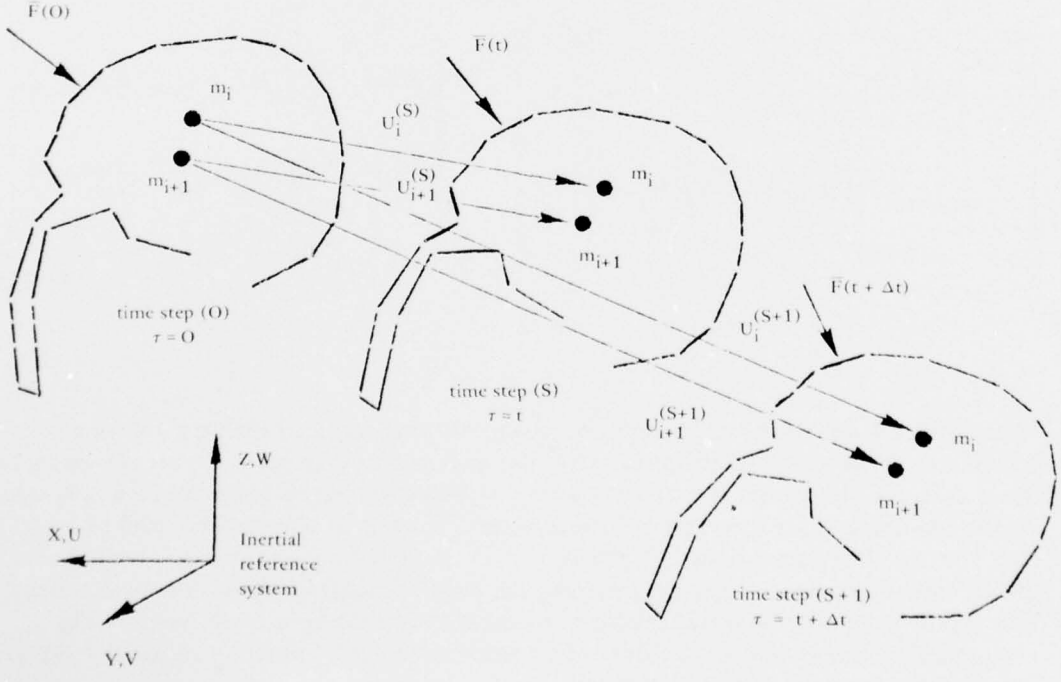

Figure 3-3. Global Displacement of Skull-Brain Model Relative to Inertial Reference System.

The mass terms m_i and m_{i+1} represent lumped masses at the two nodes in a diagonal mass matrix. The global stiffness terms $K_{i,i}$ are obtained in the direct stiffness method[14] by an appropriate summation of element stiffness terms from Equation 3-29. That is, $K_{i,i} = \Sigma k_{ij}^{n}$. The displacement vector and acceleration vector composed of U_i and $\ddot{U}_i$ terms, respectively, are unknown at time step S+1. By definition, they are referred to the inertial reference system. By choosing sufficiently small time increment $\triangle t$, it is possible to predict the acceleration terms at step S+1 in terms of known quantities from previous time steps and the unknown $U_i^{(S+1)}$. The particular prediction algorithm or integration operator employed, as previously described, is the Newmark β method.

$$\ddot{U}_i^{(S+1)} = \frac{1}{\beta\triangle t^2} U_i^{(S+1)} - \frac{1}{\beta\triangle t^2}\left(U_i^{(S)} + \dot{U}_i^{(S)}\triangle t + \ddot{U}_i^{(S)}\beta\triangle t^2\right) \qquad (3\text{-}33)$$

Substituting Equation 3-33 into Equation 3-32 and combining the unknown U_i terms on the left-hand side and taking the known terms to the right-hand side, the following equation results.

$$\begin{bmatrix} \left(K_{i,i} + \frac{m_i}{\beta\triangle t^2}\right) & K_{i,i+1} \\ \text{symmetric} & \left(K_{i+1,i+1} + \frac{m_{i+1}}{\beta\triangle t^2}\right) K_{i+1,i+2} \end{bmatrix} \begin{Bmatrix} U_i \\ U_{i+1} \end{Bmatrix}^{(S+1)} = \begin{Bmatrix} \bar{F}_i^{(S+1)} + \frac{m_i}{\beta\triangle t^2}\left(U_i^{(S)} + \dot{U}_i^{(S)}\triangle t + \ddot{U}_i^{(S)}\beta\triangle t^2\right) \\ \bar{F}_{i+1}^{(S+1)} + \frac{m_{i+1}}{\beta\triangle t^2}\left(U_{i+1}^{(S)} + \dot{U}_{i+1}^{(S)}\triangle t + \ddot{U}_{i+1}^{(S)}\beta\triangle t^2\right) \end{Bmatrix} \qquad (3\text{-}34)$$

The modified force vector on the right-hand side has been updated with the addition of inertia forces. The modified stiffness matrix on the left-hand side never requires updating for linear analyses with constant time increments. It, therefore, needs to be inverted only once (at the beginning, prior to stepping through time). The left- and right-hand sides of Equation 3-34 are then premultiplied by the inverse to obtain the solution for unknown displacements at step S+1. However, inverting and multiplication by the inverse as described here is only symbolic. In actual practice, the matrices are too large for inversion to be economical, and instead the procedure of Gaussian elimination is employed to solve Equation 3-34 for the unknown displacements.

INDIRECT IMPACT. To simulate indirect impact loads the displacement-time history resulting from impact is specified instead of force histories. For example, if the forces in Figure 3-3 are assumed zero and the displacement $\bar{U}_{i+1}(t)$ of the i+1 degree of freedom is assumed known, Equation 3-32 may be written as,

$$\begin{bmatrix} m_i & & \\ & m_{i+1} & \end{bmatrix} \begin{Bmatrix} \ddot{U}_i \\ \ddot{\bar{U}}_{i+1} \end{Bmatrix}^{(S+1)} + \begin{bmatrix} K_{i,i} & K_{i,i+1} & \\ K_{i+1,i} & K_{i+1,i+1} & K_{i+1,i+2} \\ \text{symmetric} & & \end{bmatrix} \begin{Bmatrix} U_i \\ \bar{U}_{i+1} \end{Bmatrix}^{(S+1)} = \begin{Bmatrix} 0 \\ 0 \end{Bmatrix}^{(S+1)} \tag{3-35}$$

Using the Newmark operator by substituting Equation 3-33 into Equation 3-35 we obtain,

$$\begin{bmatrix} \frac{m_i}{\beta \Delta t^2} & \\ & \frac{m_{i+1}}{\beta \Delta t^2} \end{bmatrix} \begin{Bmatrix} U_i \\ \bar{U}_{i+1} \end{Bmatrix}^{(S+1)} + \tag{3-36}$$

$$\begin{bmatrix} K_{i,i} & K_{i,i+1} & \\ K_{i+1,i} & K_{i+1,i+1} & K_{i+1,i+2} \\ \text{symmetric} & & \end{bmatrix} \begin{Bmatrix} U_i \\ \bar{U}_{i+1} \end{Bmatrix}^{(S+1)} = \begin{Bmatrix} \frac{m_i}{\beta \Delta t^2} \left(U_i^{(S)} + \dot{U}_i^{(S)} \Delta t + \ddot{U}_i^{(S)} \beta \Delta t^2 \right) \\ \frac{m_{i+1}}{\beta \Delta t^2} \left(U_{i+1}^{(S)} + \dot{U}_{i+1}^{(S)} \Delta t + \ddot{U}_{i+1}^{(S)} \beta \Delta t^2 \right) \end{Bmatrix}$$

Isolating the ith equation of Equations 3-36 and rewriting it by placing all the known terms on the right-hand side, we obtain

$$\left(\frac{m_i}{\beta\Delta t^2} + K_{i,i}\right) U_i^{(S+1)} = \frac{m_i}{\beta\Delta t^2}\left(U_i(S) + \dot{U}_i^{(S)}\,\Delta t + \ddot{U}_i^{(S)}\,\beta\Delta t^2\right) - K_{i,i+1}\,\bar{U}_{i+1}^{(S+1)} \quad (3\text{-}37)$$

Since $\bar{U}_{i+1}$ is known, the equation associated with it (the second of Equations 3-36) can be eliminated from the system and Equation 3-36 may be rewritten as

$$\begin{bmatrix} \left(\frac{m_i}{\beta\Delta t^2} + K_{i,i}\right) & K_{i,i+1} \\ \text{symmetric} & 1 \end{bmatrix} \begin{Bmatrix} U_i \\ \bar{U}_{i+1} \end{Bmatrix}^{(S+1)} = \begin{Bmatrix} \frac{m_i}{\beta\Delta t^2}\left(U_i^{(S)} + \dot{U}_i^{(S)}\,\Delta t + \ddot{U}_i^{(S)}\,\beta\Delta t^2\right) - K_{i,i+1}\,\bar{U}_{i+1}^{(S+1)} \\ \bar{U}_{i+1} \end{Bmatrix} \quad (3\text{-}38)$$

Again, in practice, Equation 3-38 is solved for the unknown U_i by Gaussian elimination rather than by actual inversion of the square matrix of the left-hand side.

When β is assigned a value of 1/6 in Equation 3-38, the integration of the equations of motion will be only conditionally stable, and the linear acceleration method results. Although the parameter β is optional in the HIM code, a value of 1/4 has been exclusively used in the development of the head injury model. In this case, the method is unconditionally stable and is termed the average or constant acceleration method. In general neither method is considered more accurate than the other. With the use of β = 1/4 the analyst does not run the risk of having the solution grow without bound for an arbitrary Δt.

The direct integration technique also provides flexibility in handling a variety of arbitrary impact loads whose frequency content may be quite varied and extensive. It is this frequency content that determines which skull/brain modes need to be integrated accurately and, hence, what size of time step is required.

4. PRELIMINARY MODEL STUDY

At the beginning of the head injury model development program, no documented evidence existed to indicate that the finite element method was a suitable analysis tool—only the suspicion that it might contribute to the study of head injury due to its innate ability to structurally model solid forms with complicated shapes and constitutive properties. Many uncertainties about its applicability to head injury modeling existed, not the least of which was due to the known semisolid or fluidlike makeup of brain matter.

Consistent with a cautious philosophy, a series of one- and two-dimensional models were constructed and numerically studied prior to attempting a three-dimensional model. These studies are reported in this section, however some readers may wish to skip directly to the three-dimensional studies presented in section 5.

One-Dimensional Models

Since it was originally envisioned that an assemblage of eight-node brick finite elements would constitute the final three-dimensional model configuration, the eight-node brick element was chosen to comprise the basic one-dimensional model used in this study.

With the proper choice of bulk and shear moduli, a Poisson ratio of zero can be obtained and, in effect, produces a one-dimensional model from a prismatic stack of three-dimensional elements as shown in Figure 4-1. Alternatively, boundary conditions can be employed to establish the same effect and retain the freedom to specify arbitrary bulk and shear moduli values. The first of these methods was employed in this study to facilitate an evaluation of the eight-node brick by comparison with classical one-dimensional wave propagation theory. The second method was used in the latter part of the study where the use of realistic skull/brain material properties was necessary. Specifically, boundary conditions were assigned to restrain, completely, lateral deformations (transverse to direction of loading) in the one-dimensional stack of elements. This was necessary to prevent physical instability induced by the zero value assigned to the shear modulus for brain material. The stack of three-dimensional eight-node brick elements was subjected to short stress pulses typically found in stress wave problems. It is important to point out that pulse durations typical of head injury are very often larger, producing wavelengths much in excess of cranial dimensions. As a result, the head injury problem belongs, most often, in the vibration domain, and the code's ability to propagate stress waves accurately is not of primary significance. Nevertheless, many engineers heretofore have investigated the dynamics of head injury from the stress-wave standpoint; their main concern being the potentially injurious effect of discrete tensile waves in brain matter if and when they occur (again, they owe their existence to relatively small pulse durations). Because of the influencing nature of these past investigations and because it is conceivable that small pulse durations may be found to exist among causative head injury loads, it is desirable to know how well the intended formulation performs in such instances.

An individualized summary of each model used in the study follows. The information includes geometry, material properties, input loads, acoustic velocity and critical time step

values as well as the computed stress wave results. It is believed that a one-dimensional model does not adequately represent the cranium; thus, no conclusions contained in this section are intended to be applicable to head injury.

Equilibrium Model. The primary objective of the equilibrium model was to verify that the FEAP code and particularly the eight-node brick were operating correctly. An equilibrium check in finite element work is usually the means used to make such a verification. If a 1.0-psi step pulse load is input as shown in Figure 4-2, the computed element normal stress σ_{yy} should take on the value of -1.0 psi. Figure 4-3 shows this stress plotted against time for three different time steps and for each of the four elements of the equilibrium model. These results, especially those for element number 1, demonstrate that the code is indeed operating correctly. Oscillation of the computed stress about the theoretical value is to be expected with any numerical integration scheme whether it is implicit or explicit.

Because the stress wave is reflected (with the same sign) from the fixed end face of the model, stresses are correctly showing a tendency in elements 2 through 4 to increase to a value of -2.0 psi.

More importantly, the effect of time step size on accuracy is illustrated. Given sufficient time (1 second) after the initiation of loading, data for the larger time step $\Delta t = 0.8$ second (approximately twice the critical value) appears as accurate as data for smaller time steps. In fact, the greater numerical damping associated with this larger time step actually appears beneficial in damping the oscillation.

Reflection/Refraction Model. Because it is of interest to know how well the FEAP code handles layered media, a simple model composed of two materials was numerically tested prior to using more realistic values for material and material layer thickness. The model is shown in Figure 4-4.

According to one-dimensional stress wave theory, a wave incident upon a material interface where the characteristic impedance changes abruptly will be both reflected and refracted. This theoretical behavior applied to the present model was computed and is shown as the dashed line response in Figure 4-5.

It can be observed that the computed solution is responsive to the reflection and refraction of waves. In Material 1, the average of the three greatest computed values for times of 2.4, 3.2 and 4.0 seconds appears to oscillate about -1.3 psi, which is close to the magnitude of the returning (reflected) wave. Since Material 2 involves a steep wave front, agreement is not good, but still the average of the computed refracted wave increases with time toward the theoretical value.

Numerical Damping Model. This model was intended for investigating the numerical damping which will occur with the Newmark β method when it is employed in systems more complex than a single-degree-of-freedom system. The model is shown in Figure 4-6.

The results of this model clearly show the numerical damping effect of large time steps on the stress wave solution. Figures 4-7, 4-8, and 4-9 each illustrate the stress wave solution at various times as computed by the FEAP code for three different time step sizes; they are time steps equal to the critical value, twice the critical value, and four times the critical value.

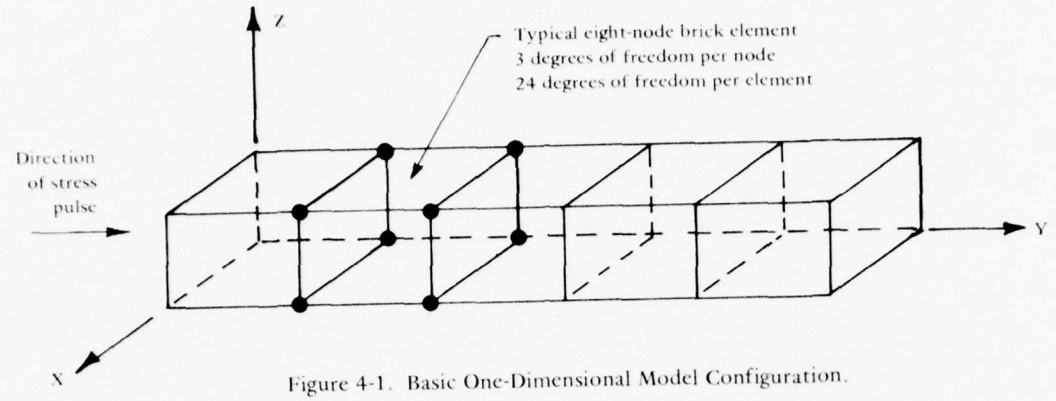

Figure 4-1. Basic One-Dimensional Model Configuration.

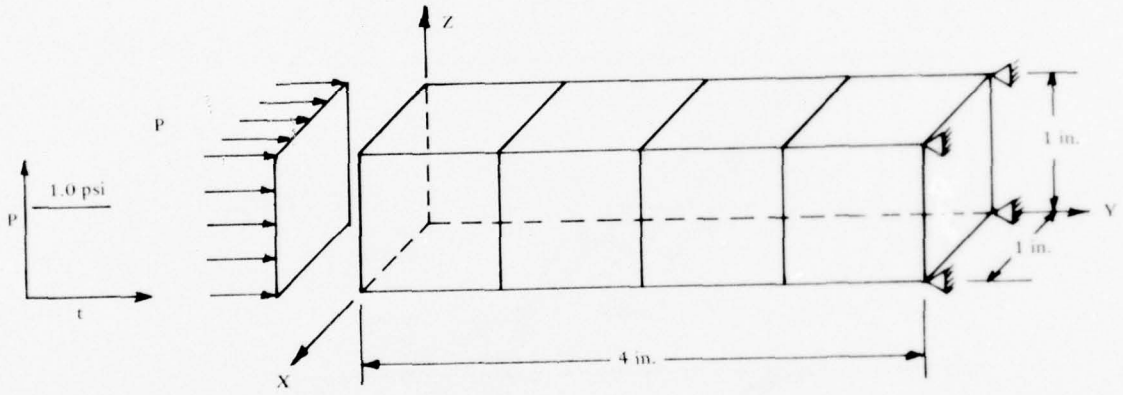

$K = 2.0$ psi, $G = 3.0$ psi } note $\mu = 0$

$\rho = 1.0$ (lb-s^2)/in.^{4}

$C_e = 2.45$ in./s

$\Delta t_{cr} \cong 0.4$ s

Figure 4-2. One-Dimensional Equilibrium Test Model.

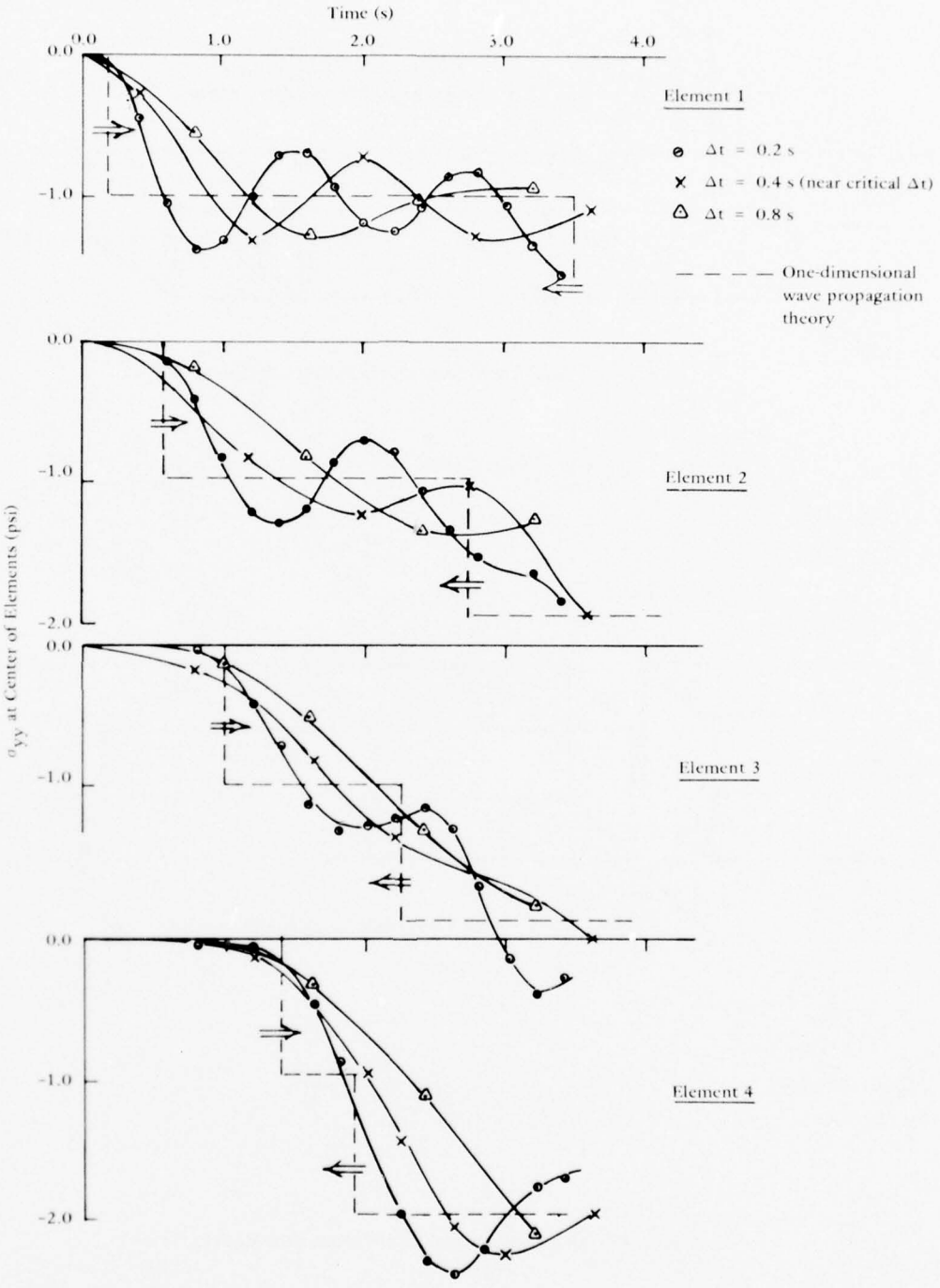

Figure 4-3. Element Stresses for Equilibrium Model.

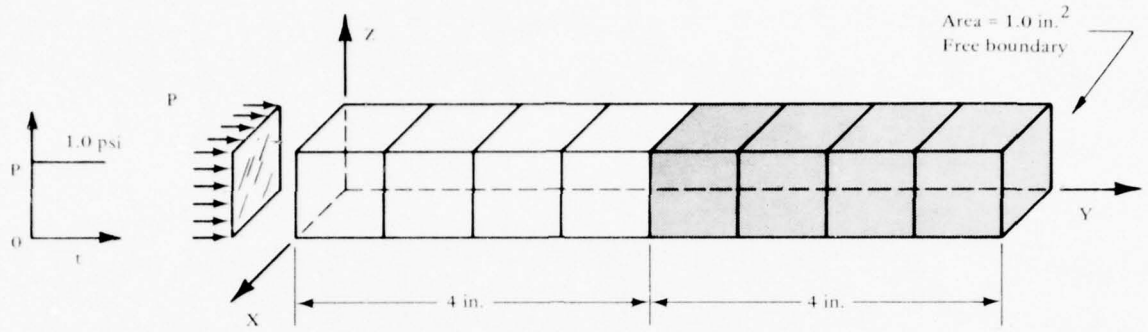

Material 1		Material 2	
K	= 2.0 psi	K	= 4.0 psi
G	= 3.0 psi	G	= 6.0 psi
ρ	= 1.0 (lb-s^2)/in.^{4}	ρ	= 2.0 (lb-s^2)/in.^{4}
C_c	= 2.45 in./s	C_c	= 2.45 in./s
Δt_{cr}	$\cong$ 0.4 s	Δt_{cr}	$\cong$ 0.4 s

Note: Characteristic impedance mismatch ratio

$$\frac{(\rho C_c)_2}{(\rho C_c)_1} = 2.0$$

Figure 4-4. Reflection/Refraction Model Description.

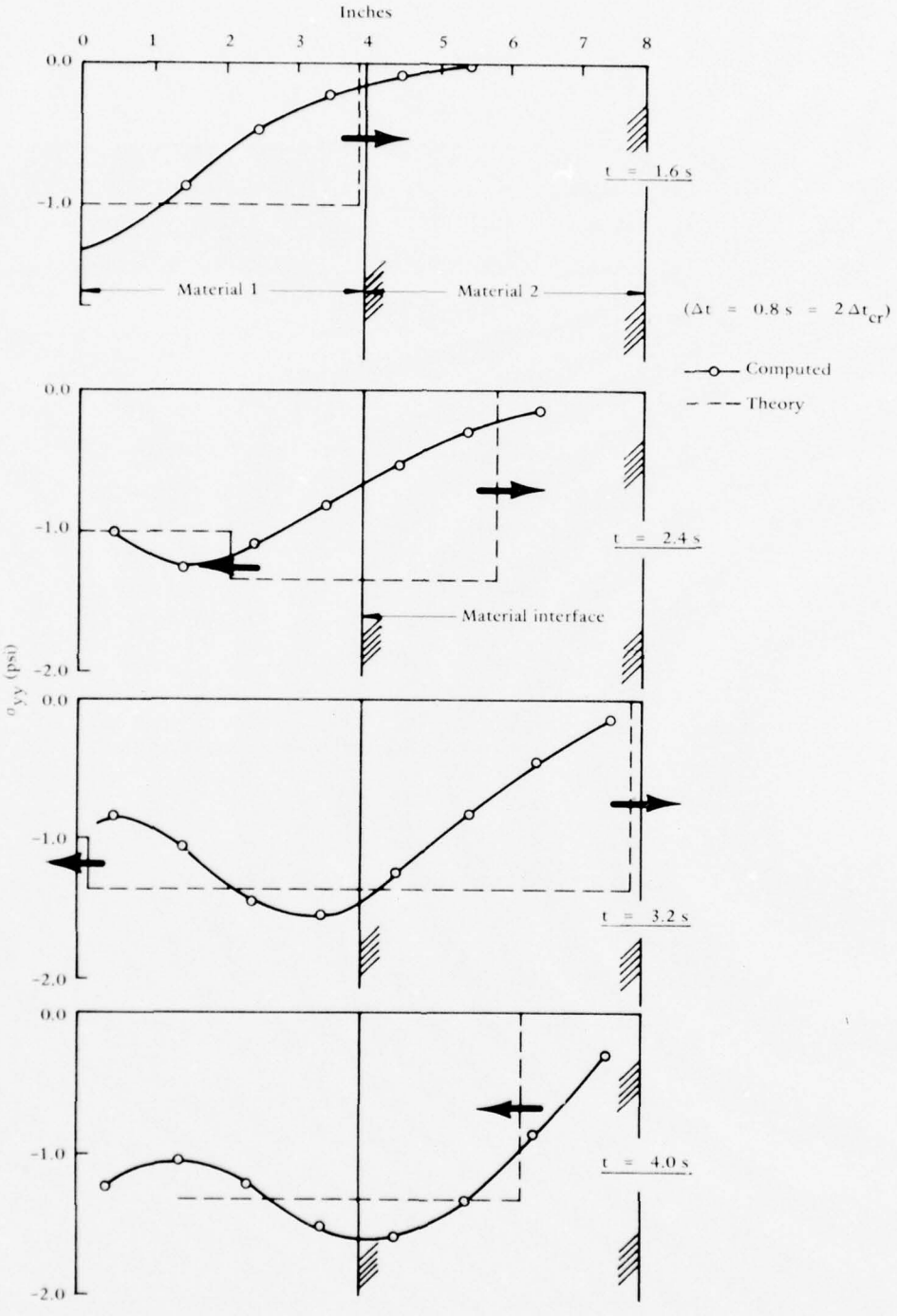

Figure 4-5. Normal Stress Profile Solutions in Dissimilar Materials.

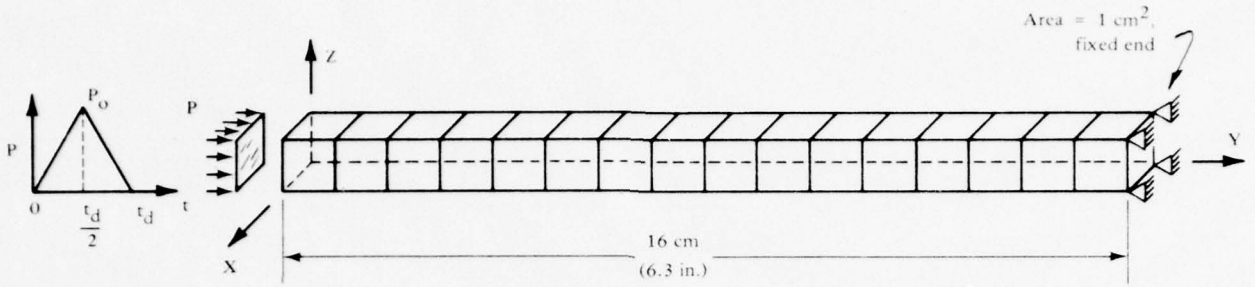

P_o = 545 psi
t_d = 5.51 x 10^{-5} s

Properties of Brain Matter

K = 3.05 x 10^5 psi
G = 0
ρ = 9.33 x 10^{-5} (lb-s^2)/in.^{4}
C_e = 57,180 in./s
Δt_{cr} = 6.886 x 10^{-6} s

Figure 4-6. Numerical Damping Model Description.

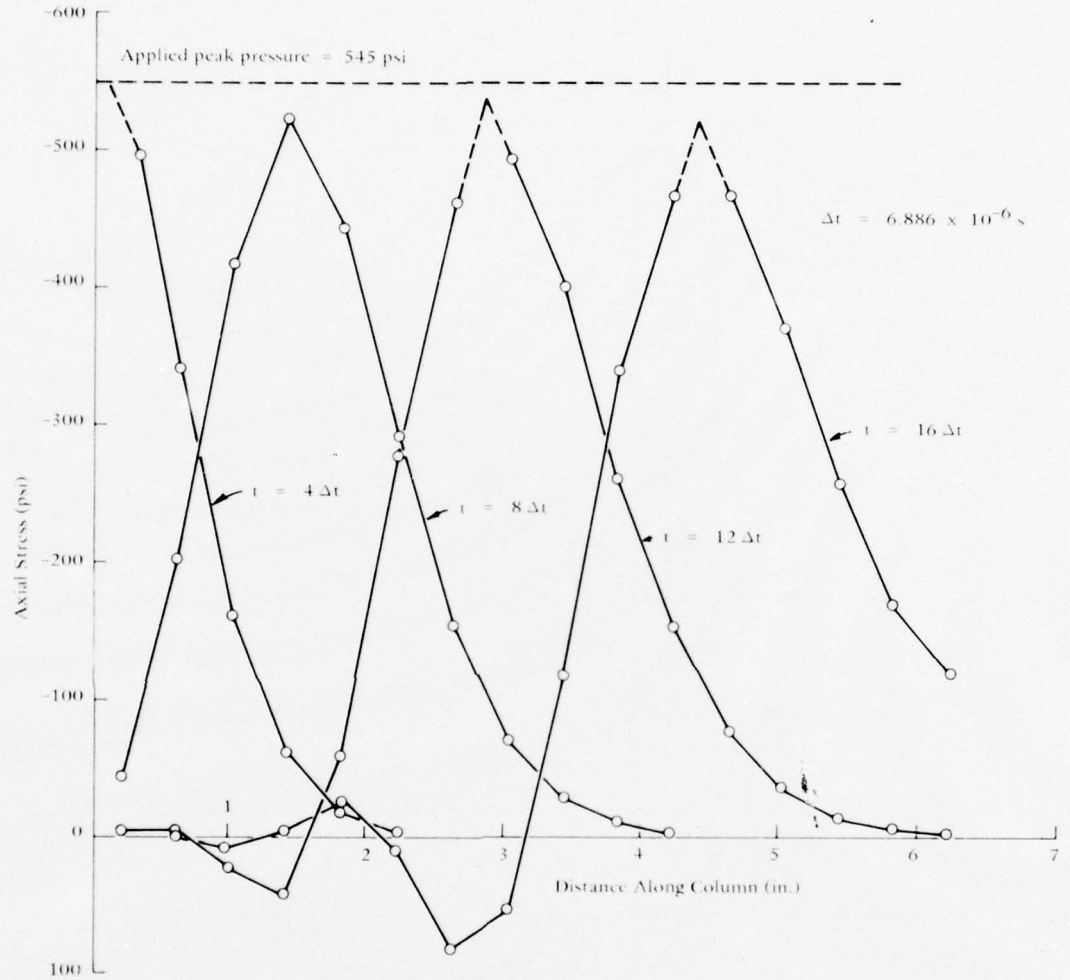

Figure 4-7. Propagation of Triangular Pulse, $\Delta t = \Delta t_{cr}$.

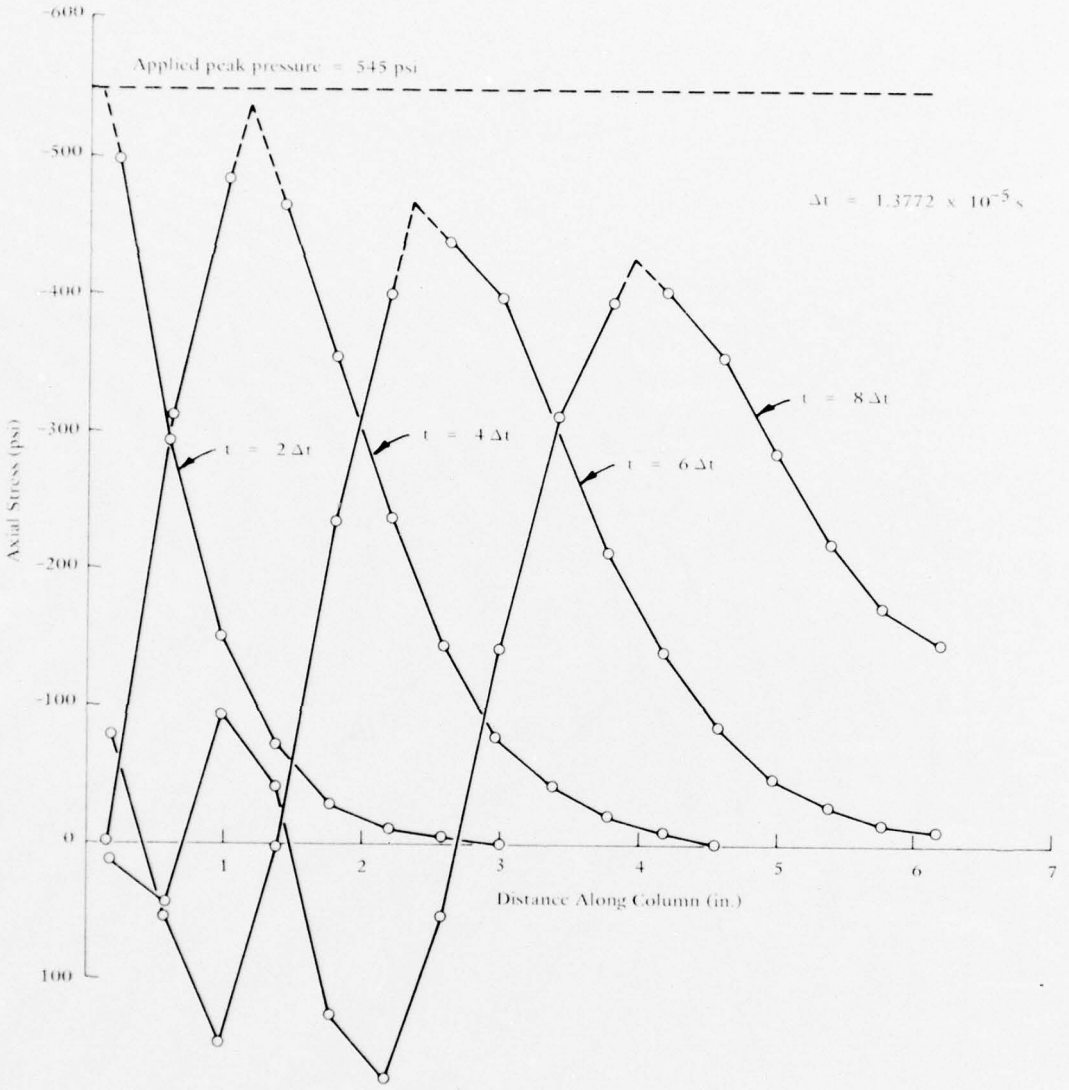

Figure 4-8. Propagation of Triangular Pulse, $\Delta t = 2 \Delta t_{cr}$.

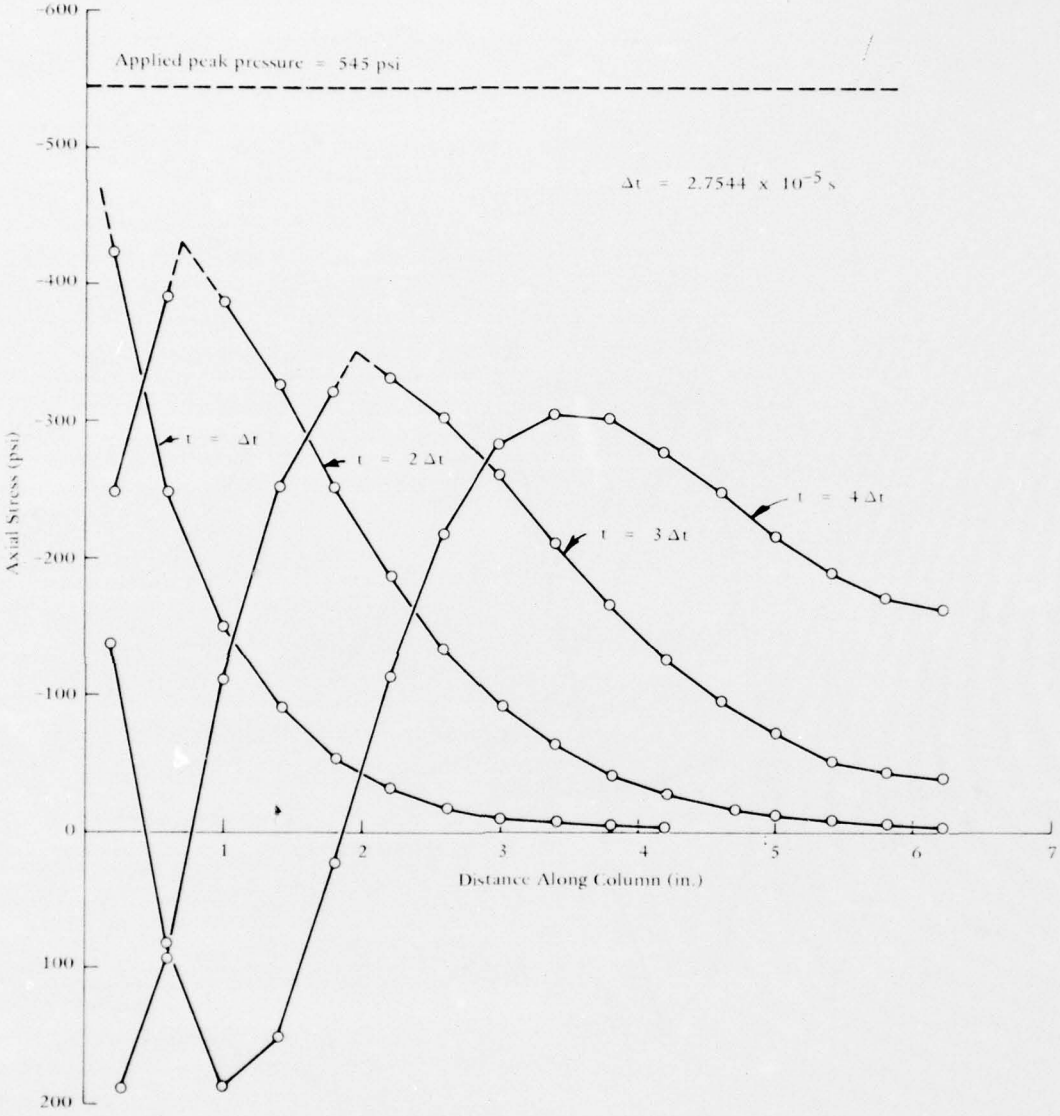

Figure 4-9. Propagation of Triangular Pulse, $\Delta t = 4\,\Delta t_{cr}$.

As a result of this study, an idea can be gained as to the relative merits of the cost/time step size tradeoff. Generally, the smaller the time step, the more accurate and costly the analysis will be. This is characteristic of any implicit scheme, but more importantly, the tradeoff between cost and accuracy can be controlled. On the other hand, an explicit integration scheme would be unstable for any time step size greater than the critical value and thus no such control would exist.

These results suggest that a time step size greater than critical but less than twice critical may be acceptable in any subsequent analyses involving discrete waves. Certainly it appears that too much damping is present with a time step size equal to four times the critical value.

Two additional observations can be made. First, numerical damping retards the wave propagation speed. This can be seen, for example, by comparing the magnitude of the leading edge of the wave at the 3-inch station along the column for the three different time steps. This value is highest in Figure 4-4 and lowest in Figure 4-6. Secondly, the tensile stresses in the trailing edge of the waves are due to numerical noise and become more pronounced with larger time step sizes.

Layered Media Model. A triangular pulse identical to the one used in the previous model was applied to a layered media model as shown in Figure 4-10. The only difference between the two models is the layered bone caps at both ends of the stack of brain elements that are added to the present model. Therefore, a direct comparison of Figure 4-7 and the results for this model (Figure 4-11) illustrates the influence of the bone caps. The data from both computer runs were based on the same time step size with relatively little change to brain element discretization.

Overall the elastic bone caps appear to reduce slightly the subsequent peak stresses in the brain matter and subject the brain elements to an earlier pulse. Otherwise, the effect of the elastic bone characterization on transmitted stress waves is very minimal in this study. The slight stress reduction could be attributed to numerical damping that was not present in Figure 4-7 but may exist in the present model because the time step is much larger (by about 7 times) than a computed critical value for the bone elements.

Summary of One-Dimensional Model Study Results. Familiarity with the characteristics of input data format and, more importantly, with computed output data using the FEAP code was gained. The study was decidedly oriented to the wave mechanics realm and the implicit technique of integration evaluated within this environment. In any future analyses with the FEAP code that may require small time steps, it is expected that accurate results using near critical time steps can be achieved. Also, in analyses involving problems where wavelengths are on the order of cranial dimensions and beyond, it is expected that accurate results can again be achieved with a corresponding savings in cost through the use of time steps substantially greater than critical values. Control over the decision between cost and accuracy is provided.

Specific conclusions resulting from this study follow.

1. Equilibrium checks on a nominal one-dimensional homogeneous model with step loading showed that the FEAP code is capable of matching trends of classical theory solutions.

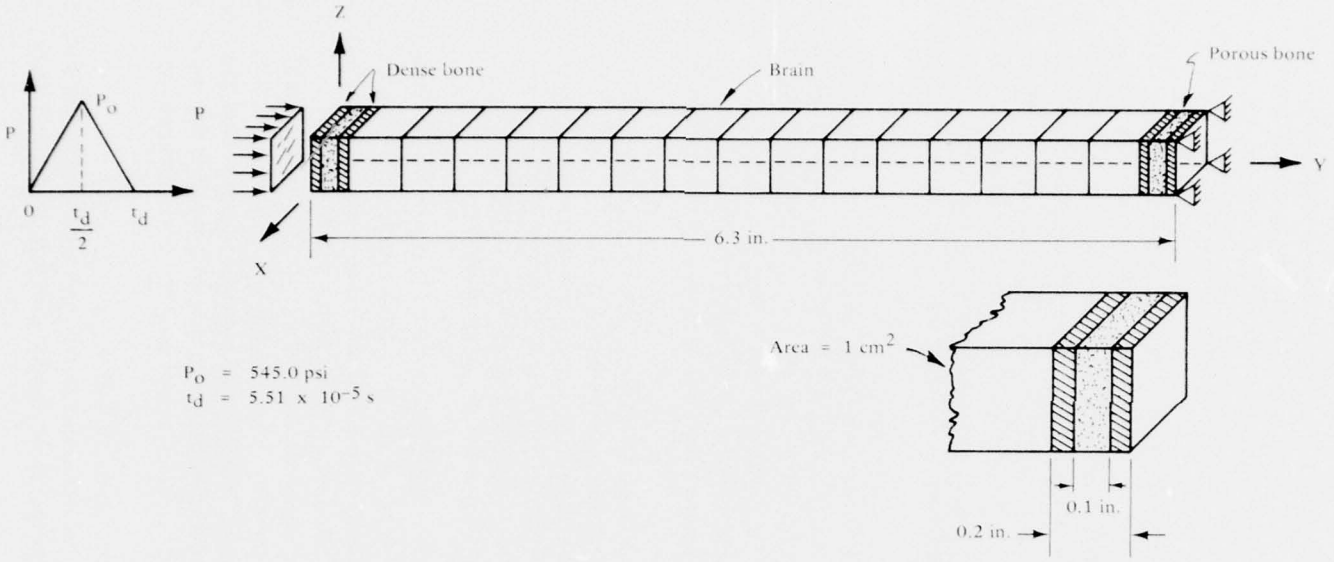

P_o = 545.0 psi
t_d = 5.51 x 10^{-5} s

Material	Bulk Modulus (psi x 10^5)	Shear Modulus (psi x 10^5)	Density ($lb\text{-}s^2/in.^4$)	Wave Speed (10^5 in./s)	Δt_{cr} (s x 10^{-6})
Dense bone	13.33	8.0	0.0002	1.095	0.456
Porous bone	1.333	0.8	0.00002	1.095	0.456
Brain	3.05	0.0	0.0000937	0.5705	6.89

Figure 4-10. Layered Media Model Description.

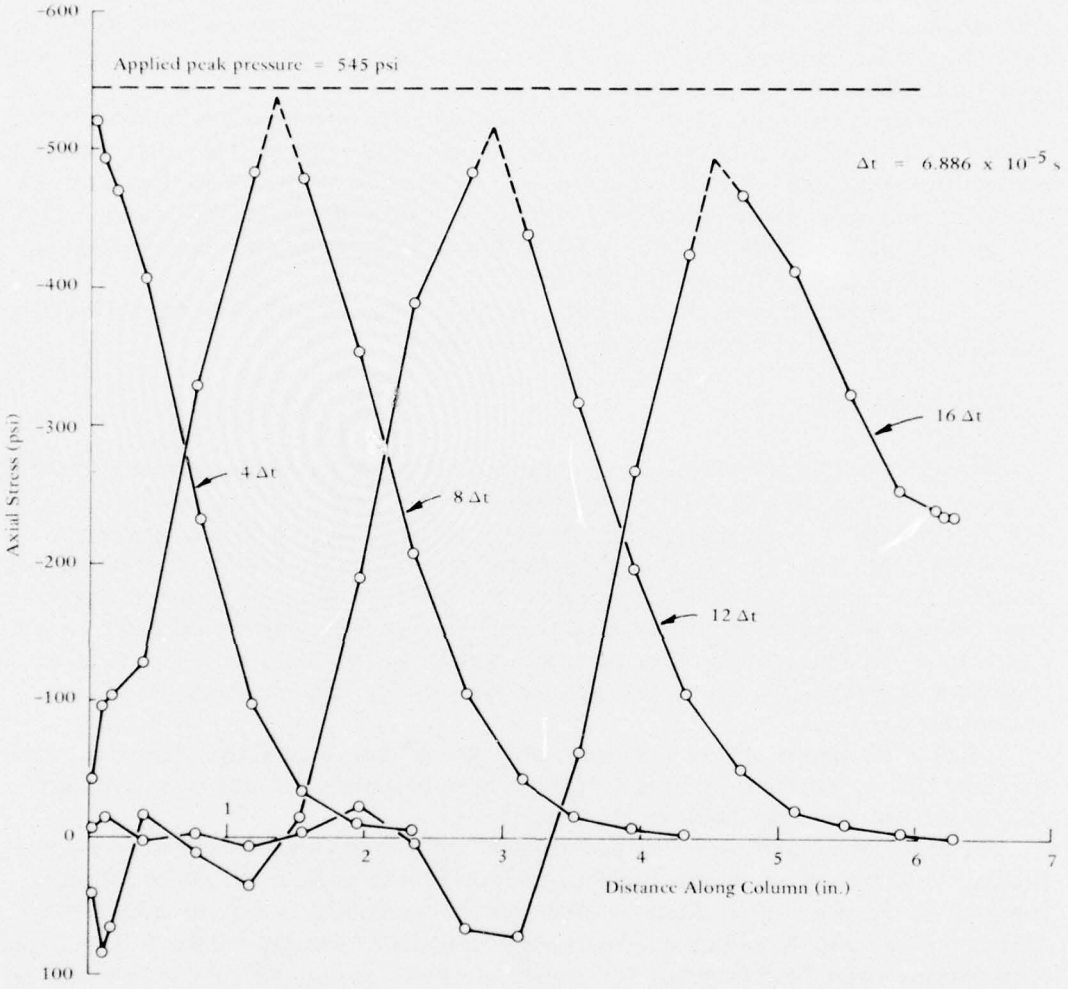

Figure 4-11. Propagation of Triangular Pulse Through Layered Media.

2. Reflection/refraction tests on a nominal one-dimensional dissimilar material model with step loading showed that, on the average, the FEAP code captured well the reflected wave magnitude. Results for the refracted wave were less accurate due to the severity of the wavefront but the tendency to capture it was evident.

3. Investigation of the effect of time step size on a one-dimensional brain model with a triangular pulse loading of short duration showed that critical time step sizes yield results in excellent agreement with theoretical prediction. However, as the prescribed time step size increases, significant numerical damping increases and adversely affects the solution. Also, the use of larger time steps resulted in a retardation of wave propagation speed and an increase in noise in the trailing portion of the waves.

4. The addition of elastic layered bone caps to the one-dimensional brain model had negligible effect on the stress wave response in the brain.

Axisymmetric Model

The objective of this model was to determine whether or not the finite element method was able to function as a head injury modeling technique. Many investigators have used, and are still using, axisymmetric analytical models for head injury modeling, and it was felt that if the finite element method could duplicate some results previously obtained from the models it too could be used as a viable analysis tool and be, in principle, easily extended to more realistic head injury modeling. Even though the geometry is simplified in the axisymmetric form, the ability of the finite element method to handle a very soft material encapsulated by a very stiff (albeit not rigid) material was of primary concern and required demonstration.

A finite difference study by Merchant and Crispino[50] was used in the comparison with the finite element analysis. These investigators, in turn, found good agreement between their model and the closed form work of Engin[51].

The design of the axisymmetric finite element model was somewhat affected by conflicting requirements: on one hand, the objective was to compare with a finite difference solution; on the other, it was desired to demonstrate the model as a valid head injury study tool in its own right. The finite difference study contained a two-layered skull. The present writer believed that a three-layered skull representing the table/diploë complex was mandatory, based upon the work of Hardy and Marcal[18], and therefore implemented the three-layer simulation. Despite the difference, the models are believed to be of sufficient similarity for comparative purposes since the diameters, degree of discretization, and the material properties were the same for both models.

---

[50] University of Washington, Department of Mechanical Engineering. A dynamic analysis of an elastic model of the human head, by Howard C. Merchant and Anthony J. Crispino. Seattle, Wash, 1972.

[51] Ali E. Engin. "The axisymmetric response of a fluid-filled spherical shell to a local radial impulse - a model for head injury," Journal of Biomechanics, vol. 2, 1969, pp 325-341.

The finite element model can be seen in Figure 4-12. The brain mesh was obtained by means of a Laplacian generation scheme where all unspecified nodal points are computed iteratively until they are uniformly spaced and consistent with specified node points for the skull. This technique is discussed in more detail in section 5.

Material properties are summarized in Table 4-1. Different dimensional systems were employed, but all values are equivalent. The tabulated mechanical and physical properties for hard bone and brain are traceable to Goldsmith[52]. However, for diploë, material properties were computed as suggested by Melvin, et al.[53]. Namely, bulk and shear muduli were calculated by multiplying their respective values for hard bone by the weight density ratio between diploë and hard bone. In this case the ratio was one-tenth and the resulting bulk and shear moduli for diploë are 1.333×10^5 psi and 0.80×10^5 psi, respectively. Note that with this ratio technique the elastic sonic velocity is the same for both hard bone and diploë.

Prior to conducting dynamic studies with this model, a static axisymmetric load was applied radially at one pole of the sphere while restraining the opposite pole against all displacement. A computed hydrostatic pressure state was expected in this simulation but did not occur despite the mechanical properties for the internal elements being specified as those for a fluid (see Table 4-1). What was computed was a highly variable and random pressure distribution (predicted magnitudes varied from +6 to -194 psi) within the sphere. This apparent anomaly was really a misinterpretation of the simulation because the outer brain elements are attached everywhere to the inner skull elements, in contrast to the actual behavior of fluid that would not attach itself to the skull elements. Thus, the computation was correct but the initial interpretation of the simulation was incorrect since, in this case, the desire was to create a hydrostatic pressure. Means were sought to eliminate the inherent and troublesome displacement continuity between the skull and brain finite elements. The difficulty was that bending and shear modes were being transferred from the shell elements into the interior elements because of nodal point compatibility at the shell/interior interface. It was believed that the model must include a mechanism to simulate the apparent discontinuity between the skull and brain that arises due to the presence of the subarachnoid space. Therefore, the model must either relinquish compatibility between the nodes of the shell and the nodes of the core or provide a substitute mechanism. Detaching or coalescing nodes at a common interface in the finite element method can become difficult and expensive where a large number of nodes are concerned. Therefore, an alternative approach was taken which resulted in the development of a brain element.

---

[52] W. Goldsmith. "Biomechanics of head injury," Biomechanics, Its Foundations and Objectives, ed. Y. C. Fung, N. Perrone, and M. Anliker. New York, Prentice-Hall, 1972, pp 585-634.

[53] J. W. Melvin, P. M. Fuller, and I. T. Baradawala. "The mechanical properties of the diploe layer in the human skull," in *Proceedings of Spring Meeting*, Society for Experimental Stress Analysis, Westport, Conn, 1970.

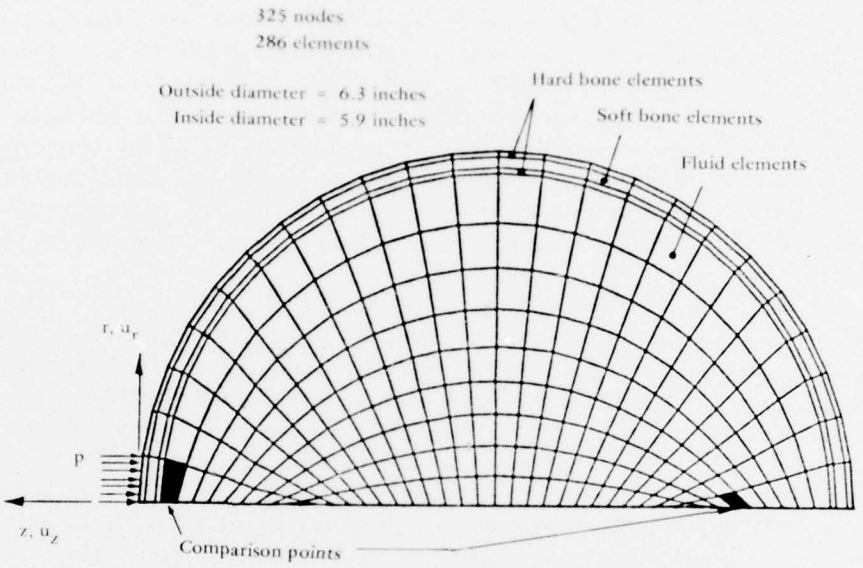

Note: No constraint in the z direction.

Figure 4-12. Axisymmetric Fluid-Filled Spherical Shell Model.

Table 4-1. Mechanical and Physical Properties for Axisymmetric Models

Property	Engin and Goldsmith[b]	Crispino and Merchant[a]	CEL
	a. Bone (inner and outer layer)		
ρ	0.0772 lbm/in.^{3} (2.14 g/cm^3)	2.14 g/cm^3	2.0×10^{-4} lbf-s^2/in.^{4}
K	(1.333×10^6 psi)	9.23×10^4 bars (1.333×10^6 psi)	1.333×10^6 psi
G	(0.8×10^6 psi)	5.53×10^4 bars (0.80×10^6 psi)	0.8×10^6 psi
C_1	(109,500 in./s	278.5 cm/ms (109,500 in./s)	109,500 in./s
E[b]	2×10^6 psi	(2×10^6 psi)	2×10^6 psi
γ	0.25	(0.25)	0.25
	b. Brain		
ρ	0.0362 lbm/in.^{3} (1.0 g/cm^3)	1.0 gm/cm^3	0.937×10^{-4} lbf-s/in.^{4}
K	(0.305×10^6 psi)	1.96×10^4 bars (0.084×10^6 psi)	0.305×10^6 psi
G	(0)	0	0
C_1	57,100 in./s	144 cm/ms 56,700 in./s	57,100 in./s
E[b]	(0)	(0)	0
γ	(0.5)	(0.5)	0.5

[b]E = 2×10^6 psi is for hard bone; for diploë, E = 2×10^5 psi (assumed).
[a]Values in parentheses are converted from authors' values.

The material characteristics of brain matter have been reported and are generally accepted as exhibiting a nearly incompressible, constant bulk modulus, and a very small time-dependent shear modulus.

In Reference 54 the use of a very compressible, "effective," bulk modulus for brain material is discussed. In many cases of finite element modeling, the use of effective material property constants is justifiable because the actual values are either unknown or because, through their specification, the solution becomes intractable. If brain injury is to be modeled, the correct and unique value relating a state of strain to a state of stress in brain material is desireable. This relationship can be provided by a high (liquid) bulk modulus ($\approx$305,000 psi). An "effective" bulk modulus which results from observed distensibility of the entire central nervous system, or even the cranial compartment itself may not necessarily be required. The distensibility mechanism can be provided, for example, by simulating a compressible subarachnoid space.

The characteristics of an ideal fluid imply the presence of hydrostatic stress proportional to volume change and the absence of shear stresses. From a classical mechanics viewpoint, a fluid can be characterized very simply by specifying the appropriate bulk modulus and setting the shear modulus to zero for those regions representing the fluid. However, when employing the finite element technique, further precautions must be taken to avoid erroneous results. Specifically, the standard use of high order numerical integration techniques to obtain the element stiffness matrix must be replaced by a reduced numerical integration (in this case, a first-order integration) capable of determining the volume change of the element independent of the assumed interpolation functions for the displacements.

The reason for this reduced integration is to insure that the strain energy of the element responds only to deformation modes that are associated with volume change rather than deformation modes such as shear and bending. Not only did this approach work well but also proved a very inexpensive coding modification. From this, it was learned how a brain element could be provided. In summary the brain element was constructed from the standard linear isoparametric solid element with a specified bulk modulus and zero shear modulus; and, in place of the standard 2 x 2 Gaussian integration scheme, one point at the element center was used.

When this element was incorporated into the code, another attempt was made at executing the axisymmetric model; this proved successful and verified the viability of the element. No distortional components were transferred into the interior elements, and the element pressures compared favorably with a hydrostatic distribution (pressures varied from -3.4 to -4.0 psi throughout the interior elements).

---

[54] Y. K. Liu, "Discussion of Paper No. 751163: The development of a detailed finite element brain model," SAE Transactions, Jan 1977.

The applied load used in the finite difference study was not typical of skull impact loads. Originally, Engin applied a step pulse; for comparison, Merchant and Crispino chose the same load magnitude as Engin. However, they terminated the pulse at 0.0614 ms, as shown in Figure 4-13 which was far below typical load pulse durations. (The initial disturbance reached only two-thirds of the sphere diameter by the time the pulse was terminated.) Nevertheless, this load was used in the present comparison study. It was applied uniformly over a half angle of 7.5 degrees (equivalent to 0.53 square inches of surface area) and was directed radially inward (see Figure 4-12).

Pressure history comparisons are shown at two points (see Figure 4-12) along the axis colinear with the load. The comparisons of results are shown in Figures 4-14 and 4-15. The time step size employed was 3 μs and is approximately twice the critical time step size required for the finite difference study. Finite element data shown has been sampled every three time steps.

Surprisingly good overall agreement can be seen for the pressure-time history within the brain element nearest the pole (Figure 4-14). The primary difference appers to be a time shift or lag between the two responses. Also noted is a difference between the responses for the peak compressive and peak tensile pressures. These differences are minor considering the dissimilar manner in which the skull bone was modeled and the dissimilarities in the finite element and finite difference techniques.

Pressure magnitude decreases considerably for points away from the pole as shown for point 2 (Figure 4-15). At the same time, agreement between the two responses deteriorates. Two explanations are offered beyond those already mentioned. First is that perhaps the coarse sampling rate of the finite element data prevented better agreement. Second, and probably more significant, is the effect of the two areas of ill-conditioned finite elements along the z-axis (see Figure 4-12). In the proximity of these elements, finite element pressure values appear to be amplified with what must be regarded as numerical noise. The finite difference mesh was better conditioned and did not exhibit these errors. It is therefore believed that by increasing the sampling rate of data and by improving the mesh the agreement would be improved.

With regard to computation of wave speeds in the spherical model, finite element data agrees well with wave propagation speeds computed by finite difference and by analytical methods. For example, taking a diametrical path through the brain material, the first disturbance at the counterpole is expected at about 0.11 ms. Taking a circumferential path through the skull bone material, the first disturbance should arrive at the counterpole in about 0.09 ms. Results of the finite element model show that both the brain wave and skull wave have arrived at the counterpole at 0.12 ms.

To study the influence of time step size on computed dynamic response, the axisymmetric model described above was employed. A more realistic load was applied so that the model's performance is more properly evaluated. Patrick, et al.[55] measured force histories

---

[55] L. M. Patrick, H. J. Mertz, Jr., and C. K. Kroell. "Cadaver, knee, chest, and head impact loads," in Proceedings of the Eleventh Stapp Car Crash Conference, Oct 10-11, 1967.

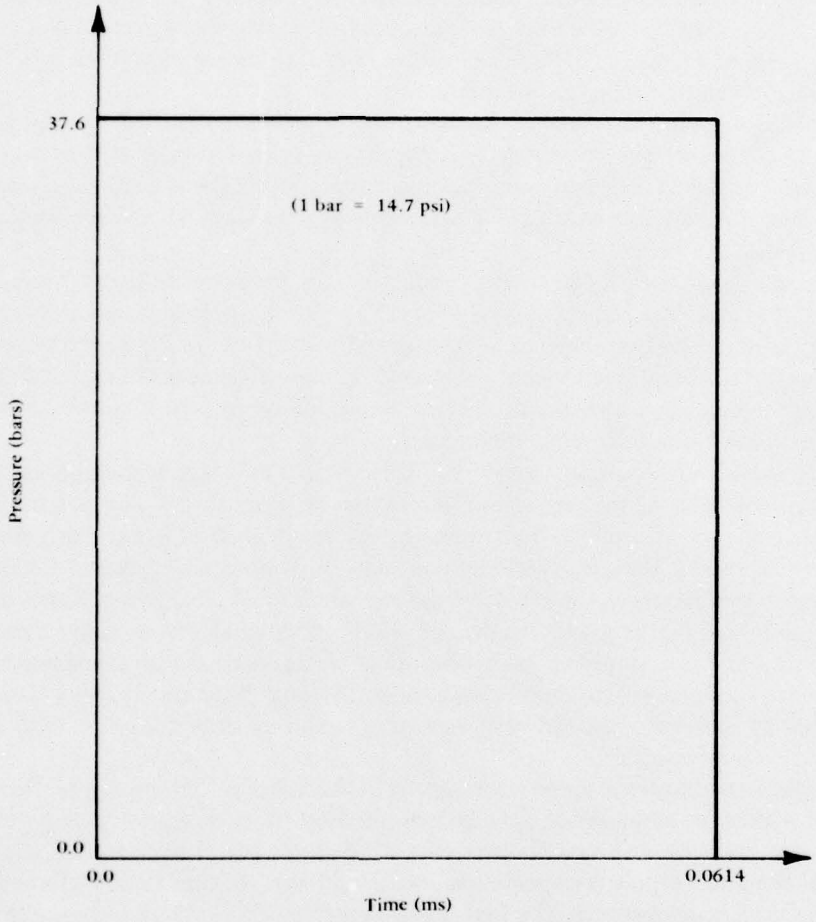

Figure 4-13. Short-Duration Load Pulse.

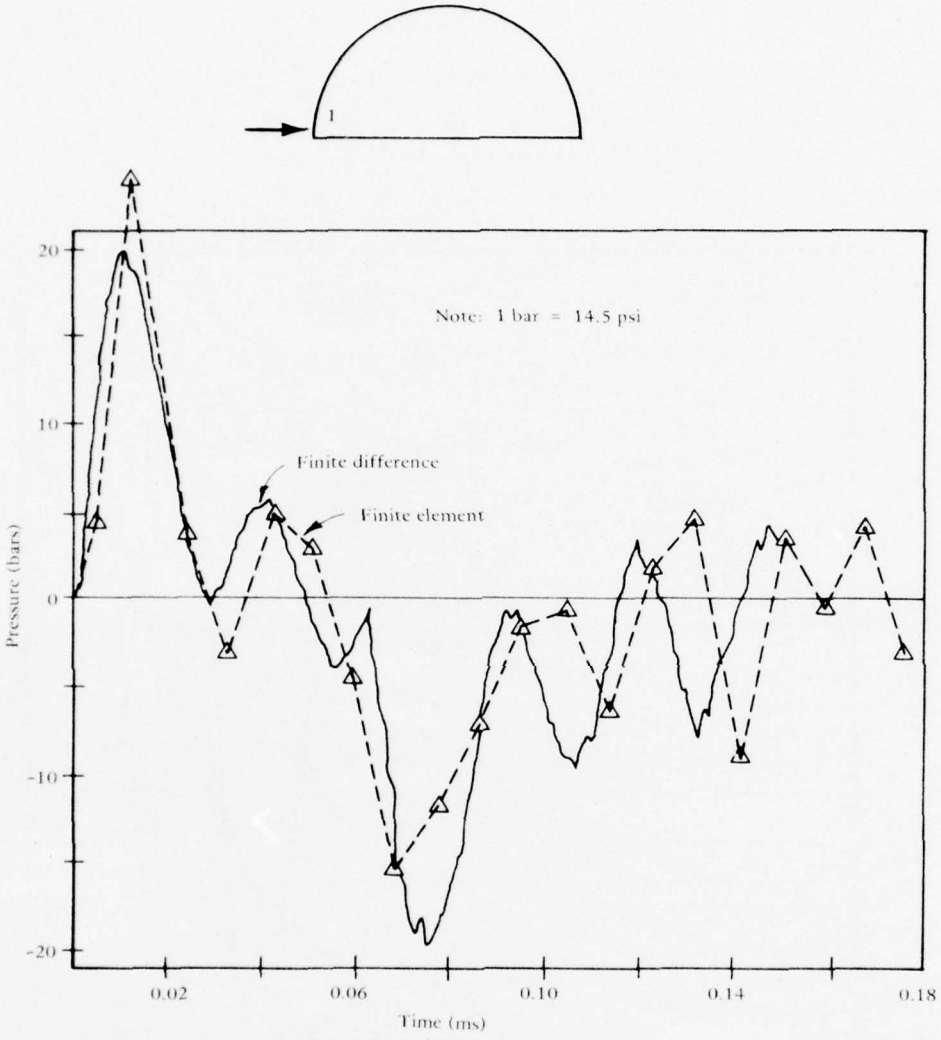

Figure 4-14. Pressure History Comparison at Point 1.

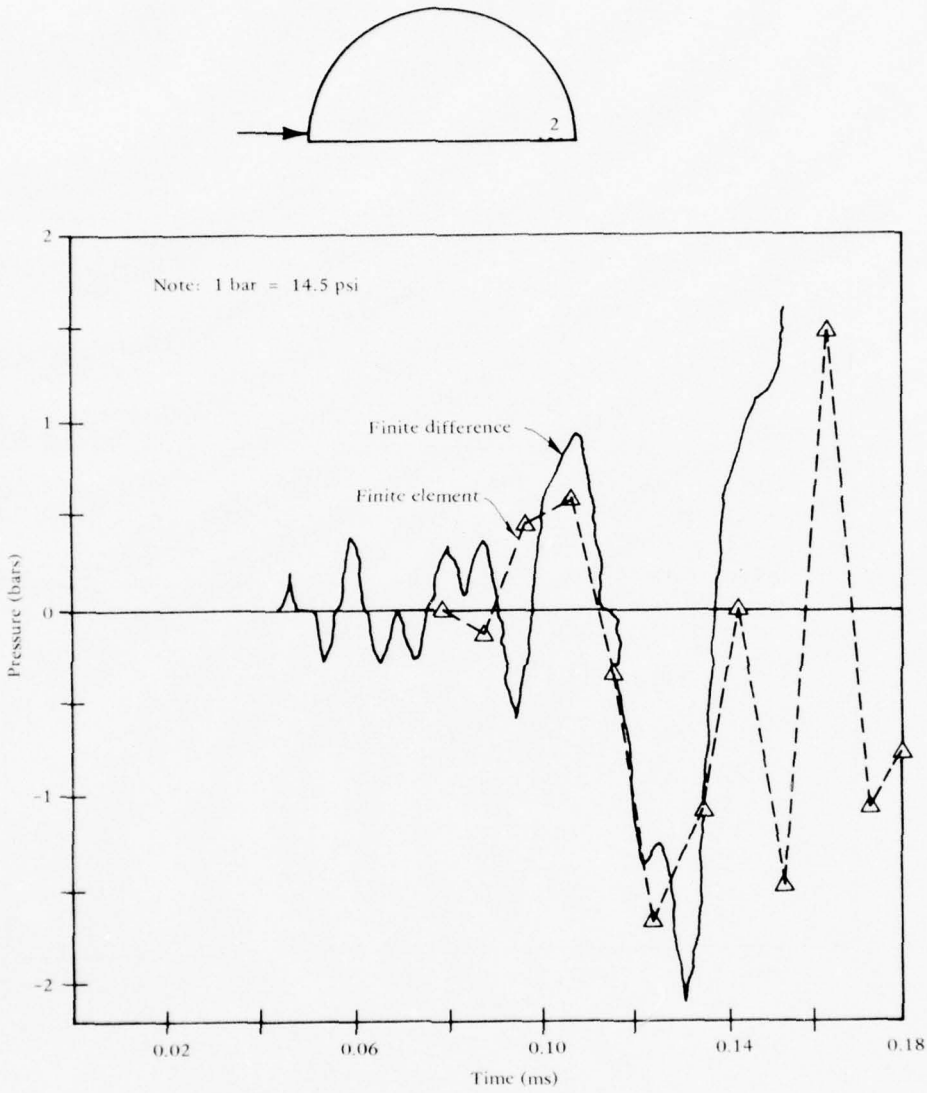

Figure 4-15. Pressure History Comparison at Point 2.

from skull collisions against padded force transducers. From this data a force of 2,650 pounds with a duration of 10 ms was selected as a typical head injury load. An equivalent pressure (distributed over 0.530 sq in.) was computed and applied to the model. This equivalent pressure-time history is shown in Figure 4-16.

Results of this study were encouraging for two reasons. First of all working with typical load pulse durations, the computed finite element data was found to be smooth and not obscured by jagged response data as was seen for the short duration pulse. Second, accurate results were obtained with very large time steps, and thus analyses of typical load pulses are expected to be economical and suited to the finite element method.

Since no changes in the axisymmetric model were made, the critical time step size remained the same; about 0.0026 ms. Computer runs were made for each of the following specified time step sizes: 0.005, 0.1, 0.2, and 0.4 ms. Thus, ratio values of specified to critical time step size of about 2, 40, 80, and 160 were investigated.

Figure 4-17 shows the compressive stress in the outer table bone layer directly beneath the site of the applied load. No noticeable difference in the stress response is observed among the investigated time step size parameters. Also the results indicate that the model satisfies equilibrium. Figure 4-18 shows the pressure history response within the brain at points 1 and 2 (see Figure 4-12). Again no noticeable difference is observed. These results demonstrate that no accuracy loss occurs due to the use of very large time step sizes.

Although in this study the main intent was to demonstrate only the applicability of finite element modeling to head injury study, some data pertinent to head injury was collected and is shown in Figure 4-19. Stress profile data were collected from the computer run associated with the largest specified time step size, 0.4 ms. The buildup and decay of compressive and tensile pressures within the brain at the pole and counterpole, respectively, can be observed. Note that there is no indication that tensile pressures exist at the poles directly beneath the applied load. This is contrary to the data shown previously (Figure 4-8) and is ascribable to the relatively long, but more typical, duration of the load pulse applied in this study.

To verify the predicted or computed rigid body motion of the axisymmetric model, the theoretical rigid body displacement solution was first generated in the manner of particle dynamics. Knowing the composite mass properties of the model (Table 4-1) and the forcing function applied to the model (Figure 4-15), a closed form expression for the acceleration can be written and then integrated twice.

The results of the comparison are shown in Figure 4-20. It can be seen that the finite element data is in good agreement with the theoretical rigid body displacement solution at those times when the applied load is nearly terminated ($t>0.008$ second). Prior to that time the periodical displacement component is significant, and since averaging finite element data tends to nullify this component the agreement can't be expected to be as good. Alternatively, neglecting the periodical component in the theoretical solution produces good agreement at all times.

The foregoing results from the axisymmetric model enable the following conclusions regarding the applicability of the finite element modeling technique in head injury studies.

(1) Acceptable agreement between finite element and finite difference results for an axisymmetric head injury model was achieved for a short duration load pulse.

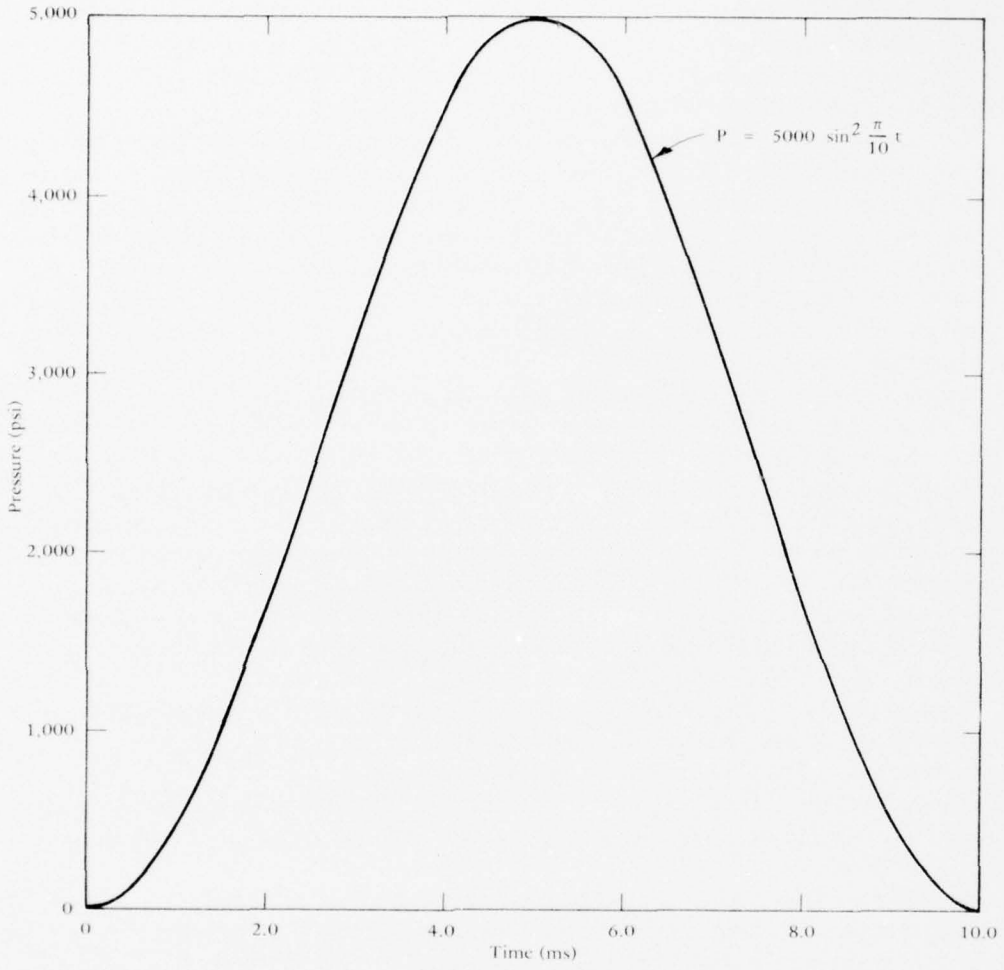

Figure 4-16. Pressure History Applied to Axisymmetric Model.

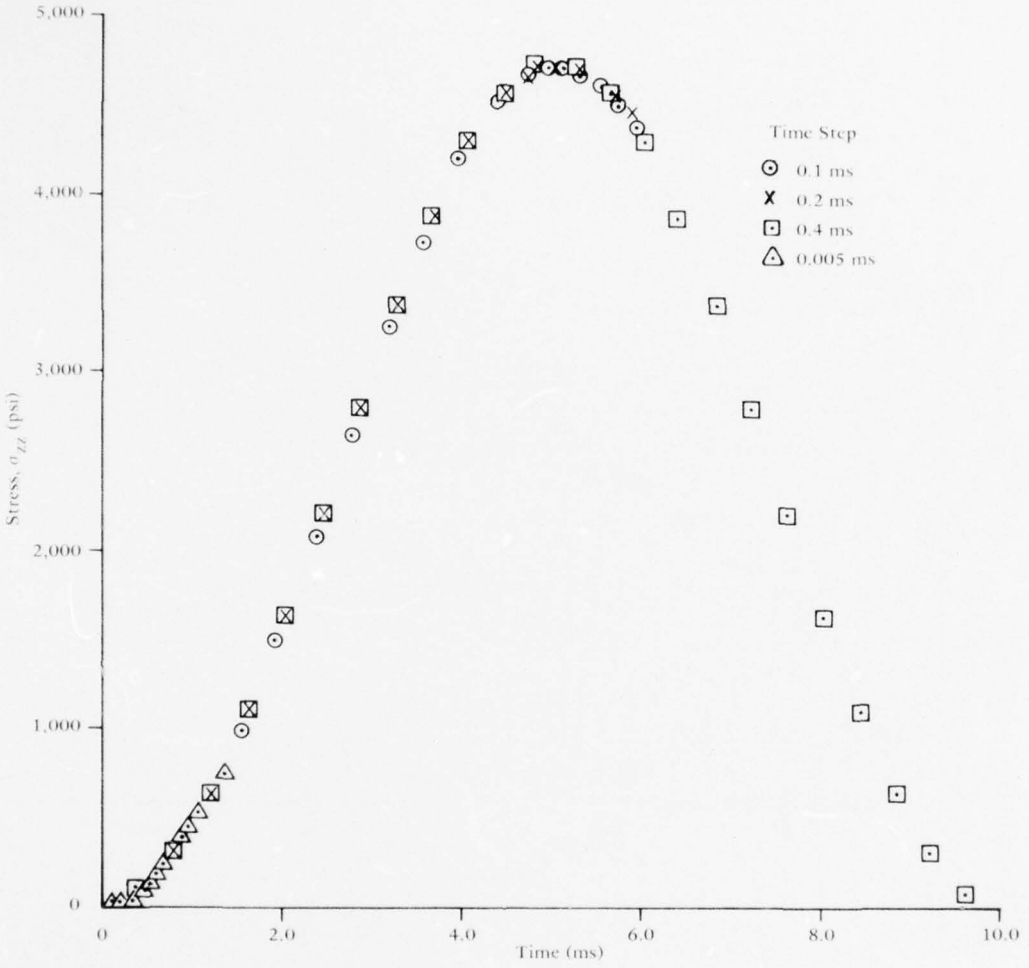

Figure 4-17. Computed Skull Element Stress Beneath Applied Load.

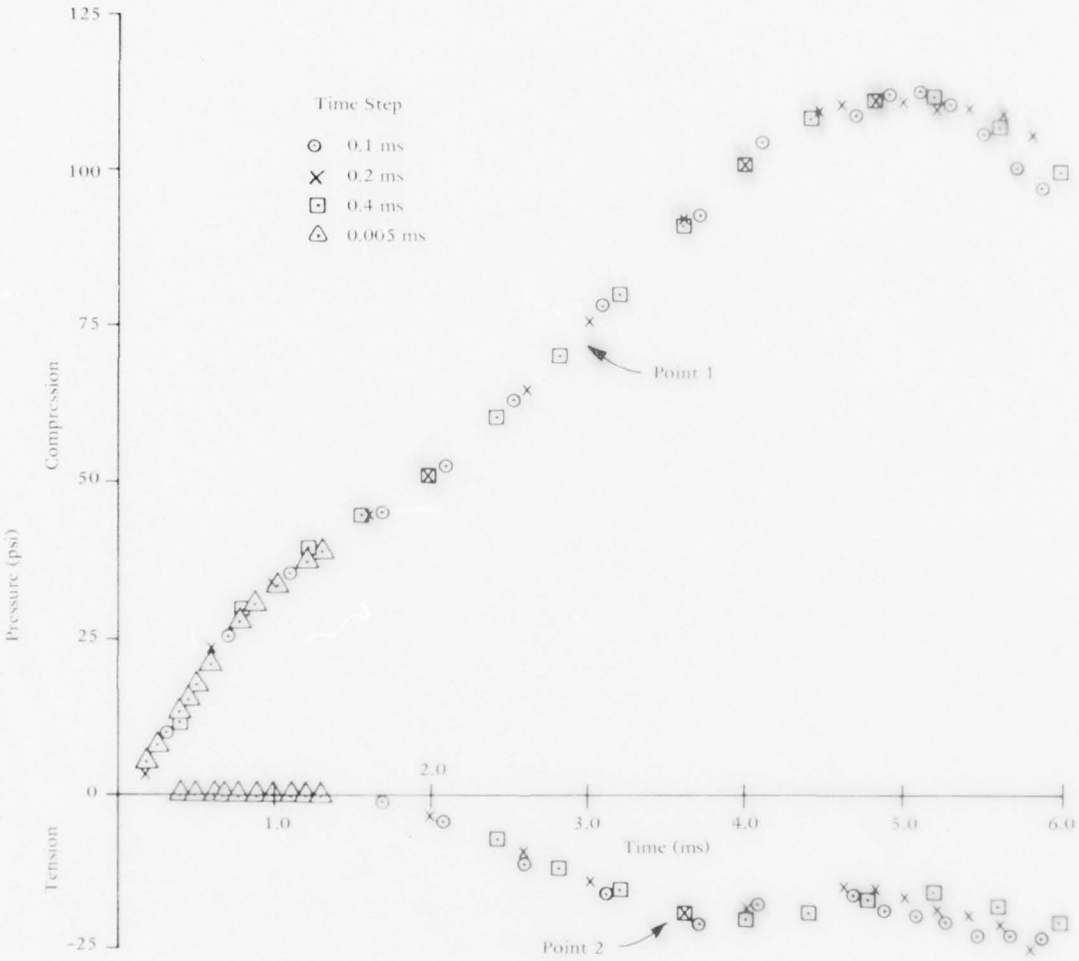

Figure 4-18. Influence of Time Step Size on Computed Pressure Histories.

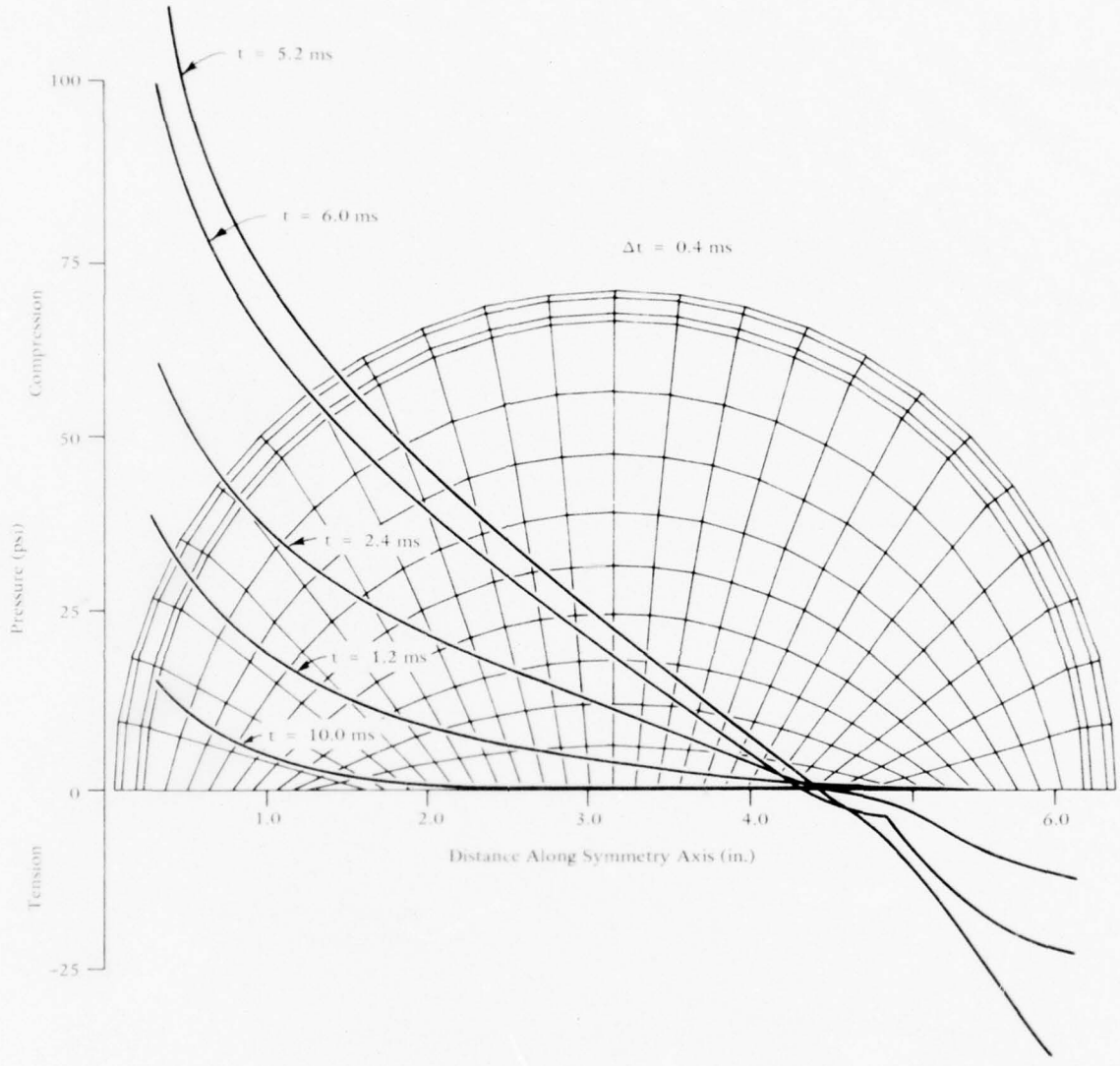

Figure 4-19. Pressure Distribution in Fluid Interior Along Symmetry Axis.

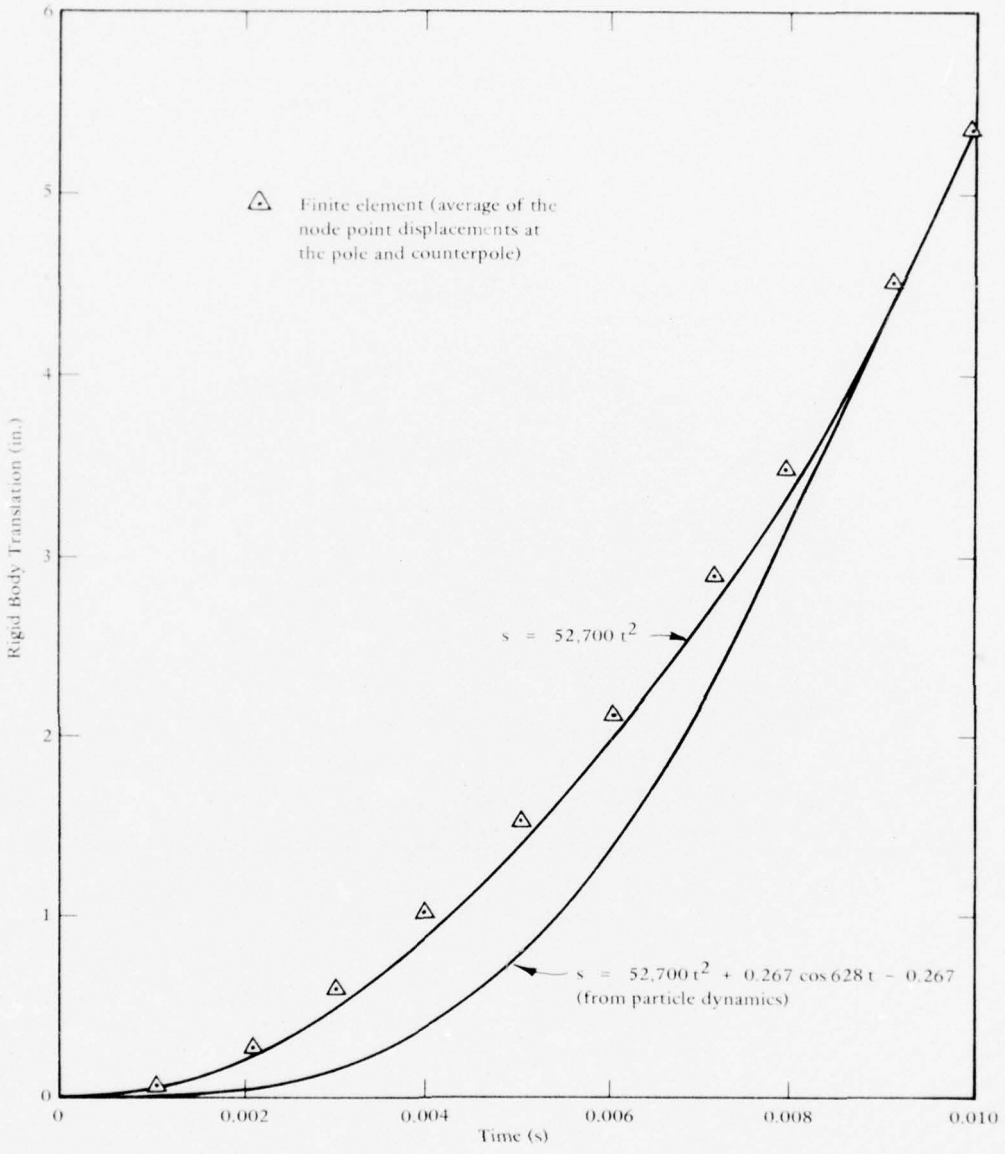

Figure 4-20. Rigid Body Displacement for Axisymmetric Model.

(2) Specified step sizes associated with the implicit integration scheme of about 2, 40, 80, and 160 times critical time step size exhibited nearly identical results. This is indicative of the efficient utility of the implicit scheme in head injury studies with typical applied load durations.

(3) The time history of rigid body translation was predicted accurately for the axisymmetric head injury model.

(4) Simulation of brain material was achieved successfully be degenerating the isoparametric element's spatial integration to one-point quadrature at the element center, and by specifying the shear modulus and the bulk modulus value for brain material.

(5) To the extent that an axisymmetric, spherical shell is a valid head injury model, the finite element method is shown to be an accurate method for head injury analysis.

(6) These results and the versatility of the finite element method encourages its application to more geometrically complex head injury models.

Plane Strain Model

Of interest in this model study was the influence of more realistic geometry on skull bending and on distribution of intracranial pressures. Knowledge acquired of these parameters could contribute to what has been learned previously concerning head injury from axisymmetric models and also intimate what can be expected in the eventual extension to three-dimensional modeling.

A plane strain model was constructed to simulate the geometry of a unit slice of the midsagittal plane of the human cranium. This model is shown in Figure 4-21. The geometry was developed from measured data taken from the plane of symmetry of a plastic replica of the human skull. A total of 420 four-node quadrilateral elements and 469 nodes constitute the discretization. As in the axisymmetric model, the skull bone is simulated with three layers of elements through the thickness, and the reduced quadrature elements characterize the encapsulated brain matter. Loading was prescribed as a uniformly varying pressure with a variation in the form of a haversine function. The duration of loading was 10 ms which is typical of durations in vehicle accidents. A time step size of 0.4 ms was employed in the integration of the equations of motion. Boundary conditions were chosen to simulate restraint against large rigid body motions at the base of the cranium near the neck juncture. In this model the skull was treated as a closed container.

Previous experimental measurements of pressures in the midsagittal plane have indicated pressure gradients to be linearly varying from compression to tension in an anterior to posterior (A-P) sense. Results of the plane strain model demonstrate that this could only be true for pure translation of the skull in the A-P direction. In actuality, for the same blow, the pressure profile will be determined by the neck constraints and the resulting relative "mixture" between translation and rotation of the head. In Figure 4-22 the pressure profiles are quadratic in the A-P direction with considerably more tensile pressure than would result from a linear profile. Figures 4-23 and 4-24 show the pressure histories in the brain and the stress histories in the outer table bone, respectively.

Two additional computer runs were made with the two-dimensional plane strain model of the midsagittal plane. The objective of these two runs was to evaluate the influence of a

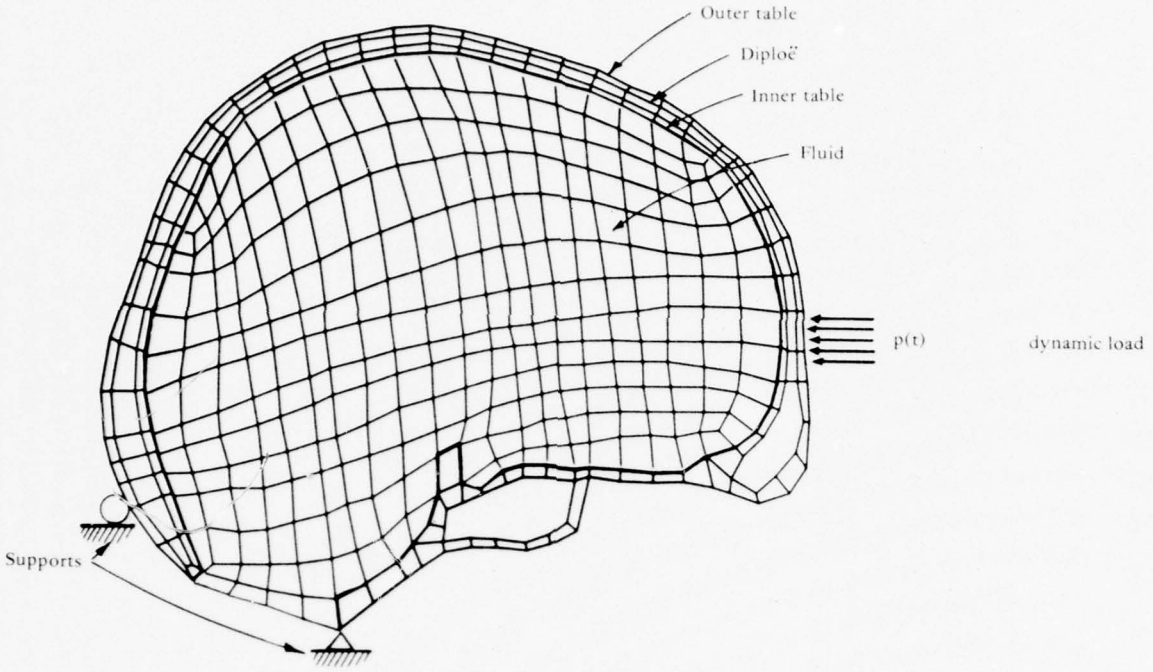

Figure 4-21. Plane Strain Model of the Human Cranium.

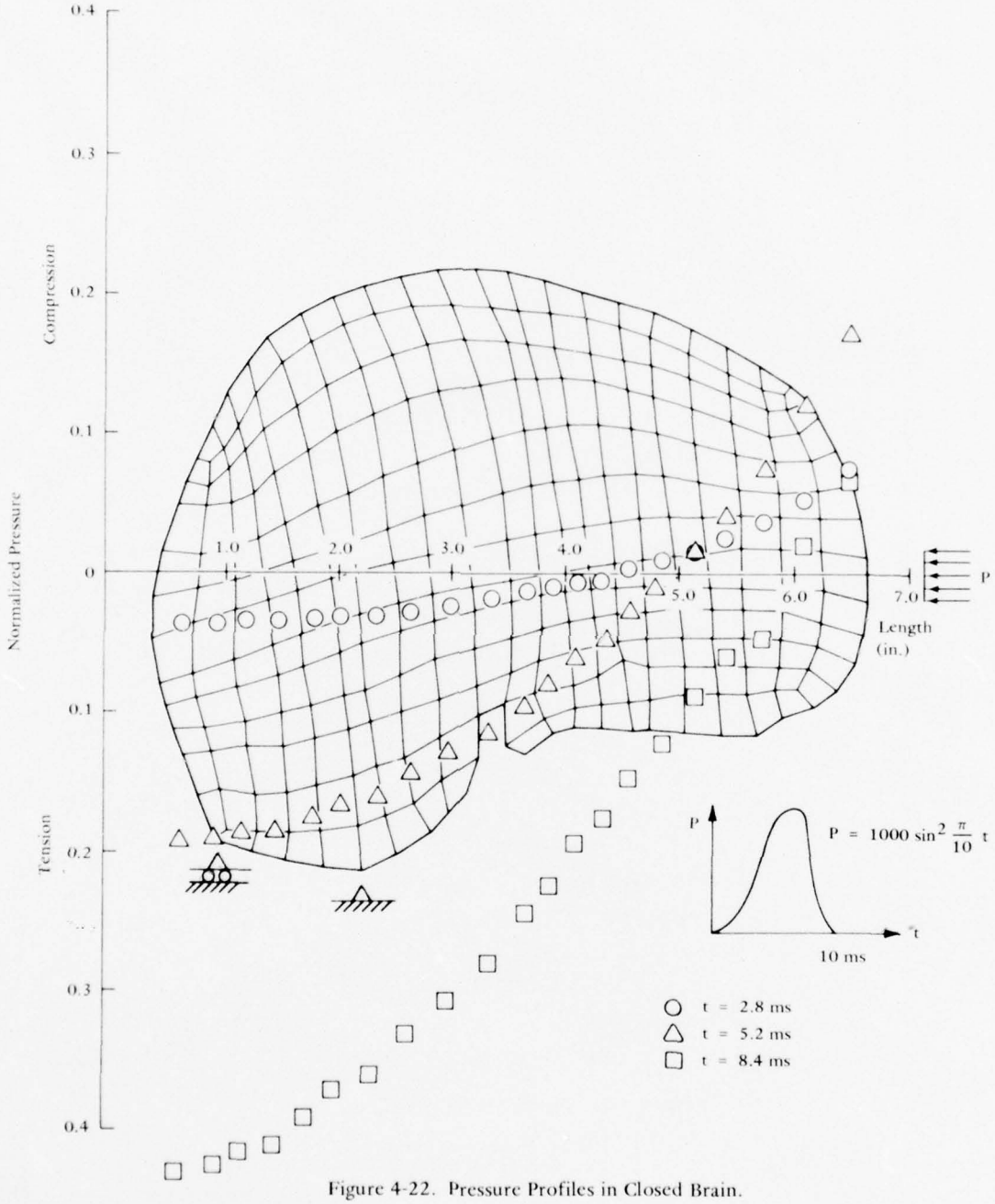

Figure 4-22. Pressure Profiles in Closed Brain.

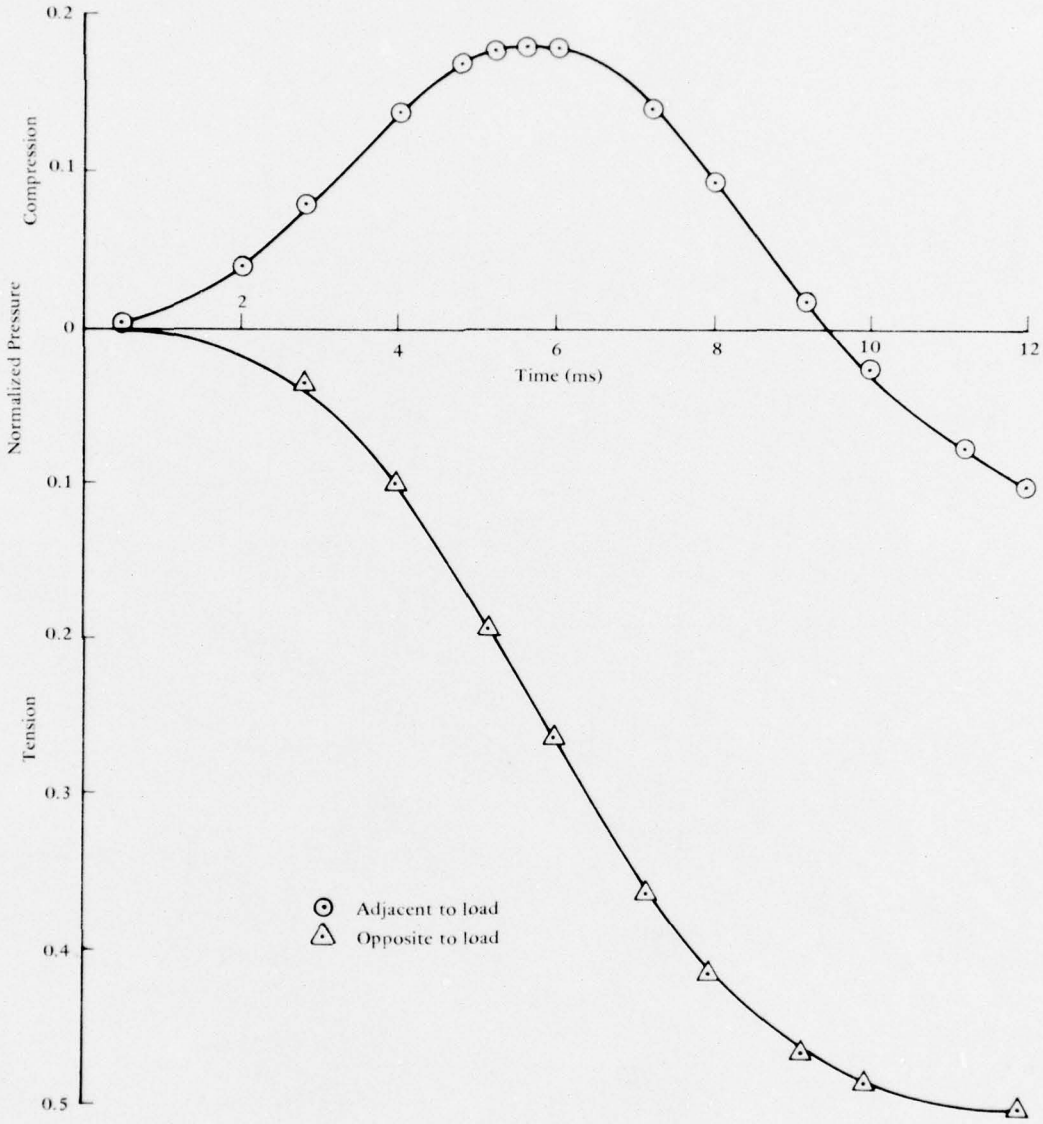

Figure 4-23. Pressure History in Closed Brain.

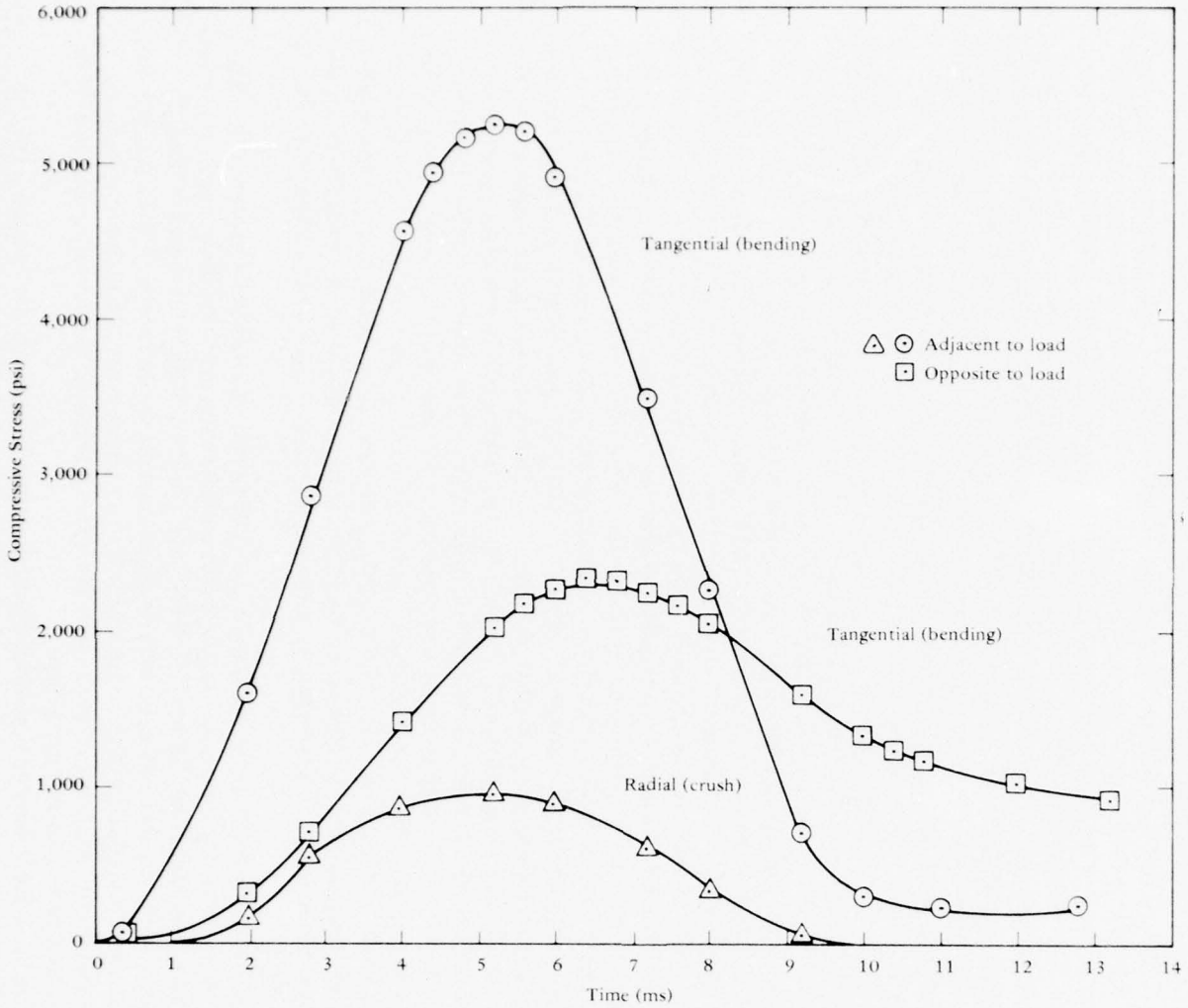

Figure 4-24. Outer Table Bone Stress.

viscoelastic shear modulus characterization of brain matter. The geometry possessed a "vented," instead of closed, skull configuration by providing an opening at the foramen magnum. Constraints were provided against translation and rotation near the opening, and the dynamic load was applied to the forehead region just as for the previous runs with this model. The material properties for the brain shown in Table 4-2 were chosen so that the shear modulus was strongly viscoelastic; thus, the initial shear modulus value was 15,500 psi and at the end of 10 ms the shear modulus decayed to 2,242 psi. While the shear response was made strongly dependent on time, the bulk modulus was considered as elastic. To establish a basis for comparison, a completely elastic characterization of brain matter was employed in the second computer run. Figure 4-25 shows the stress histories for both computer runs. Initially, no difference in the response was noted, but eventually the inherent damping properties of the viscoelastic material manifest themselves by dissipating the energy at a continuously increasing rate with time. At 7.5 ms, for example, approximately one-half the elastic stress response has been damped by the viscoelastic characterization. Figure 4-26 shows the bending stress history in the outer fibers of the skull bone at the site of the blow. Since the brain is, in effect, softer in the viscoelastic case, the elastic skull bone must deflect more and develop higher stresses than the elastic brain case.

Obviously a viscoelastic characterization has a great influence. The difficulty is in the determination of a more accurate and representative viscoelastic shear modulus formulation. The one used in this analysis, shown in Table 4-2, was arbitrarily based on a Poisson's ratio value of 0.475; but from this information an idea can be gained as to the sensitivity of dynamic skull response to viscoelastic brain matter. This information will assist in the characterization of brain material properties in subsequent three-dimensional model analyses.

The computed bending shape of the skull resulting from the loading and boundary conditions described above is presented in Figure 4-27. Since this is a linear analysis, only the shape (as opposed to magnitude) is of interest. The largest bending stresses occurred as tensile stresses on the inside cranial surface adjacent to the location of applied pressure. Tensile stresses are known to be conducive to linear fracture in cranial bone. They are indicated on either side of the skull surface where they occur. Note the location of inflection points which indicate a sign reversal for bending stresses in the cranial bone. Thus, while the model suggests that the area most conducive to linear skull fracture is on the inside surface near the loading, an alternative location would exist on the ouside surface near the top of the skull.

All bending stresses in the skull were observed to rise and subside synchronously with the haversine loading function. Displacement components due to bending, therefore, would also follow the same time history. However, the resultant movement lagged behind the loading history. In this instance a very slight counterclockwise rotation of the cranium was observed as the applied pressure displaced it "up and back over" the restraining support. Furthermore, this motion occurred while the applied pressure was subsiding and was therefore, considered to be an inertial effect.

This behavior is further evidenced by the intracranial pressure data shown in Figure 4-28. Pressure contours continued to form well after the applied load has peaked and begun to subside ($t \geq 5$ ms). Contour values normalized on the applied pressure are listed in Table 4-3. Brain damage is often observed clinically to occur on the opposite side of the skull

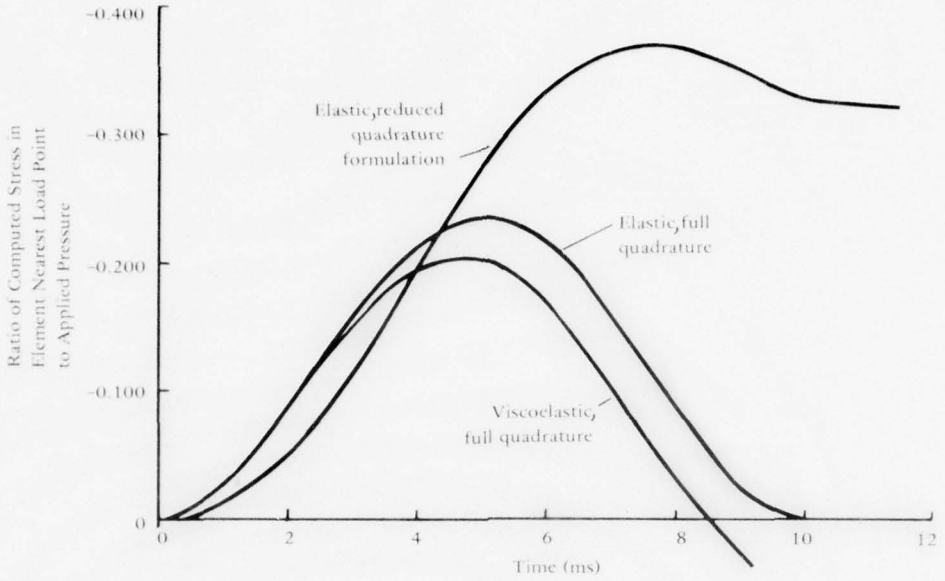

Figure 4-25. Influence of Material Properties on Intracranial Response.

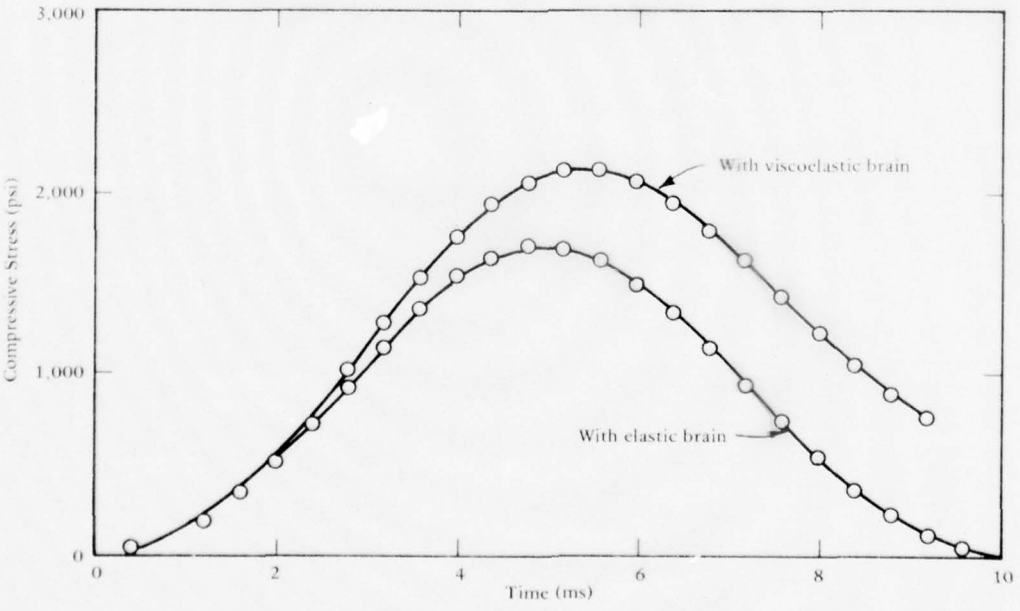

Figure 4-26. Outer Table Bone Stress History.

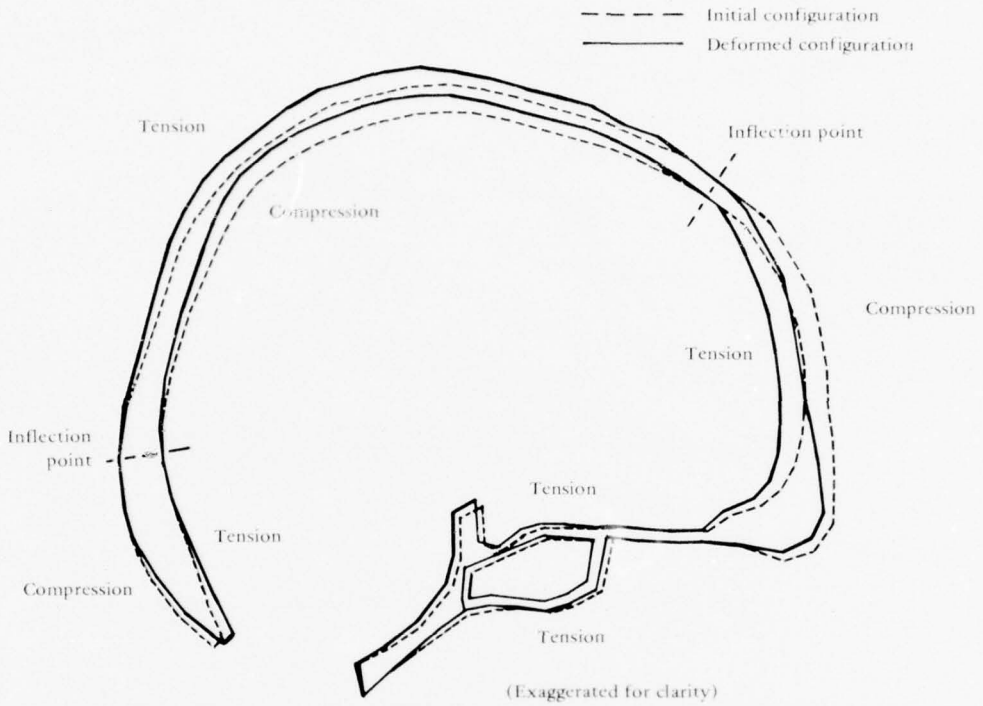

Figure 4-27. Resultant Displacement of Skull.

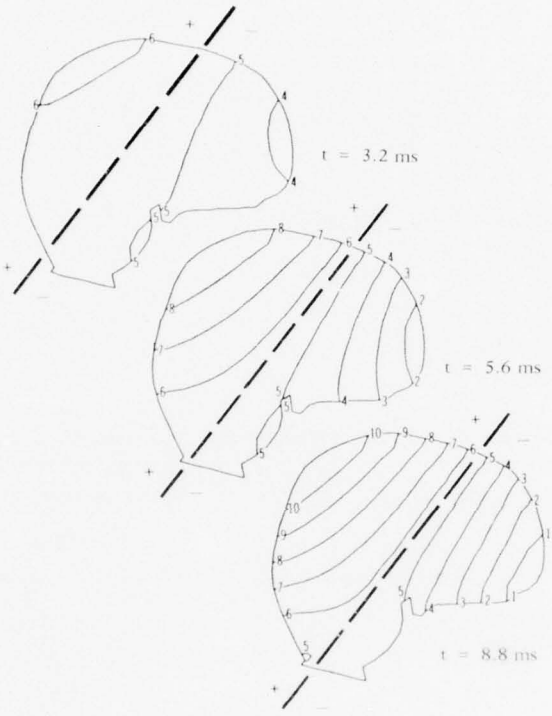

Figure 4-28. Pressure Contours in Brain.

Table 4-2. Brain Material Properties for Plane Strain Model

Characterization	K (psi)	G (psi)	ν
Elastic	305,000	15,500	0.475
Viscoelastic	305,000	G(t)[a]	ν(t)
Fluid	305,000	0	0.5

[a] $G(t) = 5{,}800\, e^{-132t} + 9{,}700e^{-264t}$
$G(0) = 15{,}500$
$\nu(0) = 0.475$
$G(0.01) = 2{,}242$
$\nu(0.01) = 0.4988$

Table 4-3. Normalized Pressure Contour Values

Contour Number	Pressure Ratio[a], p/p_a
1	-0.350
2	-0.265
3	-0.180
4	-0.096
5	-0.011
6	+0.073
7	+0.158
8	+0.243
9	+0.328
10	+0.413

[a]Minus sign indicates compression in brain; positive sign indicates tension in brain

from site of the blow and is termed contrecoup damage. Evidence indicates that lesions occurring in this manner on the surface of the brain are attributable to negative (tensile) pressures which rupture surface capillary blood vessels. Determining the location of negative pressures is, therefore, an important function of a head injury model. The contours show that the location of the maximum negative pressure occurred near the back and top of the brain. This result is related to the direction of inertia forces which are, in turn, governed by the particular combination of loading, geometry, and restraints employed. All three of these parameters must be simulated accurately in head injury models because, as seen in this example, they have an important influence on predicting both skull bending modes and intracranial pressure distributions.

5. THREE-DIMENSIONAL DISCRETIZATIONS

The two-dimensional models discussed in the preceding chapter were intended to be preparatory for a three-dimensional analysis. Since the finite element method is a viable three-dimensional analysis technique, there seemed little reason to dwell on the two-dimensional studies after they had served their preliminary purpose, and to proceed toward the ultimate goal of the project—a three-dimensional model. It is felt, however, that these simple models can be exploited further—that there is more to learn from them—and should not be discarded.

A primary consideration in the development of the HIM code was attainment of accurate geometrical simulation of the cranial anatomy. The term "recognizable geometry" is employed to distinguish this feature from previous head injury model studies employing rotationally symmetric geometry.

The effort to develop a recognizable three-dimensional discretization of the skull paralleled the preliminary model study effort as pointed out in the ORGANIZATION PLAN section 2. As expected, it was a very involved procedure, taking approximately 1 year from start to finish. This chapter describes the procedure and the considerations made during that time. This description should familiarize potential users of the HIM code with various parts of the total discretization, the various orders of discretization, and other options bearing on effective use of the model.

Components of the Discretization

The first consideration in discretizing the skull was to determine which anatomical structures should be included. Besides the cranial bone and brain structures (obvious components of a head injury model), other structures could have required inclusion. Among these were the neck, facial bones, subarachnoid space, and the major intracranial membranes such as the falx and tentorium. The inclusion of these structures and other more intricate intracranial structures had to be weighed with the added complexity and cost associated with meaningful discretizations of each. Their relative importance had to be assessed by the extent to which each participates in common head injury mechanisms. Ultimately, the deciding factor, however, had to be whether (for feasibility or economic reasons) certain of these structures could be included in a finite element model. The result of having omitted some of these structures could have adversely affected the scope of the model's applicability; to obtain reliable information, the effort nevertheless had to proceed.

Skull Bone Structure. A detailed study of the anatomy of skull sutures was made with the intent of incorporating their influence on the structural behavior of the skull. Eight bones constitute the human cranium—frontal, occipital, two temporal, two parietal and two sphenoidal as shown in Figure 5-1. The sutures shown in Figure 5-2 are the natural interfaces found between these bones and may form a failure mechanism under certain loading conditions and for certain age groups. At birth, unossified membranous intervals (fontanels) exist between the skull bones but will close within two month after birth except the anterior which closes at about 2½ years of age. Apparently this process merely closes the gap

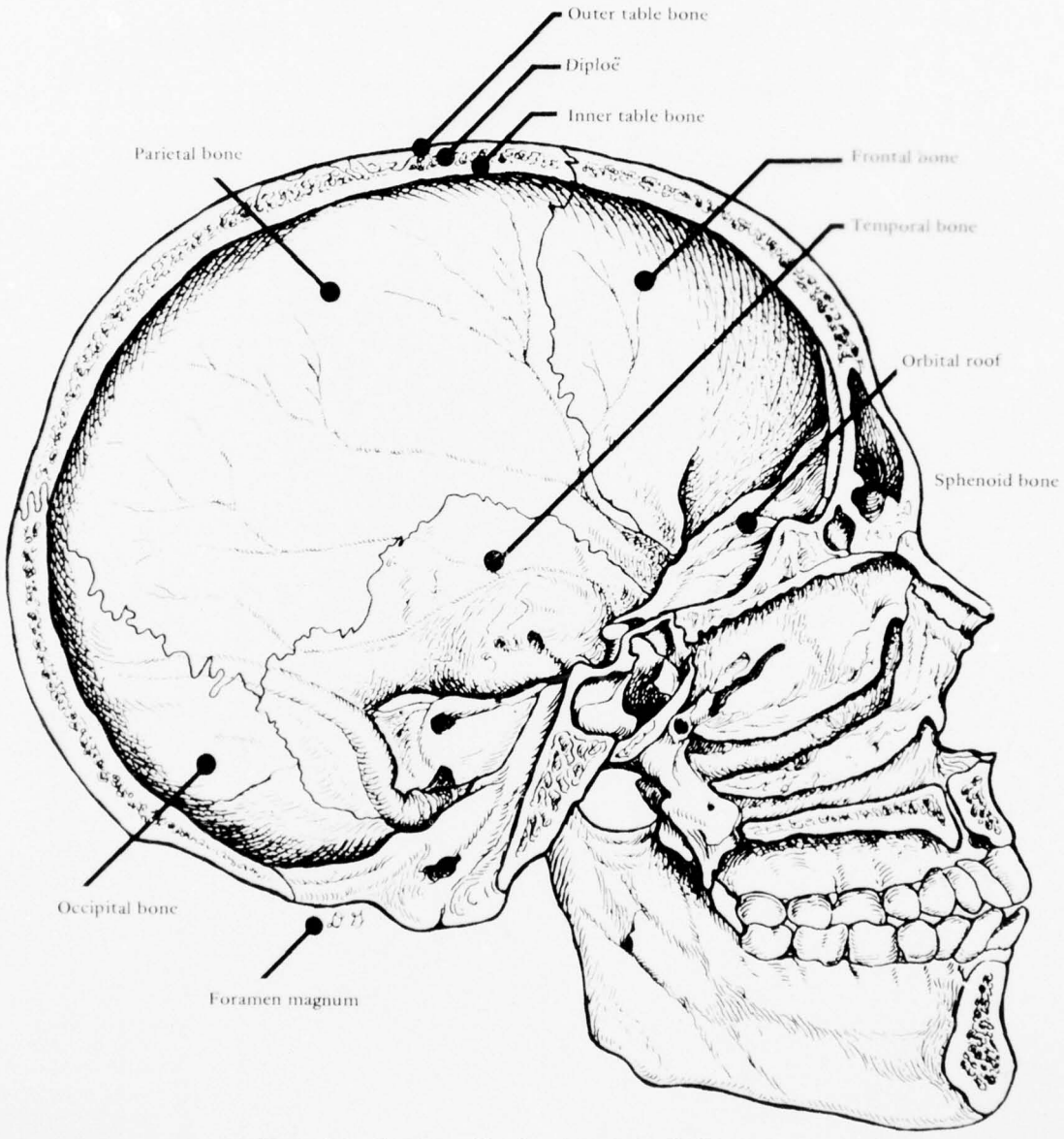

Figure 5-1. Cranium: Hemisection of the Skull.

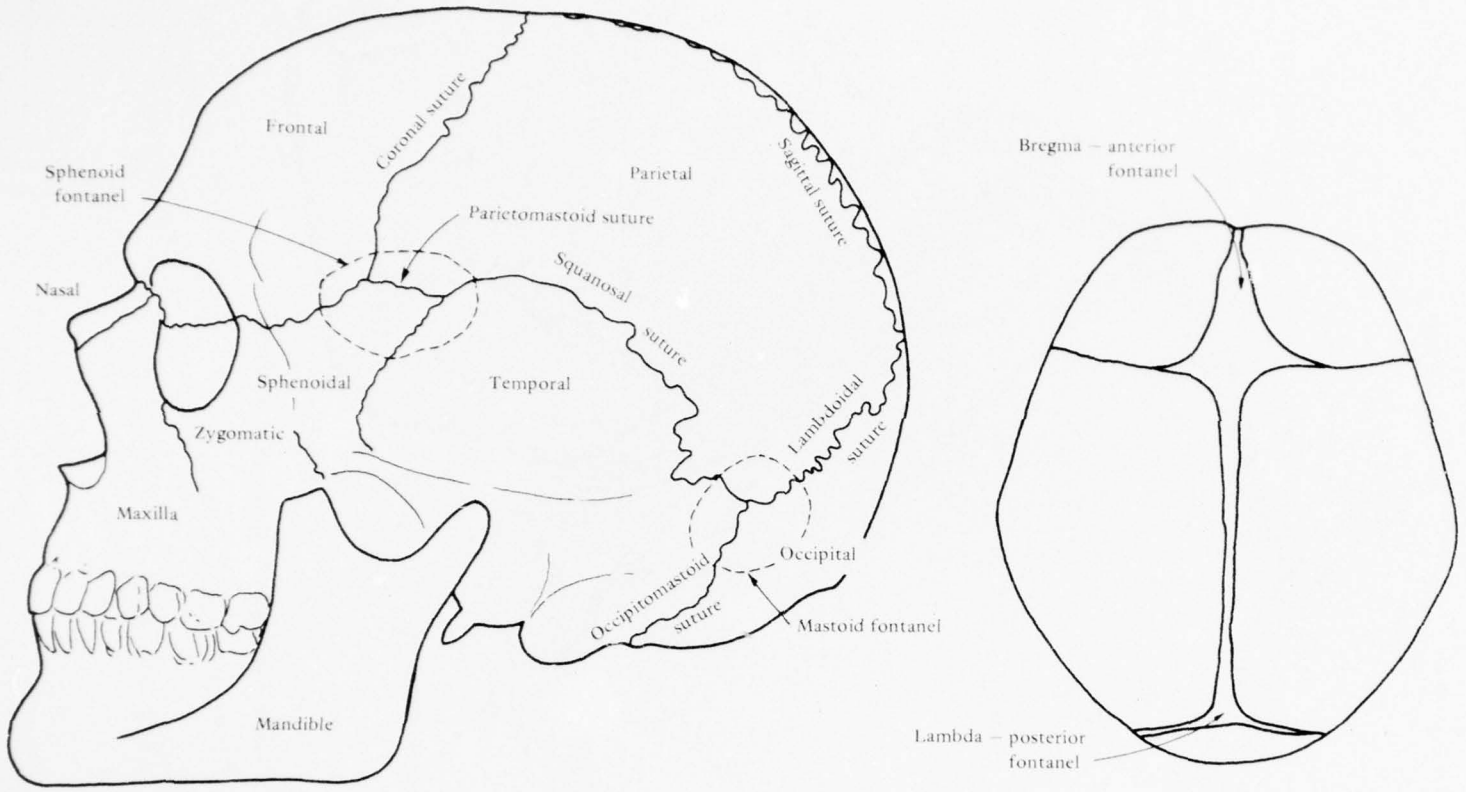

(a) Side view of adult skull.

(b) Skull at birth.

Figure 5-2. Skull Bone Structure and Sutures.

between bones but does not solidify them together. Suture closure begins at about age 22 years when ossification converts the soft hyaline cartilage coating at the joints into bone. First the sagittal and sphenoidal fontanels ossify, then at age 24 years the coronal suture ossifies, and at age 26 the lambdoidal and occipitomastoid sutures ossify. Between the age of 26 and 30, ossification is very rapid compared to thereafter when it slows down. A final burst of ossification occurs in old age. Apparently this ossification is independent of sex.

A trial discretization of the skull surface which included "suture elements" was made, anticipating the specification of mechanical properties for these elements (see Figure 5-3). Difficulty had been envisioned when the entire cranium, including the contents, was to be discretized in a manner consistent with the suture discretization; the two seem to be conflicting requirements. Thus, the idea of including suture elements was discarded. At the same time the scope of the head injury model might be more applicable to adults than to younger individuals.

Studies with a previous finite element model of the cranial structure[18] concluded that the structural significance of the sandwiched or layered construction existing naturally in the skull bone is important and should be included somehow in the simulation. Though this work made use of composite shell-type elements and the present effort will make use of solid elements, it is a simple matter to effect this simulation. A decision to include a layered skull discretization in the HIM code was primarily based upon the above cited recommendation. This recommendation was based upon consideration for proper skull strength simulation. Yet there was still another advantage in the present investigation for doing this. Actual skull bone is comprised of three distinct layers of bone through its thickness. The innermost and outermost layers are a dense bone material and are referred to as the inner and outer table bone. The middle layer is by contrast a very porous bone material and in general, is thicker than the other two layers; this layer is referred to as the diploe layer. By simulating this structure with three layers of solid elements, one not only captures the natural variation of skull bone material stiffness through the thickness (transverse anistropy), but also presumes to obtain the actual stress-strain behavior of the skull bone. This is important because such information can be correlated directly with skull bone fracture. Whereas a simulation with a single layer of shell elements can adequately represent the overall stiffness of the skull bone, it cannot yield useful stress-strain information because the assigned material properties must of necessity be averaged or smoothed values.

There are several reasons why the cranial structure should be simulated carefully despite the fact that, generally, brain damage can occur from impact in the absence of skull fracture. A linear head injury model must be capable of predicting the onset of skull fracture, if not the fracture process itself. Inclusion of the skull bone renders the model more usable in the management of brain trauma. When brain damage accompanies a severe fracture, the prognosis can be considerably complicated by intracranial infection.

The elastic and inertial forces causing brain tissue alteration are partially the result of the particular way in which the skull deforms and absorbs impact energy in each instance. Thus, notwithstanding that skull fracture is in itself an important component of injury, correct simulation of the cranial bone structure is also necessary in order to predict the input forces to the brain.

Figure 5-3. Trial Discretization of the Skull Surface Including Suture Elements.

Linear skull fractures are the most commonly observed types of skull fracture. Linear fractures tend to occur radially from a point of maximum deflection but this pattern is somewhat modified by irregular areas of bony strength. Two observations are important in regard to linear fracture. First, when the blows cause very localized bending the inner table is more severely fractured than the outer table. Second, the location of the blow and the path followed by the propagating fracture are related. For frontal blows the paths tend to radiate and very often fracture the thin bone of the orbital roofs. For vertical blows the paths classically radiate outward over the top of the skull. For occipital blows, the paths run toward the base and the foramen magnum. Finally, for parietal blows the paths radiate toward the temporal bone. Depressed skull fractures are usually caused by more blunt impacts and are characterized by depression or collapse of the cranial bone's sandwiched structure. Large flat areas of impact can cause extensive collapse of the bone and greatly modify the subsequent energy transmitted to the brain.

The skull bone structure can be thought of as comprised of cranial bones and facial bones. The cranial bone complex contains and protects the brain and is the more important of the two types. The skull bone discretization should reflect this importance, but the inclusion of the facial bones is necessary because their inertial properties substantially influence the resulting motion (acceleration) of the skull. As it happens in finite element technology, a reasonable simulation of a structure's inertial properties can be effected with a surprisingly coarse discretization. (The same is not true of a structure's elastic properties.)

In this case all that is required is a reasonable simulation of the inertial properties while no quantitative stress-strain information is sought in the facial bone structure. Therefore, a coarse facial bone discretization has been included in the HIM code geometry.

Another important consideration is the neck structure and whether or not it should be included as part of the head injury model. What is of primary concern is that many so-called head injuries are actually neck injuries or neck-related injuries; for example, damage to the spinal cord and brainstem from either the hyperextension or hyperflexion modes of injury is very common. A complete, all-inclusive head injury model should be able to simulate them. Furthermore, damage to the brain stem even though caused by hyperextension or hyperflexion is often intracranial damage because the brainstem is largely situated within the cranium.

From a practical modeling standpoint however, there is a jurisdictional dilemma arising from the discontinuous nature of the head/neck skeletal structure and the continuous nature of the central nervous system. The anatomical structure of the vertebral column suggests strongly that the neck be modeled continuously with a thoracic model[56] instead of with a skull model. Yet, because the brainstem and spinal cord are continuous at the head/neck interface, deleting the neck from the skull model is undesirable because the deletion limits the scope of the head injury model to injury prediction exclusive of neck-related trauma. At this time practical economics and modeling feasibility prohibit the ideal consideration of a combined head/neck model.

---

[56]Department of Transportation, National Highway Traffic Safety Administration. Final Report DOT HS-801 710: Thoracic impact injury mechanism, volume I, by M. M. Reddi, et al. Washington, D. C. Aug 1975.

Without a neck structure discretization interacting at the base of the skull, the forcing function of the neck on the skull base must be treated as necessary input information to the skull model. This force is extremely difficult to estimate. This basic difficulty is not removed with the inclusion of a good neck discretization because the same problem would exist with the specification of an input forcing function at the base of the neck.

Brain and Intracranial Structure. Simulation of the proper support conditions for the brain is of fundamental importance since the brain is not rigidly supported within its confines (see Figure 5-4 for reference to brain anatomy). It is tethered at its base by the exit of cranial nerves and the brainstem from the cranium. The falx and tentorium membranes lend major support. These membranes are not shown, but the falx lies in the midsagittal plane and extends downward between the two cerebral hemispheres. The tentorium forms a partition between the cerebrum and cerebellum. The semisolid medium of the brain is surrounded by cerebral spinal fluid (CSF) which is displaced when the brain shifts from one tethered position to another.

Intracranial volume shifts induced by impact give rise to two basic types of injury. Coup brain injuries occur if at the point of impact the energy is sufficient to damage the brain tissue. The extent of damage will be proportional to the applied force magnitude. Contrecoup brain injury, occurring opposite the impact, will be dependent upon the direction of the applied force vector as well as the magnitude. This direction will determine where, along the skull/brain interface, the brain tends to separate greatest from the skull. The seriousness of the injury will depend on whether or not bony irregularities exist or whether existing nerve roots exist at that particular section of cranial wall.

Three kinds of brain tissue alteration or failure can be defined as a result of impact. They are concussion, contusion (bruise), and compression of the brain. The first is not explained by clinical or pathological findings as are the latter two. Concussion is attended by loss of consciousness, no matter how brief, and is caused either by damage to the cortex or to the arousal mechanism in the brainstem. Contusions of the brain are generally associated with the coup and contrecoup injury mechanisms and are pathologically observable, as is compression of the brain that results from internal bleeding (subdural hematomas). Anatomically the lesions of concussion, contusion, and compression are distinctly different. Because of this and because they were not simply related, each will most probably require a separate failure theory. There is no reason to believe that such theories cannot be based upon the fundamental mechanical phenomenon of stress or the geometrical pheonomenon of strain. If not stress and strain, then one might ask, what other factors are there? The quantities of velocity, acceleration, and force must all ultimately manifest themselves in some form of stress and strain patterns within the brain tissue. It seems as though these patterns offer the best and most direct route to predicting brain damage.

As can be seen in Figure 5-4, the human brain is structurally very complex. It becomes obvious that some degree of idealization is necessary when discretizing this structure. The analysis tools with which we must proceed (finite element technology) do not easily allow separation (displacement discontinuities) of the various intracranial components depicted, even though they are separate components. If this capability were available, the finite element method could allow an analysis which would include these components as separate

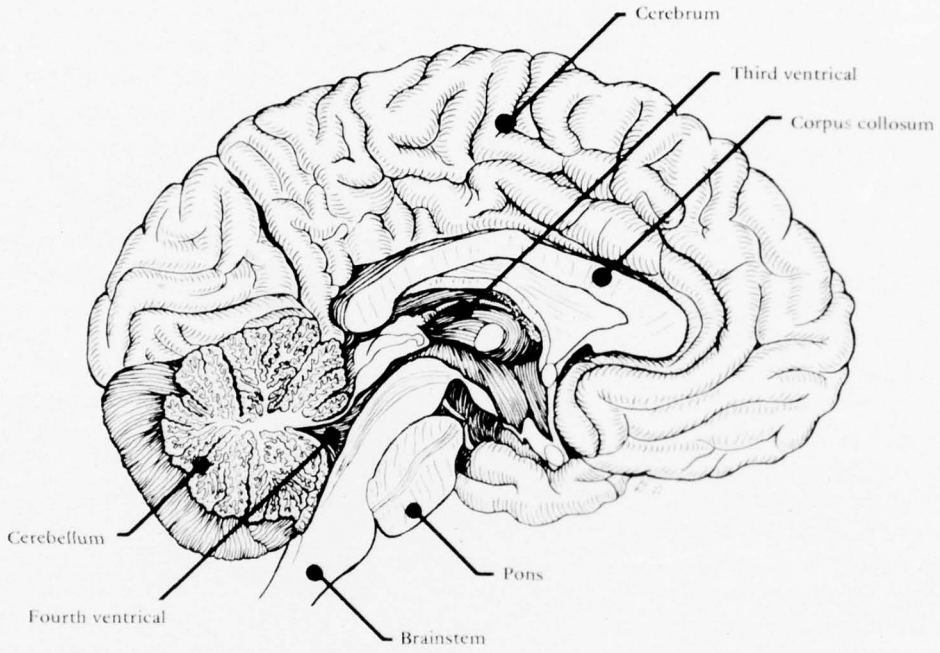

Figure 5-4. Brain: Medial Surface.

entities in the brain. It is not presently available; therefore, the major idealization in modeling the brain is the consideration of a homogeneous intracranial structure possessing a geometry roughly equivalent to that of the intracranial vault.

In any dynamic finite element stress analysis the two internal forces sought implicitly are the inertial and elastic forces. The inertial force is merely the product of the mass and acceleration of a typical node point in the finite element mesh. If the individual mass densities of the intracranial substructures are fairly uniform then the field of inertial forces will be homogeneous and everywhere directly proportional to the acceleration field. Therefore, correct simulation of the inertial force field is not significantly affected by the assumption of a homogeneous intracranial structure since intracranial materials do have mass densities that are fairly uniform.

This is not the case with internal elastic forces. These forces are dependent upon the correct simulation of the conditions of displacement continuity between the intracranial substructures. These conditions are not always continuous and are difficult to define. Of course, the elastic forces are also dependent upon the mechanical properties of these materials but this is not the difficulty. Even though these mechanical properties are known or can be estimated fairly accurately and can be individually prescribed, the elastic forces still cannot be accurately simulated unless the displacement continuity (or discontinuity) conditions can first be correctly prescribed. Since this cannot be done as a practical matter with present state-of-the-art capability, it appears inadvisable to think in terms of more detail in the construction of the brain discretization. In this connection, it should be mentioned that mesh uniformity has import beyond that of esthetics. Where possible, the mesh discretization should be constructed uniformly for the sake of computational accuracy. This is especially true for certain finite element types such as those based upon incompatible finite element formulations. Naturally, more detail in a discretization puts a needless strain on the uniformity requirement and will adversely influence numerical accuracy in those cases where the additional detail is ineffectual or unwarranted.

There are some exceptions to the idealization approach which utilizes a completely homogeneous intracranial structure and uniform discretization. These will be discussed separately in sections following.

Since the brain is not attached continuously along the internal cranial wall but is supported and tethered at their interface, a method must be devised to approximate this suspension. The single layer of elements which simulate the subarachnoid space was provided in the basic HIM code configuration for this eventuality. In this way provision is made for the possibility of relative motion* between the skull and brain at their interface. The anatomy suggests that this motion might occur because the brain is not continuous with the skull. Indeed the interface appears to be lubricated with cerebral spinal fluid. Also neurosurgeons speak a great deal about intracranial volume shifts and the "brain slosh" mechanism[57] where the primate brain has been observed through lucite calvariums to displace relative to the internal cranial wall. But just providing a layer of elements does not in

---

*In this context, relative motion means relative motion in both a normal and a tangential direction at a point on the skull-brain surface.

[57] R. H. Pudenz and C. H. Sheldon, "The lucite calvarium—a method for direct observation of the brain," Journal of Neurosurgery, vol. 3, 1946, pp 487-505.

itself simulate the subarachnoid space. An appropriate set of material properties must be assigned to those elements, depending on what the "physics" of the situation is believed to be. The particular set of mechanical properties recommended for use in the HIM code is discussed in Chapters 6 and 7, but it should be said here that this specification, like any other material property specification, is optional to the HIM code. The user may prescribe any set of material property values for any region of the discretization.

The falx and tentorium membranes may well present another exception to the concept of a completely homogeneous idealization of the intracranial structure. These membranes separate the intracranial vault into separate compartments and can provide major support which would resist intracranial volume shifts. This is an important structural influence and therefore simulation of these membranes was given careful consideration in the HIM code development. Besides the anatomical evidence supporting a decision to include them, it initially appeared a structual simulation could be easily effected with basic two-dimensional, membrane finite elements. There was, however, a dissenting note represented by the experimental work reported by Roberts, et al.[58]. They concluded that the existence of the membranes made little difference to the intracranial pressures which they measured. Nevertheless, it was decided initially to incorporate the effect of the falx and tentorium membranes into the HIM code.

Many obstacles appeared in the initial attempts to discretize the intracranial contents. During the development of the discretizing process, some simplifications were necessarily made to the model to achieve a working discretizaiton. One of these simplifications was deletion of the requirement for the membranes and relegation of their inclusions as a recommended feature for future work. Thus, the present HIM code does not possess the influence of the intracranial membranes. It is believed, however, that the mesh discretizing technique used can eventually be modified to include the membranes.

One other problem relating to the membranes will still have to be overcome. It is not clear how the two-dimensional membrane elements can be kinetically isolated from adjacent brain elements so as to adequately simulate their interaction. As these membranes exist in the skull, they are not affixed continuously with adjacent cerebral material. For example, motion of the cerebrum in an anterior-posterior direction is not resisted by the in-plane stiffness of the falx membrane. However, if in the simulation, the membrane elements are not correctly isolated (displacement compatibility relinquished), the adjacent cerebral elements would be stiffened artificially and incorrectly in the anterior-posterior direction. Therefore, an adequate simulation of the falx and tentorium is not necessarily achieved by merely including two-dimensional finite elements in the discretization unless provision is also made for their proper interaction with adjacent three-dimensional, cerebral elements.

It is believed that there is yet a third exception to the homogeneous intracranial concept and that it involves the brainstem simulation. Here again the HIM code does not account for the rather fibrous nature of the brainstem's constitutive makeup, but rather assumes it to be a homogeneous material identical to the surrounding intracranial material.

---

[58] V. L. Roberts, V. R. Hodgson, and L. M. Thomas. "Fluid pressure gradients caused by impact to the human skull," Biomechanics Monograph, ASME, 1967.

The reasons for this are the same as those offered in the discussion of the membranes. First, the constraints imposed by the brainstem's geometrical complexity prevented the realization of a viable intracranial discretization and, second, the inability to simulate the brainstem's kinematic interaction with surrounding material makes any attempt to do so inadvisable during the initial development of a head injury model. Because the brainstem is generally thought to participate widely in closed brain injury, however, it does deserve additional attention in the modeling process.

Methods of Discretization

At the outset of the project, geometrical detail of the model was assigned major importance. Automatic mesh generation schemes, which are frequently associated with ordinary finite element problems, were initially ruled out because they were thought to be efficient only with simple or analytically describable geometry. A more arduous manual approach, but one that was expected to be more appropriate for discretizing complex geometry, was first embarked upon. This decision resulted in a delay in the realization of a workable finite element discretization of the skull-brain system. Though eventually an automatic mesh generation scheme was employed successfully, it is believed useful to first discuss the original discretization attempts.

Manual Mesh Generation. A life-sized plastic skull replica was immersed in an epoxy bath for subsequent mechanical discretization. Once the assembly was completely cured, it was removed from the mold and then rectangularly shaped in a flycutting operation and thereafter polished. The resulting processed cast is shown in Figure 5-5. Next the assembly was sliced into thin sagittal sections, each of which would be discretized by superimposing a grid over the slices. Measurements relative to the reference coordinate system shown would be made of the discretization and eventually coded for input to the finite element model of head. The reference coordinate system is an established system for cranial anatomy. The x- and y-axes lie in the Frankfort plane. This plane contains the auditory meatuses and the orbital notches. The y axis is co-linear with the line connecting the auditory meatuses, and the z-axis is formed by the right-hand rule.

The epoxy cast was sliced four times in planes parallel with the midsagittal plane, creating five epoxy slabs. The slabs are shown assembled in Figure 5-6. A finite element mesh was designed and superimposed on each slab. Each superimposed mesh was composed exclusively of quadrilateral subregions. In this way the three-dimensional elements are formed as irregular, six-sided bricks, and the discretization is devoid of tetrahedrons or triangularly shaped elements. In addition to merely discretizing the cerebral volume, the finite element mesh has been designed to include the geometrical detail attending the falx of cerebrum membrane and the tentorium of cerebellum membrane.

During this development period it was also necessary to determine the number of elements and nodes required for an adequate structural idealization while keeping the model's size economically tractable. Roughly 400 elements constituted the initial discretization which included about 375 brick-type elements and about 25 membrane-type elements. For simulated dynamic load applications in the midsagittal plane, symmetry was taken advantage

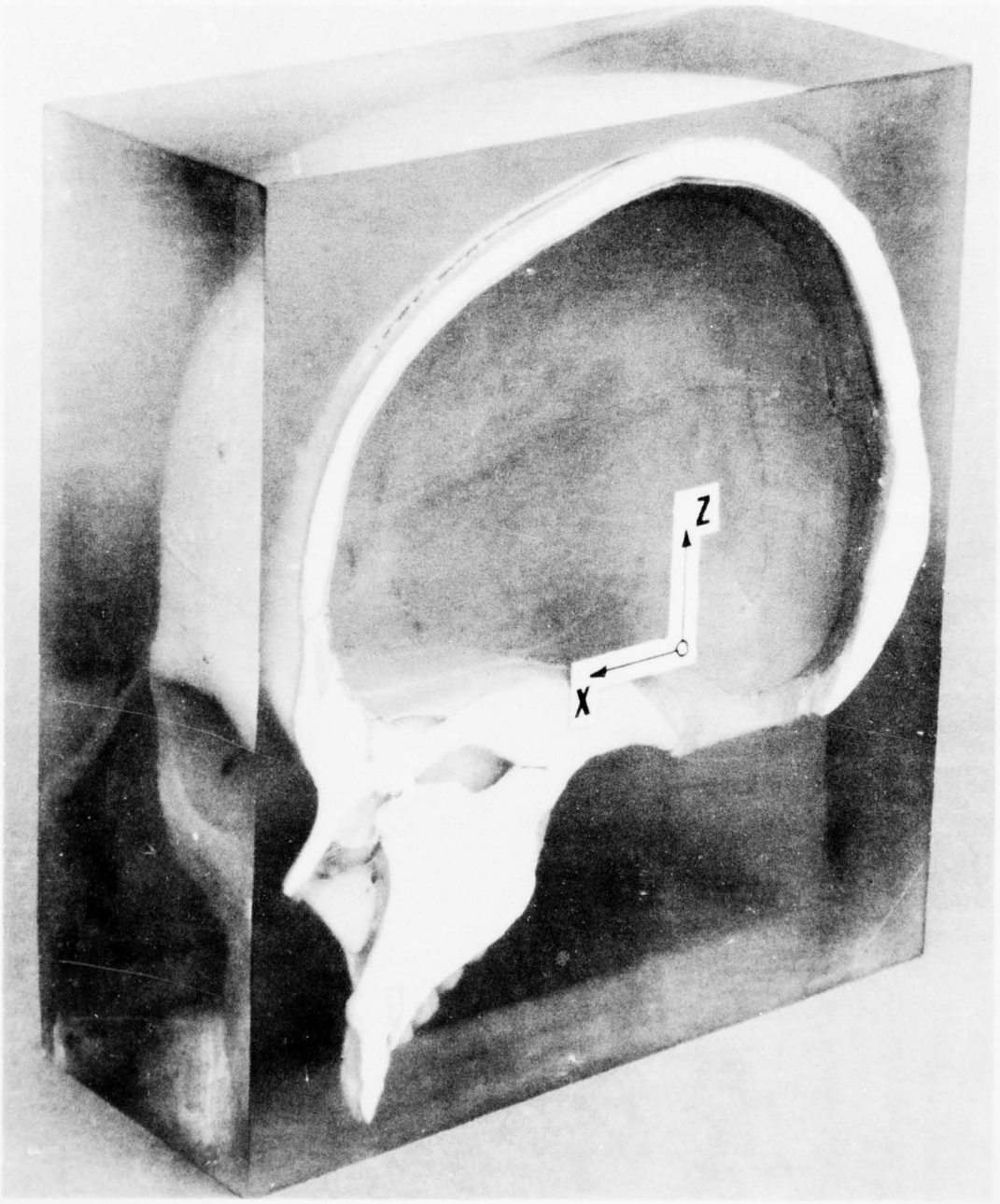

Figure 5-5. Machined Epoxy Cast.

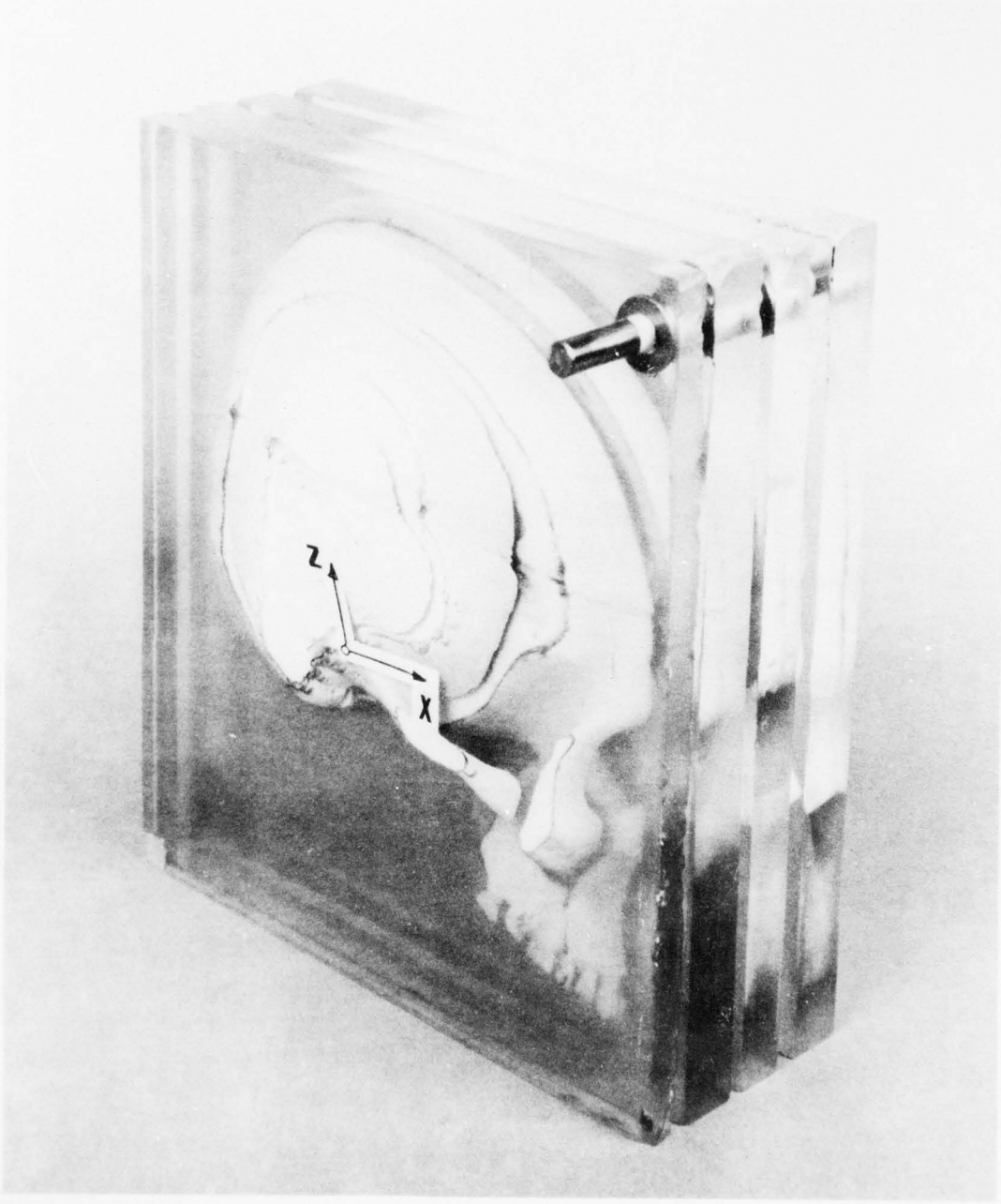

Figure 5-6. Sliced and Reassembled Epoxy Cast.

AD-A043 605 CIVIL ENGINEERING LAB (NAVY) PORT HUENEME CALIF F/G 6/2
A FINITE ELEMENT HEAD INJURY MODEL. VOLUME I. THEORY, DEVELOPME--ETC(U)
JUL 77 T A SHUGAR

UNCLASSIFIED CEL-TR-854-1 NL

2 OF 3
AD A043605

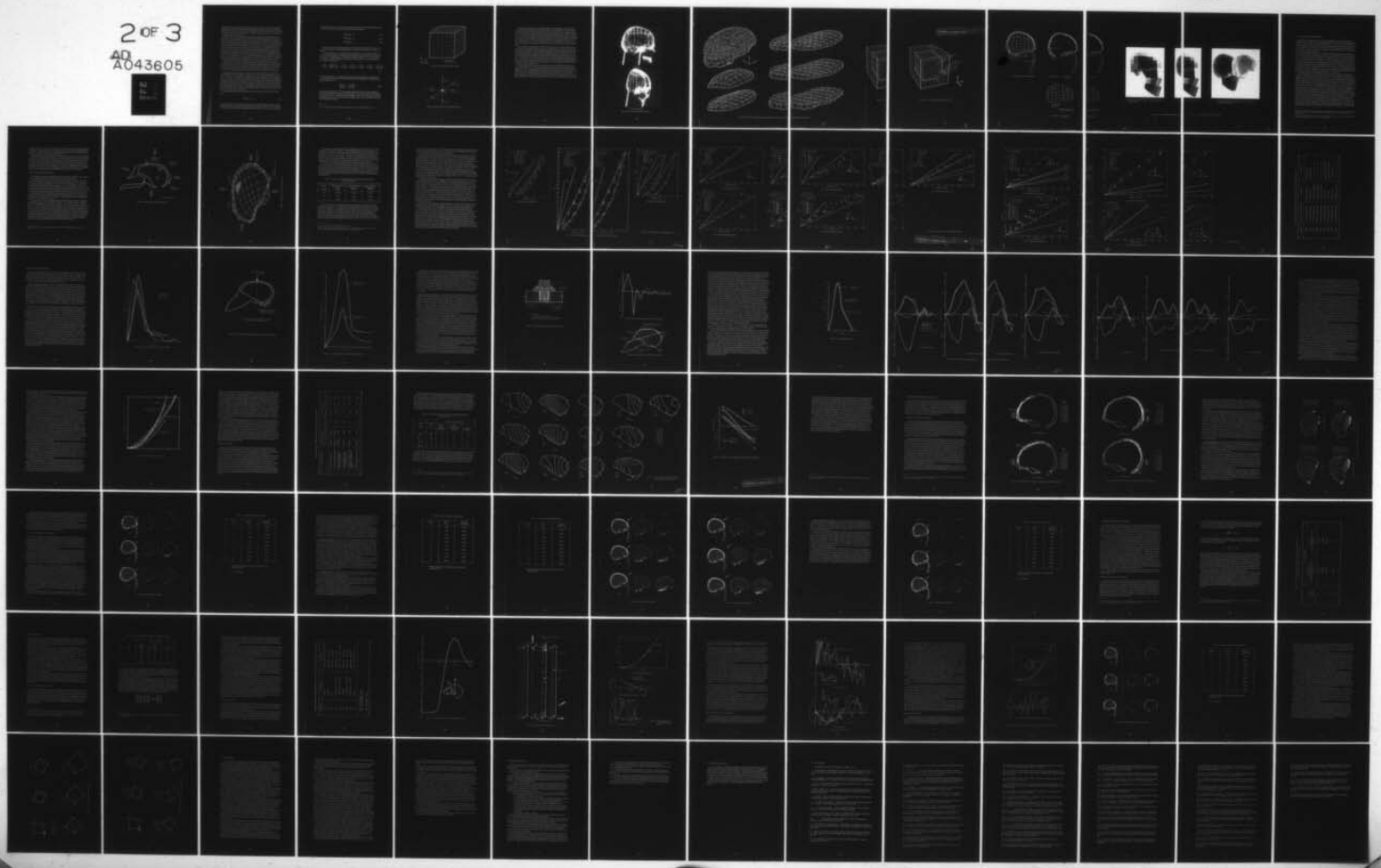

of and the discretization was made about twice as fine. However, for unsymmetrical load application the coarseness shown is approximately what must be used because 400 additional elements will have to be generated for the opposite half of the skull. It was estimated that 800 to 1,000 elements are nearly the computer's storage capacity and will adequately represent the geometry of the skull.

The difficulty with the epoxy cast procedure arises from the parallel plane concept upon which it is based. With the restriction that no triangularly shaped elements are to be allowed, an increasingly finer discretization occurs in planes farther from the midsagittal plane. This presents an unacceptable mesh size gradation. It would be better from the standpoint of mesh gradation if the fineness of discretization would increase with radial distance inward from the skull surface towards the center of the brain. Because with this latter concept the primary generators of the mesh must be radial lines, as contrasted with parallel sections, the epoxy cast procedure would have no particular advantage. Instead, it was thought that a tractable approach could be effected with pliable, fine wire lengths placed radially in the plastic skull to act as main generators of the mesh. Two difficulties were foreseen with this approach. First, a few tetrahedron elements must inevitably be included due to the convergence of the radial generators. Mixing these elements with six-sided brick elements was to be avoided for computational accuracy. Second, node point coordinate measurements would not be accomplished as easily as with the plane slices of epoxy.

Although some effort was expended on the radial wire approach and the original epoxy cast procedure did culminate in a usable three-dimensional discretization, neither method proved to be satisfactory. These point-by-point discretization methods were too arduous and did not produce sufficiently uniform discretizations of the skull-brain system. As a result they were finally abandoned in favor of an automatic mesh generation approach.

Automatic Mesh Generation. This approach to the discretization of the skull-brain system is primarily, but not completely, automatic in its computation of nodal point coordinates. Obviously some geometrical information must be put manually into the computer before it can begin to discretize the cranium and its contents. However, from a minimum of user-specified input data, this method resulted in an automatically computed and optimally uniform discretization of the skull-brain continuum. There may be some loss of capability for capturing detailed geometry, but the overall ease and expediency of the method far outweighs that disadvantage. However, the big disadvantage of the automatic scheme approach was the additional effort required to develop the necessary methodology and computer program, which did not exist at the time.

The automatic skull-brain mesh generator relies on Laplace's equation in three dimensions,

$$\nabla^2\Psi(X,Y,Z) = 0 \qquad (5\text{-}1)$$

to uniformly discretize the intracranial contents. This classical form is applied to the I-J-K integer space of the conceptualized brain discretization shown in Figure 5-7. The function Ψ is replaced by the unknown rectangular Cartesian coordinates X, Y, and Z, which describe

the skull-brain system. These functions are now written in terms of the independent integer variables I, J, and K forming three independent Laplace equations,

$$\nabla^2 X(I,J,K) = 0 \tag{5-2}$$

$$\nabla^2 Y(I,J,K) = 0 \tag{5-3}$$

$$\nabla^2 Z(I,J,K) = 0 \tag{5-4}$$

These three partial differential equations are then cast into finite difference form, and each is solved separately using standard iterative techniques as described, for example, by Smith[59].

As an illustration, the X-coordinate function of Equation 5-2 is found by solving a system of difference equations comprised of one equation for each internal node. This results in a system of 125 equations (5 cubed) for the example of Figure 5-7. If a central difference scheme is employed using the coordinates shown in Figure 5-8, a typical equation in the system can be written as

$$X^{(N)}_{I,J,K} = \frac{1}{6}\left(X^{(N-1)}_{I+1,J,K} + X^{(N)}_{I-1,J,K} + X^{(N-1)}_{I,J+1,K} + X^{(N)}_{I,J-1,K} + X^{(N-1)}_{I,J,K+1} + X^{(N)}_{I,J,K-1}\right) \tag{5-5}$$

The superscripts (N,N-1, etc.) represent the iteration number during the convergence process. Typically this number can be between 30 and 40, depending upon the prescribed convergence tolerance e; i.e.,

$$\left(X^{(N)}_{I,J,K} - X^{(N-1)}_{I,J,K}\right) \leqslant e \tag{5-6}$$

It is obvious from Equation 5-5 that the Laplace method results in a simple averaging formula for computing the coordinates of internal nodes. This results in an optimally uniform brain discretization. It is worth noting that Gallagher[14] has observed that mesh uniformity is desirable for accuracy in the finite element solution process. This is particularly true with some incompatible elements.

---

[59] G. D. Smith. Numerical solution of partial differential equations. London, Oxford University Press, 1965.

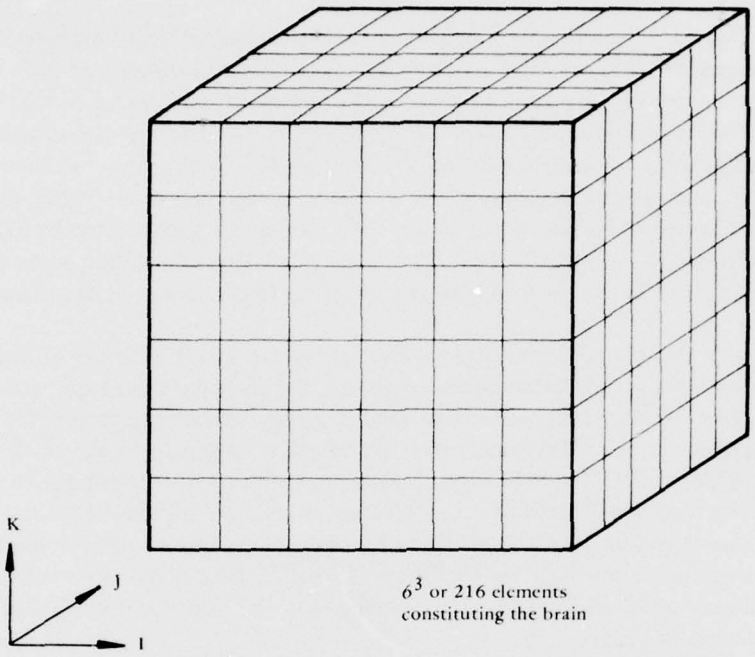

Figure 5-7. Conceptualized Brain Discretization.

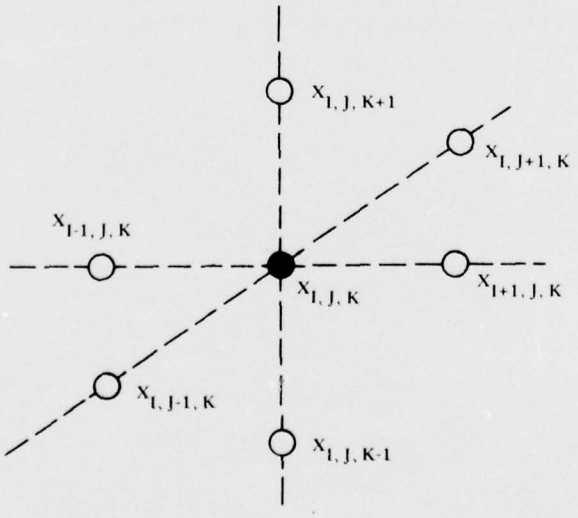

Figure 5-8. Isolated Internal Node and Neighboring Nodes.

During the iteration process the neighboring nodes surrounding an internal node near the surface will periodically lay on the cube's surface. The coordinates of such nodes are prescribed data for the Laplace scheme and are fixed and not subject to change during iteration. Put another way, these data form the boundary conditions for the solution of Equation 5-1. These data are taken from actual skulls or plastic skull replicas as shown in Figure 5-9. Because accurate geometry of both the skull and brain surface is sought, the prescribed geometrical data are recorded for the internal skull surface as opposed to the external surface. Along with the X-, Y-, and Z-coordinate values of a typical surface node, the local skull bone thickness is also recorded. Graphical results of the iteration are shown in Figure 5-10.

The skull-brain mesh generator, besides discretizing the brain with the Laplace scheme, discretizes the skull bone into three layers representing the inner and outer table bone and the middle layer of diploe. This is accomplished directly (without iteration) by computing the outward normal at each prescribed node, assigning its length to be the skull thickness and then appropriately dividing the length into three segments. Everywhere the inner and outer table thickness is one-fourth the skull thickness, and the diploe is half the skull thickness. A fourth layer is also provided at the same time (using the inward normal) and simulates the subarachnoid space between the brain and skull. Its thickness is arbitrarily selected as being everywhere equal to the table bone thickness. The conceptualized skull-brain discretization is shown in Figure 5-11.

Typical skull-brain discretizations that result from the skull-brain mesh generator are depicted in Figure 5-12. The coarse facial bone discretization was constructed manually subsequent to the automatic generation of the mesh. Scale factors are provided to alter the shape or size of an existing discretization (within certain limitations), thus avoiding the necessity for having to re-generate the mesh when studying the influence of skull size and shape. If warranted, more detail in the brain can be provided by prescribing the coordinates of internal nodes to coincide with intracranial structures or more detailed brain surface shape.

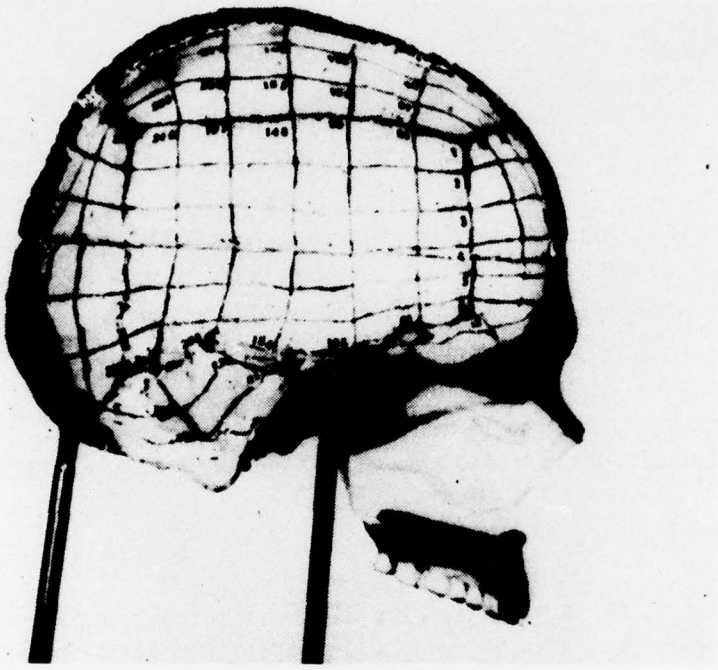

(a) Side view.

(b) Three-quarter view.

Figure 5-9. Source of Mesh Generator Input Data.

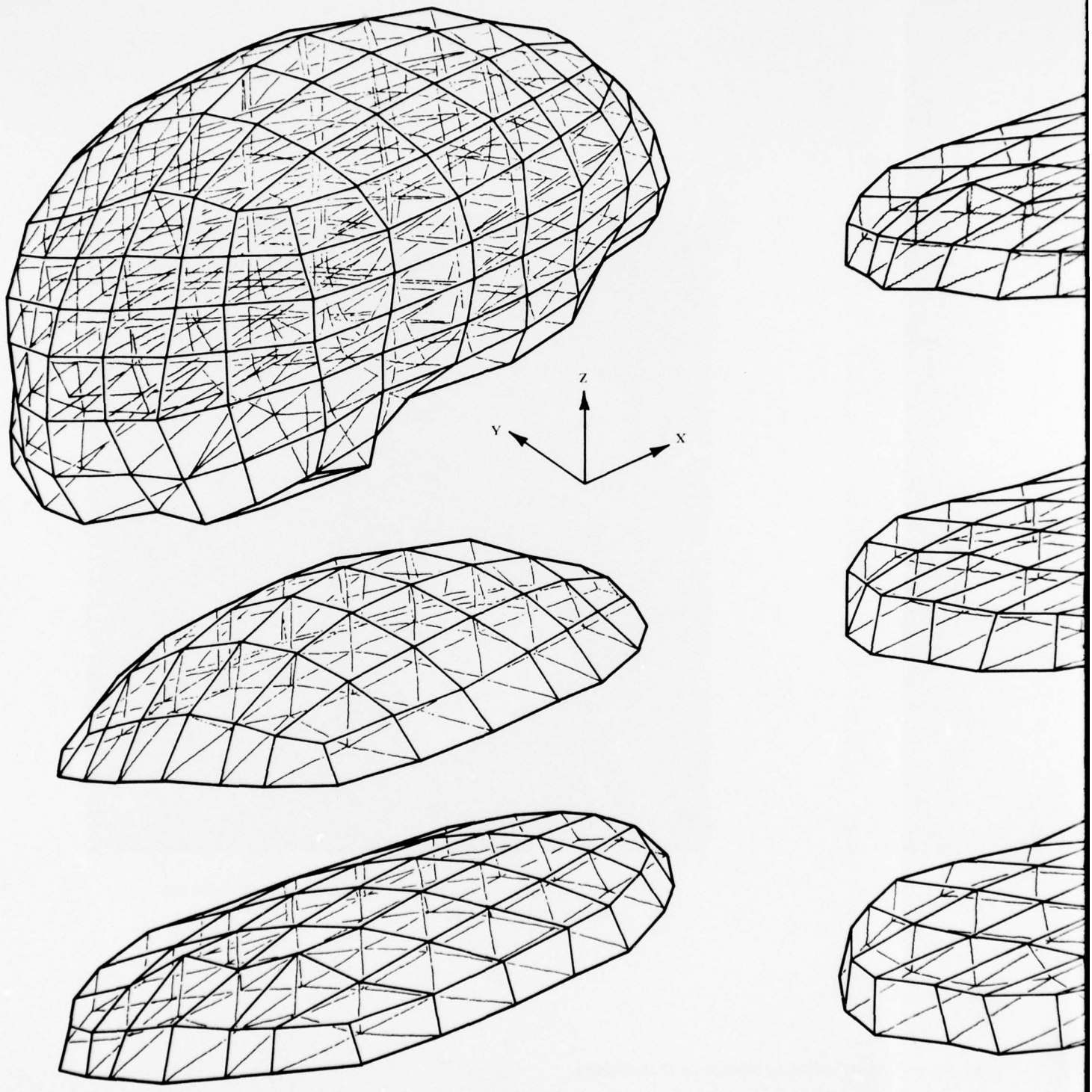

Figure 5-10. Posterior View of Brain Discretization and Horizontal Layers of Elemen

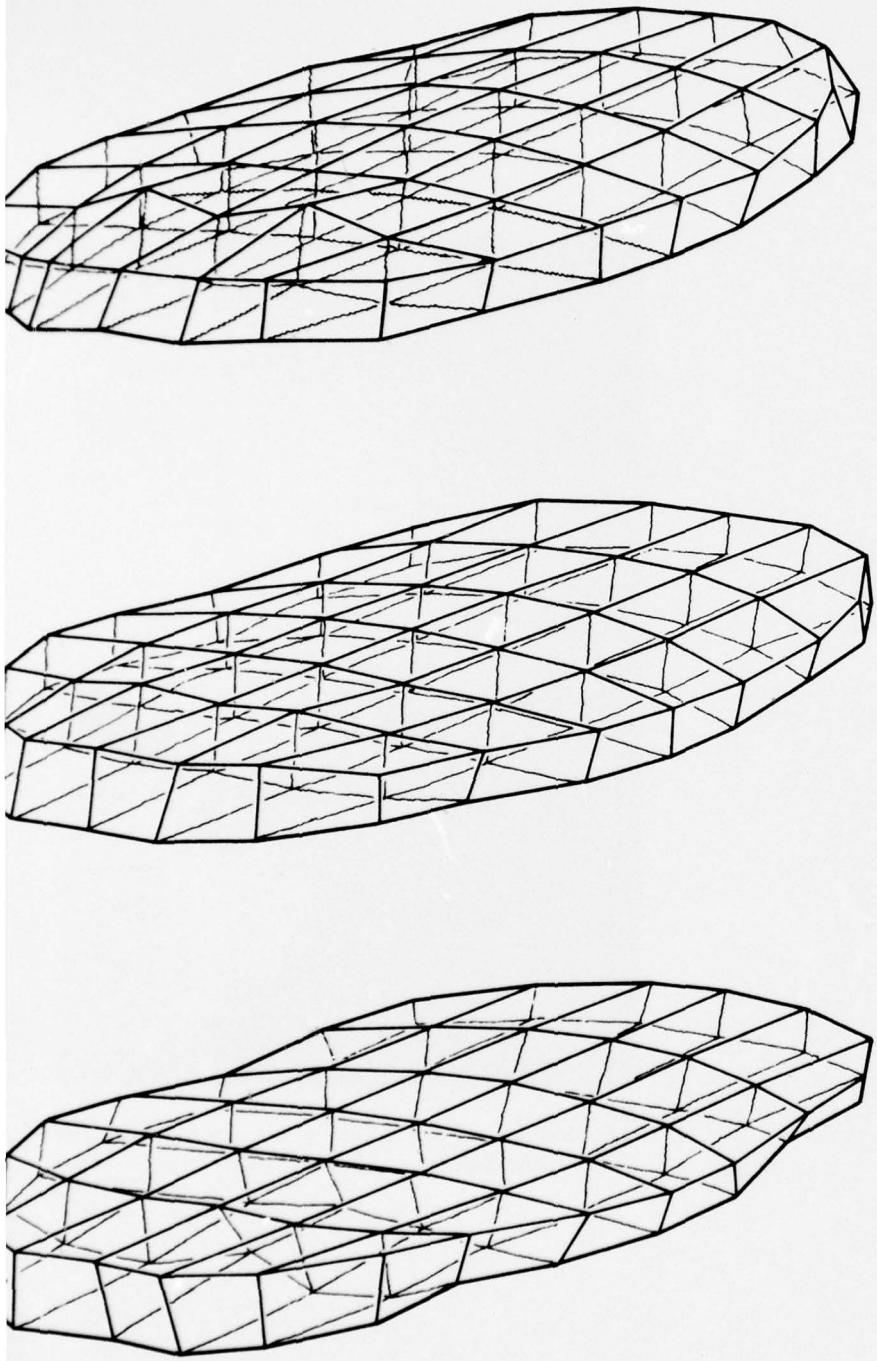

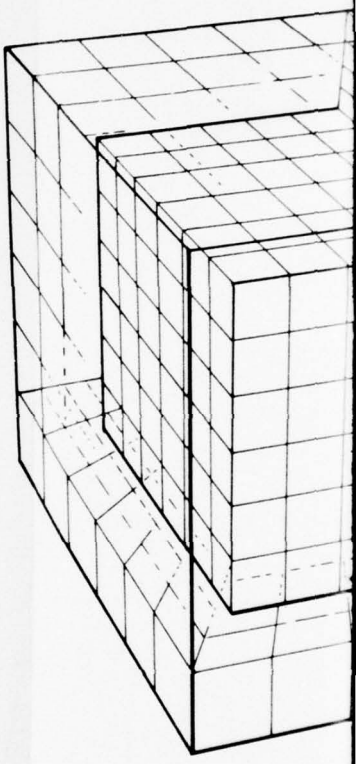

Figure 5-11. Co

Horizontal Layers of Elements.

2

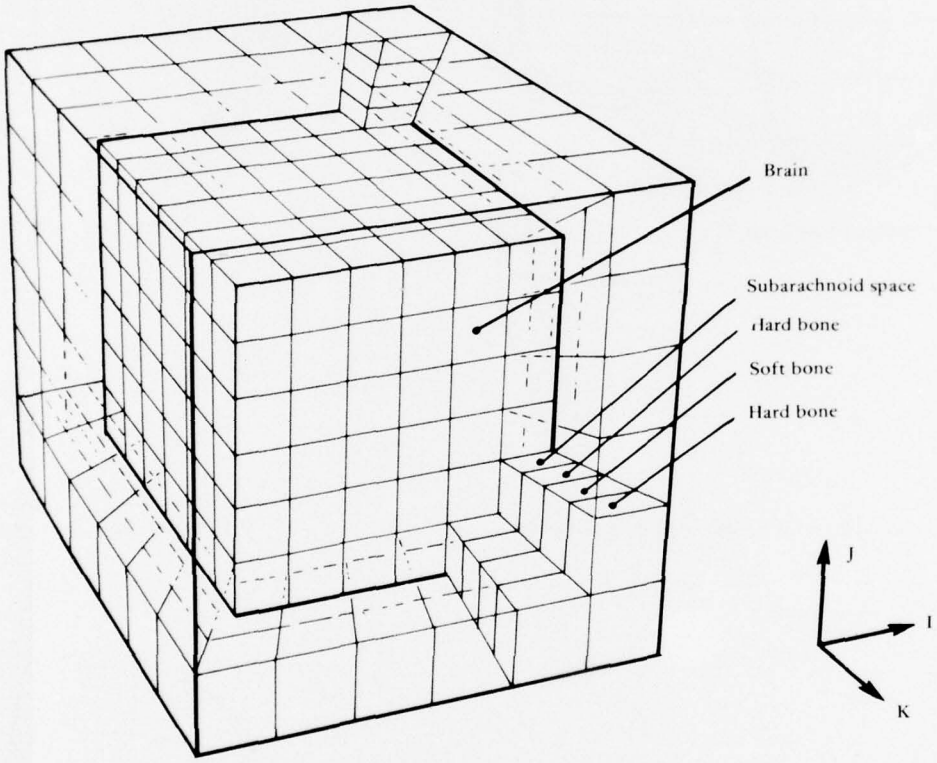

Figure 5-11. Conceptualized Skull-Brain Discretization.

3

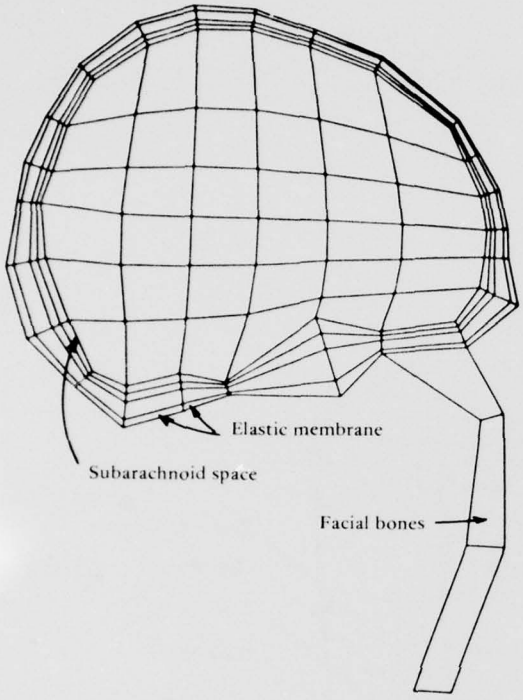

(a) Combined mesh – midsagittal plane.

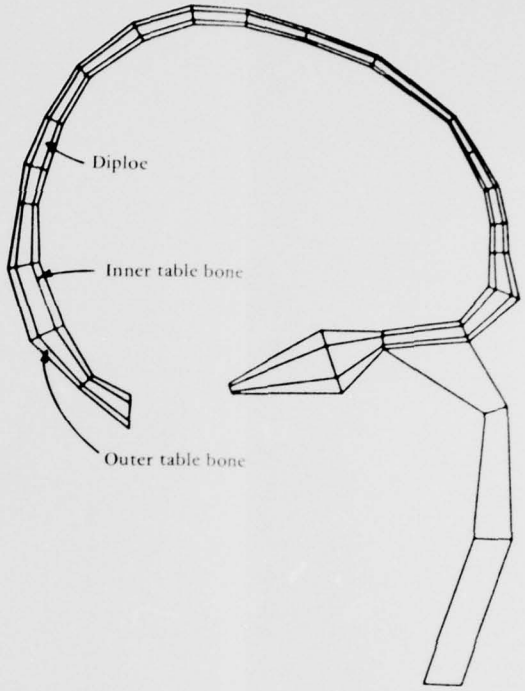

(b) Skull bone mesh – midsagittal plane.

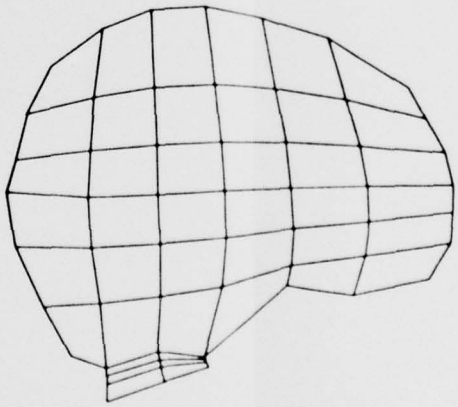

(c) Brain mesh – midsagittal plane.

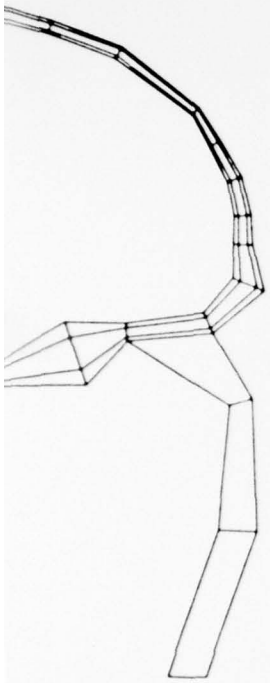

midsagittal plane.

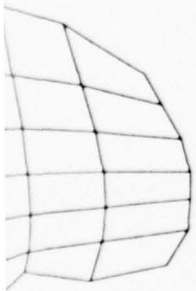

tem elements treated
ly incompressible tissue

lsagittal plane.

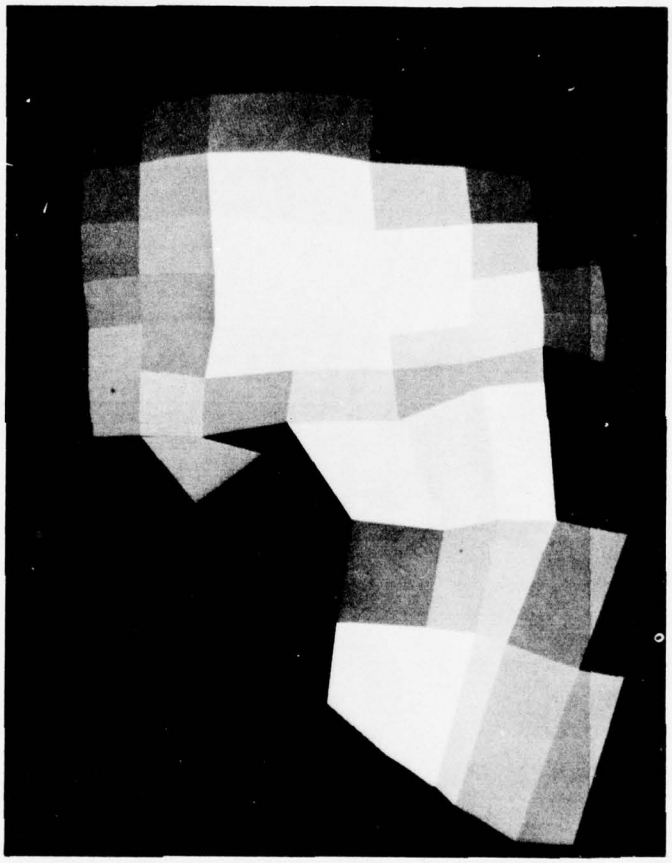

(d) HIM external skull shape profile – continuous tone computer graphics display.

(e)

Figure 5-12. Three-Dimensional Skull-Brain Discre

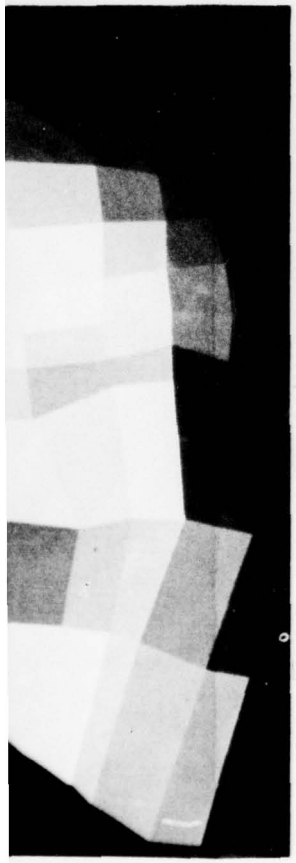

– continuous tone computer

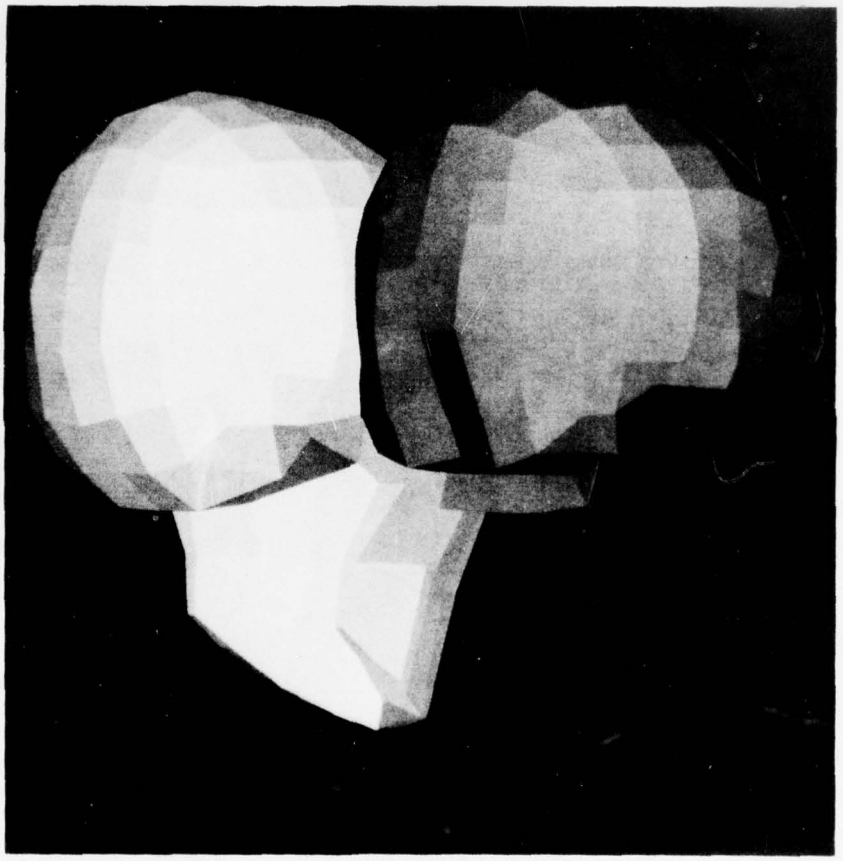

(e) HIM external skull and brain, right rear view – continuous tone computer graphics display.

Figure 5-12. Three-Dimensional Skull-Brain Discretization.

6. VALIDATION OF THE HIM CODE

Kornhauser[60] has suggested that with proper validation the advanced computer or mathematical model approach is the ultimate quantitative prediction method in biodynamic modeling. There is, however, very little information on just what "proper validation" entails. Verification of biomechanical models is more complex than verification of inanimate system models. This is because it must inevitably deal with experimentally obtained in vivo or in vitro data, where the experimental technique and repeatability of data are adversely affected by physiological processes.

Exact solutions are available only for simple problems, and oftentimes experimental results are questionable. Verification or making sure the program does what it is intended to do is the responsibility of the originator. Verification, however, is a haphazard process; there is no such thing as absolute verification. It has been proposed by Griffin[61] that verification be replaced by "level of confidence." The level of confidence of a program would encompass a number of things, including qualifications of the programmer, the complexity of the model, determination of whether solution procedures are standard or advanced, degree of approximation, comparison with theory and experiment, and the length of time the program has been in use. Ultimately, however, it is the user who is the final debugger and he should not accept any program as being absolutely verified but should scrutinize all the data and then feed back to the program developer any errors noted.

The linear head injury model development was viewed as primarily an application of existing technology and consequently use of available computer programs was indicated as opposed to the development of a distinctly new code. The computer program upon which the HIM code is based was developed by Taylor[26] and is termed the FEAP (Finite Element Analysis Program) code. This section was primarily based on the FEAP code's potential for allowing the specification of a general purpose code of moderate size to the unique problem of head injury modeling. It was not large and unwieldy and possessed the generality believed sufficient for the task. Modifications of both an unforeseen and an anticipated nature could be effected by delving into the code. The element library contained standard two- and three-dimensional isoparametric elements, but the FEAP code's unusual capability for combining these elements with linear viscoelastic material behavior was decisively influential. Many different structural analyses had been successfully performed in the past with the FEAP code, and it was sufficiently well-documented. Since its modification to the HIM code form, there have been close to 90 static and dynamic head injury simulations performed. Many of these were developmental and of a debugging nature. To date there are no known errors either in the logic or in the coding. For the past few years, the finite element method has been established as a viable three-dimensional analysis technique. Two of the HIM code's features—recognizable geometry and linear viscoelasticity—are well within

---

[60] M. Kornhauser. "Biodynamic modeling and scaling: anthropomorphic dummies, animals, and man," paper presented at Symposium on Biodynamic Models and Their Applications, Wright-Patterson Air Force Base, Dayton, Ohio, Oct 1970. (AMRL-TR-71-29)

[61] D. S. Griffin. "The verification and acceptance of computer programs for design analysis," On General Purpose Finite Element Computer Programs, ed. P. V. Marcal. New York, ASME, 1970.

the state-of-the-art. The equations of motion are linear and are solved by standard solution techniques. The finite element formulations (element types) are also standard eight-node, compatible, isoparametric elements. Indeed these standard features were initially selected to enhance the level of confidence of the HIM code.

Correlation with experimentally measured data in primates has been from the beginning an objective in the HIM code development. The results thus far have not been completely successful. The primary difficulty is that the experimentally measured parameters are basically different in kind that the computed parameters. Nevertheless, all of the efforts to verify the HIM code by correlation with experimental data are presented and discussed in this chapter. All of the experimental data were supplied by the Highway Safety Research Institute (HSRI) at the University of Michigan under contract DOT-HS-031-3-749 with the Department of Transportation, National Highway Traffic Safety Administration.

Static Skull Bone Structural Validation

Static validation consists of comparisons between two kinds of measured and computed data; load-deflection data and load-strain data for an empty rhesus skull.

A midsagittal plane view of the actual rhesus skull is shown in Figure 6-1. The three directions and regions of loading, A-P, L-R, and S-I, are shown relative to the strain gage rosette locations employed by HSRI. In Figure 6-2, the midsagittal plane view of the corresponding three-dimensional finite element model is shown. Although not shown, the facial bone discretization was actually included in the computer simulation. HSRI provided CEL with the actual rhesus skull from which the experimental data was obtained. This skull was discretized as described previously for human skulls by the automatic mesh generator.

The numbered finite elements shown were those whose computed strain response was compared with the measured strain response from the strain gage rosettes. Two elements, 468 and 540, are designated in the occipital bone region because the corresponding strain gage rosette is on their common border.

To account for the variance among published mechanical property data for skull bone, two limiting values were used for Young's modulus. Thus, computed data are designated either as corresponding to a "high range" modulus or a "low range" modulus. The high value is 1.78×10^6 psi and is taken from McElhaney et al[62] directly for compact bone. The low value is 0.82×10^6 psi and is derived as follows. Instead of compact bone properties, it is based on experimental composite skull bone properties which include the porous diploe layer along with the compact bone. Additionally its derivation excludes, as being too stiff, all mechanical property data obtained from embalmed material. Furthermore, its premise is that the simulation of three homogeneous elements through the thickness must behave on the whole as does the composite bone. Mechanical properties for the middle skull layer (diploë) are taken as one-tenth the values for the inner and outer layers.

---

[62] James H. McElhaney, et al. "Mechanical properties of cranial bone," Journal of Biomechanics, vol. 3, 1970, pp 495-511.

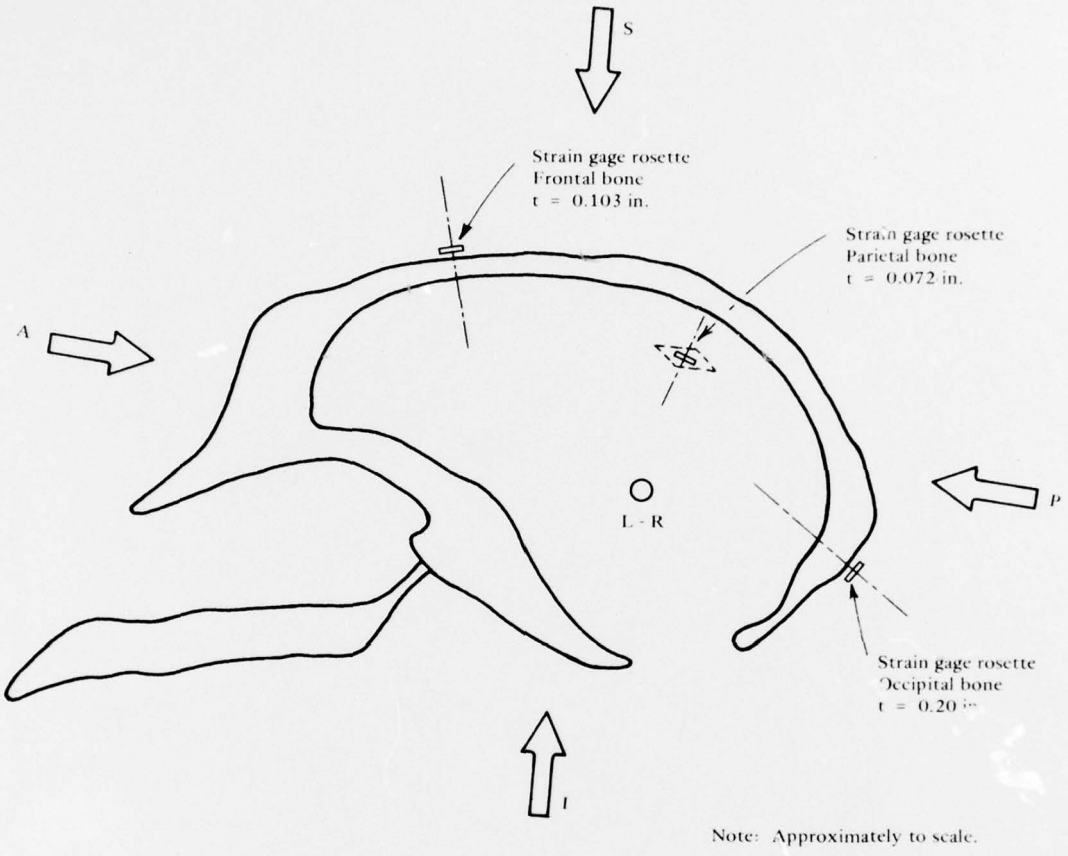

Figure 6-1. Midsagittal Plane of Actual Rhesus Skull

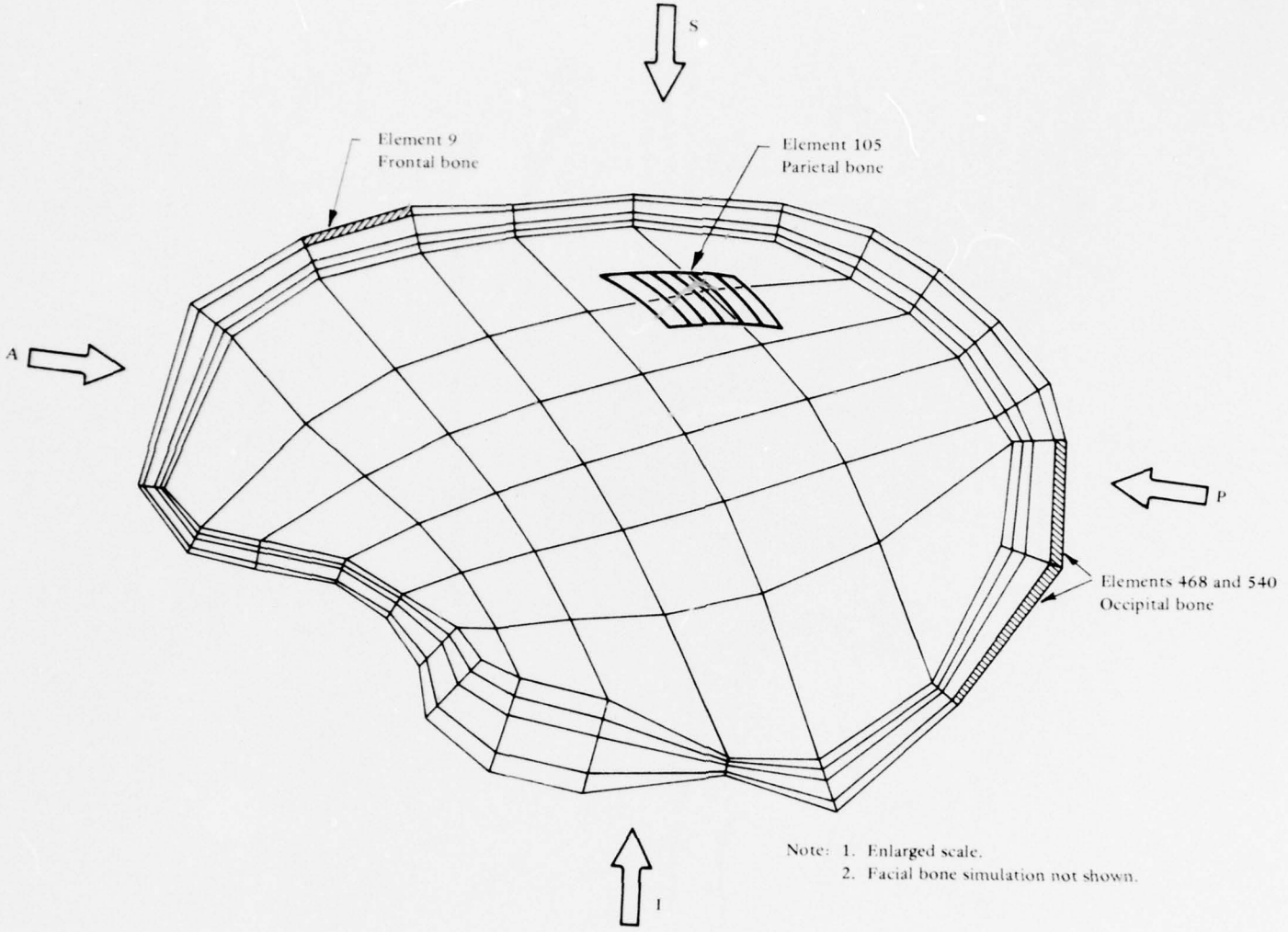

Figure 6-2. Midsagittal Plane of Modeled Rhesus Skull.

A comparison of computed and measured load-deflection results for the A-P, L-R, and S-I directions is presented in Figure 6-3. The loading portion of the experimental curves demonstrate the linearity of actual skull deflections within the range of applied load. (The loading rates varied from 3 to 9 lb/sec.) However, the unloading portion consistently exhibited a nonlinear, hysteritic behavior. The HIM code is linear and does not account for this phenomenon. The essence of this data involves a comparison between measured and computed slopes (average of the slopes for experimental data). These values are a measure of the skull's structural stiffness in each of three roughly orthogonal directions.

A summary of the data is presented in Table 6-1 and shows clearly that the finite element model is from 1.2 to 2.2 times more stiff for the lower modulus and from 2.7 to 4.7 times more stiff for the higher modulus than the actual skull. At first it was believed that this discrepancy was due to errors in simulated skull thickness values. But after carefully reconstructing the geometrical simulation, only a small improvement was achieved. It is now believed that the difficulty is with the particular finite element formulation used for the skull element.

Table 6-1. Comparison of Experimental and Computed Structural Stiffness for Rhesus Skull No. 1

Direction of Loading	HSRI Experimental Stiffness (lb/in)	Computed Stiffness Using Low E (lb/in)	Computed Stiffness Using High E (lb/in)
A-P	12,600	15,527	33,693
L-R	3,700	8,011	17,367
S-I	3,087	5,777	12,470

The element employed is the eight-node brick, and it cannot effectively capture large bending stress gradients.* In the region of the skull bone directly beneath the load the deformation is primarily due to bending. However, in regions only a small distance away the bending stress gradients become small and the membrane stress values predominate. Here the element formulation is expected to work well. But in areas of large bending stress gradients, the solution is to use a different finite element formulation; either a 20-node brick, or a nonconforming formulation. To correct the problem an eight-node, incompatible finite element has been developed and checked by Taylor, et al.[63] and has been added to

*Several concomitant cantilever beam model studies verified this.

[63] Robert L. Taylor, Peter J. Beresford, and Edward L. Wilson. "A nonconforming element for stress analysis," International Journal for Numerical Methods in Engineering (submitted for publication, 1975).

the FEAP code element library. The element has demonstrated improved bending response and has been coded to list strains on the element surfaces. Unfortunately funds expired prior to incorporation of this element into the HIM code.

Comparisons of computed and measured strains are presented in Figure 6-4. The data are shown in "load versus principal strain" format. Loads were experimentally applied quasi-statically in 15 tests which are numbered consecutively from 3 to 17. Basically, the experimental data is acceptable and once again demonstrates the linearity of skull bone for the range of loading employed. In some load cases the spread in data is larger than in others. A trained eye may be able to discount some of it, but all the data received from HSRI is plotted in this validation effort. The computed data is shown for both the high and low elastic modulus E with a solid line and a dashed line, respectively. Each line is numbered corresponding to the element from which the computed principal strain was extracted. Also in each figure a Mohr's circle for strain is qualitatively sketched for both the measured and computed strain states. From figure to figure the relative circle size describes qualitatively the relative strain magnitudes occurring from test to test. The solid semicircle represents the measured values.

The primary consideration in looking over the strain comparisons is that the measured values are surface strains and the computed values are subsurface strains taken from an element in the vicinity of the strain gage. Within the element the computed strain is everywhere constant, but it portends to be most accurate at the element's centroid. The result is that comparisons are being attempted of measured and computed strains at points which differ in location; i.e., the gage point and the element centroid. Depending on the strain variation in the neighborhood of these two points, this difference may or may not be significant. Generally, however, it is known that the shear strain at subsurface position is nonzero (tends towards a maximum at the midthickness point) whereas on the free surface, the two shear strain components must always be zero in the absence of a traction force. Since shear strain is equivalent to the Mohr circle radius, the computed Mohr circles (for subsurface strains) are always expected to be larger than the measured Mohr circles and the results do bear this out.

In spite of the above limitations, at least qualitative evaluation can be made of the comparison presented in the nine parts of Figure 6-4. The results range from acceptable correlation to no correlation at all. This qualitative evaluation is summarized in Table 6-2.

Figures 6-4(d) and (e) show the computed strains bracket the experimental strains nicely. This is true to a somewhat lesser extent in Figures 6-4(c) and (i) if we choose to key on element 468 instead of 540. In all cases, element 468 seems to correlate better than element 540. Thus, in these four cases if an average Young's modulus were employed the computed strains would correlate acceptably well with average measured strains. This could also be true of the results in Figure 6-4(a) although the experimental data spread simply precludes any meaningful evaluation. The results show correlation ranging from poor to none at all in Figures 6-4(b), (f), (g), and (h). Results of Figures 6-4(b) and (h) demonstrate a qualitative agreement. Again assuming an average modulus, their error ranges from 50 to 100%. However, the results shown in Figures 6-4(f) and (g) show the model to be predicting much more strain (more than 100%) than what is being measured.

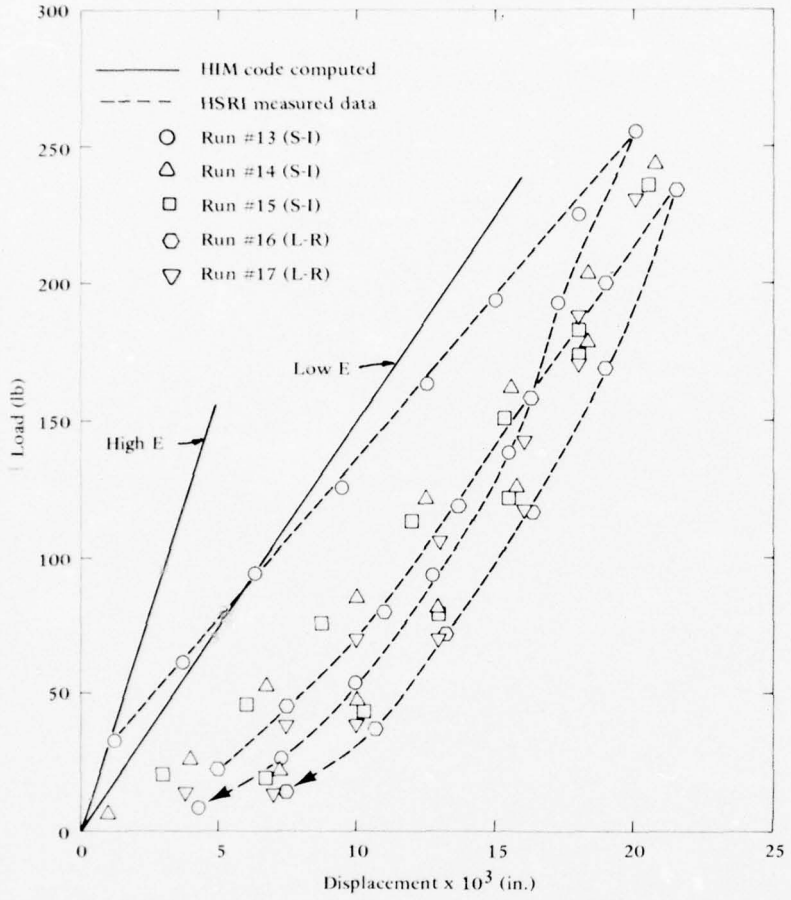

(a) A-P load versus A-P displacement.

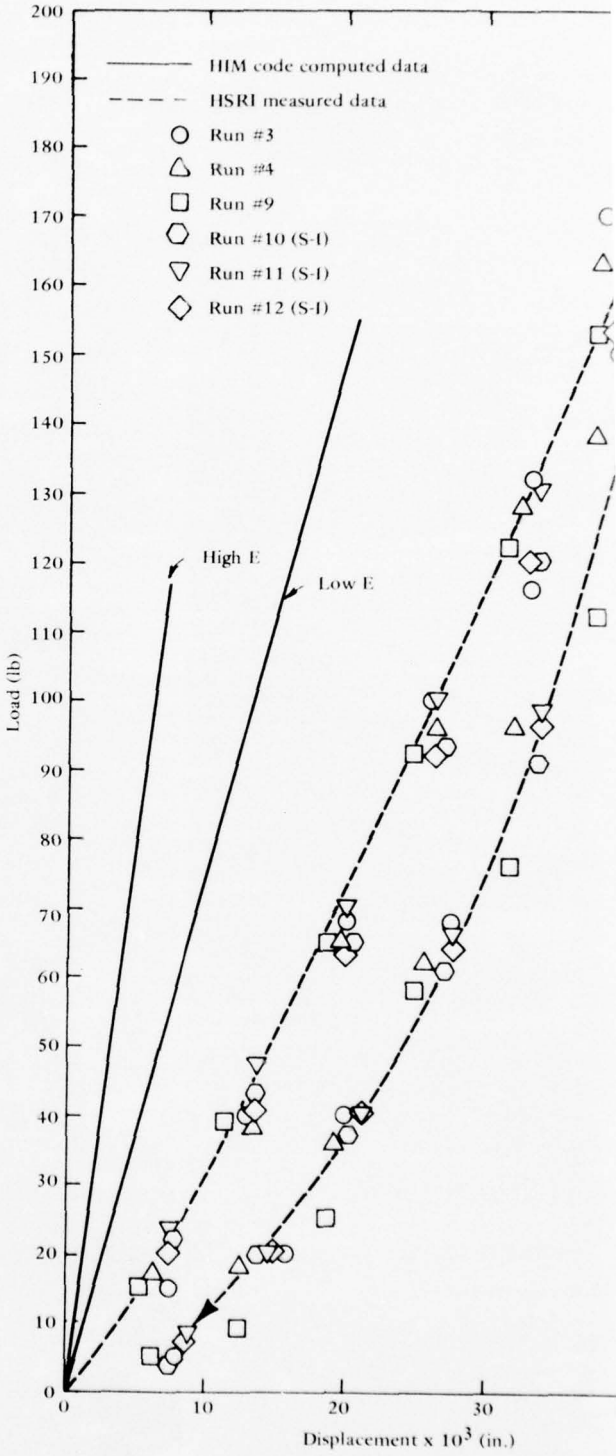

(b) L-R load versus L-R displacement.

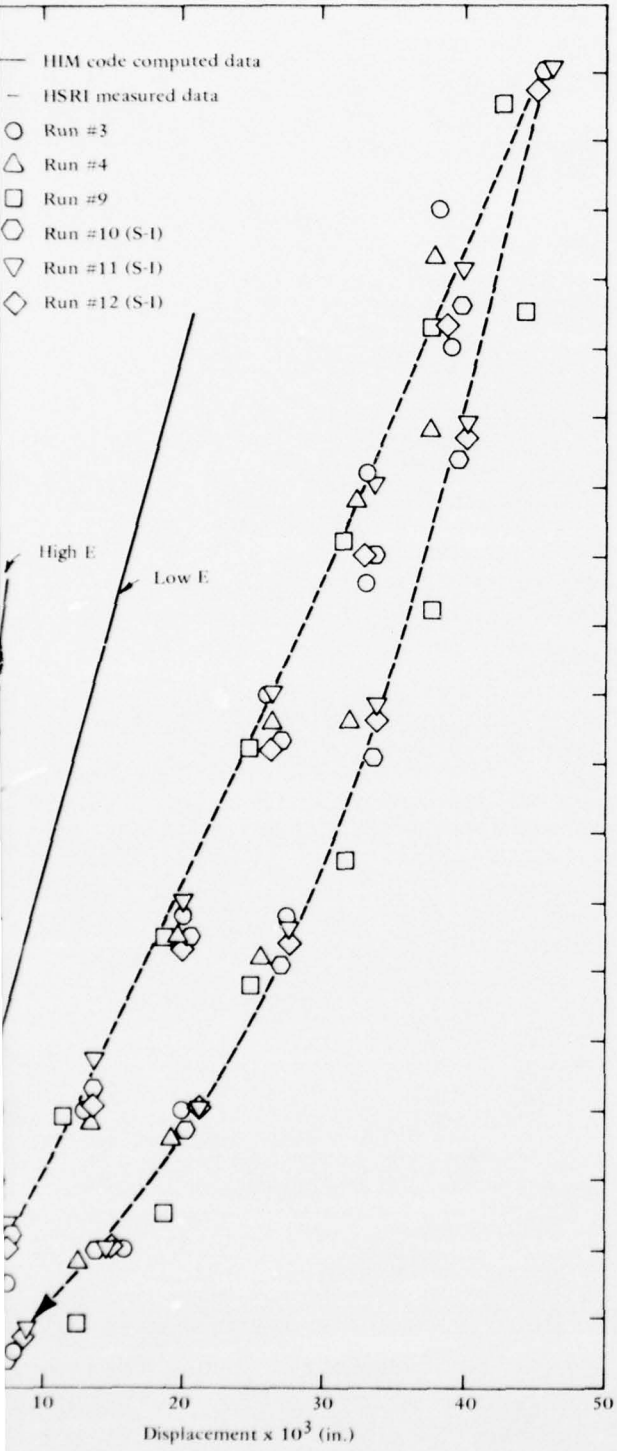

(b) L-R load versus L-R displacement.

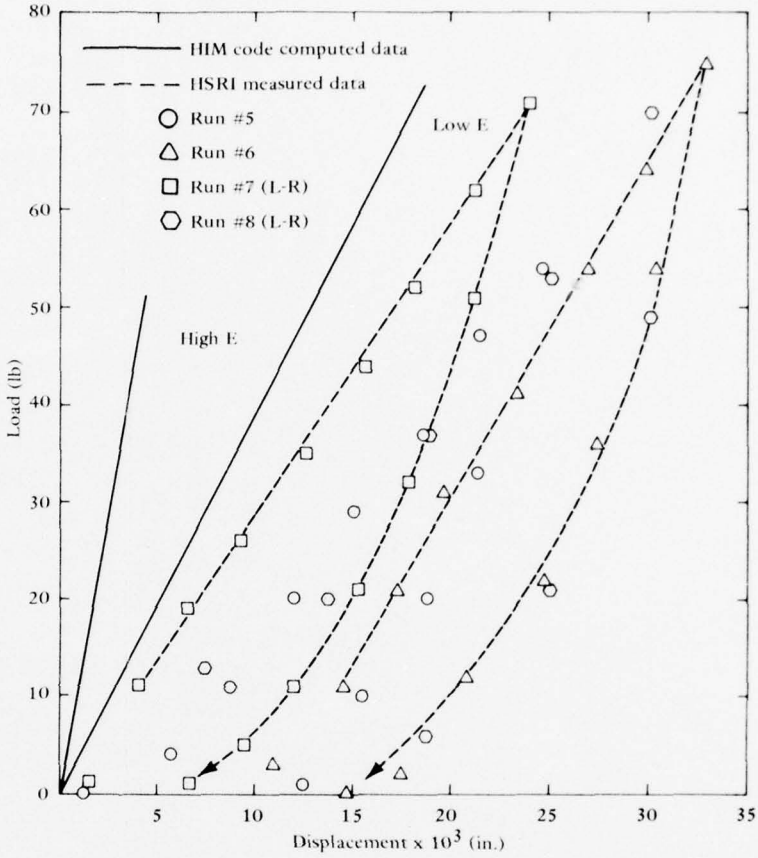

(c) S-I load versus S-I displacement.

Figure 6-3. Load and Displacement for Rhesus Skull No. 1.

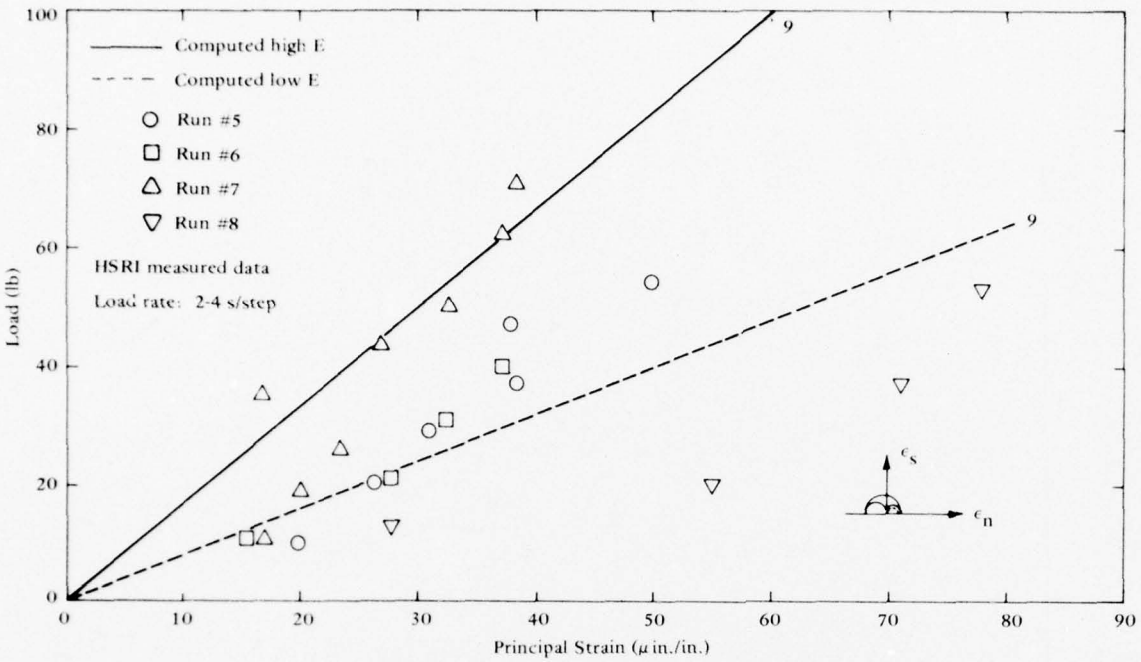

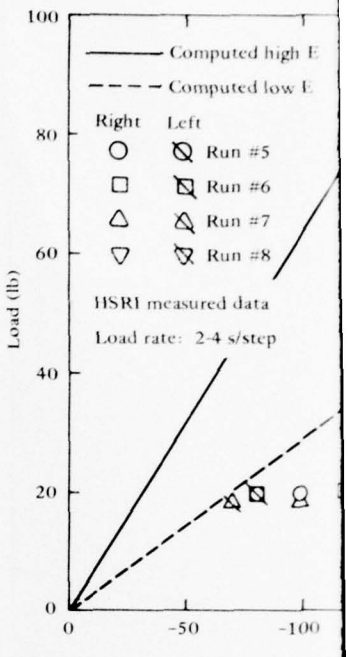

(a) S-I load versus frontal strain, E1.

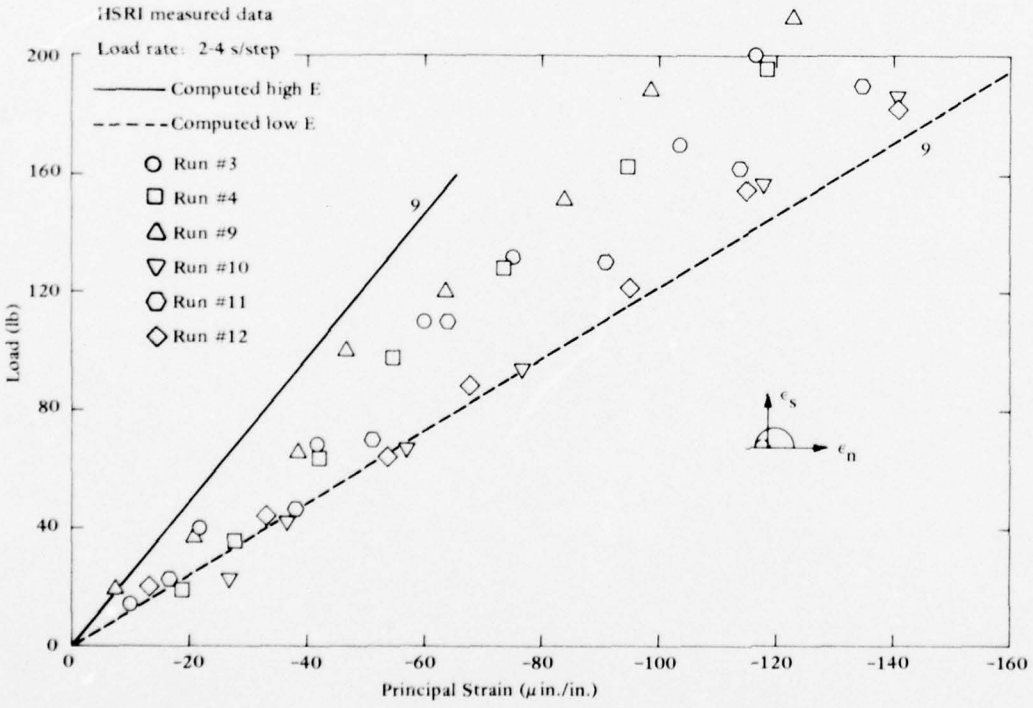

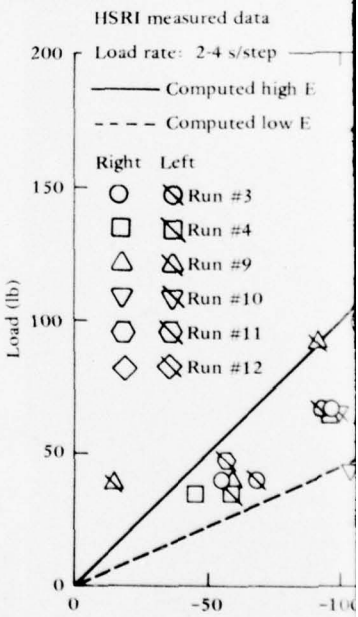

(d) L-R load versus frontal strain, E2.

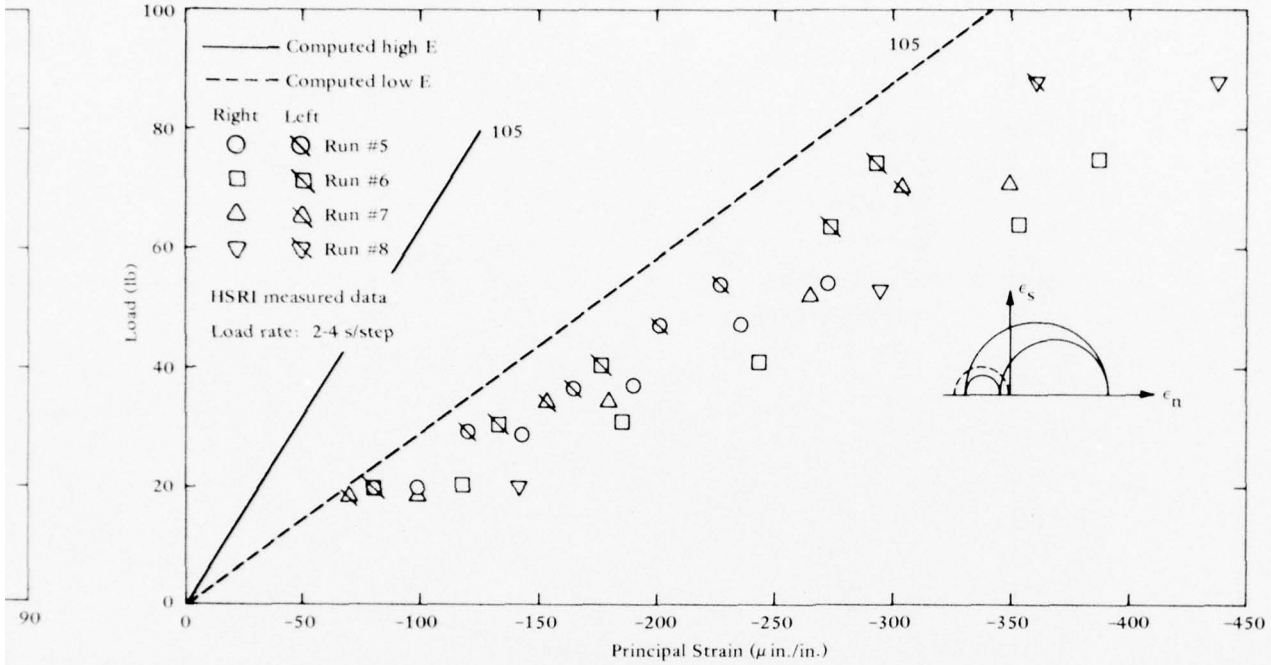

(b) S-I load versus parietal strain, E2.

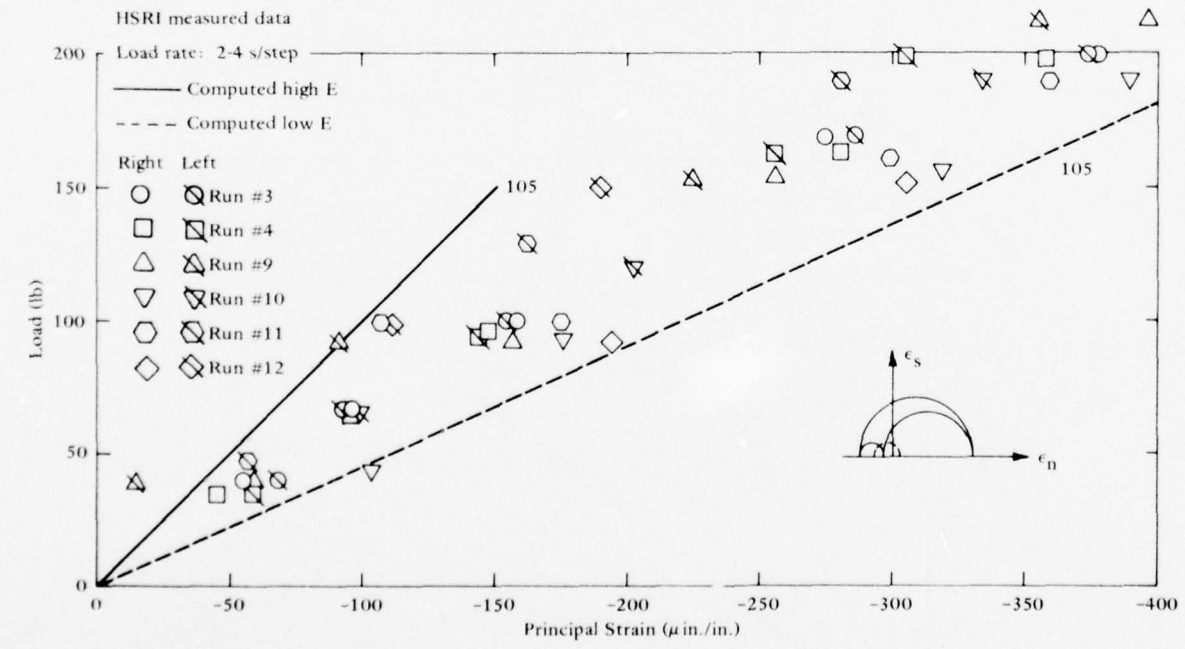

(c) L-R load versus parietal strain, E2.

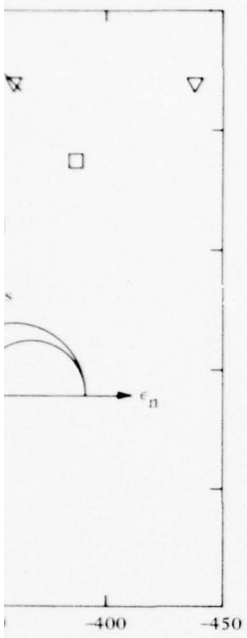

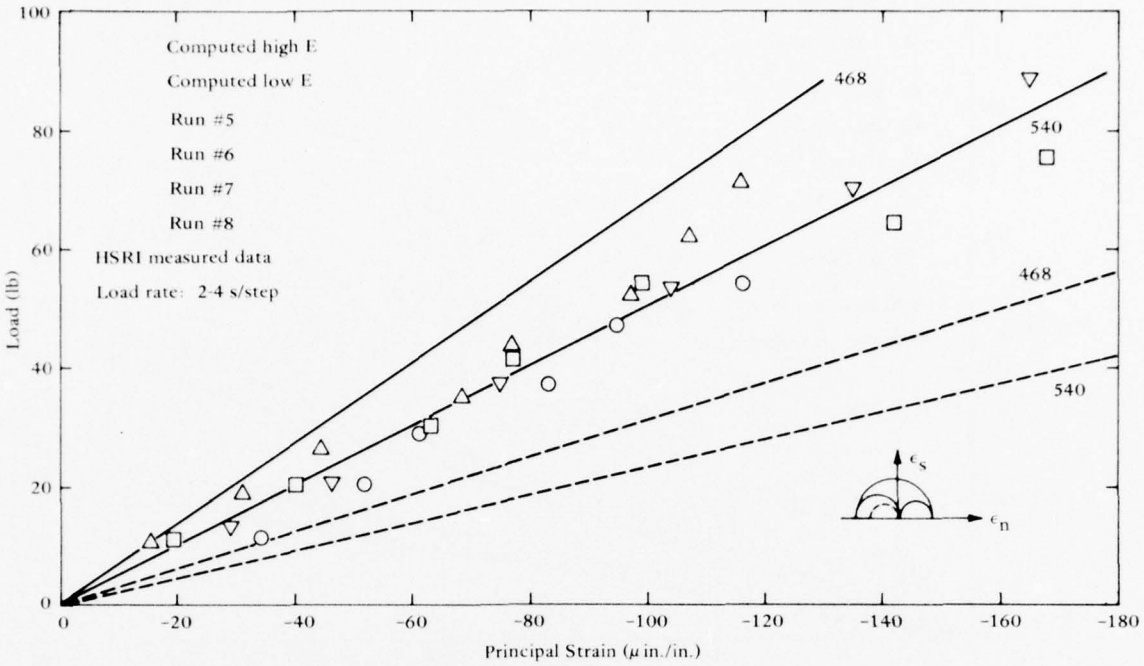

(c) S-I load versus occipital strain, E2.

Figure 6-4. Load and Various Strains for Rhesus Skull No. 1.

3

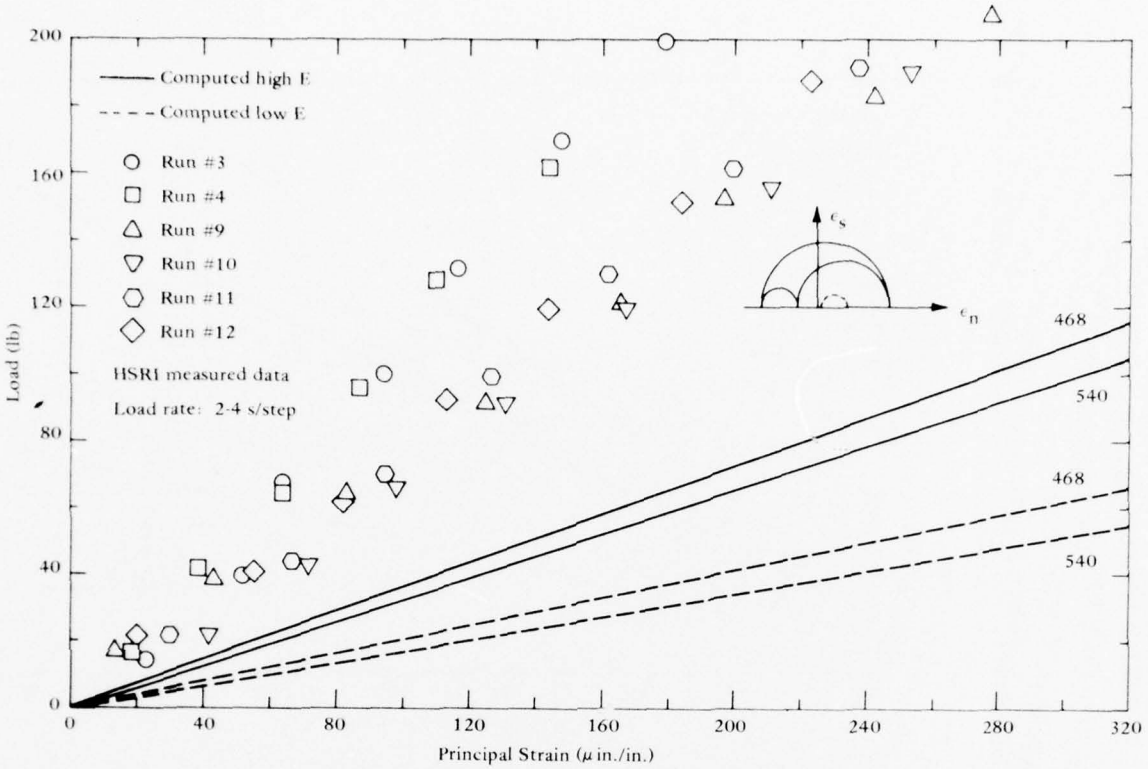

(f) L-R load versus occipital strain, E1.

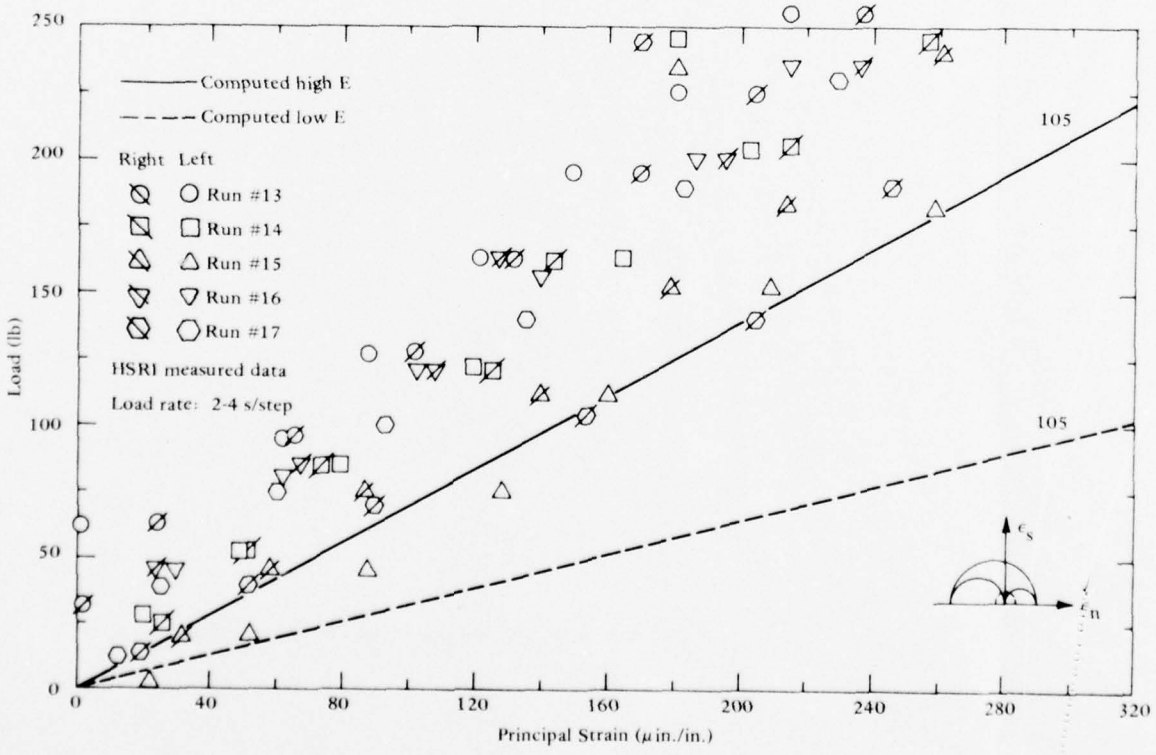

(h) A-P load versus parietal strain, E1.

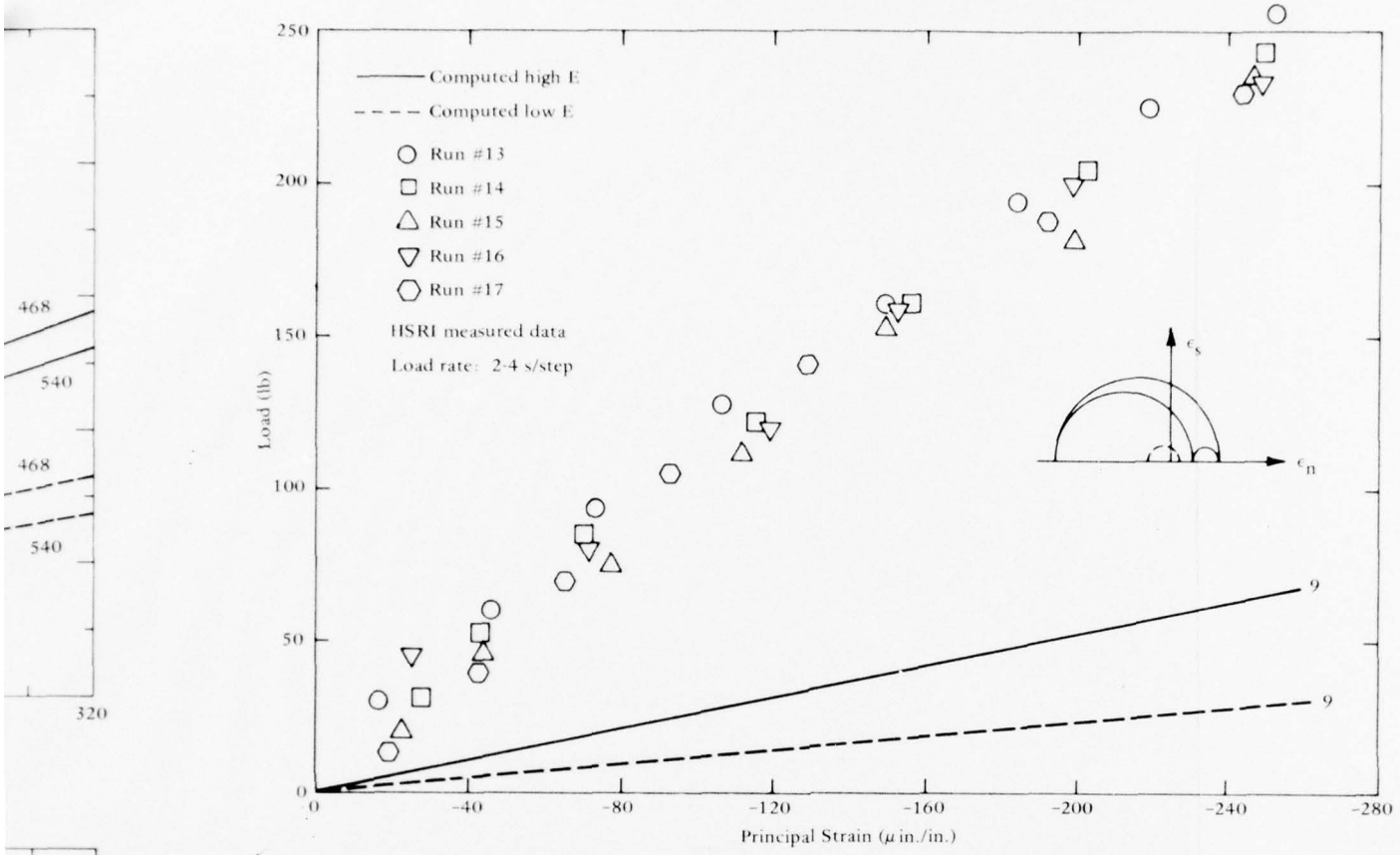

(g) A-P load versus frontal strain, E2.

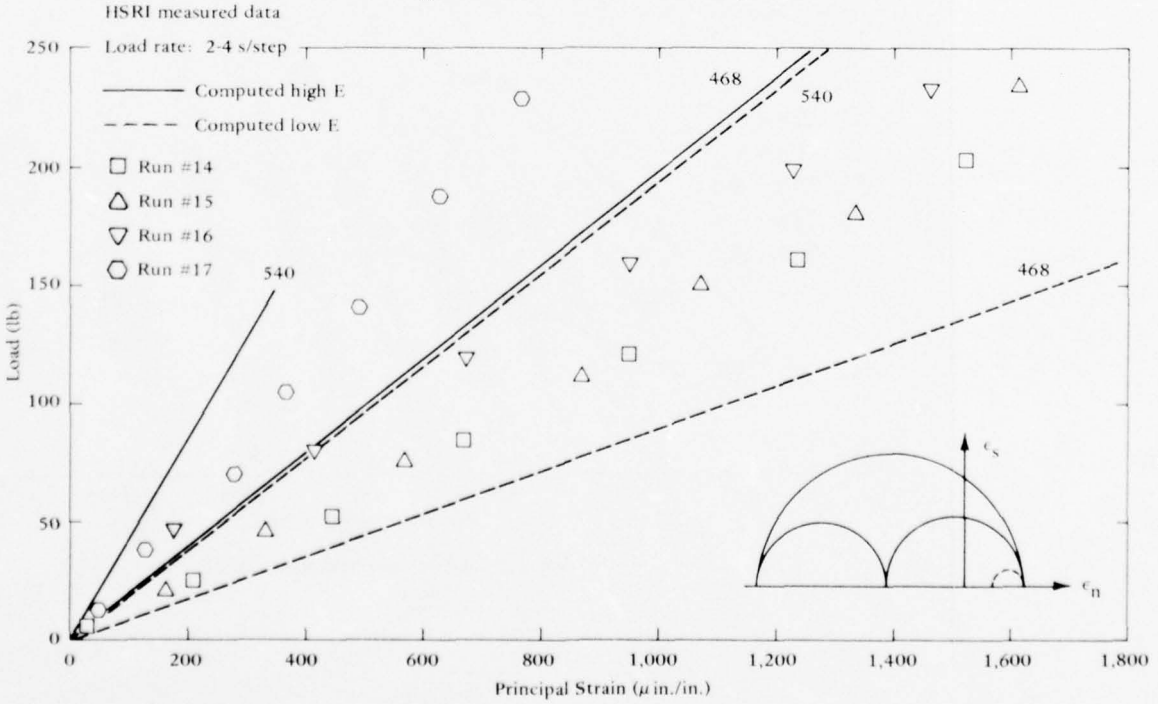

(i) A-P load versus occipital strain, E1.

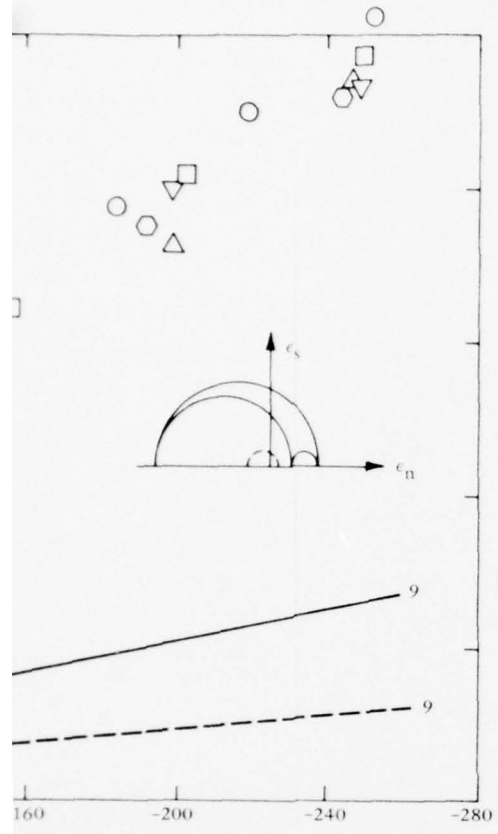

l strain, E2.

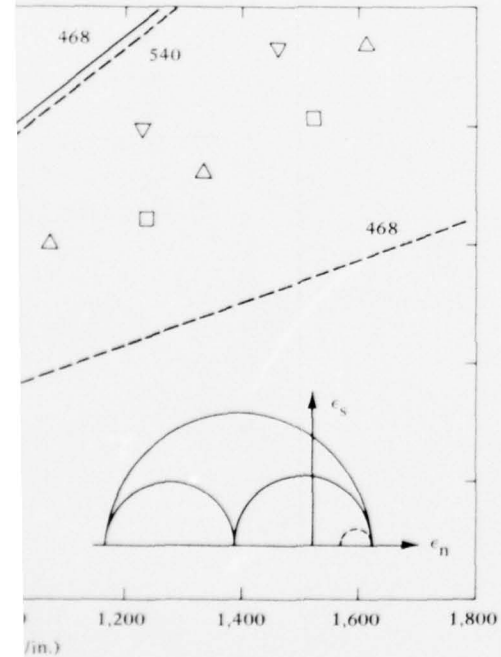

l strain, E1.

Figure 6-4. Continued.

Table 6-2. Qualitative Evaluation of Static Strain Correlation for Rhesus Skull No. 1

Figure No.	Type of Load and Strain	Evaluation	Comments
6-4(a)	S-I load, frontal strain	Possible correlation	Insufficient data
6-4(b)	S-I load, parietal strain	Poor correlation	≈ 50% difference
6-4(c)	S-I load, occipital strain	Acceptable correlation	———
6-4(d)	L-R load, frontal strain	Acceptable correlation	———
6-4(e)	L-R load, parietal strain	Acceptable correlation	———
6-4(f)	L-R load, occipital strain	No correlation	Computed values too large
6-4(g)	A-P load, frontal strain	No correlation	Computed values too large
6-4(h)	A-P load, parietal strain	Poor correlation	≈ 100% difference
6-4(i)	A-P load, occipital strain	Acceptable correlation	———

Dynamic Experimental Validation

There are two kinds of data and two different configurations involved in the dynamic validation phase which immediately followed the static validation effort. Dynamic cranial bone strains in both a dry rhesus skull and a live rhesus were to be used as correlative data. These strains were induced by impacts in a controlled laboratory environment. More importantly, dynamic intracranial pressure data recorded for the live animal impacts were to be used to correlate measured and predicted brain response.

Dynamic Skull Bone Response. In the first configuration the empty rhesus skull was anchored to a laboratory test frame with a wall-anchor bolt assembly inserted through the skull's foramen magnum so that the skull base was immovable against various dynamic impacts. Four strain gage rosettes were located on the frontal, the two parietal, and the occipital cranial bones. The HSRI principal strain data shown in Figure 6-5 were recorded for a 3.8 ms impact on the superior surface in the S-I direction. The peak load was 63 pounds applied over an area of 1/2 sq. in. The strain magnitudes are typical of this series of experimental tests. The first impression of these measured strains were that they appeared too low. They are on the whole about five times smaller than the strains recorded during the static validation tests at equivalent peak load levels. This difference can be explained from an examination of the geometry of the applied load and boundary condition at the skull base.

In the static load cases the applied S-I loading was equilibrating, causing the rhesus skull to be "pinched" in the S-I direction (see Figure 6-1). In the dynamic case the applied S-I load vector does not pass through the base support but rather forward of it, and instead of pinching the skull it bends the skull as in a cantilever. The configuration of the corresponding HIM code simulation illustrates this in Figure 6-6. This causes rigid body motion of the skull about its support, but motion not present in the static tests. Thus, the dynamic strain levels recorded may well be below those recorded for the static case as mentioned above.

If the test setup had been arranged so that the dynamic load vector passed through the support, subsequent simulation of the test would have gone more smoothly. Review of HSRI high speed film revelaed that the wall-anchor bolt assembly deflected elastically under the impact of the controlled blow. This meant that the corresponding HIM code simulation had to account for this motion instead of merely constraining the nodal points at the foramen magnum against movement. Several load-deflection tests of the wall-anchor bolt assembly had to be conducted at CEL to determine its structural properties. These properties were then translated into an equivalent wall-anchor bolt finite element which was added to the base of the simulted skull. This process is, at best, only roughly approximate. Nevertheless, the computed strains for the simulated S-I impact are shown in Figure 6-7. The upper curve represents the computed strain history for complete restraint of the skull base, and the lower curve represents the strain history for an elastically restrained skull base. Obviously the restraint greatly influences the predicted strain. Although many more computer simulations were conducted in this validative effort, the two curves represent the limits of strain response predicted.

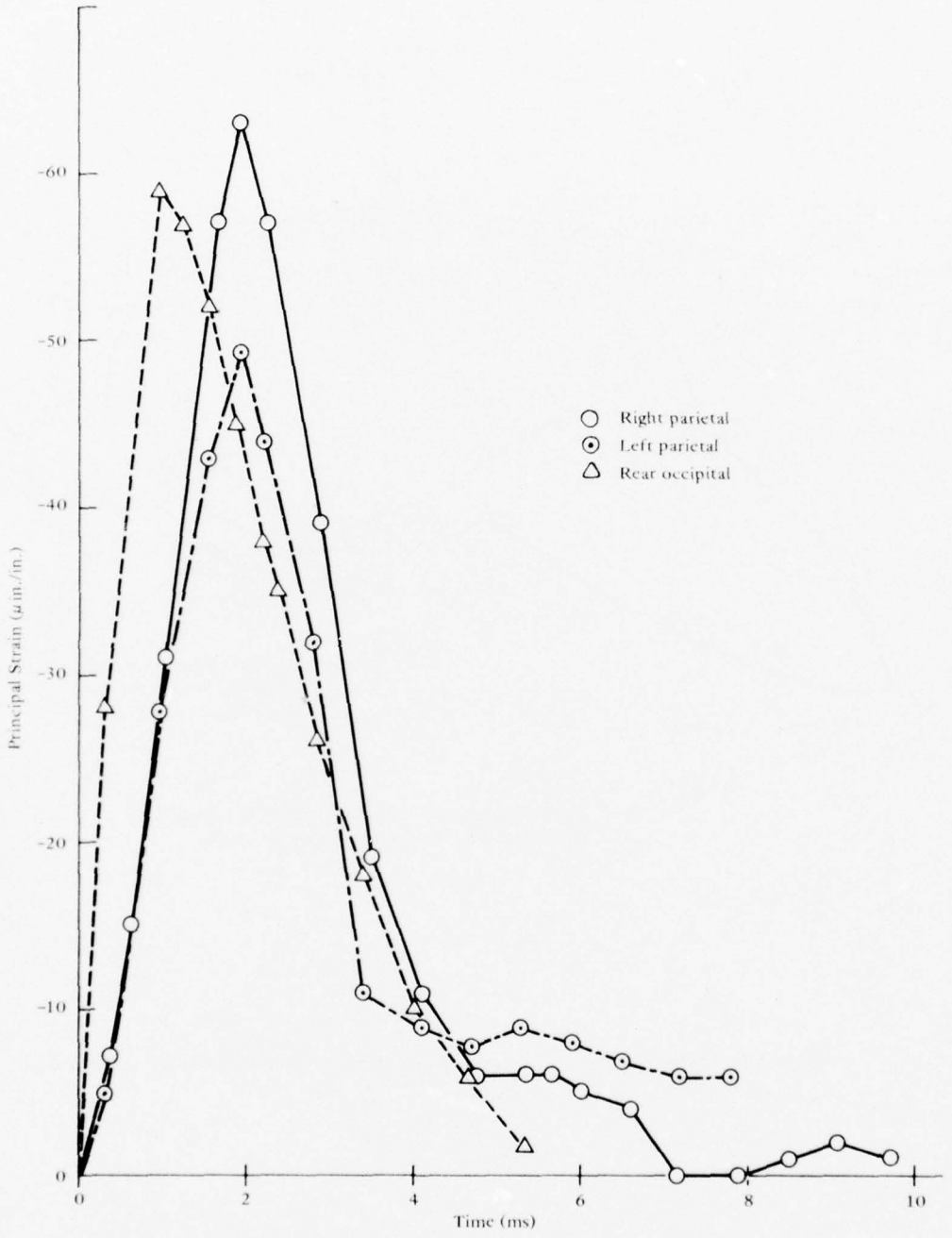

Figure 6-5. Experimental Dynamic Strain in a Rhesus Skull.

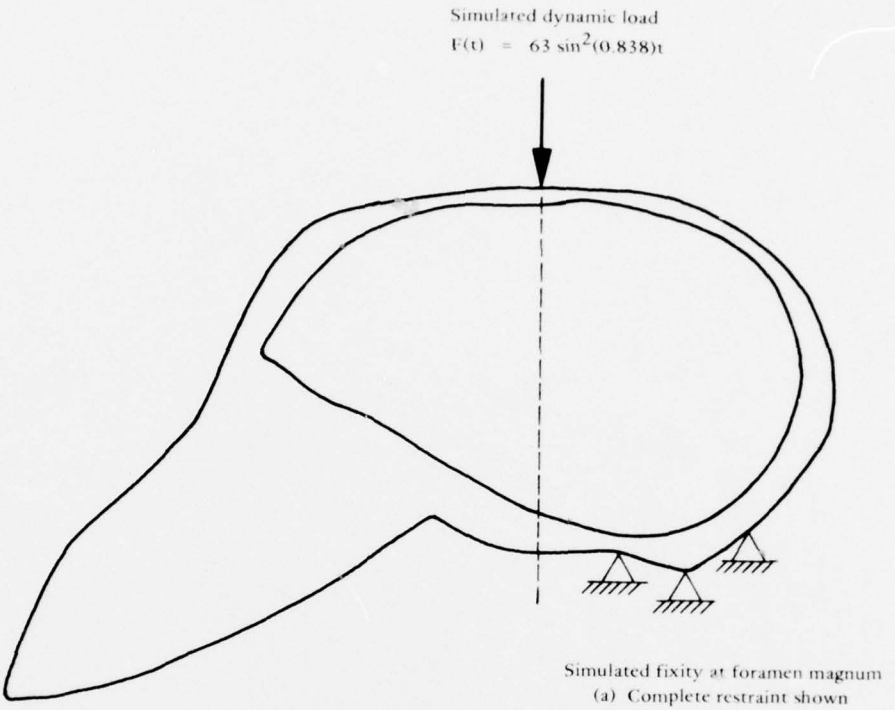

Note: Facial bone complex excluded mandible in both HSRI experimental test and corresponding simulation.

Figure 6-6. Finite Element Model for Simulating Dynamic Rhesus Skull Experiment.

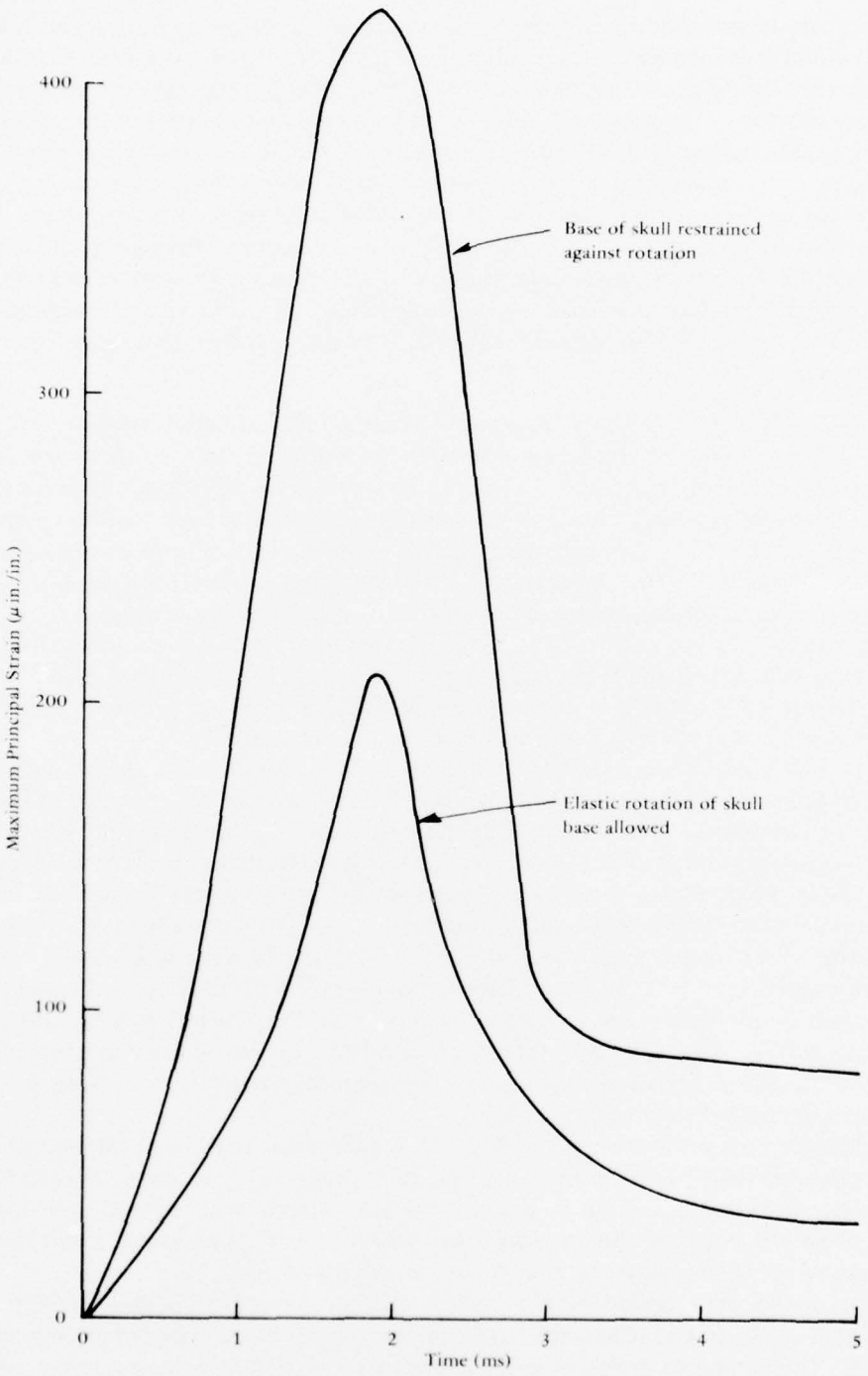

Figure 6-7. Computed Dynamic Strain in Rhesus Skull Parietal Bone.

The primary observation when comparing the measured and computed strains is that the computed strain is at least three times greater in magnitude. (Care was taken that the computed strain was sampled at a location near the corresponding strain gage rosette on the rhesus parietal bone.) Comparisons of computed and measured dynamic strains elsewhere on the rhesus skull consistently revealed that the model predicts strains by a factor between three and one order of magnitude greater than measured strains. The discrepancy was ascribed to the eight-node isoparametric element whose stiffness, as discussed in the static validation, did not adequately capture the skull bending response. Because of the inherent difficulties in attempting to match finite element model strains with those of the actual skull, it was expected that correlation would be difficult. The finite element model, however, should be capable, in this instance, of better correlation and on that basis requires improvement.

Dynamic Intracranial Pressures. A series of experimental validation tests was conducted by HSRI with live rhesus monkeys in an anesthetized condition. In the case of A-P (rear) impacts, two specially prepared pressure transducers were surgically placed in the skull to monitor intracranial pressure. One was located in the left parietal bone near the point of impact, and the other was in the forward right corner of the frontal bone over the tip of the right frontal lobe of the brain. A schematic of the pressure transducer system is presented in Figure 6-8. The transducer sensor is not located in a subdural position; instead, it is carefully placed epidurally but very close to the dura. Approximately one eye drop of silica gel fills the notch in the skull and is intended to provide a pressure transmitting medium. In this way the pressure measured is said to be equivalent to the intracranial pressure even though the sensor is not in direct contact with any intracranial material.

A typical measured pressure history is shown in Figure 6-9. In this case the data are from the front pressure transducer, and the applied load was from the rear so that the data are said to be contrecoup pressure. The applied peak load magnitude in HSRI run number 003 was 800 pounds and the duration of loading was 2 ms which amounts to fairly rigid impact. The initial peak pressure is about 13 psi tension and occurs at about 1 ms and the next peak is 19-psi compression occurring just after 2 ms. The second peak is believed due to the influence of the rhesus neck structure in reversing the forward acceleration due initially to the applied load. Since the primate is heavily anesthetized, this may be neither a voluntary nor an involuntary neck reaction but just from the physical presence of the neck and thoracic inertia. The first peak is the classical tensile pressure at the contrecoup location. More importance is placed on it because it is popularly thought that tensile pressures are more conducive to brain injury.

Several associated computer runs with the HIM code were made in an attempt to correlate the computed response with the above measured intracranial response. In each successive computer run adjustments to the model were made which were believed to be improvements in either the model or the simulation and which, it was hoped, would bring the computed pressure into closer agreement with the measured pressure.

The midsagittal plane discretization of the simulated rhesus skull is shown in Figure 6-10. Neither the scalp and other soft tissue nor the mandible are included directly in the discretization. The combined mass of these components was, however, subsequently computed and added to the model by increasing the density of the outer layer of skull bone

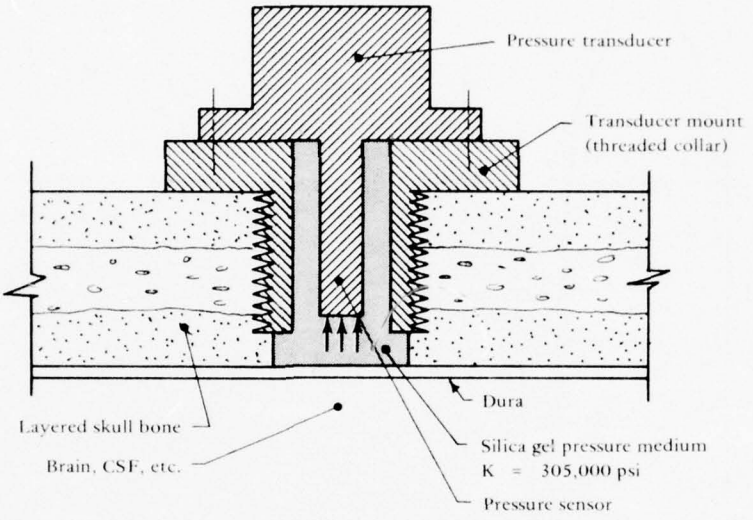

Note: 1. Not to scale.
2. Notch is from 7 to 10 mm in diameter.
3. Sensing element tip is about 2 or 3 mm off the dura surface.
4. Only an "eye drop" of silica gel is inserted into notch.

Figure 6-8. Schematic of HSRI Pressure Transducer and Mount.

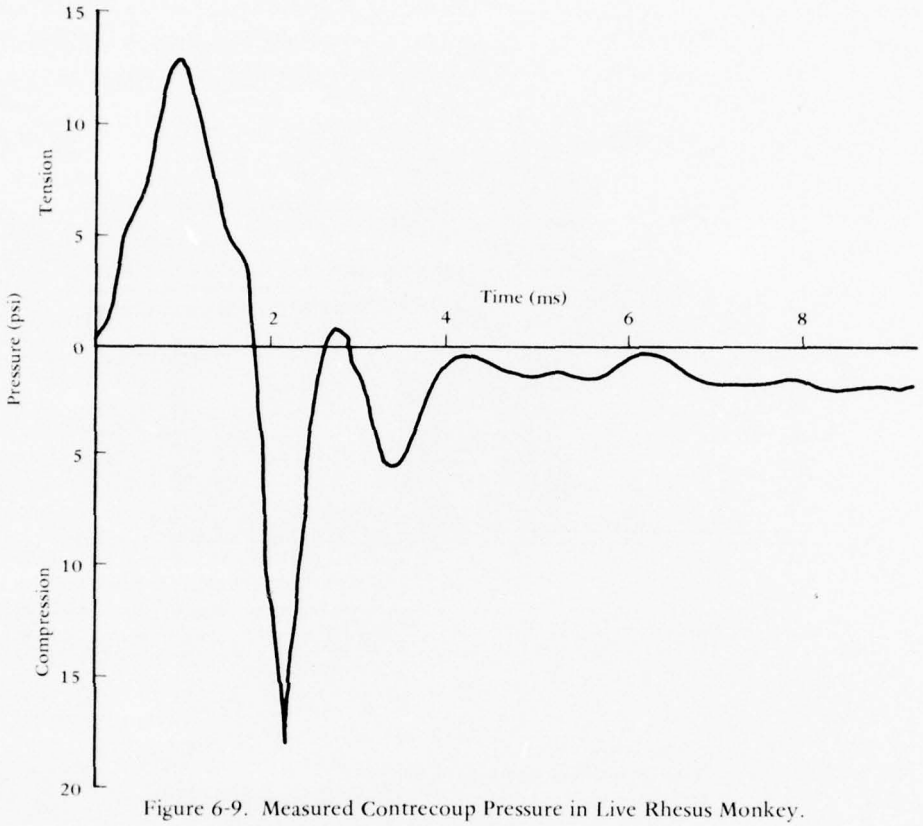

Figure 6-9. Measured Contrecoup Pressure in Live Rhesus Monkey.

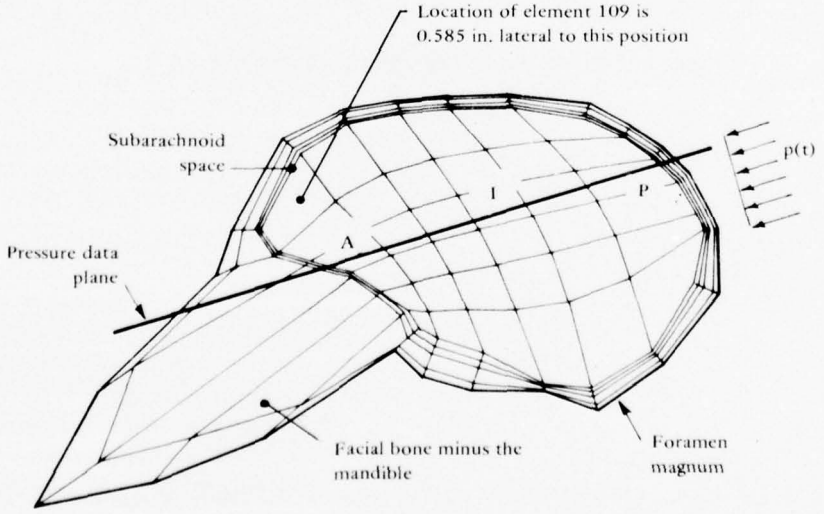

Figure 6-10. Midsagittal Plane Discretization of Rhesus Skull.

material by an appropriate uniform amount. The facial bone structure of the rhesus skull is very complex and extensive when compared to the human skull. Although much effort was expended in an attempt to include the mandible in the rhesus discretization it proved too difficult (unlike the human model in which the entire facial bone complex was included). The other facial bones were difficult and their discretization (shown in Figure 6-10) was not achieved easily. Perhaps a more important consideration in evaluating the live rhesus monkey simulation configuration is the unknown boundary condition at the base of the skull. As stated above, the neck is believed to influence the rhesus head acceleration (actually reversing it) subsequent to the impact. Since the corresponding model does not possess a neck structure, the neck reaction forcing function on the skull would normally be considered as necessary input information as is the simulated impact force. If this information were available it could easily be input to the model nodes at the base of the skull—but it is not known nor is it known how it can be measured. Therefore, the only recourse is to assume some reasonable displacement boundary condition for the nodes. The choices for this condition in the present HIM code version are completely unrestrained nodes, completely restrained nodes, or constrained nodes that slide along a prescribed flat plane. (These cases are evaluated and discussed in conjunction with the human model in the next chapter.) The best course of action appears to be to assume a completely unrestrained (free) condition for these nodes. At least the initial peak (tensile peak) in the measured intracranial pressure-history should be unaffected by the neck reaction. Indeed the HSRI experimental configuration was designed to create a "free body" condition for the live rhesus head at impact by aligning the head in front of the impactor with light supportive surgical thread attached to the primate's ears. Thus, it is believe to be better in the corresponding simulation to model the rhesus skull with no restraint at the skull base. Computed intracranial pressure data was extracted and examined at element 109, which corresponds closely to the HSRI transducer location, and also along an anterior-posterior (A-P) plane as shown. The anterior point (A), intermediate point (I), and posterior point (P) are in the midsagittal plane. Element 109 is not in the midsagittal plane.

The simulated impact force-history is shown in Figure 6-11 and was uniformly distributed over an area of approximately 1/2 sq in. It simulates the short duration blow delivered symmetrically about the midsagittal plane with a hard impactor.

Results of the HIM code simulations of the live rhesus monkey test are shown in Figures 6-12(a) through (f). An integration time step size of 130 μs was employed in all the computations except as noted. This series of six computer runs consitute the more important attempts to compute intracranial pressures which, it was hoped, would correlate with those pressures measured (Figure 6-9). More specifically the objective of the computation was to agree as closely as possible with the peak tension pressure of 13 psi observed by HSRI.

In the first simulation, Figure 6-12(a), the rhesus skull model contained no opening through the cranial base where the foramen magnum is normally found and through which the brainstem passes. This was the existing configuration of the model at that time. Though element 109 produced a relatively high peak tensile pressure of 35-psi tension, these results were initially encouraging because it was believed that the intended subsequent inclusion of the foramen magnum would uniformly lower the computed pressure. Also it was very uncommon to find any head injury model predicting peak intracranial pressures below 100 psi at that time.[16]

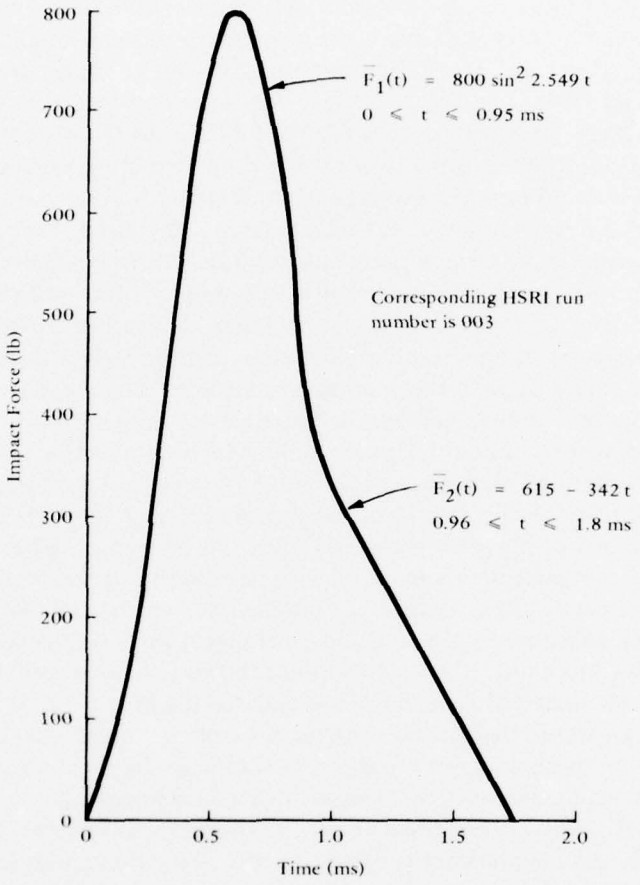

Figure 6-11. Simulated Dynamic Load.

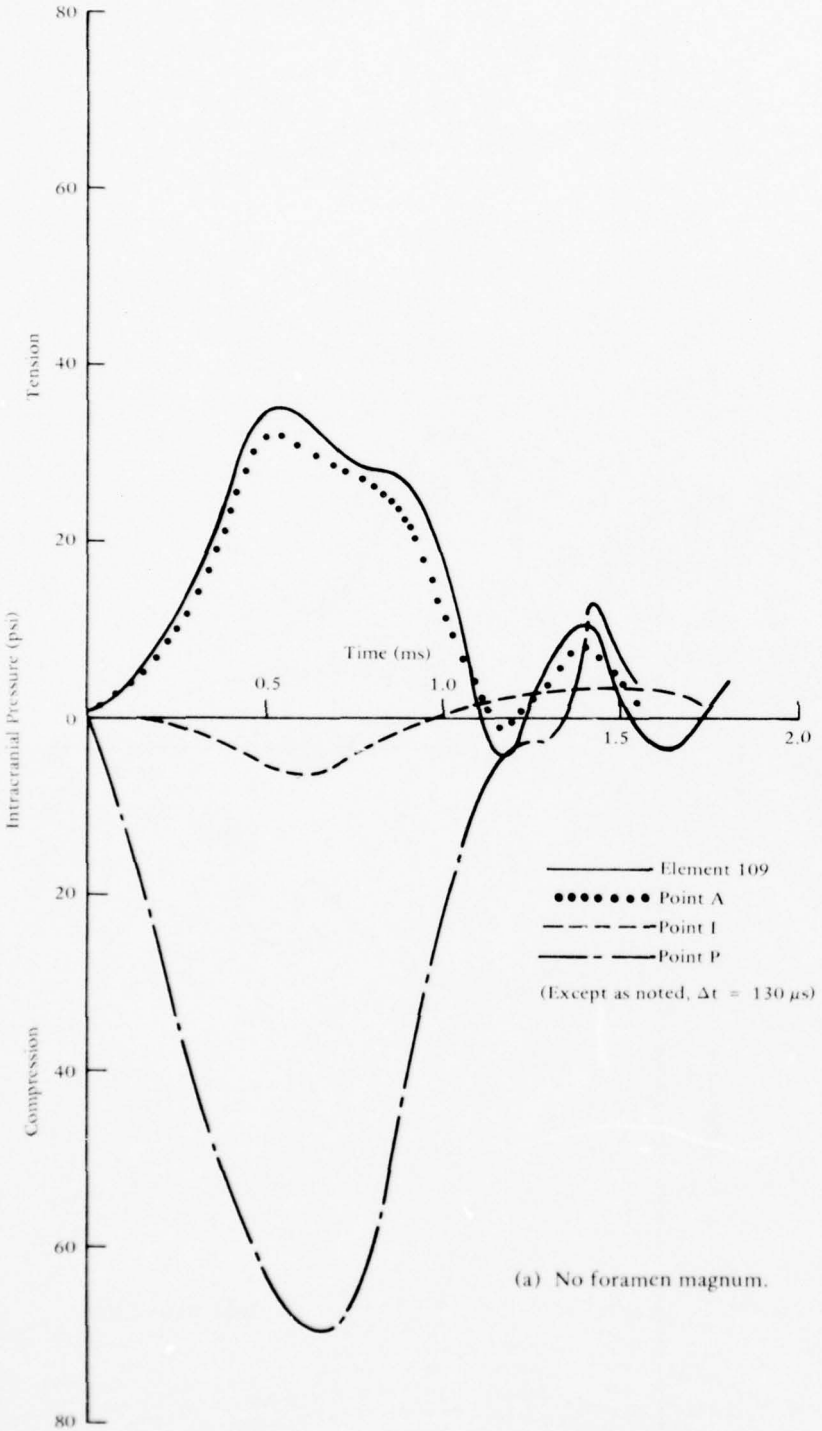

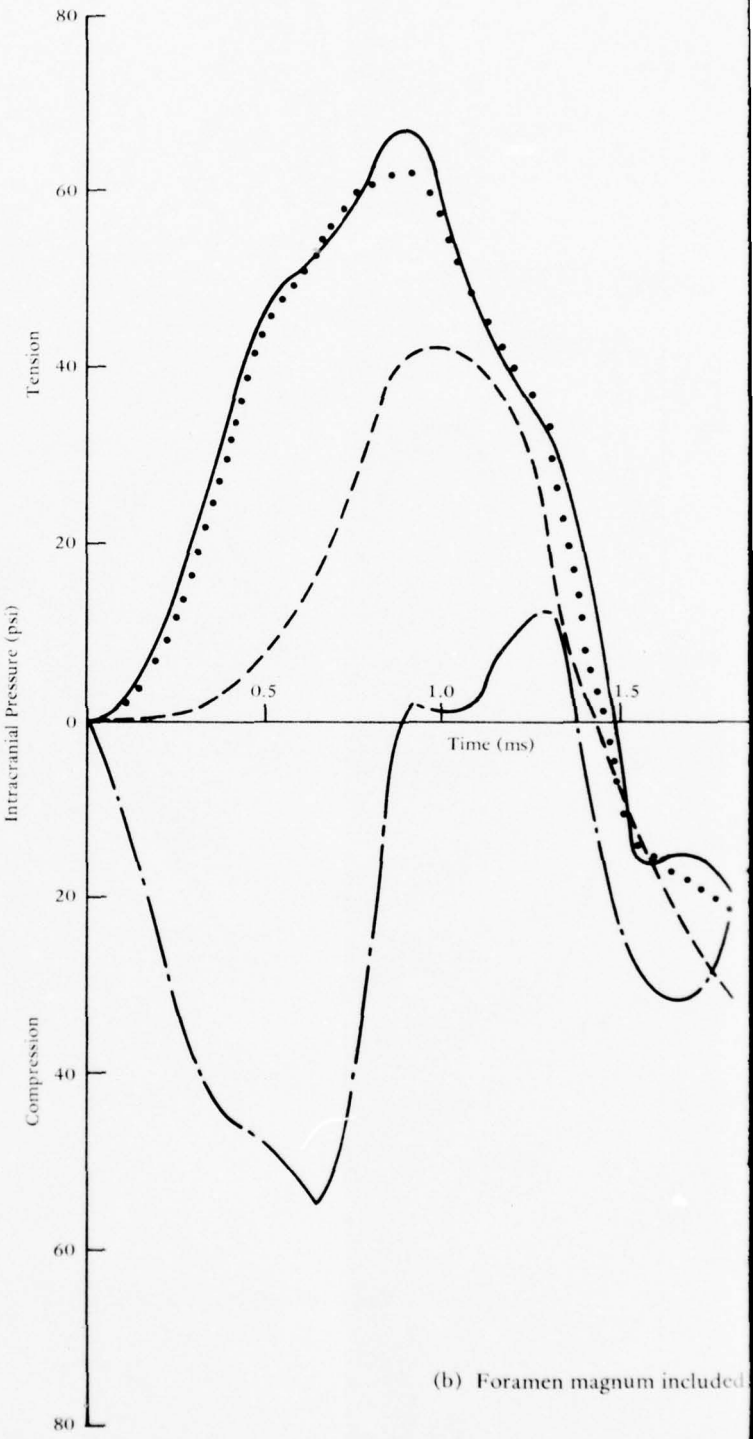

Figure 6-12. Computed Intracranial Pressure History.

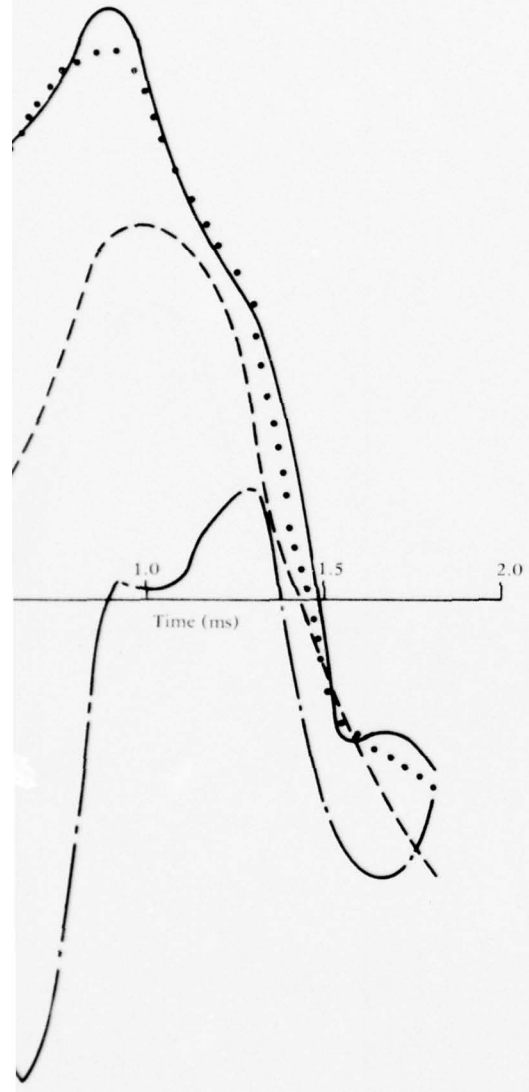

(b) Foramen magnum included.

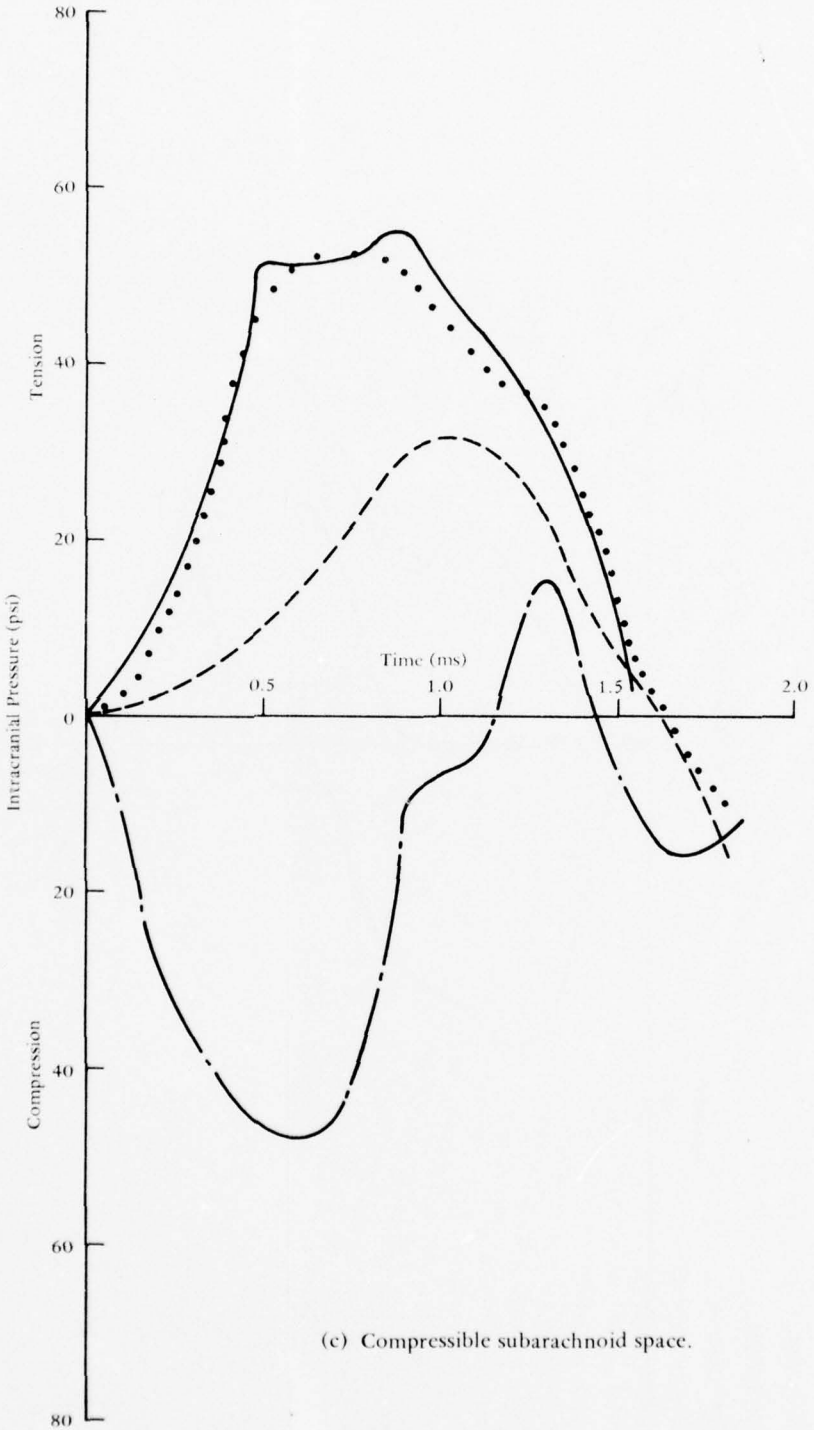

(c) Compressible subarachnoid space.

nputed Intracranial Pressure History.

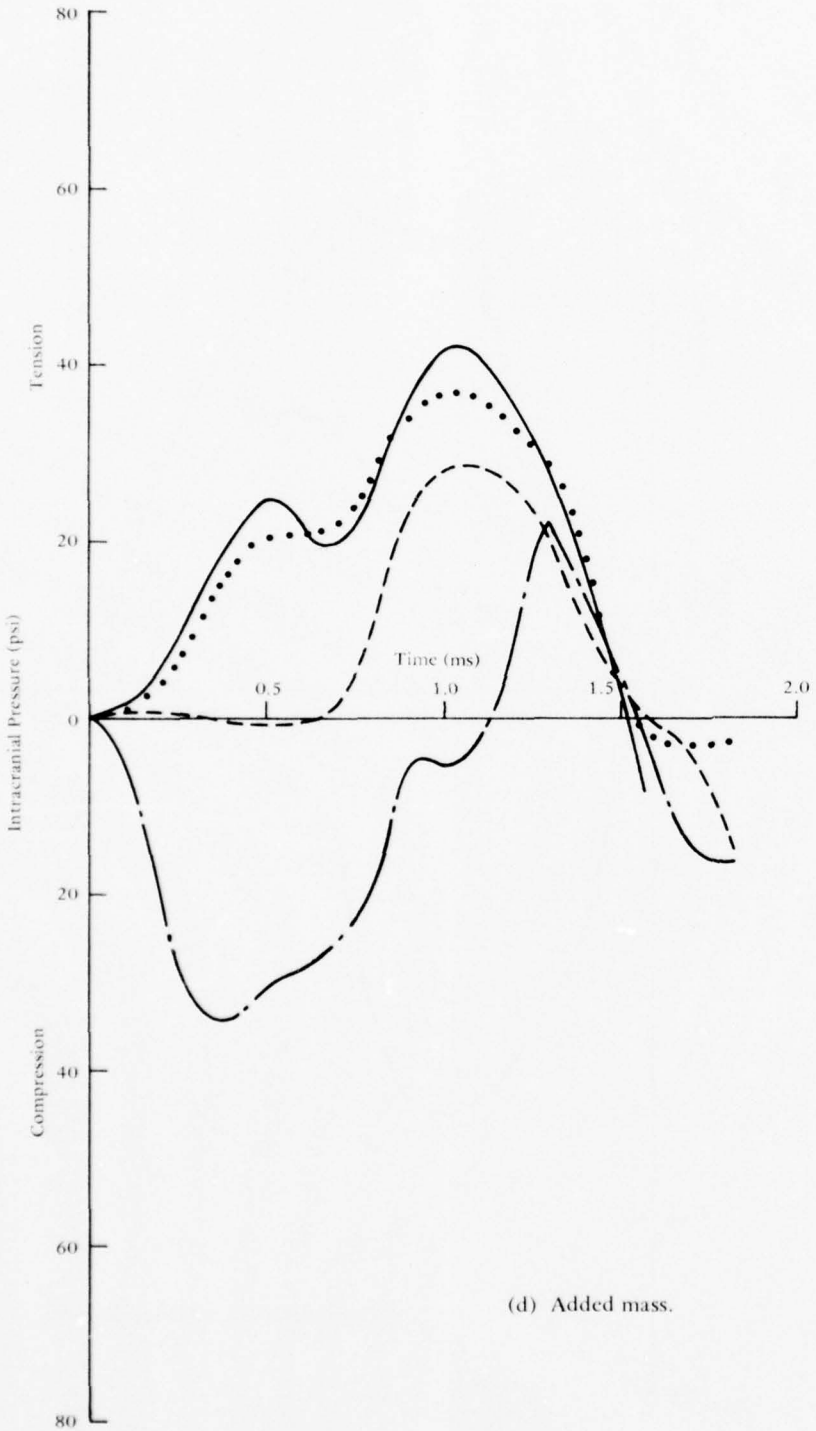

(d) Added mass.

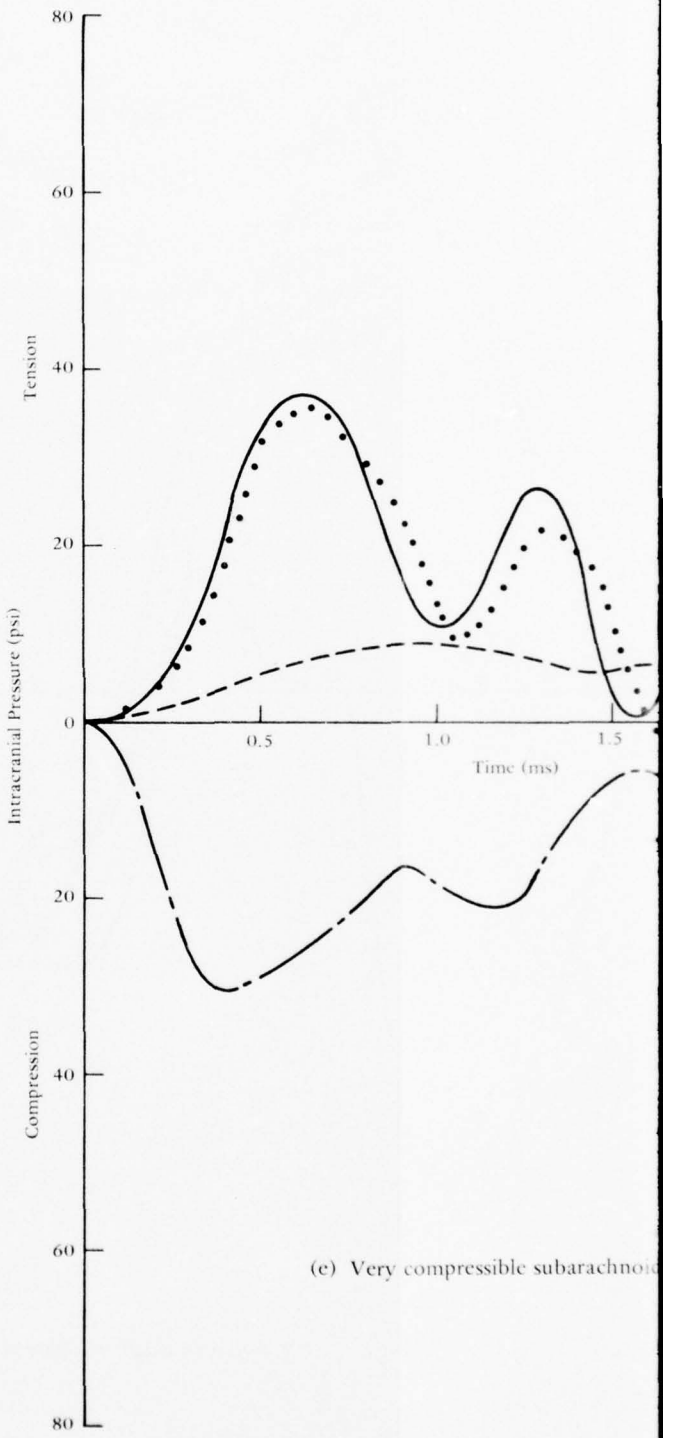

(e) Very compressible subarachnoi

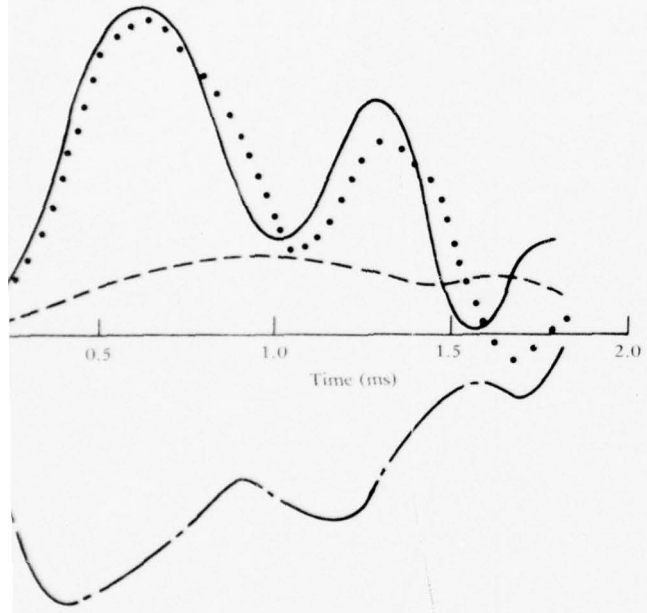

(e) Very compressible subarachnoid space.

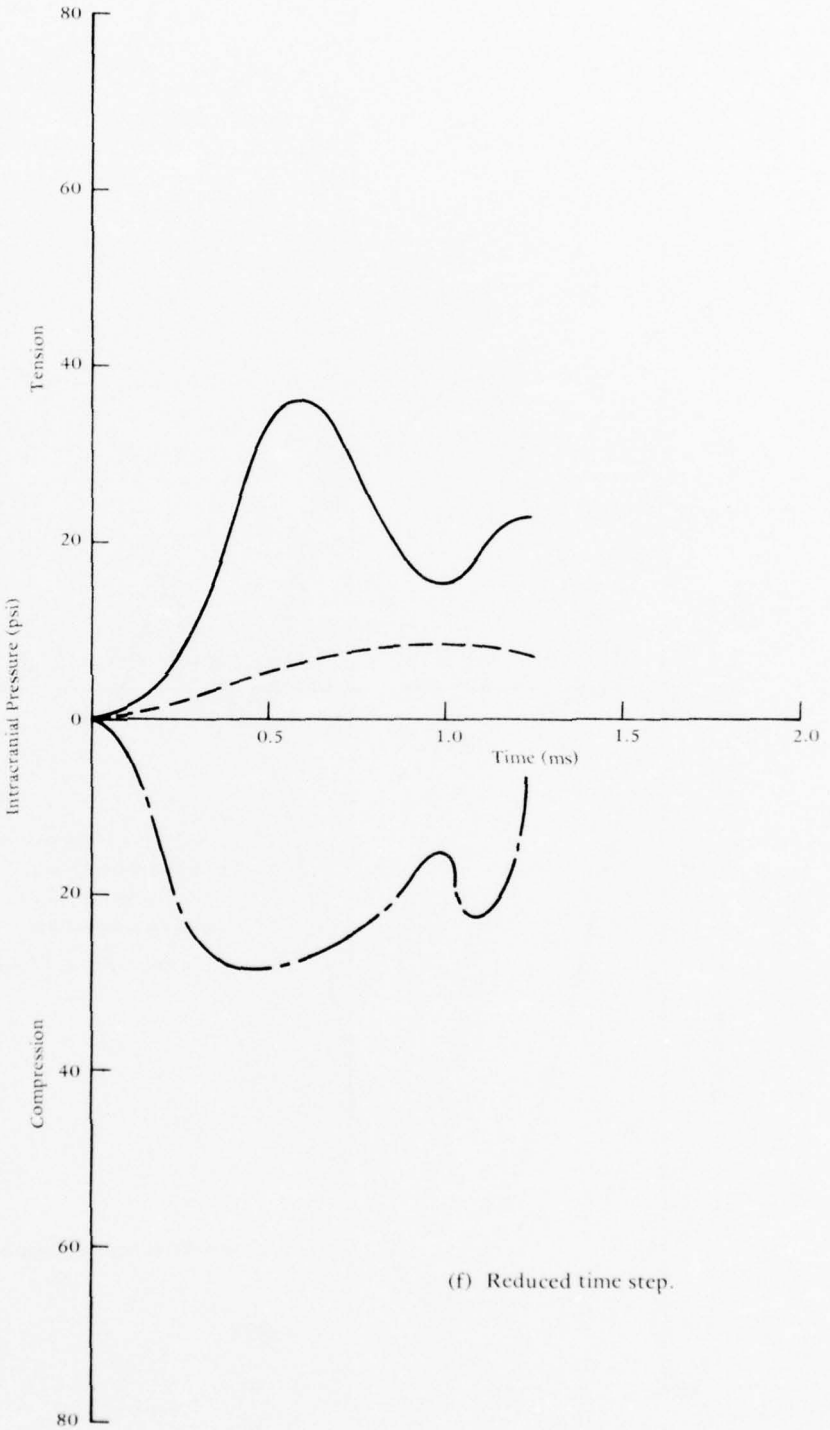

(f) Reduced time step.

In the remaining five simulations the specification of bone material properties for the finite elements in the region of the foramen magnum (see Figure 6-10) was removed and replaced as follows. The outer layer of elements were assigned to be soft and elastic in the manner of a membrane sealing over the foramen magnum aperture. The next three innermost layers were assigned the mechanical properties of the brain material and were thought of as simulating a rather truncated brainstem. In the absence of a neck model, it was hoped that this would provide a more realistic approximation to the region of the foramen magnum and brainstem while still providing containment (necessary for numerical stability) for the simulated intracranial contents.

The results in Figure 6-12(b) were very surprising, however, because while the computed pressure at point P decreased, the tensile pressure extracted from element 109 increased from 35 psi to 67 psi. A general decrease in overall intracranial pressure did not occur as was expected, but instead a shift in the distribution of the pressure materialized. This was unfortunate from the standpoint of achieving correlation of the 13-psi peak tensile pressure in the region of element 109. But for reasons which will be explained more fully in a subsequent discussion on statistics of observed head injury distribution a return to the "no foramen magnum" configuration could not be justified. Also in this simulation the applied load was improved by including both $\bar{F}_1$ and $\bar{F}_2$ exactly as shown in Figure 6-11 whereas the previous simulated load included only $\bar{F}_1$. Comparison with the measured impact force history showed that the combination of $\bar{F}_1$ and $\bar{F}_2$ gave a better approximation of the actual load. This change would explain the difference between Figure 6-12(a) and (b) in the "trailing off" portion of the computed intracranial pressures. Something still had to be done with the model to reduce the predicted pressures, and there remained a modification that had been intended but yet was untried.

Since the brain is not continuous with the internal cranial wall but is supported and tethered at the skull/brain interface, a method was devised to approximate this suspension. The single layer of elements which simulate the subarachnoid space was provided in the basic HIM code configuration for this eventuality. Up to this point, the mechanical property specification for these elements has been identical to that of the brain elements. This, combined with the displacement continuity imposed by the finite element method, effects a continuous support. However, by specifying the material for the subarachnoid elements (see Figure 6-10) as compressible, a discontinuous support between the brain and skull can be approximated. As it happens the net result should also be to reduce the deformation gradients and, hence, the intracranial pressures that develop in the brain.

The results of characterizing the subarachnoid space as compressible (bulk modulus of 3,050 psi) are shown in Figure 6-12(c). This time, as expected, the overall computed intracranial pressure was reduced. Pressures at all points were lower than they were prior to the compressibility specification in the subarachnoid space elements. The peak tensile pressure in element 109 dropped from 67 to 55 psi. This was still high compared to the experimental value of 13 psi but nevertheless was considered an improvement. Strains in the brain, though not shown, were reduced correspondingly.

Varying the compressible properties of the subarachnoid space is an attempt to deal with an intracranial area for which there exists no material property data and in which the stress-strain behavior is of no interest so long as discontinuity of displacements is simulated.

There may never be any material property data because of the discontinuous nature of the subarachnoid space. One recourse is to effect engineering approximations with regard to the mechanical behavior of this area.

In the course of continued checking of the simulation for accuracy it was thought that the mass of the connecting head tissue and the mandible, which was neglected in the model, might be more significant than at first realized. An estimate of this additional mass was made for the specific primate employed in HSRI test 003. Distribution of this additional mass, when added to the model, could not be accomplished accurately since, as described earlier, no discretization of the rhesus mandible was included. But the mass density of the outer layer of elements for the cranial bone was increased by a uniform amount, making the total mass of the model more closely equal to that for the actual animal.

To demonstrate the influence of this additional mass, the rhesus skull displacement data are presented in Figure 6-13. This information was also derived to aid in improving the simulation of the live rhesus experimental tests. If a reasonable correlation between measured and computed intracranial pressure is to occur, at least the measured and computed displacement histories of the rhesus skull should agree. Acceleration histories would perhaps have been more convincing parameters, but this information was not of sufficient quality to be usable at the time of the validation effort herein described. High speed film proved more useful in determining displacements than did the double integration of measured accelerometer data. The "particle mechanics solution" assumes perfect translation which was not the case as some rotation was present in the horizontal displacement of the frontal bone. The displacement history curve associated with the corrected or added mass is more parallel with the experimental data than any of the other curves. This means that the computed velocity agrees more closely with the measured velocity as a result of the added mass. This is not necessarily true of the acceleration, however, because that quantity depends on the curvature and not the slopes of the curves, and curvature cannot be as easily observed in this data. It does appear as though the added mass has retarded, by too much, the displacement of the frontal bone.

A distinct reduction in overall intracranial pressure computed by the HIM code as a result of the added mass can be seen in Figure 6-12(d). The peak tension stress in element 109 has been lowered from 55 to 43 psi. These results demonstrate the importance of adequately simulating the mass of the rhesus skull when computing the intracranial pressure.

At this point there were few obvious additional modifications to the simulation and model which could reasonably be proposed without revamping the entire model. Obviously the measured pressures were still well below those which were being computed. Since time did not allow any extensive modification to the model, two more simulations were conducted which required only minor changes.

The mechanical properties of the subarachnoid space being quite unknown could be guessed at with relative freedom. If a reduction of the skull modulus from 305,000 to 3,050 psi provided an improvement, then perhaps a further reduction to 305 psi, for example, would also be beneficial. The computed intracranial pressures presented in Figure 6-12(e) are for this case. An improvement was indeed realized although not as significant as before. The computed peak tensile pressure in element 109, corresponding to the pressure transducer, was reduced from 43 to 37 psi. There is a limit imposed by numerical

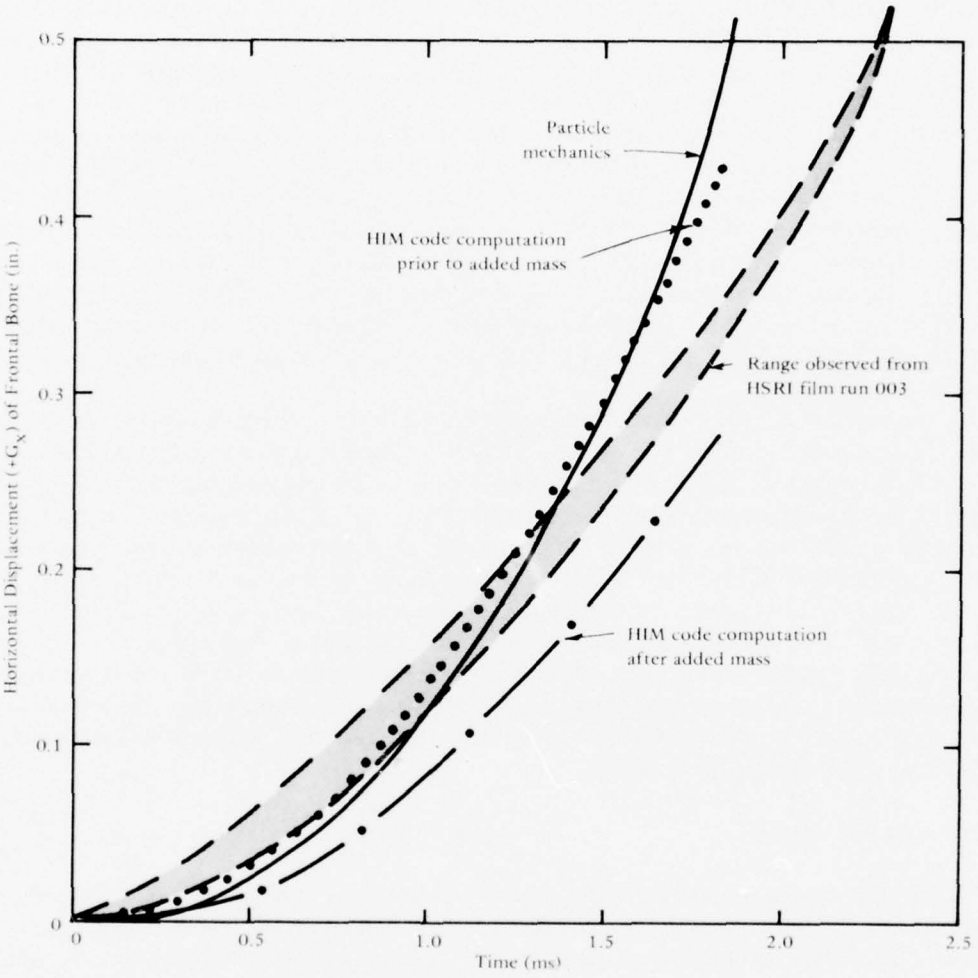

Figure 6-13. Rhesus Skull Displacement History.

stability to the amount by which the bulk modulus can be reduced or to the specified compressibility for the layer of elements designated as the subarachnoid space. The latter bulk modulus value of 305 psi is straining that limit. Any further reduction would risk computation of incompatible displacements in the subarachnoid region with the present model.

The final attempt at correlating with the measured intracranial pressures was made by testing the effect of the prescribed integration time step size. To this point 130 μs was the time step employed in all simulation and this value might appear coarse when compared with the rise time associated with the input load function (Figure 6-11). Therefore, the prescribed time step was halved to a value of 65 μs which is on the order of one-tenth of the rise time possessed by the impact load. This is ordinarily deemed adequate, and anywhere from one-eighth to one-tenth can be used as a rule of thumb. The best method, however, is to test the effect on response of various prescribed time steps. The results, in this case, are presented in Figure 6-12(f), exhibit very little difference in peak response, and show that no real benefit can be expected by undergoing the additional expense of a smaller integration time step size.

A summary of the HIM code simulations of the live rhesus impact experiment which have been discussed above is presented in Table 6-3. Here it can be seen that the best effort to correlate computed and measured intracranial pressures results in the HIM code predicting peak intracranial pressures which are about three times higher than those which were measured in HSRI test number 003. It can be seen that the predicted pressure gradient in the A-P direction is substantial. It is about 65 psi in the short space of approximately 3 inches. More detailed computed intracranial pressure data for the midsagittal plane resulting from HIM code simulation number 5 (see Table 6-3) is presented in Figure 6-14. If at a later time the position which was selected for correlation with the HSRI transducer is found to be inaccurate, this data can serve to adjust the above validation results. As evidenced by the pressure gradient size, it would not require much of an error in this position to make a significant difference in these results.

Qualitative Validation

There are some characteristic traits of typical HIM code predictions which have surfaced during the development process and which are consistent with general and experimental observation or head injury statistics. As a result they are presented here to enhance the level of confidence in the performance of the HIM code in a qualitative sense.

It is generally agreed by engineers and clinicians alike that contrecoup brain injury is an important category of head injury. When the initial development of the HIM code began there was no guarantee that this important mechanism would manifest itself in a finite element model. Yet from the preliminary two-dimensional models to the present three-dimensional models, significant tensile intracranial pressure has been consistently predicted in that portion of the brain opposite to the applied impact load. At the same time, compressive intracranial pressure in the brain adjacent to the applied load (coup pressure) is consistently predicted. This phenomenon has not only been observed clinically and pathologically, but it is a reasonable physical mechanism which should be expected from a properly simulated encapsulated, fluidlike material. The model simulates this basic mechanism very well.

Table 6-3. Summary of HIM Code Simulations of Live Rhesus Experiments

No.	Simulation Description	Bulk Modulus (psi)		Peak Pressures (psi)			
		Brain	Subarachnoid	Element 109	Point A	Point I	Point P
1	No foramen magnum	305,000	305,000	35 T	32 T	6 C	71 C
2	Foramen magnum included	305,000	305,000	67 T	62 T	42 T	55 C
3	Reduced bulk modulus of subarachnoid space	305,000	3,050	55 T	52 T	31 T	48 C
4	Added mass to account for mandible and scalp	305,000	3,050	43 T	37 T	29 T	34 C
5	Further reduction of bulk modulus in subarachnoid space	305,000	305	37 T	36 T	9 T	31 C
6	Halved integration time step	305,000	305	36 T	35 T	9 T	28 C

Some interesting statistics relating the incidence of coup and contrecoup head injuries have been compiled[64]. It is believed that this information is germane to the development of head injury models and that one criterion for a valid model is that it account for this data. The information is presented in Table 6-4. It is readily apparent from this data that the traumatic results caused by frontal and rear impacts are different.* The data suggest that frontal impacts are more apt to induce coup brain injury than contrecoup injury, while rear impacts induce predominantly contrecoup injury. Side impacts are more apt to produce contrecoup injury independent of impact location (left or right side). Symmetry of the resulting injury exists for side impacts but does not exist for front and rear impacts.

Table 6-4. Distribution of Coup and Contrecoup Brain Injuries with Location of Impact

Location of impact	Number of cases	Percent location of injuries		
		Only or mainly at impact site	Only or mainly opposite impact site	Equally distributed
Frontal	280	49	5	46
Rear	36	0	97	3
Left side	33	12	67	21
Right side	31	13	68	19

In Figure 6-15, the intracranial pressure distribution in the A-P direction are plotted for simulations 1 and 2 (Table 6-3). These data are normalized on the highest computed absolute pressure. The contrecoup pressures or tensile pressures naturally occur in the anterior brain while the coup pressures or compressive pressures occur in the posterior brain. However, note that the A-P pressure distribution curves for the closed skull intersect the zero pressure line at a position considerably anterior to where the open skull curves intersect.

---

[64] U. S. Air Force. SBNO-87936-3: German aviation medicine World War II, vol. I. Pelham Manor, NY, 1971, p. 626.

*At the very least then, a model should be capable of distinguishing between frontal and rear impacts.

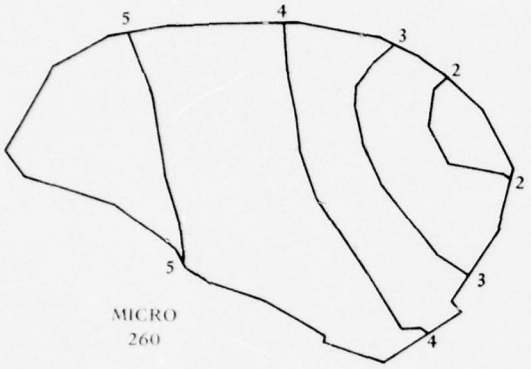

(a) Step 1.

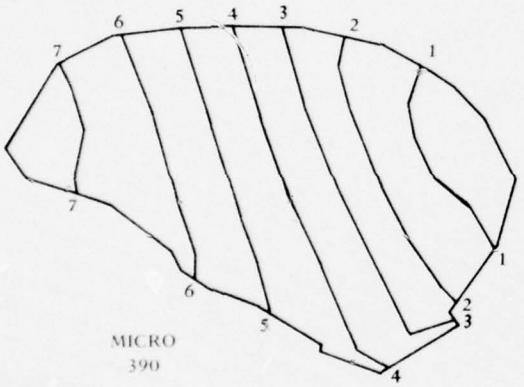

(b) Step 2.

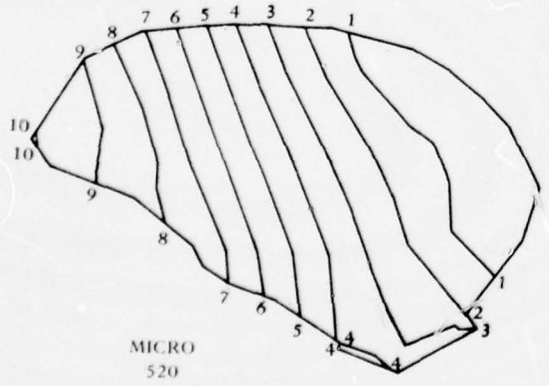

(c) Step 3.

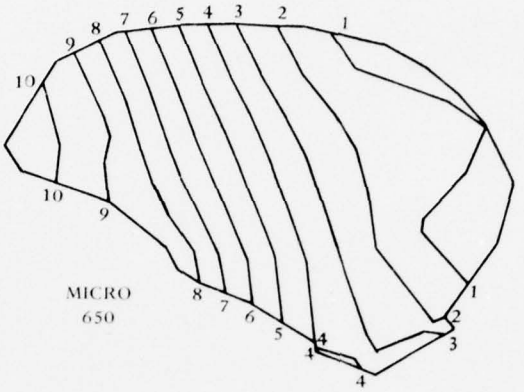

(d) Step 4.

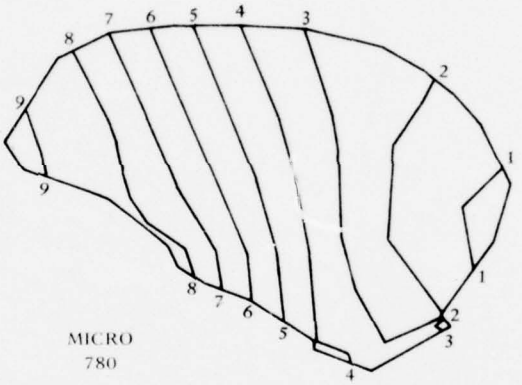

(e) Step 5.

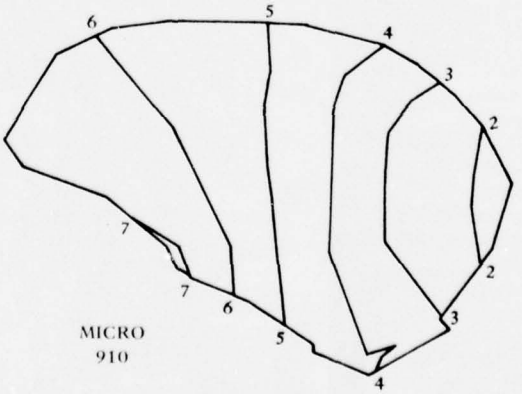

(f) Step 6.

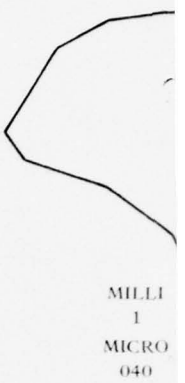

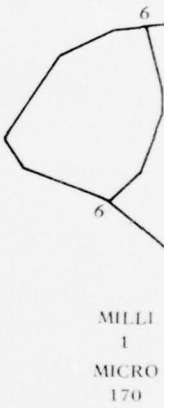

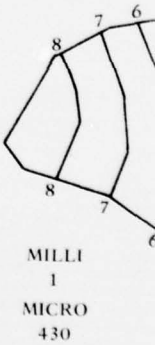

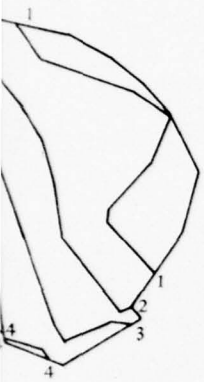

p 4.

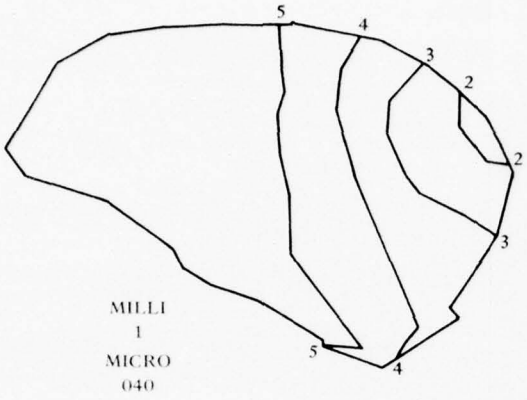

(g) Step 7.

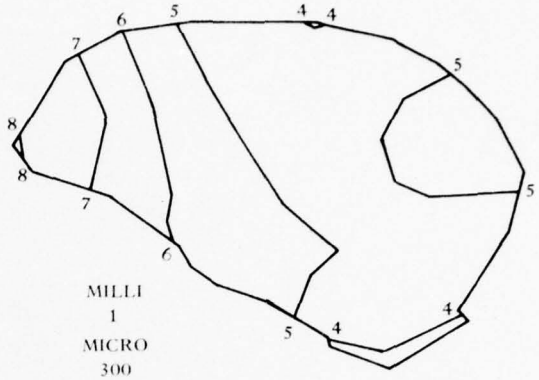

(j) Step 10.

p 5.

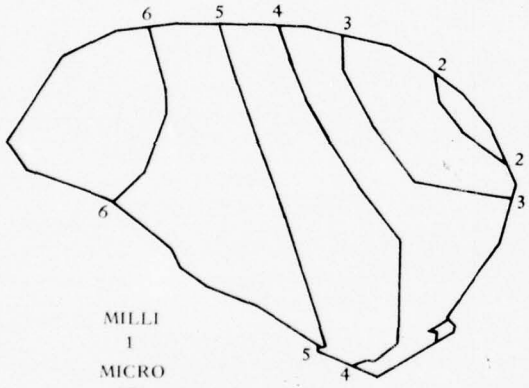

(h) Step 8.

1. 2.48×10^{01}
2. 1.75×10^{01}
3. 1.01×10^{01}
4. 2.85×10^{00}
5. 4.49×10^{00}
6. 1.18×10^{01}
7. 1.91×10^{01}
8. 2.65×10^{01}
9. 3.38×10^{01}
10. 4.12×10^{01}

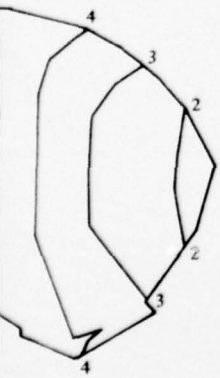

p 6.

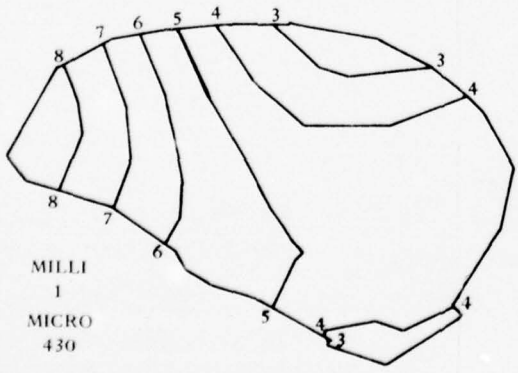

(i) Step 9.

Figure 6-14. Predicted HIM Code Intracranial Pressures Simulating HSRI Experiment No. 003.

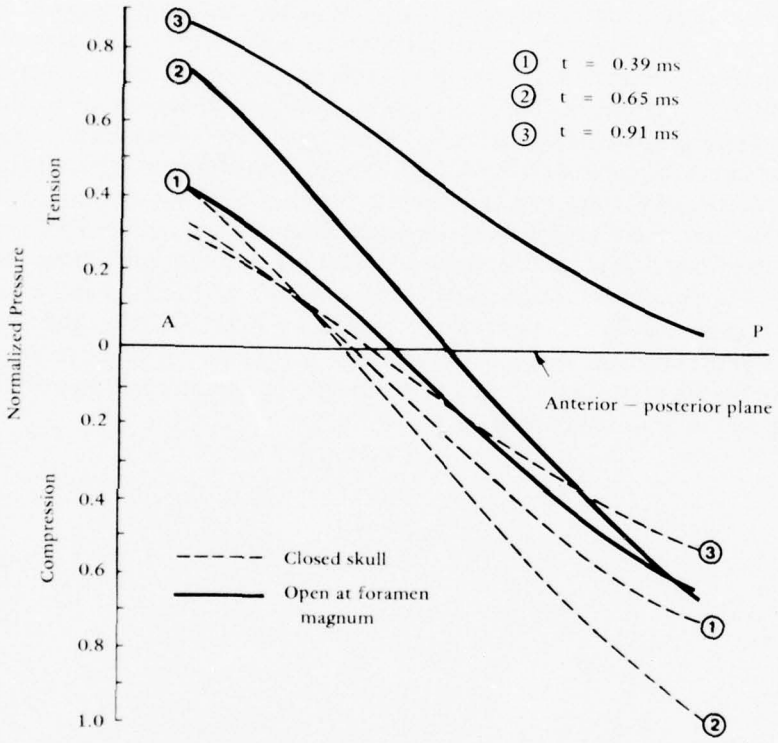

Figure 6-15. Influence of Foramen-Magnum/Intracranial-Pressure Distribution.

The net effect is that in the closed skull the contrecoup pressures are much smaller than the contrecoup pressures for the open skull case, since at any time the two cases yield nearly equal gradients.* If the vulnerability of brain material to tensile pressure is accepted, the pressure distribution occurring in the open skull is far more likely to explain the data of Table 6-4. This data indicates that, for rear impacts, in 97% of the cases brain injury occurs only or mainly at a contrecoup point, and in only 3% of the cases injury equally distributed. In no cases were the coup injuries found to occur in the absence of contrecoup injuries. Yet the closed skull simulation would predict, in absolute magnitude, coup pressures much higher than contrecoup pressures. While it may be intuitively obvious to some, this data concludes that a closed skull configuration for head injury simulations must be rejected.

Another possible explanation of the data in Table 6-4 would include the differences in the bony irregularities of the anterior and posterior internal skull surface. Since the anterior skull contains more sharp protrusions, the interface conditions between the cranial wall and brain and attending hazards will be more severe under dynamic conditions. This is undoubtedly true, but the shift in the location of zero pressure as discussed above has also been observed experimentally[58]. As shown by comparing Figures 6-12(a) and (b), the effect of the foramen magnum opening is to create larger tensile pressures for longer durations at anterior points in the brain during rear impacts. It, therefore, is regarded as an important mechanism in head injury modeling.

*The reverse is naturally true for the coup pressures; the coup pressures in the closed skull are much larger than the coup pressures in the open skull.

7. HIM CODE DEVELOPMENTAL RESULTS

In this chapter the computed dynamic response obtained from several HIM code simulations in the last part of the head injury model development program are presented. They deal with the human configuration and, in particular, with the three-dimensional discretization discussed earlier in Chapter 5. Though most of the effort described throughout this report pertains to the development of a usable tool with which to study head injury, some of the results presented in this chapter provide useful insight into the mechanical causes of head injury—an important objective of this head injury model study. Excerpts from these results were presented at an earlier date in Reference 65.

Frontal Impact Versus Occipital Impact

The human skull model employing the fine discretization (see Figure 5-12) was subjected to a typical direct impact load from the front and from the rear. In each case the peak load was 2,600 pounds and was distributed over a skull surface area of about two sq in. The impact load varied with time as a haversine function having a duration of 10 ms. The direction of loading nearly passed through the skull center of gravity, and the skull was completely unrestrained. The skull model included an elastic membrane over the foramen magnum in the same manner as previously discussed for the rhesus skull model. Additionally, a compressible bulk modulus of 305 psi was assigned the elements constituting the subarachnoid space. The integration time step size was 1 ms.

Cranial Bone Response. Minimum and maximum principal stresses in the midsagittal plane of the cranium are presented in contour form in Figure 7-1 for a frontal impact. Negative and positive values refer to compression and tension stresses in the skull bone, respectively. For the frontal load condition, the outer surface of the frontal bone sustains the maximum compression stress (6,200 psi) while the inner surface of the frontal bone sustains the maximum tension stress (2,050 psi). These are bending stresses. They appear to accumulate above the loading region where the frontal bone thickness is reduced. The relative magnitudes of compression and tension stresses are significant since tension stress is usually thought of as being more conducive to skull fracture. Yet the compressive stresses are roughly three times greater. If they were equal, then fracture would be expected to begin eventually on the inner and outer cranial surface, higher up on the frontal bone. But as the analysis shows, the larger compressive stresses may significantly alter that fracture pattern by initiating fracture on the outer surface of the frontal bone just below the indicated position for impending tensile fracture.

Principal stress data for the occipital impact is presented in Figure 7-2. Maximum compressive stress (5,160 psi) occurs just above the load region on the outer skull surface. Again these are bending stresses. The maximum tensile stress (1,820 psi), however, occurs at the

---

[65] Shugar, T. A. "Transient structural response of the linear skull/brain system," in Proceedings of the Nineteenth Stapp Car Crash Conference, San Diego, CA, Nov. 1975. pp 581-614.

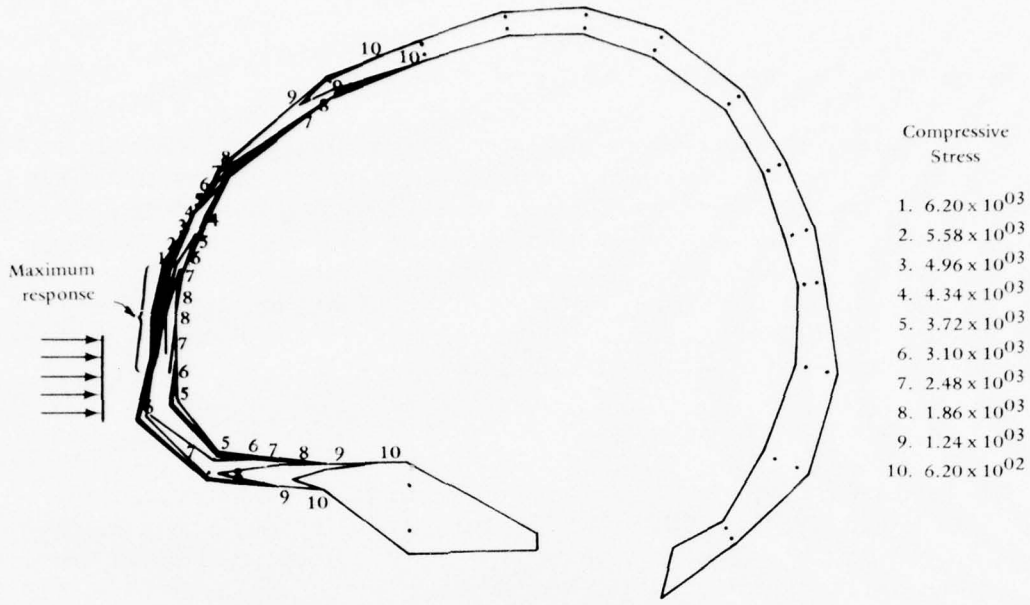

(a) Compressive stress.

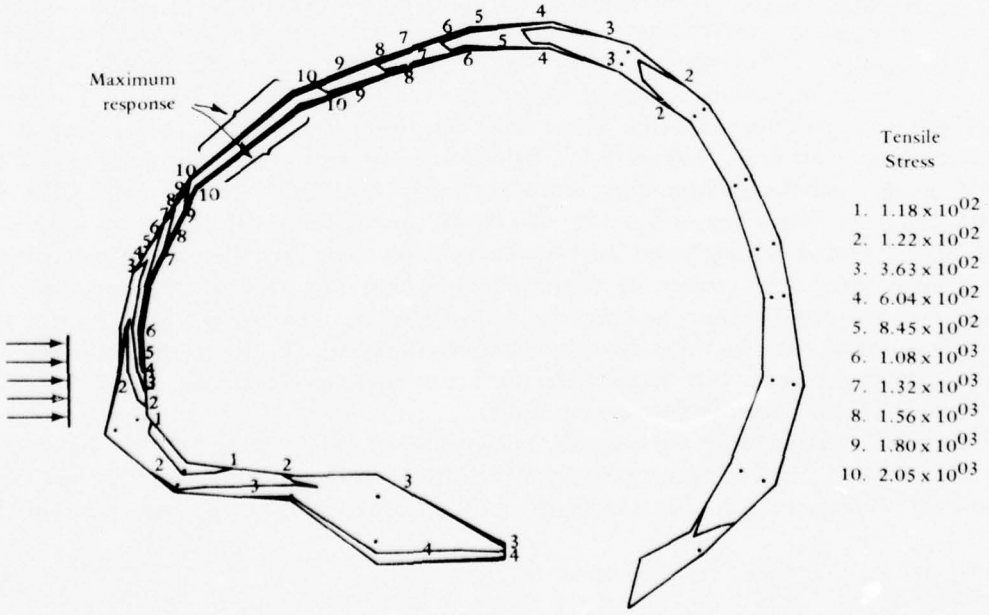

(b) Tensile stress.

Figure 7-1. Principal Stresses in Cranium for a Frontal Impact at Peak Response Time.

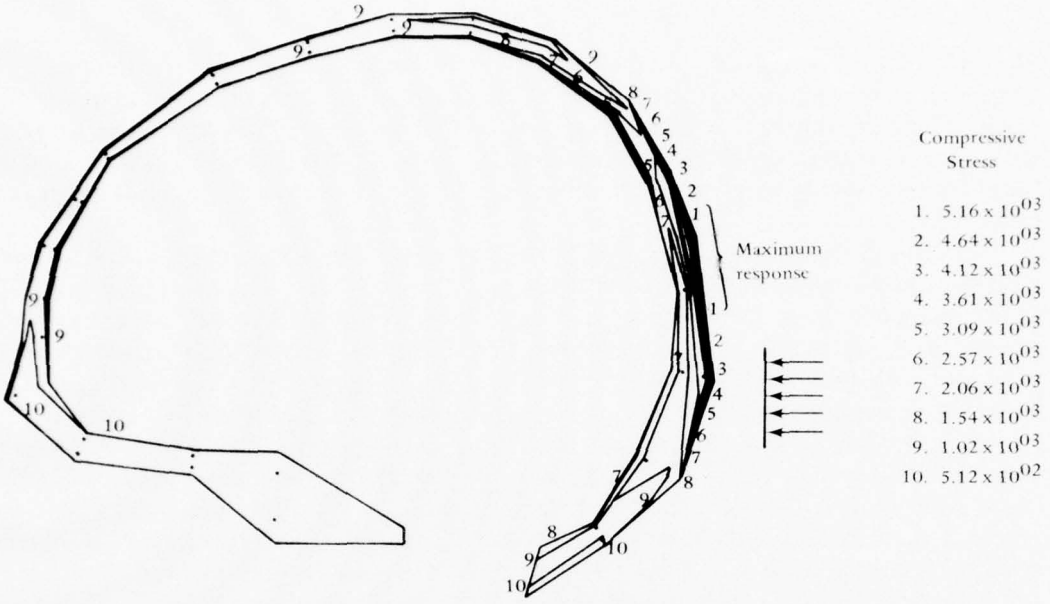

(a) Compressive stress.

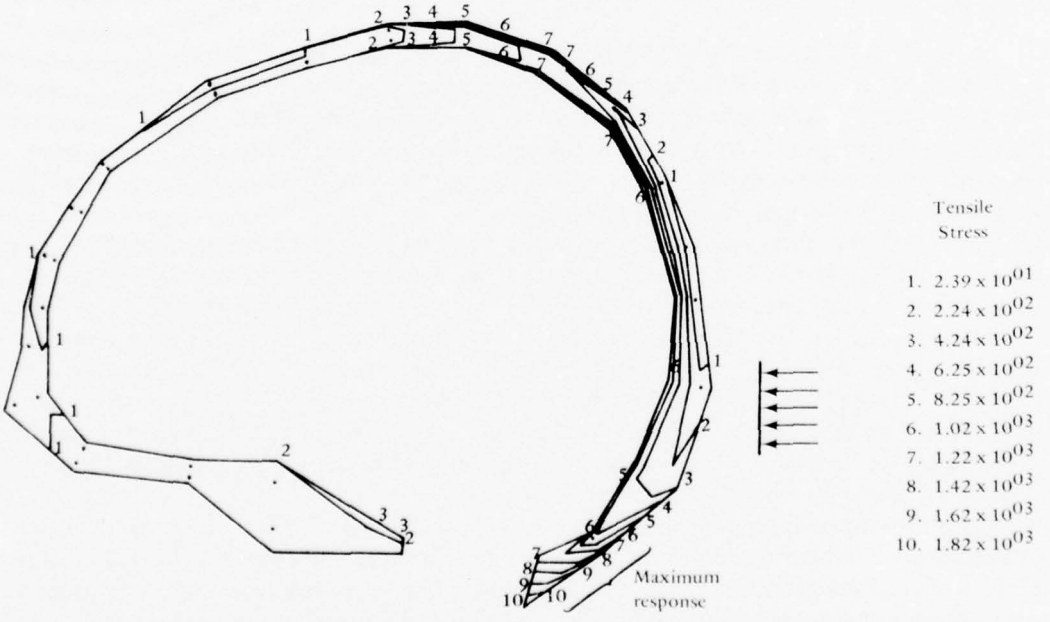

(b) Tensile stress.

Figure 7-2. Principal Stresses in Cranium for an Occipital Impact at Peak Response Time.

edge of the foramen magnum, well below the point of loading. As a result the foramen magnum appears to present an area of stress concentration not unlike that found in conventional engineering shell structures in the vicinity of apertures. The compressive stresses are again almost three times larger than the tensile stresses. As a result their contribution to linear fracture cannot be ignored even though tensile stresses may be more conducive to linear fracture.

The effect of simulating the sandwiched or layered nature of the cranial bone structure is illustrated from the concentration of stress contours in the inner and outer table bone layers, while the diploe, or middle layer of softer bone, is essentially devoid of high stresses. The layered construction of the skull is indeed very efficient in resisting the bending forces of impact. Compressive bending stresses are consistently higher than tensile bending stresses in the above two simulations. Because bone is more susceptible to failure by tension stresses, it is difficult to pin-point the exact local of impending fracture. Moreover, no acceptable failure criterion exists for skull bone subjected to two- and three-dimensional stress states. It is clear that fracture paths and areas of high stress are considerably altered by local geometrical irregularities of the cranial structure. It is also clear from the above two simulations that the occiput developes less stress for the same load than does the frontal bone and apprears to be stronger. Linear fractures are apt to originate on the inner skull surface as well as the outer skull surface. For frontal impacts the fracture of the frontal bone is likely to occur above the blow at a higher position. For occipital impacts, fracture of the occipital bone is likely to occur either above or below the impact area and perhaps as far down as the foramen magnum.

Intracranial Response. Data in this section as in all HIM code predictions are presented for the midsagittal plane of the model but is to be interpreted as predicted data for a sagittal plane just to the right or left of the midsagittal plane of a human skull. This is because the two cerebral hemispheres are actually separated by the falx membrane which occupies a good portion of the midsagittal plane. A full sagittal section of cerebral material occurs in actuality only to the right or left of this plane.

The results for each load case are presented together in Figure 7-3 for comparison. Negative and positive pressures denote compression and tension, respectively. Peak pressure that occurs as compression in the anterior brain from the frontal blow (Figure 7-3(a) and (b)) is less likely to cause brain damage than the peak pressure occurring as tension in the anterior brain as induced by the occipital blow (Figure 7-3(c) and (d)). They are nearly the same in absolute magnitude, but the brain is believed more susceptible to injury from tension. This is the same characteristic as was noted with the rhesus model and offers a good explanation for the statistically observed phenomenon of asymmetry in brain injury (see Table 6-4) caused by frontal and occipital impacts.

Maximum shear strain data when compared for the two load cases are almost indistinguishable and therefore appear to be independent of whether the impact is frontal or occipital. The peak shear strain for the occipital impact is 20% greater than for the frontal impact. Brain damage due to shear strain will most likely be found in the brainstem or possibly the cerebellum according to this data, regardless of the impact load direction. The midbrain region possesses very little shear strain.

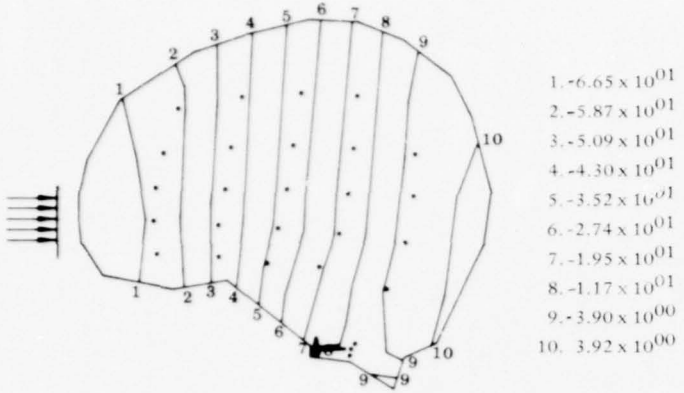

(a) Pressure at t = 5 ms.

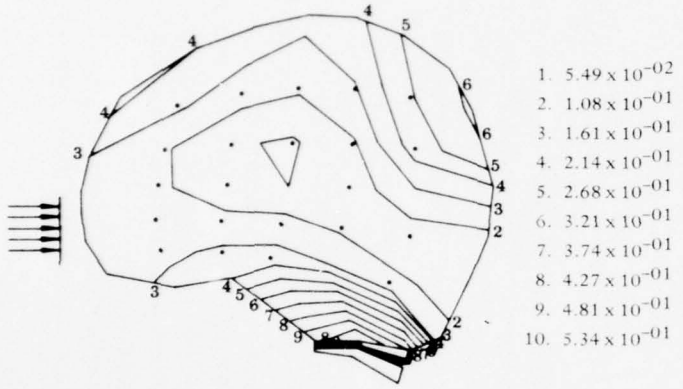

(b) Maximum shear strain at t = 7 ms.

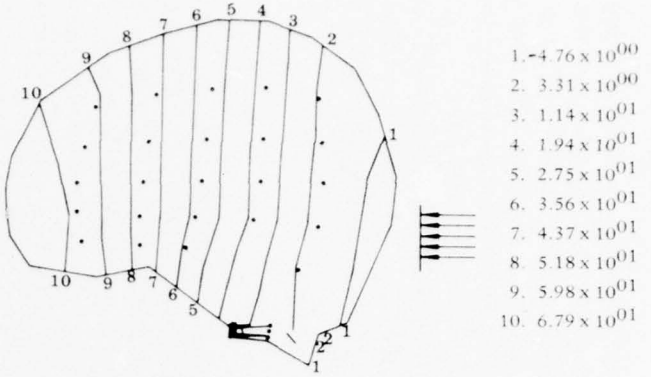

(c) Impact, pressure at t = 5 ms.

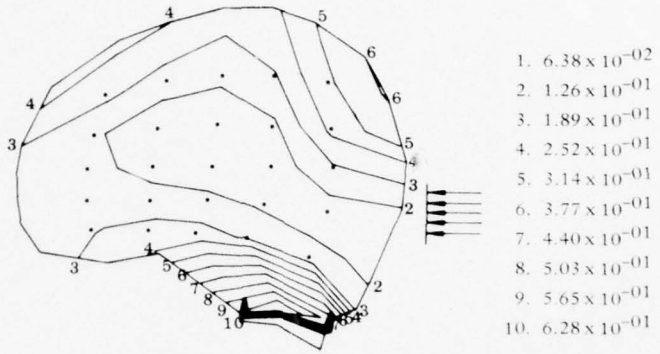

(d) Maximum shear strain at t = 7 ms.

Figure 7-3. Intracranial Response for Frontal and Occipital Impact.

These intracranial results, both pressure and maximum shear strain, surely indicate that intracranial pressure would be the mechanical phenomenon more likely to explain the statistical distribuiton of coup and contrecoup damage which is noted in Table 6-4. The most severe shear strain does not occur at either a coup or contrecoup location. The most severe pressure does occur at these positions. The location of the most severe shear strain does not vary with the load direction, but the location of the most severe pressure does.

Thus far the HIM code indicates pressure to be the most important intracranial response for predicting brain damage. However, to this point, only translation of the skull has been studied and whether or not these results will differ for rotation remains to be seen. The effect of rotation is investigated in the following section.

Varying the Skull Base Boundary Condition

A series of four HIM code simulations are presented and discussed for the primary purpose of determining the necessity for including a neck simulation with the skull model. In conducting these simulations the effect of skull rotation is also introduced. Rigid body motion of the skull and the response of the brain in terms of intracranial pressure data and maximum shear strain data are employed in the discussion. Cranial bone stresses are not discussed, but for each simulation like those of the previous section, information pertaining to linear fracture of the cranium was computed.

The effect of the boundary conditions at the skull base upon intracranial response is investigated by repeating the impact simulation for a skull which is (a) fixed against movement at the base, (b) pinned at the base allowing rotation about the base, (c) rollered at the base allowing the skull to slide along a plane, and (d) completely unrestrained at the base allowing the skull to translate and rotate. The simulated impact load was a concentrated force, varying with time as a haversine function, with a duration of 10 ms and a peak force of 1,000 pounds. The impact load is applied at an angle of 15 degrees with the horizontal on the frontal bone. Again, the numerical integration time step size was 1 ms.

Skull Fixed at the Base. The fixed skull is completely restrained at each of two node points on the perimeter of the foramen magnum. The computed displacements, stresses, and shear strains are shown in Figure 7-4 at three selected times corresponding to peak loading, prior to peak loading, and subsequent to peak loading. The sequence of displacements shows very little rigid body motion because of the restraint at the base. To display what rigid body motion did exist, the displacements were scaled to 2.5 times their actual values.

In the subarachnoid region near the top of the skull a relative motion between the inner skull elements and the outer brain elements can be observed at 5 ms (note the jog at the top along the vertical mesh lines). This is graphical evidence of the desired effect designed by specifying a relatively compressible bulk modulus in the subarachnoid elements. This result can be observed in other HIM code simulations to a lesser or greater extend. Though the relative motion is always slight, it serves to reduce significantly the stresses and strains in the brain that would otherwise develop by assuming that the brain is rigidly fixed to the inner skull surface.

The curvature of the stress contours, for which values are given in Table 7-1, demonstrates the rotation taking place to the virtual exclusion of translation. A significant amount

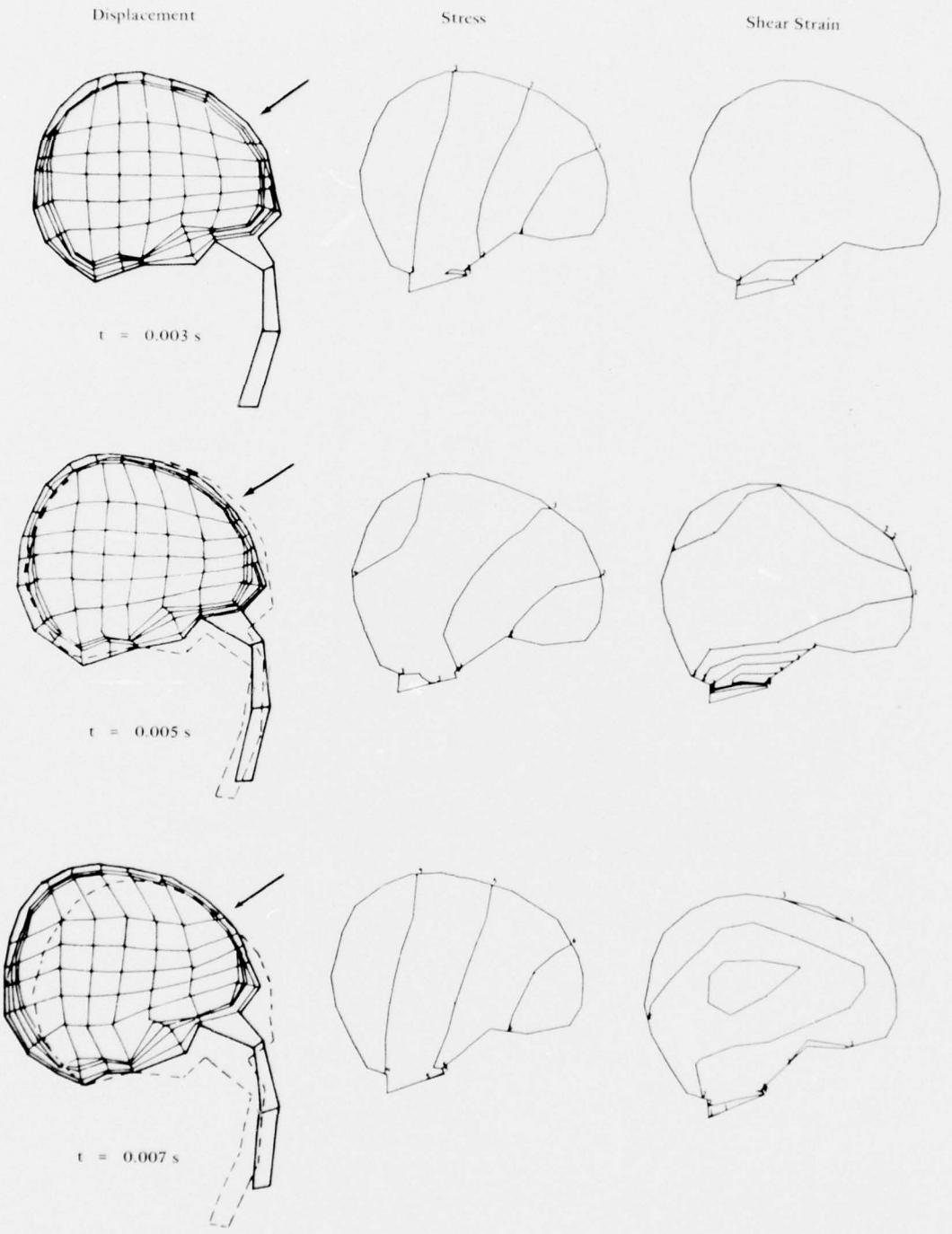

Figure 7-4. Direct Impact of Fixed Skull.

Table 7-1. Contour Values for Fixed Skull

Contour No.	Stress[a, b] (psi)	Maximum Shear Strain
1	-5.4	0.035
2	-2.2	0.070
3	+0.9	0.104
4	+3.8	0.139
5	+7.3	0.173
6	+10.4	0.208
7	+13.7	0.242
8	+16.9	0.277
9	+21.9	0.311
10	+23.2	0.346

[a] Negative sign indicates compression, and positive sign indicates tension.

[b] 1 psi = 0.069 bar.

of tension is evident in the brain in this simulation. The skull is accelerated "back over" the support, initially causing compression in the anterior and tension in the posterior brain. The skull, however, soon accelerates back in the opposite direction as the load subsides. This causes a sign reversal in the stresses of the anterior brain. Actually the peak tension stress occurred at 9 ms (not shown) on the anterior brain surface in this simulation. The elasticity of the skull bone has participated significantly because of the restraining condition.

Shear strains develop initially in the brainstem region then subside at 7 ms, only to increase again to the maximum value at 9 ms. This oscillation is a manifestation of the same phenomenon discussed above for the stress response. There is only a slight tendency for the shear strains to develop on the outer surface of the brain. The brainstem sustained virtually all the shear strain. It might reasonably be expected that this is due to the fixed support condition but results will be shown for an unrestrained skull which discount that possibility.

Skull Hinged at the Base. Only in the most rare situation would a completely restrained skull simulation be appropriate. A more realistic constraint would allow some rigid body movement of the skull. The results for a hinged skull are shown in Figure 7-5. The rotation takes place about a pinned node on the anterior ridge of the foramen magnum and can be termed noncentroidal rotation. Significant rigid body motion occurs as compared with the completely restrained skull and as a result the intracranial response is very different. First of all there is no reversal of sign in the computed intracranial response and second, the compressive stresses and shear strain are considerably larger as shown by the values in Table 7-2. This condition is therefore more severe than the completely restrained condition with regard to intracranial response. This is not true for the skull bone response.

The curvature of the stress contours, especially in the anterior brain, reflect the rotation (rigid body) that is taking place. The contrecoup response is comparatively mild as evidence in the peak response at 5 ms showing less than 13-psi tension in the posterior brain.

The maximum shear strain response peaks at 7 ms; i.e., subsequent to peak pressure response. The brainstem region sustains the more severe shear strain and the midbrain region sustains the least shear strain. Although not shown, these observations are also true of the computed normal strain distribution.

Skull Sliding on Its Base. In this instance the simulated skull is allowed to slide on a horizontal plane tangent to the skull base under the influence of the impact force. The rigid body motion in this case is primarily translational.

The intracranial response is basically similar to the hinged skull condition as shown in Figure 7-6. The stress contour values presented in Table 7-3 indicate a higher compressive stress in the anterior brain and also a slightly more severe contrecoup condition in the posterior brain. The magnitude of tensile stresses are higher and distributed over about the same amount of brain material as in the hinged skull.

The shear strain contour response, with regard to distribution, looks the same as the response for the hinged skull. However the magnitude of these contours is lower for the sliding skull that it is for the hinged skull. So, while the model predicts the translated skull to be more severe with regard to coup and contrecoup stresses, it also predicts the rotated skull to be more severe regarding the strain condition in the brainstem region.

Table 7-2. Contour Values for Hinged Skull

Contour No.	Stress[a] (psi)	Maximum Shear Strain
1	-40.8	0.093
2	-34.0	0.184
3	-27.1	0.276
4	-20.3	0.367
5	-13.5	0.459
6	-6.7	0.550
7	+0.2	0.641
8	+7.0	0.733
9	+13.8	0.824
10	+20.6	0.916

[a] Negative sign indicates compression, and positive sign indicates tension.

Table 7-3 Contour Values for Sliding Skull

Contour No.	Stress[a] (psi)	Maximum Shear Strain
1	-55.1	0.065
2	-47.1	0.128
3	-39.0	0.192
4	-30.9	0.255
5	-22.9	0.319
6	-14.8	0.382
7	-6.8	0.446
8	+1.2	0.510
9	+9.3	0.573
10	+17.3	0.636

[a] Negative sign indicates compression, and positive sign indicates tension.

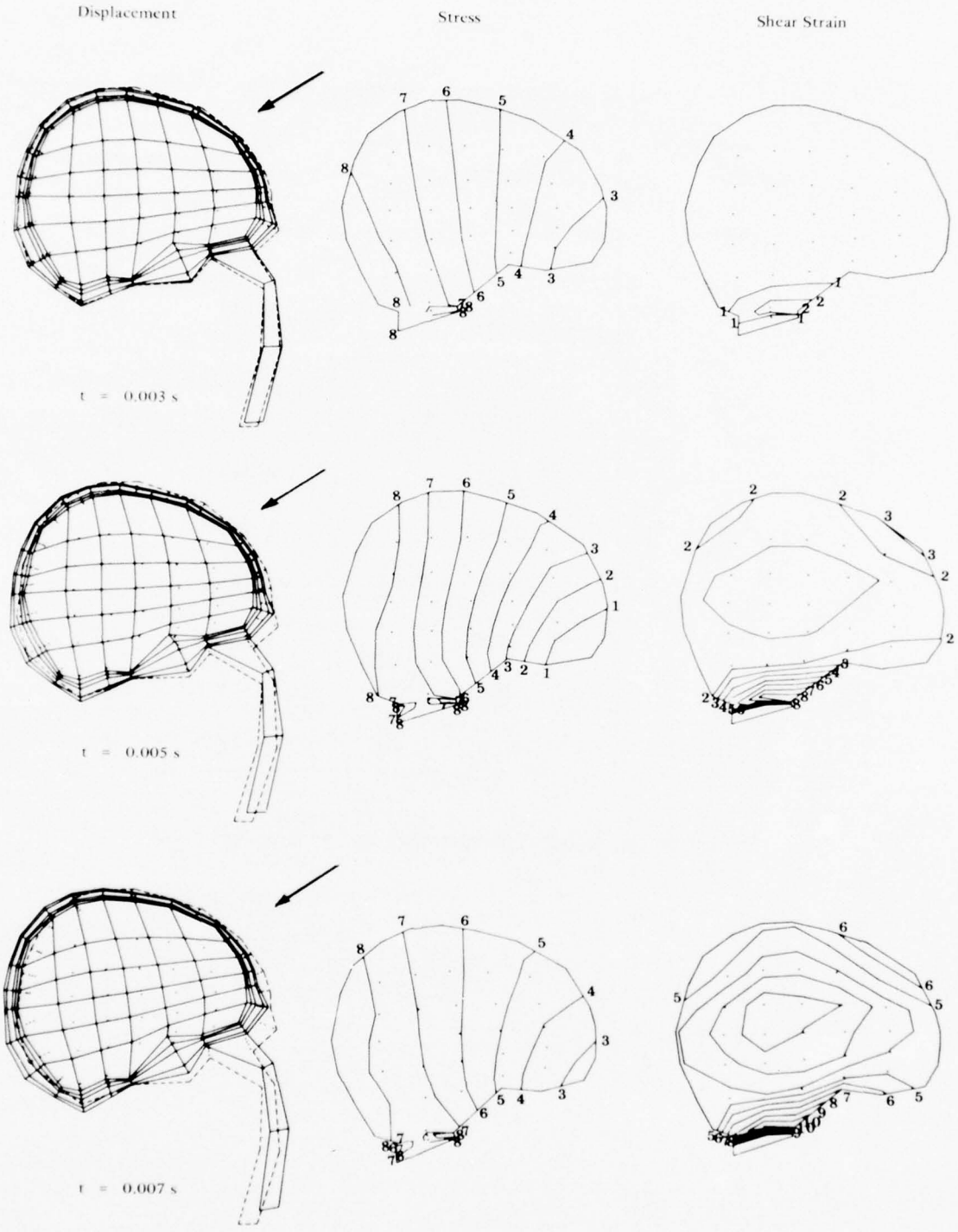

Figure 7-5. Direct Impact of Hinged Skull.

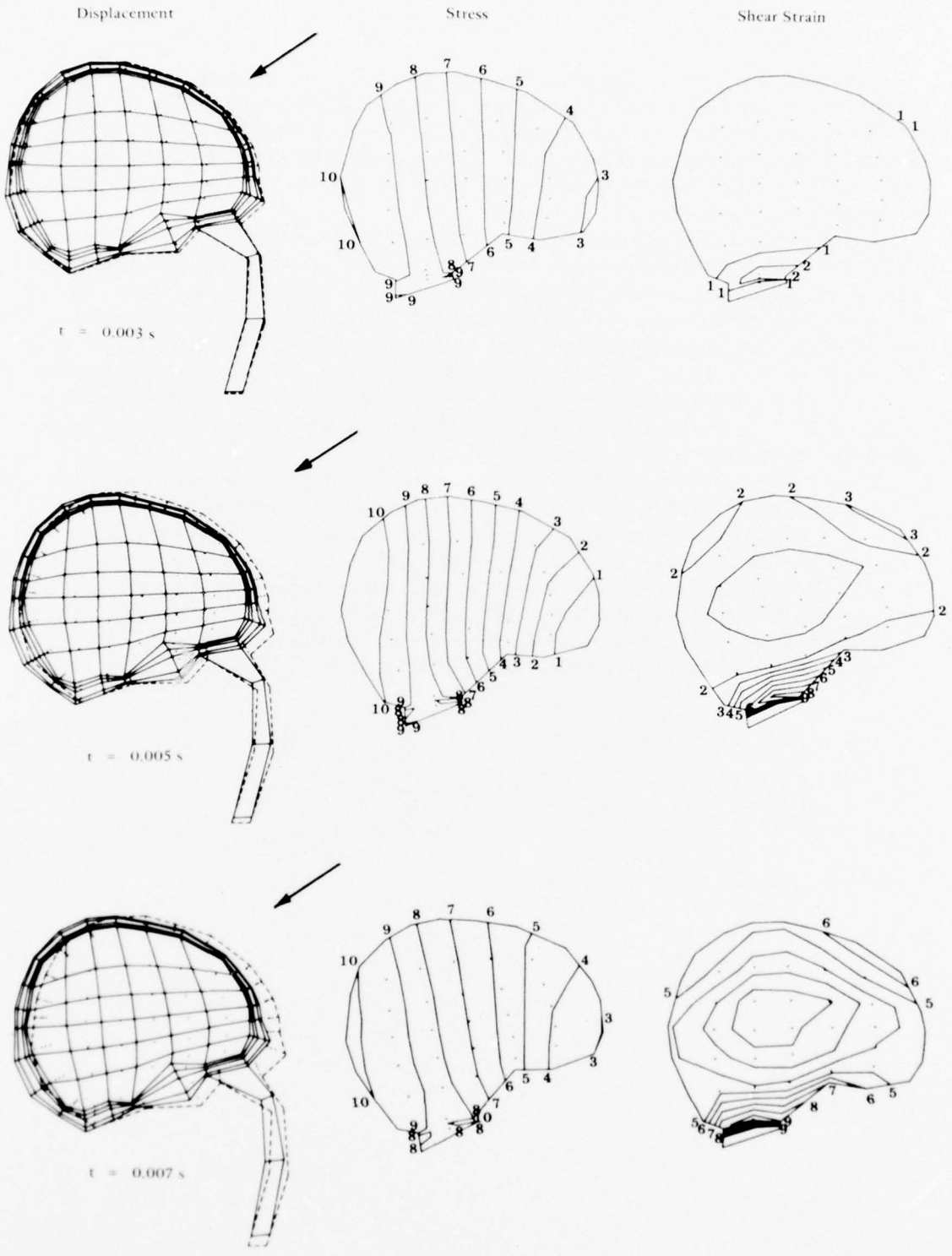

Figure 7-6. Direct Impact of a Sliding Skull.

Skull Completely Free at the Base. The response of the brain is slightly more severe than previous responses if, for the same impact load, the boundary restraints at the base of the skull are removed. The HIM code results for the impacted, free skull are presented in Figure 7-7. Here rigid body motion is significant and is a general or curvilinear state of motion combining both rotation and translation. Response parameters are presented at the same selected times as before.

The stress contour lines are generally more straight and less vertical than in the previous cases. This does not necessarily mean less rotation occurred, but only that there is in this case, more of an influence from translation. The rotational influence is manifested in the change in orientation of the rather straight contours. The stress magnitudes reported in Table 7-4 show that higher contrecoup brain stresses occurred in the free skull than in any of the previous simulations. The stress-time response follows closely the load-time specification with the peak response occurring at 5 ms. The influence of the foramen magnum is evident from the posterior location of the zero pressure region. These two observations are generally true of all these simulations.

Shear strains develop initially in the brainstem region as before. They continue to increase throughout the simulation to their maximum value. The maximum response time is 9 ms after which they subside. At any given time the shear strain diminishes with distance from the foramen magnum towards the midbrain region where the shear strain prediction is always observed to be minimal. Beginning from the midbrain region, the shear strain generally increases with radial distance toward the outer surface of the brain, particularly the superior surface. The shear effect can also be seen from the displacements in the distortion of the outer brain elements as compared with the distortion of the inner brain elements.

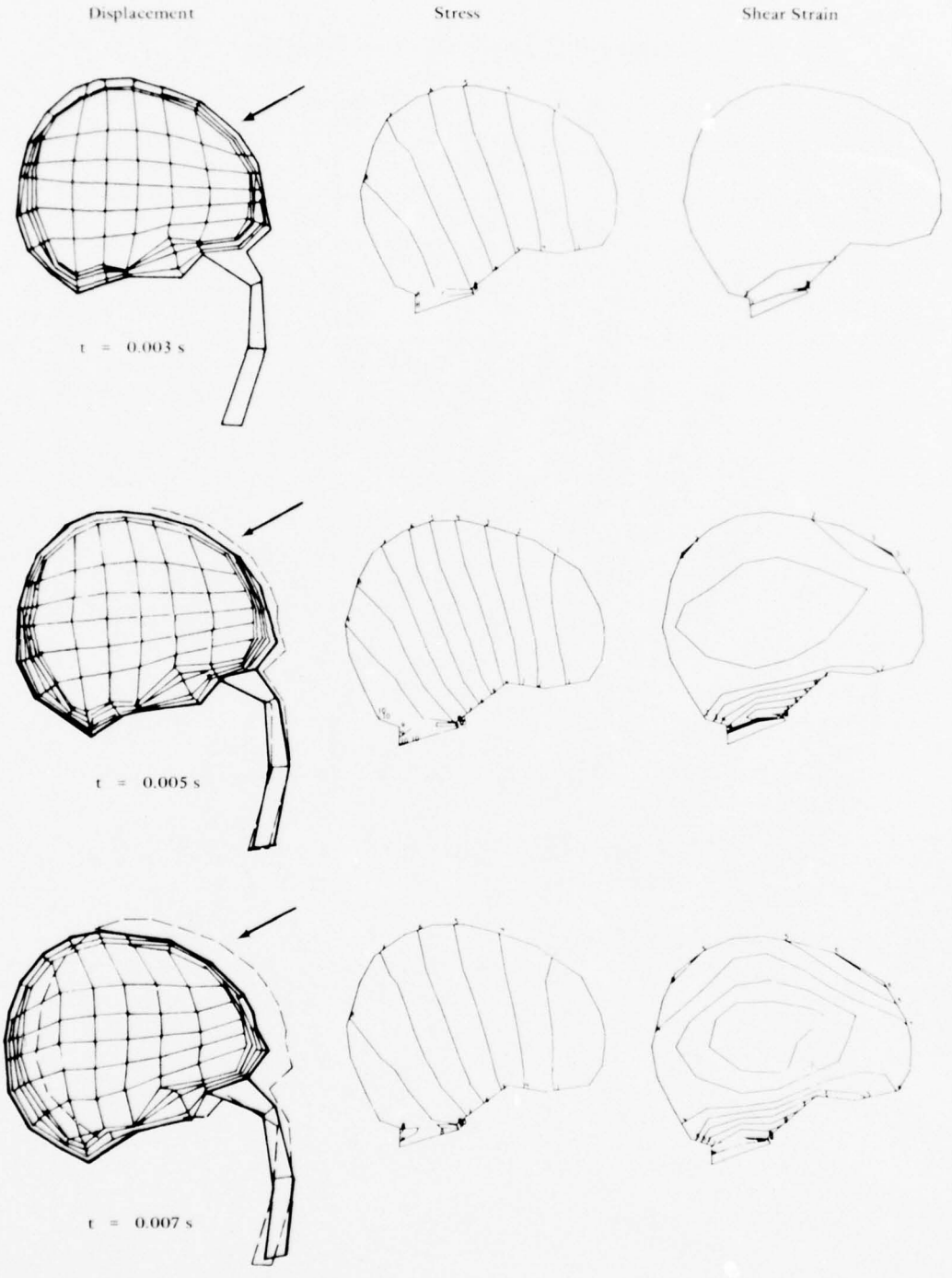

Figure 7-7. Direct Impact of Free Skull.

Table 7-4. Contour Values for Free Skull

Contour No.	Stress[a, b] (psi)	Maximum Shear Strain
1	-51.9	0.091
2	-42.0	0.180
3	-32.1	0.271
4	-22.2	0.361
5	-12.3	0.451
6	-2.46	0.541
7	+7.43	0.631
8	+17.3	0.721
9	+27.2	0.812
10	+37.1	0.902

[a] Negative sign indicates compression, and positive sign indicates tension.

[b] 1 psi = 0.069 bar.

8. INDIRECT IMPACT ACCELERATION

In many hazardous dynamic environments occupants are restrained so that their heads may not directly impact surrounding objects. Yet there is a need to determine the mechanical stress and strain response of the brain under these circumstances. This is also true of human volunteer testing where the environment should not be truly hazardous, but mechanical stress and strain predictions are necessary for correlation with measured physiological response. In these instances the impact forces are transmitted to the head at the base of the skull and subject the head to impact acceleration as described by Ewing and Thomas[66].

An intensive effort is ongoing to quantify the human dynamic response to impact acceleration and its correlation with injury and physiological effects. This research is being conducted at the Naval Aerospace Medical Research Laboratory (NAMRL), Michoud Station, New Orleans, Louisiana. Volunteer subjects and human analogs are given impact accelerations at a modern pneumatically powered sled facility. A computer-controlled data acquisition system continuously monitors all input parameters as well as selected output parameters of the subject's response. Acquired data is then applied in the development of mathematical models which are intended to complement and extend knowledge acquired experimentally. Once validation of these models is achieved and once a sufficient level of confidence has been attained with the models, they will play an active role in the design and evaluation of protective systems for humans in hazardous dynamic environments. Specifically, alternative aircraft and ship designs can be evaluated from the standpoint of crew system safety, with the mathematical models providing basic data in the evaluation process. It is never too soon, when considering the development of new high performance craft, to ask whether crews can function during normal operation and be reasonably protected during abnormal operation of high performance craft. Hydrofoils and surface effect machines are intended to travel at speeds up to 80 knots at rough sea states.

To establish the HIM code as a usable tool in instances of indirect impact, several preliminary problems required solutions. (The necessary theoretical considerations were presented in Chapter 3.)

Mass Distribution Properties of the Skull

In previous studies with the finite element head injury model, it was found that significant intracranial pressures occur well after skull deformation modes had dissipated. This suggests the importance of computing the correct rigid body response of the head due to dynamic loading. It is therefore necessary that the discretized finite element model of the head possess the correct inertial properties. To this end the capability for computing the mass moment of inertia tensor with respect to the center of gravity was added to the existing HIM code preprocessor. Eventually this computed data was to be compared with measured inertial distribution properties of rhesus skulls used in NAMRL testing. Correlation would validate the accuracy of the discretization.

---

[66] Naval Aerospace Medical Research Laboratory. NAMRL Monograph 21: Human head and neck response to impact acceleration, by Channing L. Ewing and Daniel J. Thomas. Pensacola, FL, Aug 1972.

Measurement of these properties is difficult but has been achieved for human cadaveric skulls[67] . Numerical computation of the inertia tensor for the modeled skull is conceptually very easy, however. For example, the mass moment of inertia tensor component with respect to the y-axis I_y through the skull is defined as

$$I_y = \int (x^2 + z^2)dm$$

where the integral is evaluated over the entire skull. Since, in the finite element discretization process, the skull continuum has been conveniently divided into a great many small elements, I_y can be approximated as

$$I_y = \sum_{i=1}^{e} (x_i^2 + z_i^2)m_i$$

where x_i and z_i are the distances in the x and z directions from the y-axis to the centroid of the ith element, m_i is the mass of ith element and e is the number of elements constituting the discretization. The element mass m_i is computed numerically by integrating the element volume which in turn is proportional to the determinant of the Jacobian $|J|$, which was defined in the element stiffness relationship (section 3.0). This quantity is routinely evaluated for each element during the initial check of the finite element mesh subsequent to the automatic mesh generative process and prior to HIM code execution. So the most important information for computing inertial quantities is available and little additional effort is required. It is also necessary to code the parallel axis theorem to enable evaluation of the inertia tensor with respect to various head anatomical reference systems.

Results of the mass moment of inertia computations are presented in Table 8-1 for the rhesus skull model used in the validation efforts reported in Chapter 6. The computational scheme was checked by measuring the displaced volume of an empty, dry rhesus skull and successfully comparing it with the computed volume of a discretized version of the same skull. In the absence of measured inertial quantities, no direct check of the data in Table 8-1 is possible. But the results appear reasonable and also compare well with the inertia of a solid sphere about a diametrical axis that is equivalent to the rhesus skull in total mass. The computational method does depend on having a great many small elements for accuracy.

---

[67] Naval Aerospace Medical Research Laboratory. NAMRL-1193: Measurement of mass distribution parameters of anatomical segments, by Edward B. Becker. Pensacola, FL, Oct 1973.

Table 8-1. Computed Mass Distribution Properties of a Discretized Rhesus Skull

Volume = 11.26 in.^{3}; Mass = $1.3(10)^{-3}$ lb-sec^2/in.

Inertia Tensor Component	Reference System	
	Axes Parallel to Frankfurt Plane and Passing Through Center of Gravity (lb-s^2-in.)	Principal Axes Passing Through Center of Gravity (lb-s^2-in.)
I_x	$0.87(10)^{-3}$	$1.27(10)^{-3}$
I_y	$1.13(10)^{-3}$	$1.13(10)^{-3}$
I_z	$1.24(10)^{-3}$	$0.84(10)^{-3}$
I_{xy}	0	0
I_{xz}	$0.10(10)^{-3}$	0
I_{yz}	0	0

Frequency Response

Frequency response data of the head injury model is useful for two different reasons and such data should be obtained in connection with validation. First, the data will aid in the selection of appropriate frequency response ranges for transducers used in experimental validation tests. It will provide upper and lower bounds to the spectrum of dominant frequencies possessed by the head.

No less important is the utility of frequency response data regarding selection of appropriate time step size in numerical simulations. Because the effect of discretizing the time domain during any execution of the model is to numerically filter the "true" solution, it is important that the "residual" or computed solution include the major frequency components. To achieve this condition, the selection of a time step size when executing the HIM code must be based, at least in part, on frequency response information.

Frequency components for various HIM code models were determined by using a general structural analysis computer code called SAP[68]. This code extracts the eigenvalues from large structural stiffness matrices by a technique known as subspace iteration[69]. The method is the current recommended procedure when large matrices are involved. Yet, there is some doubt as to whether subspace iteration converges to the lowest, and most important, mode. In any case the user of this method must accept the numerical results with little assurance beyond a convergence to a prescribed tolerance that the lowest eigenvalue is realistically the fundamental frequency.

The natural frequencies associated with the first four modes of the HIM code rhesus and human skull models are presented in Table 8-2. Experimental measurements of the lowest natural frequency has yielded numbers which are in the range of 1 to 20 Hz for human and rhesus skulls. So the computed values do appear high. This may be attributed to the model's skull bone stiffness which, from static validation efforts (Chapter 6), was shown to be too high.

Conversion of NAMRL Measured Data

A large data base constructed and stored at NAMRL contains the measured response of the head and neck for a great many dynamic tests of humans and human analogues. The crucial data conveying the motion of the head was extracted from this source and applied as input to the finite element head injury model. In this manner the intracranial response predicted by the model would be consistent with input motion and would also include the influence of the neck. A key issue is the technique in which the measured motion is applied over the contiuum of the head, that is, the means by which the motion is distributed to drive the skull model.

---

[68] University of California, College of Engineering. Report EERC 73-11: SAP IV, a structural analysis program, for static and dynamic response of linear systems, by K. J. Bathe, E. L. Wilson, and F. E. Peterson. Berkeley, CA, Jun 1973.

[69] K. J. Bathe and E. L. Wilson. "Solution methods for eigenvalue problems in structural mechanics," International Journal of Numerical Methods in Engineering, vol. 6, 1973, pp 213-226.

Table 8-2. Computed Natural Frequencies for HIM Code Models

Mode	Frequencies (Hz)		
	Empty Rhesus	Full Rhesus	Human
1	130	108	43
2	838	120	51
3	1,121	126	55
4	2,266	127	57

The theory in Chapter 3 demonstrates the feasibility of prescribing displacement histories of selected node points on the skull model. The method of prescribing displacement histories was selected at the outset because the current version of the HIM code did not allow for specification of acceleration histories but purported to work with prescribed displacement histories and initial velocities as well.

The following describes how the measured displacement data is transformed to provide prescribed input displacement history data for the HIM code model[70]. NAMRL data, which is supplied on magnetic tape, includes the translation of the origin of the anatomical coordinate system for the head as the subject is carried along on the sled. At selected sample times, the three-dimensional rotation of the head anatomical coordinate system is supplied along with the translation of the system. The rotation data consists either of four quaternions or three Euler angles. Thus, the displacement history of each node point on the skull-brain model selected for driving is obtained by the following transformation

$$\begin{Bmatrix} x(t) \\ y(t) \\ z(t) \end{Bmatrix} = \begin{Bmatrix} x_O(t) \\ y_O(t) \\ z_O(t) \end{Bmatrix} + \left[\Gamma(t)\right] \begin{Bmatrix} x_S \\ y_S \\ z_S \end{Bmatrix}$$

[70]Personal communication with L. S. Lustic, Naval Aerospace Research Laboratory, Detachment, Michoud Station, New Orleans, LA, 16 Sep 1975.

where the subscript zero denotes the location of the anatomical system origin in laboratory coordinates at time t and the subscript s denotes the location of a selected node point on the model in the anatomical coordinate system. The term [T(t)] is the transformation matrix from the anatomical coordinate system to the laboratory coordinate system at time t and is defined in Table 8-3.

Because the HIM code does not allow a variable time step specification, the transformed displacement histories must be for a constant time interval. This presents no problem when sensor data is transformed because it is currently supplied at equally spaced, 1-ms intervals. However, if the data is supplied from high speed photography it is currently only approximately equally spaced (2-ms intervals) and interpolation will then be necessary. Since Euler angles can be discontinuous they are unsuited to interpolation; quaternion would be recommended in cases where interpolation is necessary.

Because NAMRL data acquisition is completely three-dimensional, it senses and records the inevitable movement of the skull, which is not symmetrical with the midsagittal plane. The HIM code can provide a completely three-dimensional discretization, but a half-skull discretization is being employed in this effort for economical reasons. This means that any data contributing to unsymmetrical displacement must be filtered in the transformation process. This is relatively easily accomplished by zeroing out the first and third Euler angles prior to entering into the transformation equation, along with the y translational displacement component after going through the computation. The computed angular displacement of the head in the midsagittal plane is shown in Figure 8-1.

The selection of node points whose displacement histories are to be prescribed requires some elaboration. Basically, a minimum of three noncollinear nodes should be selected, and they should be on the skull bone. Since the transformation computation may involve some error, no matter how slight, the prescribed displacements for several nodes will not be exactly consistent with rigid body motion. Therefore, a fictitious strain will have been introduced into the skull bone and will depend on the error magnitude. This difficulty can be minimized by selecting a minimum number of nodes and nodes which are physically located at large distances from one another and also by carrying out the prescribed displacement computation to the maximum number of decimal places allowed by computer word length. The extent to which the fictitious skull strain affects the brain response is believed to be negligible. And since the brain's response in indirect impact simulations is what is primarily sought, the significance of the fictitious skull strain is mitigated.

Preliminary Simulations

A preliminary study of the HIM code's ability to operate with prescribed displacements was initiated with a simple model (Figure 8-2), but one which retained the basic ingredients of a skull model. This study is important in revealing the differences in numerical behavior between solutions for direct and indirect impact.

First, the model was subjected to a prescribed forcing function (direct impact), and the resulting displacements were plotted. A curve fit to this displacement data yielded a second-order polynomial displacement history as shown in Figure 8-3(a). Next, this displacement history was prescribed in a second execution of the simple model (with a zero forcing function this time). The "intracranial pressure" results from both runs compared reasonably

Table 8-3. Definition of Transformation Matrix Coefficients in Terms of Euler Angles or Quaternions

Coefficient	Euler Angle[a]	Quaternion[b]
T_{11} =	C(3) C(2)	$Q^2(4) + Q^2(1) - Q^2(2) - Q^2(3)$
T_{12} =	- S(3) C(2)	2 [Q(1) Q(2) - Q(3) Q(4)]
T_{13} =	S(2)	2 [Q(1) Q(3) + Q(4) Q(2)]
T_{21} =	C(3) S(2) S(1) + S(3) C(1)	2 [Q(3) Q(4) + Q(1) Q(2)]
T_{22} =	- S(3) S(2) S(1) + C(3) C(1)	$Q^2(4) - Q^2(1) + Q^2(2) - Q^2(3)$
T_{23} =	- C(2) S(1)	2 [Q(2) Q(3) - Q(4) Q(1)]
T_{31} =	- C(3) S(2) C(1) + S(3) S(1)	2 [Q(1) Q(3) - Q(4) Q(2)]
T_{32} =	S(3) S(2) C(1) + C(3) S(1)	2 [Q(1) Q(4) + Q(3) Q(2)]
T_{33} =	C(2) C(1)	$Q^2(4) - Q^2(1) - Q^2(2) + Q^2(3)$

[a] S(i) = Sin Euler angle i at time t
C(i) = Cos Euler angle i at time t

[b] Q(i) = Quaternion i at time t

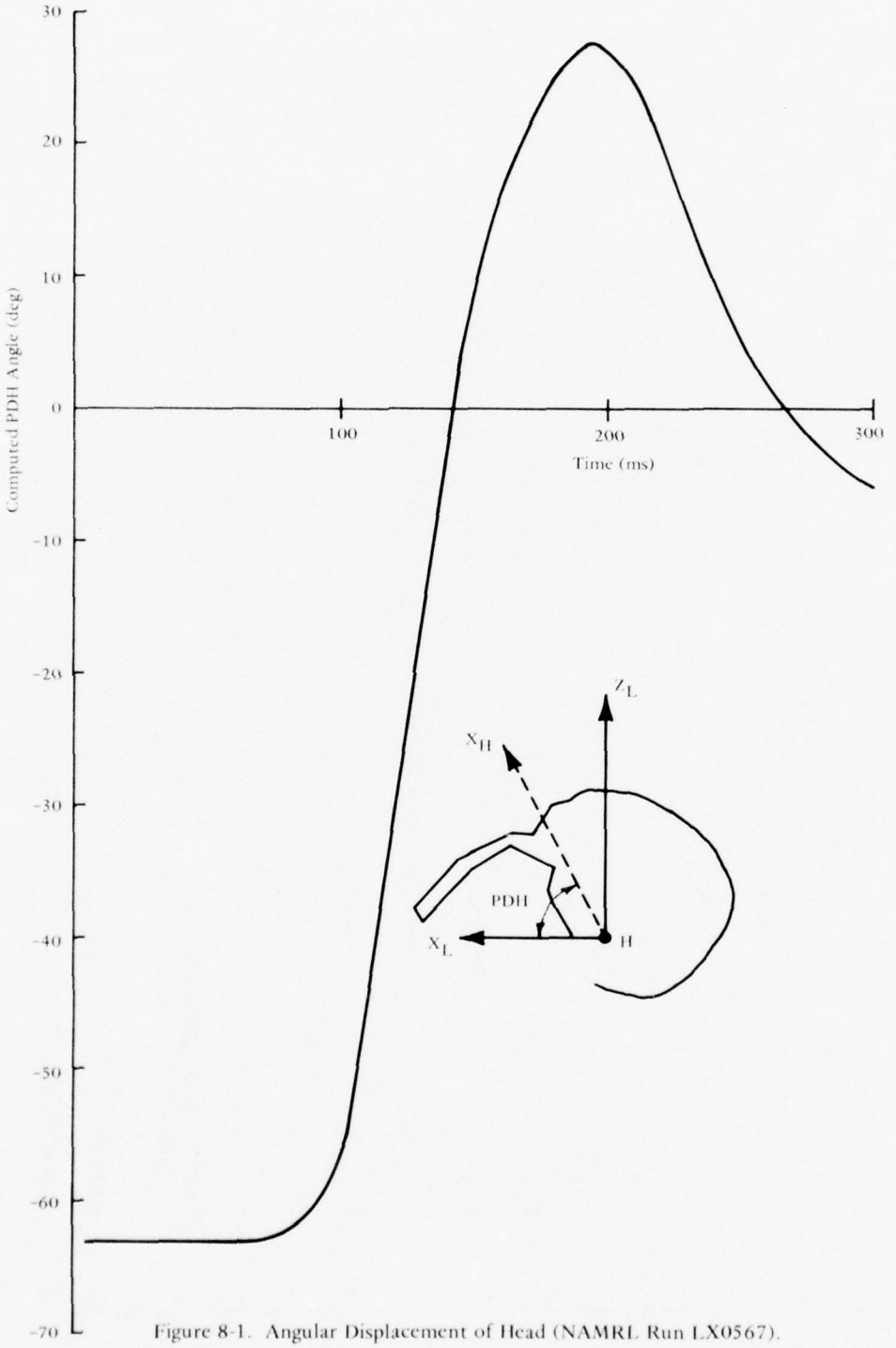

Figure 8-1. Angular Displacement of Head (NAMRL Run LX0567).

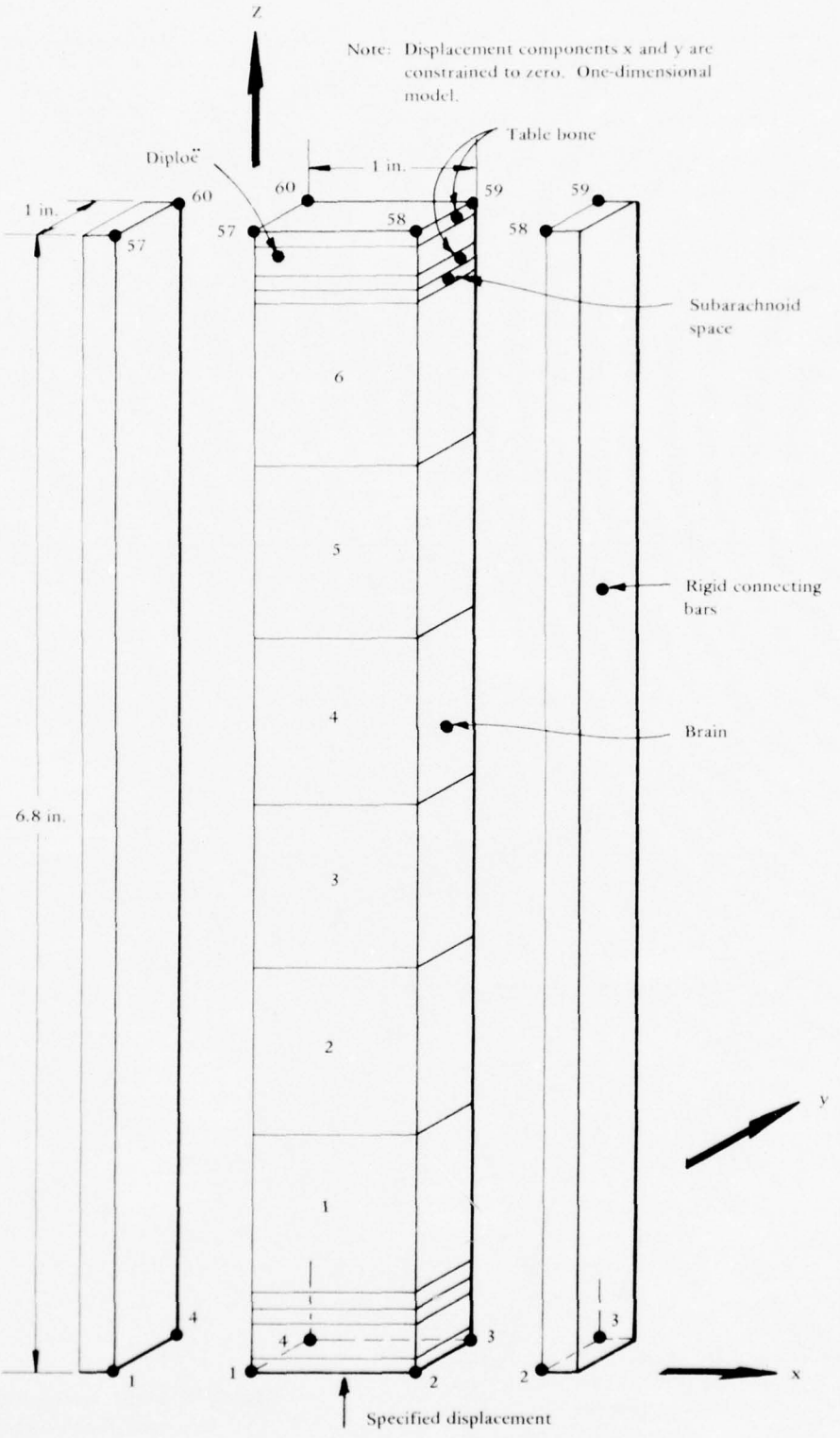

Figure 8-2. Preliminary Indirect Impact Model.

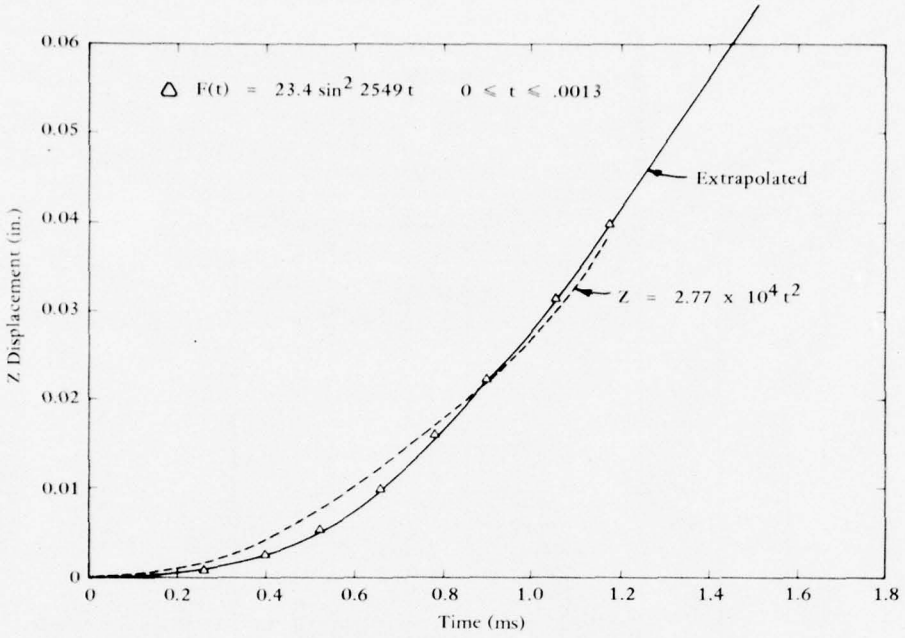

(a) Equivalent displacement history.

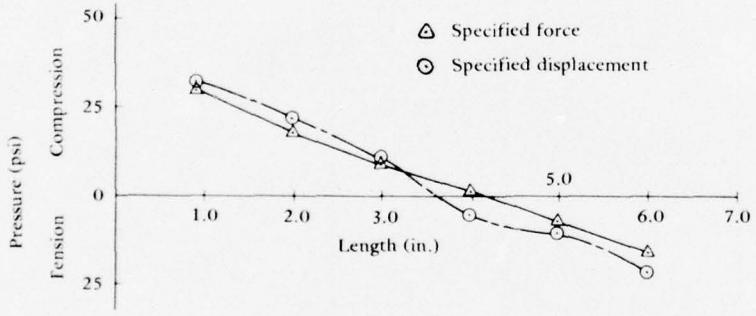

(b) Intracranial pressure gradient at t = 0.39 ms.

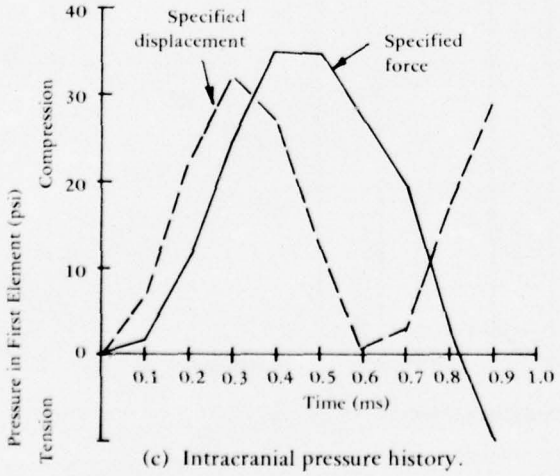

(c) Intracranial pressure history.

Figure 8-3. Initial Demonstration of Prescribed Displacements Option.

well as is seen in Figure 8-3(b) and (c) considering the differences in input. This indicated that the specified displacement option of the HIM code was apparently working satisfactorily.

Following this, further preliminary computations were conducted with two oscillating-type functions (sine-squared and sine) having longer durations. This type of displacement function was anticipated with NAMRL data extracted from both repeated load (obtained from shake table experiments) and sled tests. The input function and the results are presented in Figures 8-4(a) and (b). Computed "intracranial pressures" in each case fluctuated unexpectedly. Suspecting that the time step size was to coarse in comparison to the natural period of a typical brain element, the time step was successively reduced—first for the sine-squared function and then for the sine function. In Figure 8-4(a) it can be seen that the time step size reduction had no effect.

The initial conditions were then investigated. The sine-squared function has a zero first derivative at time zero (initial velocity), but a nonzero second derivative at time zero (initial acceleration). By assigning these initial conditions and repeating the computer run with the most coarse time step, the computed "intracranial pressures" were found to vary smoothly in an expected manner. However, a paradox arises and can be seen by writing the equation of motion for a simple, undamped, spring-mass system (see Equation 3-30). This equation is obviously not satisfied at time zero when an initial acceleration and a zero initial displacement is applied. Thus, while the sine-squared function for displacement definitely possesses a *nonzero second* derivative at time zero and through its specification the results appear satisfactory, it is not strictly valid to specify it as an initial condition for the physical system.

The sine function for displacement possesses a nonzero first derivative (initial velocity) and a zero second derivative. Specification of these initial conditions reduces considerably the computed fluctuation in pressure as is seen in Figure 8-4(b). Further reductions in time step size then show still more improvement, but this improvement would not exist without first having specified the correct initial velocity.

Therefore, it is necessary to be cognizant of initial velocity conditions and specify them when using the displacement option of the HIM code. It is also apparently necessary to employ time steps no larger than eight times the critical value to avoid excessive intracranial pressure fluctuations. Since typical NAMRL sled tests have durations of around 300 ms, the cost of using the present operator will probably be high. It may be possible to use the same operator (Newmark β method) along with some prescribed numerical damping. The fluctuations which appear in the pressure solution are not unstable (they do not grow without bound). It is seen that their mean or average value is the solution sought, and thus some form of damping ($\beta \neq 1/4$) could allow the use of larger, more economical time steps.

HIM Code Simulation of Indirect Impact

Using the human skull model, several attempts were made to compute intracranial pressure histories while specifying input displacements. In each case the intracranial pressure results exhibited the fluctuation noted in the previous section. Durations of these prescribed displacement histories varied from 10 to 100 ms and time step sizes were from 1 to

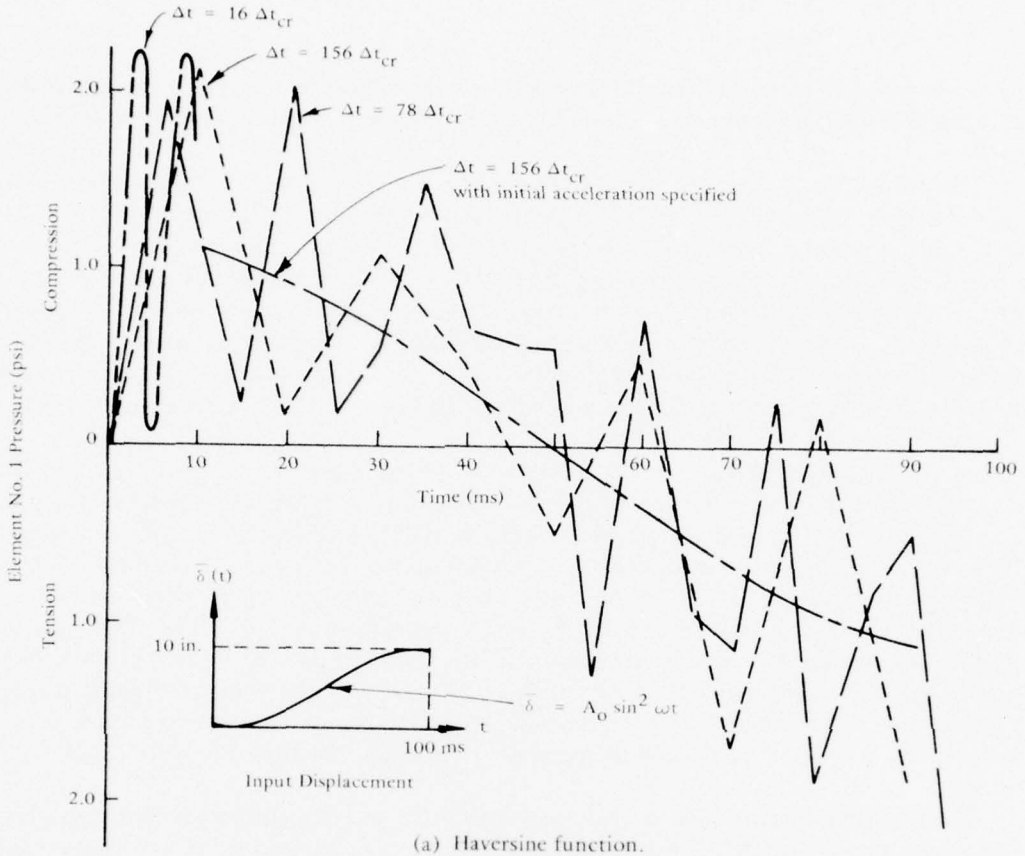

(a) Haversine function.

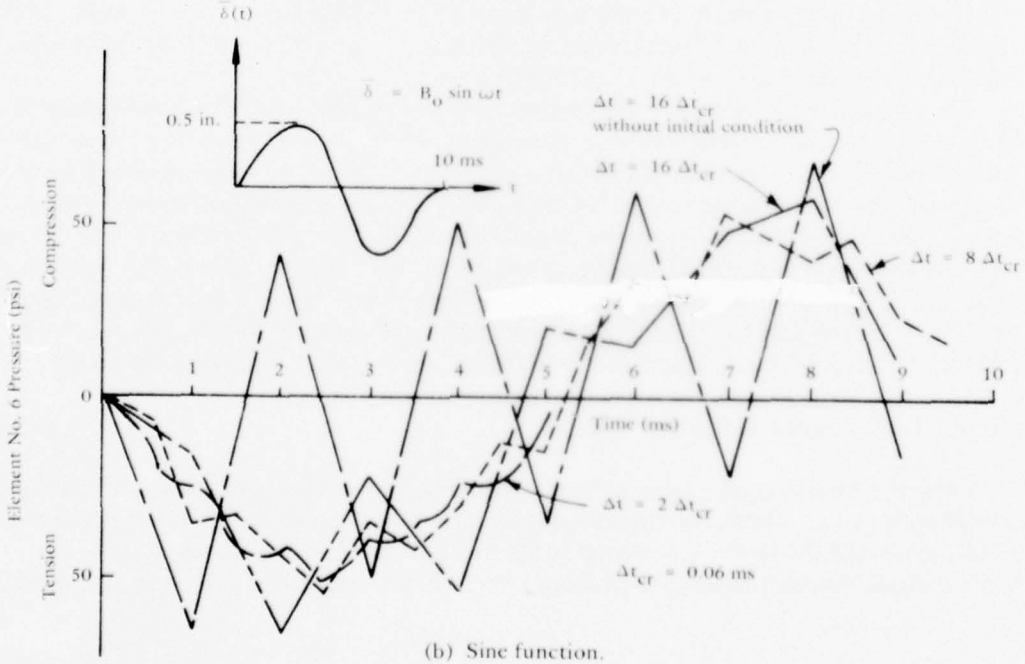

(b) Sine function.

Figure 8-4. Pressure Fluctuation.

5 ms. A typical example is illustrated in Figure 8-5. Here the input displacement (Figure 8-5a) is translational only and in this case is the measured displacement of the skull during the initial phase of NAMRL sled test no. LX0567. These displacement components were assigned to several node points surrounding the foramen magnum so that the skull model was driven at the base of the skull. Translation occurred in the $-G_X$ and $-G_Z$ directions simultaneously. As can be seen in Figure 8-1, little rotation of the head occurred during the first 100 ms of run no. LX0567. The pressure fluctuations taken from an element in the posterior brain are shown in Figure 8-5(b). This behavior was exhibited throughout the brain. The time step size, 5 ms, is believed to be too coarse for use with the brain elements, which are similar in size to those for the preliminary model discussed in the previous section. Yet a smaller time step would not be economical for a NAMRL test duration of 300 ms. This analysis cost about $200 and spanned only the first one-third of the total test run. Thus, a more economical integration scheme is required that will allow larger time steps and contain sufficient numerical damping to produce smooth computed pressure histories in the brain. The smoothed average of the pressure fluctuation exhibits a tensile pressure in the posterior brain as would be expected. Further, the pressure magnitude is considerably lower than HIM code pressure predictions for direct impact (Chapter 7). This appears to be uniformly true with comparisons of indirect and direct impact intracranial response.

A possible alternative to specifying directly an input displacement is to compute beforehand an equivalent forcing function which when specified would produce the desired displacement. The computed inertial properties (Table 8-1) of the model must be employed in this process to transform a prescribed displacement to an "equivalent" prescribed forcing function.

To demonstrate this method the nodal points on the perimeter of the foramen magnum were assigned equivalent force-time histories and a simulation was made. These nodes were constrained to translate in the $-G_X$ direction according to the displacement function $U(t) = 500\ t + 1200\ t^2$, where U is measured in inches and t in seconds. Therefore, the skull moves according to an initial velocity of 500 in./s and a constant acceleration of about 6.2 g's. Every node in the skull-brain system was automatically assigned the initial velocity value. Initial displacements were assumed zero, although provision is made for their simultaneous specification. The simulation was carried out through 10 ms.

The displacement, stress, and shear strain are presented in Figure 8-6 at 5, 7, and 9 ms. The stress state continues to increase until at 9 ms the maximum stresses are developed. A slight forward rotation is evidenced in the curvature of the stress contours of the anterior brain. It cannot be seen in the displacements because the translational movement is dominant. The stress and strain magnitudes are given in Table 8-4 and show lower magnitudes than those in the direct impacts, which, of course, involve higher acceleration levels.

Linear Model Limitation

It should be emphasized that the HIM code is a linear finite element code and that all the results discussed to this point are subject to the limitations imposed by linear elasticity theory. Two such limitations which are particularly important involve geometry and are the limitations of small displacements and small strains. The normal strain component ϵ_X of

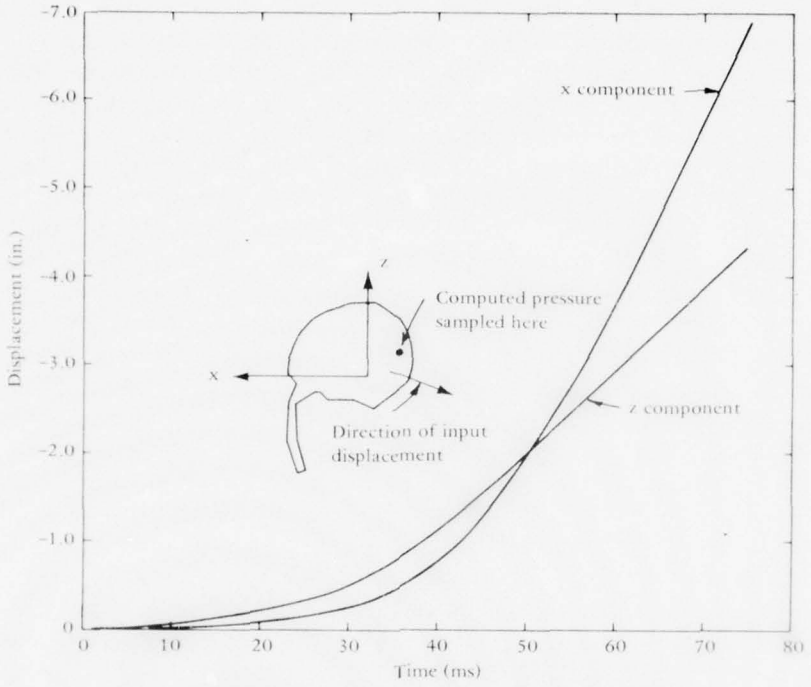

(a) Specified translational displacement history of skull.

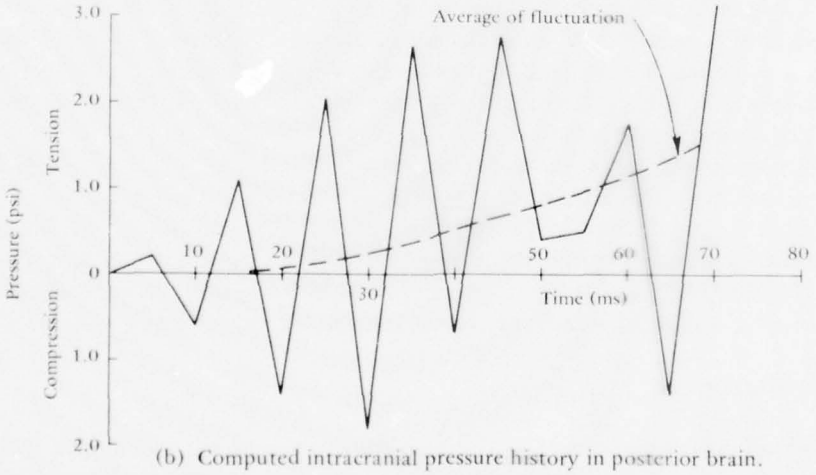

(b) Computed intracranial pressure history in posterior brain.

Figure 8-5. Typical Response of Intracranial Pressure Due to Prescribed Displacements.

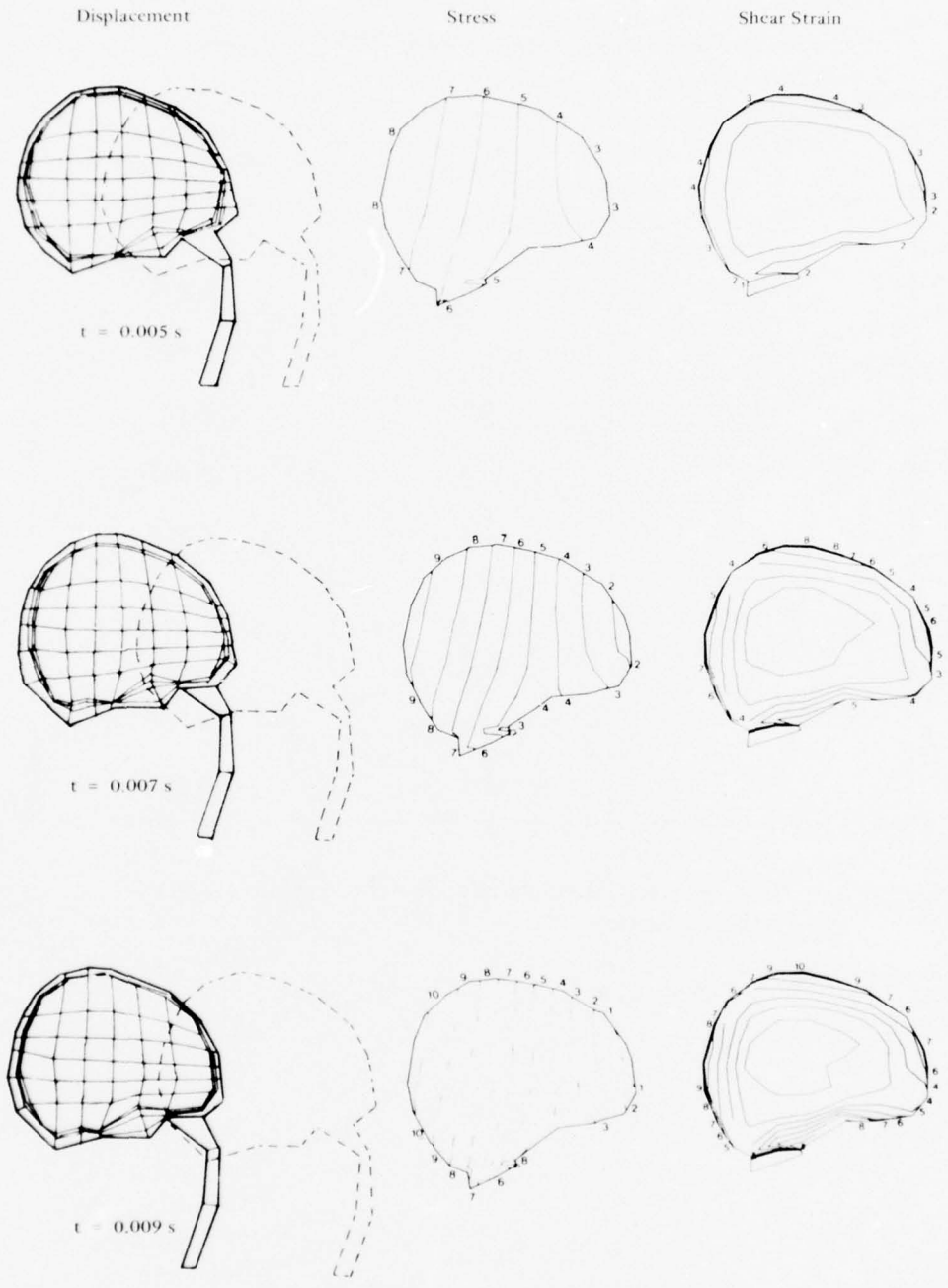

Figure 8-6. Indirect Impact Response for Translated Skull.

Table 8-4. Contour Values for Translated Skull

Contour No.	Stress[a, b] (psi)	Maximum Shear Strain
1	-9.0	0.029
2	-7.0	0.059
3	-5.0	0.088
4	-3.0	0.117
5	-0.9	0.147
6	+1.1	0.176
7	+3.1	0.205
8	+5.2	0.233
9	+7.2	0.263
10	+9.2	0.293

[a] Negative sign indicates compression, and positive sign indicates tension.

[b] 1 psi = 0.069 bar.

Equation 3-4 is defined as the change in length of a unit length originally oriented parallel to the X axis. The shear strain component ϵ_{xy} of Equation 3-5 is defined as half the angle change between two lines originally parallel to the X and Y axes. The second-order strain terms of Equations 3-4 and 3-5 extend these definitions to cases involving large movements which have rotated the original axes by gross amounts.

A study was made to determine the extent of rotation that the HIM code simulation could sustain before the linear assumption was no longer valid. Evidence of error becomes apparent when the computed displacements exhibit a uniform dilation. The study consisted merely of trying several head impact simulations allowing rotation to occur and measuring the angle of rotation. Generally it was found that dilation in the displacements began occurring at about 10 degrees of rigid body rotation. The dilation is uniform and is not accompanied by the development of any stress or strain. In fact, the stress and strain responses appear to be normal; i.e., the response as usual subsides subsequent to application of peak loading even though the rigid rotations continue beyond 10 degrees. Still the validity of the linear computation must be regarded as suspect for large rotations.

To correct the situation, a nonlinear analysis is required. One method is to update the coordinate system for the skull-brain system during the latter time steps when large rotations are being experienced. This is theoretically an easy modification in the HIM code and does not require the addition of the second-order terms in the strain formulation. After each time step the computed displacements are added to the coordinates to define a new system. Naturally it is costly computationally. Each time that the coordinate system is updated the modified stiffness matrix on the left-hand side of Equation 3-34 will change, necessitating another inversion of the system of equations. One such simulation has been made with the HIM code, and the cost was increased by a factor of 2.5.

Such corrective action merely solves the problem of large rotation; it is not sufficient when the strains themselves are large. In this event the second-order terms must be included to avoid inaccuracies. The shear strain values given in Tables 7-1 through 7-4 are large, indicating the associated linear analyses to be more accurate for simulated loads scaled down from 1,000 pounds. To solve the problem of large strain in the brain a nonlinear, nearly incompressible, finite element formulation is required. This element has been developed by Hughes, et al.[34]. Some numerical experimentation with the two-dimensional version of this element is presented in the following.

A single quadrilateral element was pinned at one corner and assigned an initial velocity at the other three corners in such a way as to induce large rotational excursion about the pinned corner. Because of the centrifugal forces setup, internal strains should develop in the element. However, with the linear version of the quadrilateral element, the computed strain in the element is everywhere zero, and the attending erroneous dilation, as described above, occurs as shown in Figure 8-7. With the nonlinear element the results are quite different for the same problem. As shown in Figure 8-8, the computed Lagrangian strain E is nonzero and the distortion of the square element is consistent with the centrifugal force. No artificial dilation occurs with large rotations in this instance.

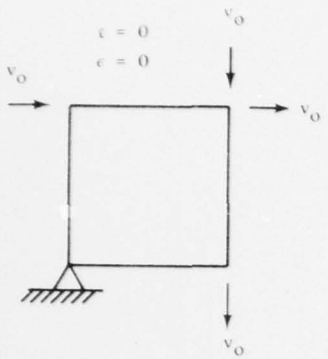

Bulk modulus = 1.0×10^6
Shear modulus = 0.4×10^6
Density = 1.0
v_o = 352

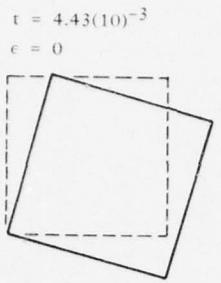

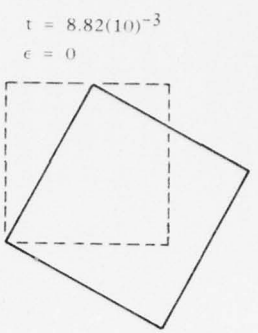

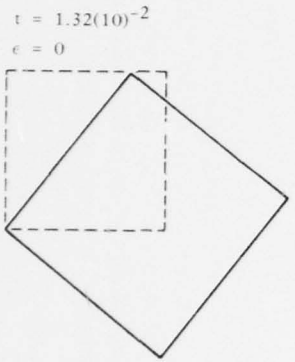

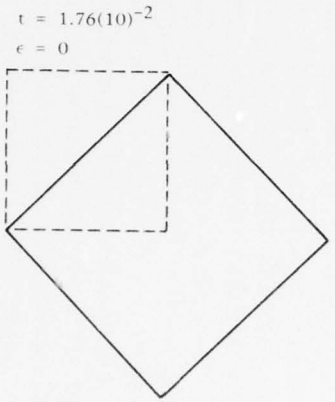

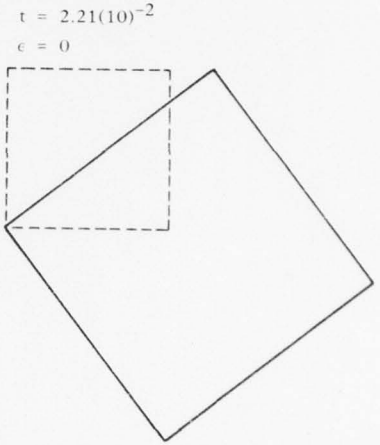

Figure 8-7. Effect of Large Rotation on Linear Element.

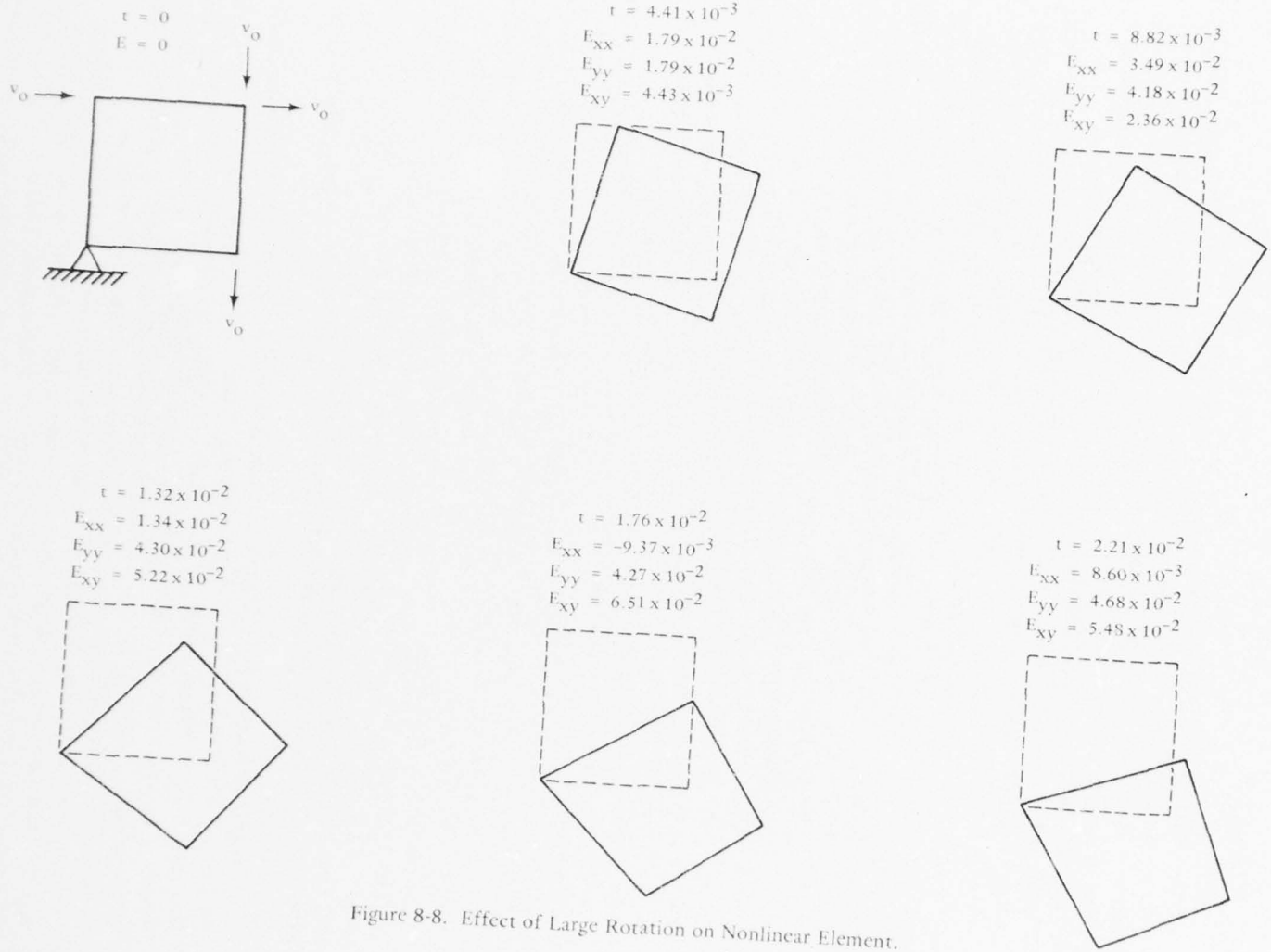

Figure 8-8. Effect of Large Rotation on Nonlinear Element.

9. CONCLUSIONS

A fully three-dimensional head injury model computer code, referred to as the HIM code, was presented. Its development from preliminary one- and two-dimensional models through to the present completed model was predicated on the importance of recognizable geom try in head injury modeling. Time histories of displacement stress and strain are computed throughout the skull-brain continuum for arbitrary direct impact loads.

The model is applicable to closed brain injury exclusive of neck-related trauma as well as skull bone injury. The advantage of the finite element approach is that is provides a generalized capability for studying head injury. The HIM code has been designed with sufficient flexibility to accommodate new information as it becomes available regarding geometry and material properties. A wide range of human and primate skulls can be easily and automatically discretized to assist in almost any head-impact study. The accuracy achieved in such studies is significantly enhanced by employing recognizable geometry. Boundary conditions and impact loads require only a minimum of idealization. Any or all parts of the skull-brain system can be idealized as being either viscoelastic or linear elastic.

A direct integration technique is used to integrate the equations of motion in the HIM code. The primary advantage of the method is that it can integrate those vibration modes which are most prominent in a response due to an arbitrary impact force, whether it be of short or long duration. Control is provided by specification of a time step size consistent with the frequency content of loading. Besides this flexibility, the direct integration method can be readily employed in an extension to nonlinear analyses.

Results from a two-dimensional axisymmetric finite element model compared favorably with results from a similar finite difference model. In those instances when an axisymmetric fluid-filled shell may be considered a useful head injury model, the finite element method is shown to be competitive with other numerical and analytical approaches. When dealing with load durations exceeding 1 ms, it is perhaps more attractive than the finite difference method and in most cases always offers more flexibility than analytical approaches.

A two-dimensional plane strain model demonstrated the importance of simulating more complex geometry. Skull bending and intracranial pressure distributions were predicted more realistically than in previous modeling efforts. Potential sites of linear skull fracture and closed brain injury were indicated relative to anatomical features. Furthermore, the sensitivity of these locations to the characteristics of loading and boundary conditions was clearly evident.

A modification of the isoparametric element formulations for simulating brain matter produced a response representative of clinically observed intracranial response. The element was obtained by a reduced form of numerical integration termed one-point Gaussian quadrature. This procedure is necessary to effect a conventional finite element analysis of nearly incompressible materials. In this way the brain is idealized as a nearly incompressible material consistent with available experimental data on brain material properties.

Coup and contrecoup intracranial response are very evident in simulations with the model. Inclusion of the foramen magnum causes a posterior shift in the null point of the otherwise symmetrical, anterior-posterior, pressure distribution. This behavior is consistent with previous experimental observations. Further, it is an explanation of the asymmetry in

statistical distribution, noted in the literature, of contrecoup and coup injury occurring as a result of frontal and occipital impacts.

The brain is simulated as being isolated from the cranial wall by including a compressible representation of the subarachnoid space. In this way intracranial volume shifts and the brain slosh mechanisms that have been clinically observed can also be observed in the model's response.

Automated mesh generators are the only practical means for developing discretizations for head injury models which depict recognizable geometry. They cannot avoid all the laborious effort of extracting measured data because a minimum of this information is necessary. Nevertheless, they are to be preferred over completely manual efforts at generating the discretizations. Automatic mesh generators result in skull-brain discretizations which are uniform as well as consistent with the specified geometry.

Techniques for efficient equation solving, including optimal renumbering of the system of motion equations, are necessary for an economically flexible head-injury model. Two basic discretizations are provided the user in the HIM code: a fine and a coarse mesh. Each allows for taking full advantage of symmetrical conditions when they exist. The present linear HIM code costs approximately $200 per simulation, including apprximately $30 of data post-processing. These costs are based upon present commercial computer rates and involve anywhere from 10 to 15 time steps with the fine discretization.

The HIM code has undergone extensive numerical testing, and all known bugs have been corrected. With the exception, perhaps, of simulating the brain material, the HIM code has been constructed with standard dynamic, finite element techniques. A qualitative validation has been established through comparisons with theory for simple models, through comparison with solutions from methods other than finite element, and through observing the reasonableness of both the skull bone response and the coup and contrecoup response in the brain. Attempts at quantitative validation have not proved successful. The present skull bone finite element characterization is found to be too stiff. To correct the problem an eight-node incompatible element has been developed which will allow more bending but, as yet, has not been incorporated and tried. Comparison of measured and computed intracranial pressures are difficult but were attempted anyway in this study. Measured epidural pressures in anesthetized rhesus monkeys were on the order of 10 psi while computed intracranial pressures of primate simulations were on the order of 37 psi. While this is only within an order of magnitude agreement, previous model attempts were known to have computed pressure in excess of 100 and even 1,000 psi. Future improvements in both experimental and modeling techniques may well establish a satisfactory quantitative validation.

Simulations with the HIM code have assisted in defining the limits of its applicability imposed by the assumptions of linearity. Rigid body rotations in excess of 10 degrees may require nonlinear strain terms if the response of interest has not already subsided. Shear strains were predicted which are in the realm of large strain analysis and indicate a requirement for nonlinear formulations independent of large rotations. Efforts are presently underway to effect a nonlinear analysis. Meanwhile the linear HIM code predictions can yield useful insight into the mechanical causes of skull and brain injury.

Qualitative information obtained from the linear HIM code can provide useful insight into the mechanical-clinical relationships of head injury. Though this report, in the main,

describes the development of a head injury analysis tool, some results derived during the course of the project do fall under this category and are discussed in the following paragraphs.

The skull bone stress response induced by an occipital impact suggests that impending skull fracture would occur along a path between the point of loading and the foramen magnum. While the skull is thick in this region, the foramen magnum presents an area of stress concentration.

The relative displacement between the skull and brain observed in the predicted response has also been observed in tests involving primates with implanted lucite calvariums. This motion appears beneficial in alleviating somewhat the stress in the brain. But the beneficial effect is true only up to a point. Strain develops at the brain's surface when further relative motion is prevented by either geometrical or mechanical constraints at the skull-brain interface. The tendency for brain elements nearest this interface to deform more than those in the midbrain area is very apparent in the graphics of the deformed mesh.

The boundary condition specification has been shown to influence significantly the computed intracranial response by a comparison of a restrained skull, a partially restrained skull, and an unrestrained skull, all subjected to the same impact load. Predicted intracranial stress distributions develop null pressure regions which tend to locate above the foramen magnum independent of the direction of impact. Thus, for unrestrained impacts, significant contrecoup tensile stresses will exist for impacts to the occiput and significant coup compression stresses will exist for impacts to the frontal bone. The contours at the anterior and posterior brain surfaces locate closely the sites of potential coup and contrecoup damage in the midsagittal plane.

Shear strain predictions for direct impact loads have shown the brainstem region to be most vulnerable. Besides the brainstem region, the outer surfaces of the brain developed shear strains. The midbrain region evidenced little or no shear strain. This response is true also of the indirect impact load case except that the maximum shear strains occurred at the brain surface as opposed to the brainstem region.

The results are generally independent of the restraint conditions at the base of the skull and thus the neck is not expected to modify them greatly.

10. RECOMMENDATIONS

Recommendations can be divided into two categories. The first category pertains to the linear HIM code and the second category pertains to the development of a nonlinear head injury model.

First, with regard to improving the linear HIM code and its validation with experimental data, three specific recommendations are made.

1. The linear isoparametric element, eight-node brick used to model the skull bone structure should be replaced with an incompatible finite element formulation to allow more effective modeling of the bending stress gradient across the simulated three-layered cranial thickness. The skull element should remain three-dimensional, as is now the case, as opposed to a two-dimensional shell element.

2. Employ reduced integration (one-point quadrature) with the dilatational terms of the brain element stiffness matrix only, while using the normal quadrature rule for the distortional energy terms. This should preserve the present, nearly incompressible, formulations for the brain element while reducing the strain magnitudes, which are typically very large in the present HIM code computations.

3. Improvement of the HIM code running efficiency can be made by the following:
   (a) Incorporating the bandwidth minimizing routines directly into the HIM code so that their use is transparent to the user.
   (b) A more efficient procedure can be adapted for solving the equilibrium equation if special hardware features available on the CDC 6600 are employed.
   (c) Direct access I/O should be used in processing the right-hand side vectors. This would be especially useful for dynamic analyses of multiload vectors.
   (d) The inner product calculations involved in backward reduction could be done more efficiently. The same techniques noted in (b) above should be adapted.
   (e) I/O methods currently employed in the program could be reworked advantageously.
   (f) The program should be overlayed.

With these improvements it is estimated that the running costs could be reduced by 50%. Further recommendations would include the following.

1. Injury or "failure" criteria for the simulated structures of the brain and skull should be developed and incorporated into the HIM code; then the computed results summarized into a printed description of injury hazard for each HIM code simulation.

2. Additional parameter studies should be conducted for the purpose of generating a head injury data base which would facilitate directly the preparation of safety standards.

3. Preprocessor and postprocessor integration into the HIM code would greatly enhance use of the code and analysis of the data. These routines have been completed, but remain separate from the HIM code.

Recommendations pertaining to the nonlinear head injury model are less specific than the above recommendations. A nonlinear computer code similar to the basic HIM code exists, but the HIM code input module (geometry, etc.) must be incorporated and checked out first before more detailed and specific recommendations can be made regarding a nonlinear code. Assuming this is accomplished, the following recommendations can be made:

1. Repeat selected linear HIM code runs with the nonlinear model to discern the differences and further define the limitations of the less expensive linear model.

2. With the large-rotation/large-strain capability, simulate the large head rotation data typical of NAMRL test sled runs.

3. Investigate appropriate temporal integration techniques to eliminate numerical noise associated with the use of the Newmark method along with prescribed displacement data input.

4. Develop a capability to input prescribed acceleration data to eliminate any error associated with numerical smoothing (double integration) of measured acceleration data.

5. Develop a capability to synthesize the nonlinear head injury model code and the contact/impact prediction code. In this way, the dynamic impact of both the simulated skull and target can be included in one computer run.

11. ACKNOWLEDGEMENTS

Dr. Lee J. Ovenshire of the National Highway Traffic Safety Administration, initiated funding for this work under Interagency Agreement DOT-4S-289-550 1A. Subsequently, funding support was provided by Dr. Channing L. Ewing, Naval Aerospace Medical Research Laboratory, Michoud Station, New Orleans. Their enthusiastic sponsorship is greatly appreciated. Also the writer would like to thank Mssrs. David Corrente, Michael Katona, and John Crawford of the Civil Engineering Laboratory for their able and timely assistance.

Appreciation is also expressed to Dr. Ken Saczalski of the Office of Naval Research and Dr. Hank Christiansen of Brigham Young University for making available the funds for and construction of the continuous tone computer graphics of the simulated skull-brain geometry.

12. REFERENCES

1. National Safety Council. Accident facts. Chicago, Il, 1976.

2. National Highway Traffic Safety Administration. NHTSA DOT-HS-801715: Effect of the fuel shortage on travel and highway safety, by E. C. Cerrelli. Washington, DC, Aug 1975.

3. S. P. Desjardins. "Vehicle crashworthiness," Numerical and Computer Methods in Structural Mechanics, ed. S. J. Fenves, et al. New York, Academic Press, 1973, pp 557-584.

4. Army Air Mobility Research and Development Laboratory. TR-71-22: Crash survival design guide. Fort Eustis, VA, Oct 1971.

5. K. J. Saczalski, et al. "A critical assessment of the use of non-human responding surrogates for safety system evaluation," in Proceedings of the Twentieth Stapp Car Crash Conference, SAE, 1976.

6. T. Hayashi. "Study of intracranial pressure caused by head impact," Journal, Faculty of Engineering, University of Tokyo, 1969, pp 30-59.

7. A. E. Engin and Y. King Liu. "Axisymmetric response of a fluid-filled spherical shell in free vibrations," Journal of Biomechanics, vol. 3, no. 1, Jan 1970.

8. Y. C. Lee and S. H. Advani. "Transient response of a sphere to torsional loading—a head injury model. Math," Biosciences, vol. 6, 1970, pp 473-486.

9. Naval Air Development Center. Report No. NADC-CS-7113: Impact analysis of the skull-brain system, by Stephen L. Gordon. Warminster, PA, Dec 1971.

10. ———. Interim Report No. NADC 73065-40: Analysis of head impact, by Stephen L. Gordon. Warminster, PA, Apr 1973.

11. J. V. Benedict, E. H. Harris, and D. U. von Rosenberg. "An analytical investigation of the cavitation hypothesis of brain damage," Journal of Basic Engineering, vol. 92, Sep 1970, pp 597-603.

12. Anthony James Crispino. A dynamic analysis of an elastic model of the human head, M. S. thesis, Department of Mechanical Engineering, University of Washington. Seattle, WA, 1972.

13. O. C. Zienkiewicz. The finite element method in engineering science. London, England, McGraw-Hill, 1971.

14. Richard H. Gallagher. Finite element analysis: Fundamentals. Englewood Cliffs, NJ, Prentice-Hall, 1975.

15. Shugar, T. A., "Simulating and Modeling the Human Head's Response to Impact," Aircraft Crashworthiness, Eds K. Saczalski, G. T. Singley III, W. D. Pilkey, and R. Huston, University Press of Virginia, Charlottsville, 1975, pp 213-234.

16. A. I. King and C. C. Chou. "Mathematical modeling, simulation and experimental testing of biomechanical system crash response," paper presented at Eleventh Annual Meeting, American Institute of Aeronautics and Astronautics, Washington, DC, Feb 1975. (AIAA paper no. 75-272)

17. W. Goldsmith. "The physical processes producing head injury," in Proceedings of the Head Injury Conference, Lippincott, Philadelphia, PA, 1966, pp 350-382.

18. Office of Naval Research. Technical Report No. 8: Elastic analysis of a skull, by C. H. Hardy and P. V. Marcal. Washington, DC, Nov 1971. (Contract No. N00014-67-A-0191-0007)

19. V. H. Kenner and W. Goldsmith. "Dynamic loading of a fluid-filled spherical shell," International Journal of Mechanical Sciences, vol. 14, 1972, pp 557-568.

20. T. B. Khali, W. Goldsmith, and J. L. Sackman. "Impact on a model head-helmet system," International Journal of Mechanical Sciences, vol. 16, 1974, pp 609-625.

21. H. S. Chan. "Mathematical model for closed head impact," in Proceedings of the Eighteenth Stapp Car Crash Conference, Ann Arbor, MI, Dec 1974, pp 557-578.

22. Ernst Schrem. "Computer implementation of the finite-element procedure," Numerical and Computer Methods in Structural Mechanics, ed. S. J. Fenves, et al. New York, Academic Press, 1973, pp 79-117.

23. C. C. Ward. A dynamic finite element model of the human brain, Ph. D. thesis, Department of Engineering, University of California at Los Angeles. Los Angeles, CA, 1974.

24. C. C. Ward and R. B. Thompson. "The development of a detailed finite element brain model," in Proceedings of the Nineteenth Stapp Car Crash Conference, San Diego, CA, Nov 1975. pp 641-670.

25. West Virginia University, Biomechanics Laboratories, Department of T and AM. Head injury model construction program data compilation and review. Morgantown, WV, Jun 1971. (Contract No. PH-43-67-1137)

26. University of California, Department of Civil Engineering. Finite element analysis program, by R. L. Taylor. Berkeley, CA.

27. J. W. Pugh, et al. "Elastic and viscoelastic properties of trabecular bone: dependence on structure," Journal of Biomechanics, vol 6, no. 5, Sep 1973.

28. Y. C. Fung. "Stress-strain-history relations of soft tissues in simple elongation," Biomechanics, ed. Y. C. Fung, N. Perrone, and M. Anliker. Englewood Cliffs, NJ, Prentice-Hall, 1972. pp 181-208.

29. R. C. Tennyson, R. Ewert, and V. Niranjan. "Dynamic viscoelastic response of bone," Experimental Mechanics, Nov 1972.

30. H. C. Wang and A. S. Wineman. "A mathematical model for the determination of viscoelastic behavior of brain in vivo—I Oscillatory response," Journal of Biomechanics, vol 5, 1972, pp 431-446.

31. X. T. Truong. "Visco-elastic propagation of longitudinal waves in skeletal muscle," Journal of Biomechanics, vol 5, 1972, pp 1-10.

32. J. E. Galford and J. H. McElhaney. "A viscoelastic study of scalp, brain, and dura," Journal of Biomechanics, vol 3, 1970, pp 211-221.

33. Civil Engineering Laboratory. Contract Report CR-75.007: Finite element formulation and solution of contact-impact problems in continuum mechanics, by T. J. R. Hughes, R. L. Taylor and J. L. Sackman. Berkeley, CA, University of California, May 1974.

34. ————. Contract Report CR-75.008: Finite element formulation and solution of contact-impact problems in continuum mechanics—Part II, by T. J. R. Hughes, R. L. Taylor, and J. L. Sackman. Berkeley, CA, University of California, Jan 1975.

35. ————. Contract Report CR-77.001: Finite element formulation and solution of contact-impact problems in continuum mechanics—Part III, by T. J. R. Hughes, R. L. Taylor, and J. L. Sackman. Berkeley, CA, University of California, Jul 1975.

36. ————. Contract Report CR-77.002: Finite element formulation and solution of contact-impact problems in continuum mechanics, Part IV, by T. J. R. Hughes, R. L. Taylor, J. R. Sackman, and W. Kanoknukulchai. Berkeley, CA, University of California, 1976.

37. T. J. R. Hughes, et al. "Finite element formulation and solution of a class of contact-impact problems in continuum mechanics," paper presented at Third Conference, Structural Mechanics Reactor Technology, London, England, 1975.

38. R. L. Taylor. "An approximate method for thermovisco-elastic stress analysis," Nuclear Engineering and Design, vol. 4, 1966, p. 21.

39. I. Fried. "Finite element analysis of incompressible material by residual energy balancing," International Journal of Solids-Structures, vol. 10, 1974, pp 993-1002.

40. D. J. Naylor. "Stresses in nearly incompressible materials by finite elements with application to the calculation of excess pore pressures," International Journal for Numerical Methods in Engineering, vol. 8, 1974, pp 443-460.

41. T. A. Shugar and M. G. Katona. "Development of finite element head injury model," Journal of Engineering Mechanics Division, ASCE, vol. 101, EM3, Jun 1975, pp 223-239.

42. R. S. Dunham, R. E. Nickell, and D. C. Stickler. "Integration operators for transient structural response," Computers and Structures, vol 2, no. 1/2, Feb 1972. pp 1-16.

43. R. W. Clough and J. Penzien. Dynamics of structures. New York, NY, McGraw-Hill Book Company, 1975. p. 271.

44. R. D. Cook. Concepts and applications of finite element analysis. New York, NY, John Wiley and Sons, Inc., 1974. pp 252-253.

45. Nathan M. Newmark. "A method of computation for structural dynamics," Journal of the Engineering Mechanics Division, ASCE, EM3, Jul 1959.

46. University of California. SESM Report 68-1: A computer program for the dynamic stress analysis of underground structures, by E. L. Wilson, Berkeley, CA, Jan 1968.

47. John C. Houbolt. "A recurrence matrix solution for the dynamic response of elastic aircraft," Journal of Aero Science, vol. 17, 1950, p. 540.

48. P. D. Lax and R. D. Richtmeyer. "Survey of the stability of linear finite difference equations," Communications on Pure and Applied Mathematics, vol. 9, no. 2, May 1956.

49. Robert E. Nickell. "On the stability of approximation operators in problems of structural dynamics," International Journal of Solids and Structures, vol. 7, 1971, pp 301-319.

50. University of Washington, Department of Mechanical Engineering. A dynamic analysis of an elastic model of the human head, by Howard C. Merchant and Anthony J. Crispino. Seattle, WA, 1972.

51. Ali E. Engin. "The axisymmetric response of a fluid-filled spherical shell to a local radial impulse—a model for head injury," Journal of Biomechanics, vol. 2, 1969, pp 325-341.

52. W. Goldsmith. "Biomechanics of head injury," Biomechanics, Its Foundations and Objectives, ed. Y. C. Fung, N. Perrone, and M. Anliker. New York, Prentice-Hall, 1972, pp 585-634.

53. J. W. Melvin, P. M. Fuller, and I. T. Baradawala. "The mechanical properties of the diploë layer in the human skull," in Proceedings of Spring Meeting, Society for Experimental Stress Analysis, Westport, CT, 1970.

54. Y. K. Liu. "Discussion of Paper No. 751163: The development of a detailed finite element brain model," SAE Transactions (to be published Jan 1977).

55. L. M. Patrick, H. J. Mertz, Jr., and C. K. Kroell. "Cadaver, knee, chest, and head impact loads," in Proceedings of the Eleventh Stapp Car Crash Conference, Oct 10-11, 1967.

56. Department of Transportation, National Highway Traffic Safety Administration. Final Report DOT HS-801 710: Thoracic impact injury mechanism, volume I, by M. M. Reddi, et al. Washington, DC, Aug 1975.

57. R. H. Pudenz and C. H. Sheldon. "The lucite calvarium—a method for direct observation of the brain," Journal of Neurosurgery, vol. 3, 1946, pp 487-505.

58. V. L. Roberts, V. R. Hodgson, and L. M. Thomas. "Fluid pressure gradients caused by impact to the human skull," Biomechanics Monograph, ASME, 1967.

59. G. D. Smith. Numerical solution of partial differential equations. London, Oxford University Press, 1965.

60. M. Kornhauser. "Biodynamic modeling and scaling: anthropomorphic dummies, animals, and man," paper presented at Symposium on Biodynamic Models and Their Applications, Wright-Patterson Air Force Base, Dayton, Oct 1970. (AMRL-TR-71-29)

61. D. S. Griffin. "The verification and acceptance of computer programs for design analysis," On General Purpose Finite Element Computer Programs, ed. P. V. Marcal. New York, ASME, 1970.

62. James H. McElhaney, et al. "Mechanical properties of cranial bone," Journal of Biomechanics, vol. 3, 1970, pp 495-511.

63. Robert L. Taylor, Peter J. Beresford, and Edward L. Wilson. "A non-conforming element for stress analysis," International Journal for Numerical Methods in Engineering (submitted for publication, 1975).

64. U. S. Air Force. SBNO-87936-3: German aviation medicine—World War II, vol. I. Pelham Manor, NY, 1971, p. 626.

65. T. A. Shugar. "Transient structural response of the linear skull brain system," in Proceedings of the Nineteenth Stapp Car Crash Conference, San Diego, CA, Nov 1975. pp 581-614.

66. Naval Aerospace Medical Research Laboratory. NAMRL Monograph 21: Human head and neck response to impact acceleration, by Channing L. Ewing and Daniel J. Thomas. Pensacola, FL, Aug 1972.

67. Naval Aerospace Medical Research Laboratory. NAMRL-1193: Measurement of mass distribution parameters of anatomical segments, by Edward B. Becker. Pensacola, FL, Oct 1973.

68. University of California, College of Engineering. Report EERC 73-11: SAP IV, a structural analysis program, for static and dynamic response of linear systems, by K. J. Bathe, E. L. Wilson, and F. E. Peterson. Berkeley, CA, Jun 1973.

69. K. J. Bathe and E. L. Wilson. "Solution methods for eigenvalue problems in structural mechanics," International Journal of Numerical Methods in Engineering, vol. 6, 1973, pp 213-226.

70. Personal communication with L. S. Lustic, Naval Aerospace Research Laboratory, Detachment, Michoud Station, New Orleans, LA, 16 Sep 1975.

AD-A043 605 CIVIL ENGINEERING LAB (NAVY) PORT HUENEME CALIF F/G 6/2
A FINITE ELEMENT HEAD INJURY MODEL. VOLUME I. THEORY, DEVELOPME--ETC(U)
JUL 77 T A SHUGAR

UNCLASSIFIED CEL-TR-854-1 NL

3 OF 3
AD A043605

END
DATE FILMED
9 -77
DDC

Appendix A

CLINICAL DESCRIPTION OF HEAD INJURY

This appendix is a reproduction of a report submitted in March 1974 by Richard B. Small, M.D. of the University of Southern California Medical Center in fulfillment of CEL Contract No. N62399-73-C-0006.

CLINICAL DESCRIPTION OF HEAD INJURY

By

Richard B. Small, M.D.
Los Angeles County-
University of Southern California Medical Center
Department of Neurosurgery
March 1974

Contract No. N62399-73-C-0006
Civil Engineering Laboratory
Naval Construction Battalion Center
Port Hueneme, California 93043

INTRODUCTION

Historically man has long recognized the serious nature of head injuries. Early human societies developed mechanisms for dealing with head injury as evidenced by the development of helmets for protection of the head in warfare. Some of these societies also practiced trepanation, however its use cannot be related to head injury. Later cultures have recorded rather sophisticated observations regarding head injury. In the Edwin Smith surgical papyrus (circa 1600 BC) several cases of head injury are presented along with the observation of contralateral weakness and the poor prognosis associated with feeble pulse and fever. In the Hippocratic writings there are a number of observations referring to head injury and the first treatise devoted solely to the subject. Included are recommendations for elevation of depressed fractures and trepanation. Attention was not directed to the neurological condition of the patient until much later. Delineation of the presently recognized syndromes comprising the post-traumatic encephalopathies was not accomplished until the late 18th Century.

Commotio Cerebri. The symptomatology of concussion of the brain was presented by Lanfranci of Milan in his Chirgia Magna (1296 AD). This was presented as a classic rather than an original description. Essentially the same description can be found in the writings of Ambrose Pare (1561), a number of 18th Century writers including Littre (1705), Jean-Louis Pettit (1774) and Benjamin Bell (1783), and recent reviews including Courville (1951) and Ward (1966).

Contusio Cerebri. Concerning cerebral contusions Pare (1561) recognized that in some injuries "by the violence of the blow the veins and arteries may be broken." Shortly thereafter Fallopius (1569) described similar findings contralateral to the impact. The significance of the observations was well recognized prior to 1766 when the Academie Royale de Paris offered a prize for "etablir la theorie dea contracoups dans les lesions de la tete et les consequences qu'on peut en titer." This subject has continued to be of considerable interest.

Compressio Cerebri. It is possible (Courville, 1951) that Celsus recognized that intracranial hemorrhage or sanguanous effusion resulted from head injury. Pare described subdural hematoma and suggested tearing of veins as its etiology (Flamm, 1972). The first definite distinction of the symptomatology of compression from concussion, however, is found in Le Dran (1731).

Nevertheless considerable confusion has persisted to the present time concerning the interrelationship of cerebral concussion, contusion and compression. This is manifested in the concept, which developed in the middle of the 19th Century and persists today, of these entities as a continuum particularly in clinical evaluation. Anatomically the lesions are distinctly different. Biomechanically their linear relationship is not substantiated by present evidence.

Experimental studies of head injuries were carried out during the 19th Century by Gama (1835) and others, but well controlled studies were not performed until earlier in the present century. Basic to modern studies was the neuropathological work of Ramon y Cajal. This work was extended to human material by Spatz and co-workers in Germany and Rand

and Courville in this country. Clinical and experimental studies by Denny-Brown and Russell (1932, 1940, and 1945) stimulated the investigation of the clinico-pathologico-mechanical correlation of head injury, which is the ultimate objective of this present project.

Theoretical Considerations. The mechanism by which the impact of a closed head injury produces damage and dysfunction in the central nervous system has been a subject of interest to clinicians and pathologists for some time. That there is no concensus of opinion is reflected in a rather extensive literature. Early vascular and humoral theories have been discarded, and there is general acceptance that mechanical forces produce intracranial injuries. The oldest mechanical theory is that of vibration which was the consensus of the Parisian Royal Academy of Surgery. Another supporter was Gama who developed the first experimental model of head injury in 1835. He imbedded black threads in a gellatin filled flask. To-and-fro movement of the threads was noted when the flask was struck. The theories derived from this model included vibration of the skull, pressure gradients in the brain and propagation of waves of force or compression through the brain. Experimental measurements have tended to discredit these theories as the pressure changes measured were propagated too slowly to explain effects observed with intermediate high speed cameras (1000 - 4000 frames per second). Such studies have been performed by Pudenz and Sheldon (1944), Ommaya (1969) and Gosch et al (1970). They have confirmed the movement of the brain relative to the skull postulated by Russell (1932) and Holbourn (1943-44). Holbourn is the first of a number of physicists who have contributed a great deal to the study of the biomechanics of head injury. His theory is based on shear forces developed within the cranium by rotational acceleration of the head. Such forces are also invoked in the explanation of the axonal injuries described by Strich and others. Many authors have suggested less severe and reversible damage by shear forces to fiber systems in mild and moderate degrees of post traumatic encephalopathy. Rotational acceleration has also been used with some success in describing the distribution of contusions. Further evidence of the existence of shear forces in head injury is derived from high speed camera studies of photoelastic models.

Another physical scientist suggested a theory based on a simple model not unlike Gama's. Gross' model was a fluid filled flask in which intermediate high speed photography revealed cavitation following impact. Collapse of these cavities is postulated to produce high local accelerations leading to shear forces. Further development of this theory has been carried out by Unterharnscheidt and Sellier (1966) and by Kopecky and Ripperger (1969). In their model the negative pressures produced by acceleration and elastic deformation of the skull do not necessarily drop so low as to produce cavitation, however, they produce pressure differentials across cell membranes sufficient to cause disruption of their integrity.

A divergent mechanism of injury is invoked very successfully by Lindenberg (1960) to explain a selected group of fatal human head injuries. Thus elastic deformation of the skull and translational acceleration or "mass movement" of the brain in the "line of impact" is shown to be reasonable mechanism.

The brain is not rigidly supported within its own confines, but is tethered somewhat at its base by the exit of cranial nerves and the spinal cord from the cranium. Bridging veins

from the dural venous sinuses to the cortex add another minor stabilizing force. The falx and the tentorium lend more major support. Yet the brain is a semisolid medium with surrounding cerebrospinal fluid. Blows to the head cause significant shifts of brain tissue within the cranium. Let us consider the intracranial compartment.

The skull is a rigid cavity with a capacity of 1400 - 1500 cc's, an irregular base, and a smooth vault which is composed of an inner and an outer table of bone with innerposed cancellous bone. This arrangement provides greater strength with an economy of weight, as well as a certain degree of insulation. The cranial vault is not uniform in its thickness, but varies from 2 mm. in the temporal region to greater than 1 cm. in the mid-frontal and parietal occipital regions. Irregularities of the base, particularly the sphenoid ridges and the orbital plate areas, greatly modify the formation of fractures, and the overall planes of energy transfer through the skull and thus through the brain.

The base of the skull is a membranous structure with a cancellous or diploic layer only in certain areas. The three main divisions of the base are the anterior, middle, and the posterior fossae. The anterior fossa is formed by the horizontal or orbital portion of the frontal bone laterally, the lesser wing of the sphenoid and the body of the sphenoid posteriorly, and the cribiform plate of the ethmoid in the midline. Projecting upward from the midline of the cribiform plate in its forward portion is the crista galli, to which is attached the falx cerebri. The middle fossa is formed by the greater wing of the sphenoid (containing the pituitary fossa) in the middle, and squama and the anterior aspect of the petrous portion of the temporal bone laterally and posteriorly. The anterior and middle fossae are separated by the sphenoid ridge, with its sharp, knife-like edge fitting against the junction of the frontal and temporal poles of the cerebral hemispheres. The posterior fossa is formed by the posterior aspect of the petrous portion of the temporal bone anteriorly and the occipital bone posteriorly. The foramen magnum is in the center of the posterior fossa, with the basilar process of the occipital bone and the posterior part of the body of the sphenoid forming the base of the skull in front of the foramen magnum. To further complicate the area, numerous perforations which provide avenues of egress for cranial nerves are distributed acrosss the base. The main vascular supply to the intracranial contents also penetrates the skull via this area. Fractures occurring through the base may produce injury to any of the cranial nerves or vascular structures which are intimately associated with the area. These injuries are produced either by direct shearing effects, or by the accumulation of hemorrhage within a foramina with subsequent compromise of space and compression. In addition, fractures through this area may produce dural tear with cerebrospinal fluid leak via a route of cranial nerve egress.

Linear fracture lines tend to occur radially from a center of inbending or deformation secondary to an energy transfer to the skull. These fractures are modified by areas of bony strength. Fracture lines are predetermined by the site of impact as well as the strength of the skull. Most often:

1. Blows frontally cause linear fractures into the orbital roofs;
2. Vertical blows cause radiating fractures;
3. Occipital blows cause fractures running toward the base and foramen magnum;
4. Parietal blows cause fractures directed toward the temporal region.

Depressed fractures are usually caused by a relatively sharp point of contact with laceration of scalp being common. With massive quantities of energy transfer, large flat objects may cause extensive depression of bone.

In considering the intracranial volume, dural and meningeal supporting structures may be considered as inconsequential. Appropriate values for the remaining intracranial contents include:

1. Brain 88.8% (65% H_2O);
2. Blood 2,3%;
3. Cerebrospinal fluid 8.9%.

The skull is rigid and allows only minimal expansion through the foramen magnum and the smaller foramina that transmit blood vessels and nerves. In addition, dural reflections divide the intracranial cavity into fossae that normally protect the brain against excessive movement but limit the amount of compensary shift and displacement that can develop in response to abnormal conditions.

In this regard, the tentorium cerebelli divides the cranial vault into anterior and posterior fossae. The rigid dural extension leads posteriorly from the petrous ridges and anterior clinoid processes, sloping downward and laterally from its medial edge to attach to the occipital bone along the line of the lateral sinus. Extending posteriorly into the center of the tentorium from the posterior clinoid processes is a large semioval opening, the incisura or tentorial notch, whose diameters are usually between 50 and 70 mm. in the fronto-occipital axis and 25 and 40 mm. in the interparietal axis.

The temporal lobes rest on the tentorial incisura and their medial surfaces protrude over its edge, so that 3 to 4 mm. of the medial anterior portion of the temporal unous bulges into the notch. A small segment of the hippocampal gyrus also overhangs the edge and becomes more narrow posteriorly.

It is important to retain the fact that changes in the relationships between the tentorial incisura and its surroundings explain most of the complications in supratentorial volume shifts. The midbrain occupies the anterior portion of the notch. The cerebellum lies in juxtaposition to the dorsum of the midbrain and fills the posterior portion of the notch. Ventral to the brainstem lies the basilar artery, which divides into two diverging posterior cerebral arteries just caudal to the incisura. Each posterior cerebral artery crosses the oculomotor nerve that emerges caudal to it. The artery then circles the homolateral cerebral peduncle and the adjacent lateral midbrain and reaches the vental surface of the hippocampal gyrus of the temporal lobe, where it crosses the tentorial edge and proceeds toward the occipital lobe.

The oculomotor nerves penetrate the medial-basal surface of each cerebral peduncle caudal to the tentorium. They traverse the basal cistern (tentorial gap), initially passing between the superior cerebellar and posterior cerebral arteries, and then passing in close proximity to each temporal lobe uncus at the point where the uncus overhangs the lateral incisural edge, and finally passing over the petroclinoid ligaments to enter the cavernous sinus.

Considering that the brain may move within the skull, it is evident that two types of injury may be produced by a blow to the skull:

1. If energy is sufficient at the point of impact the brain will be damaged to a degree compatible with the force. This is called a COUP type injury.

2. The delivered energy will cause the brain to shift in a direction dictated by the force vector of injury, causing it to rebound off the inner cranial wall, and inflicting injury proportional to the force and related to the configuration of the particular section of the cranial wall, a CONTRECOUP type injury.

The importance of intracranial volume shifts in the production of brain injury cannot be overestimated. Vascular and neural injury secondary to these displacements are often responsible for injuries which produce irreconcilable results. Mesial shift of the lateral hemisphere may force the cingulate gyrus under the falx cerebri. Downward displacement of the hemispheres and basal nuclei may compress and displace the diencephalon and the adjoining midbrain rostrocaudally through the tentorial incisura. In such transgressions the pituitary stalk may be partially avulsed and marked changes may occur in the diencephalon and brainstem. More posterior mesial shift may result in compression of the midbrain against either the free edge of the tentorium of some other resistant structure such as the petroclinoid ligament. Herniation at the incisura also has direct effects upon the brain stem and upon the delicate vascular penetrations of the structures as well. Stretching of the perforating branches of the basilar artery occurs because the artery is tethered to the circle of Willis and cannot shift caudally. Thus, infarction and hemorrhage are produced within the brain stem to further complicate existing injury.

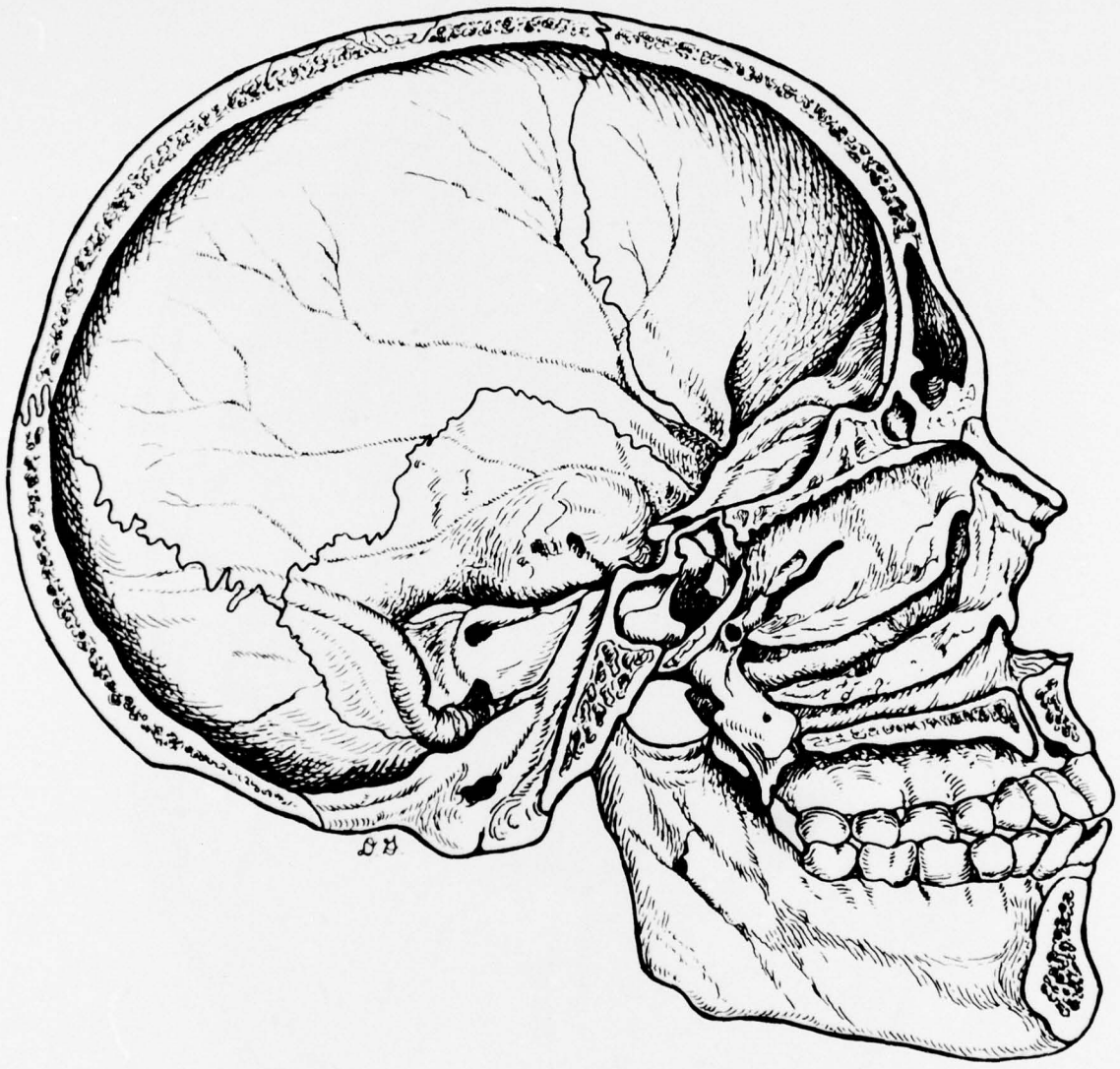

Figure A-1. The Cranium – hemisection of the skull.

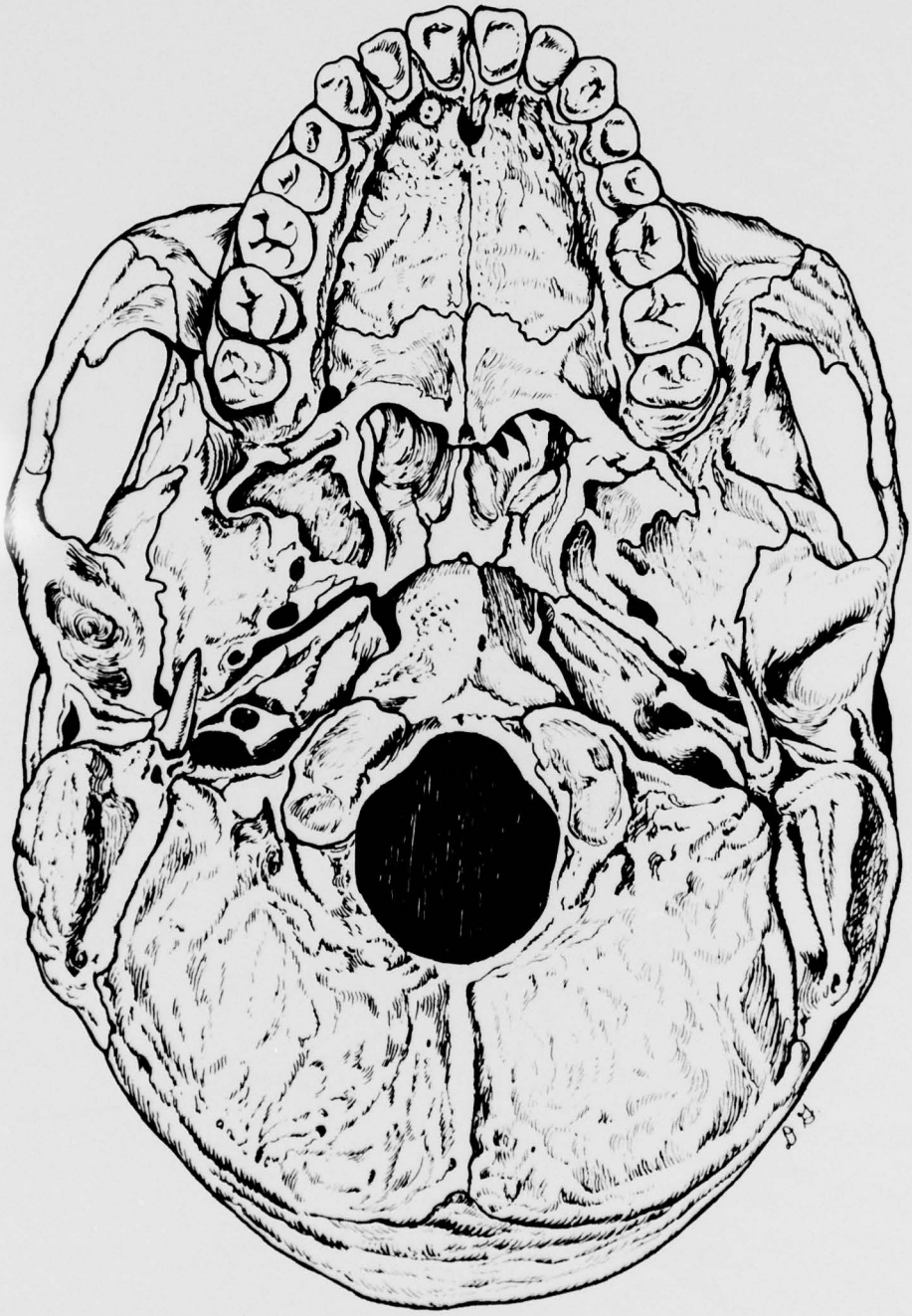

Figure A-2. The Cranium — basal view of the skull.

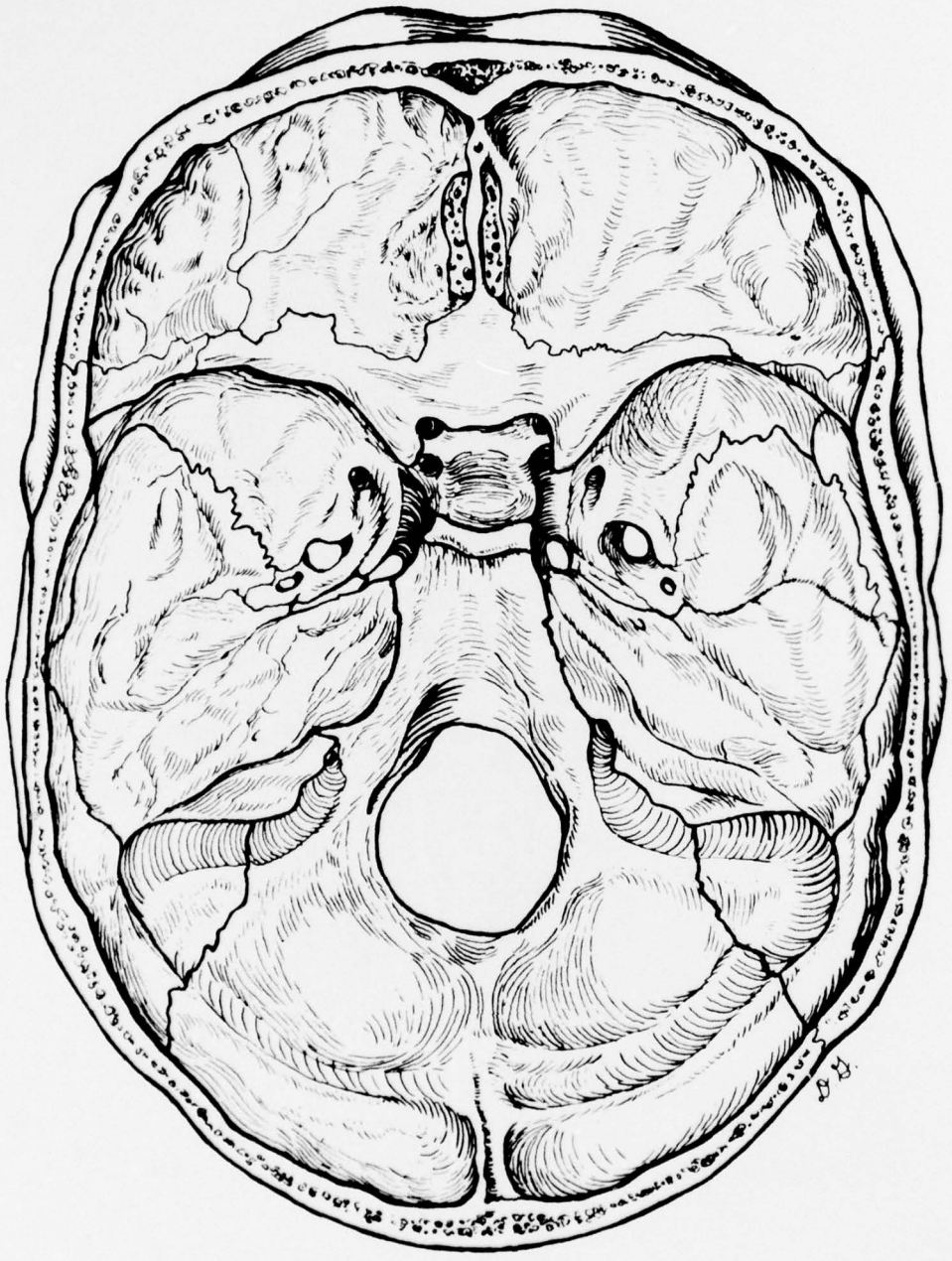

Figure A-3. The Cranium – floor of the cranial cavity.

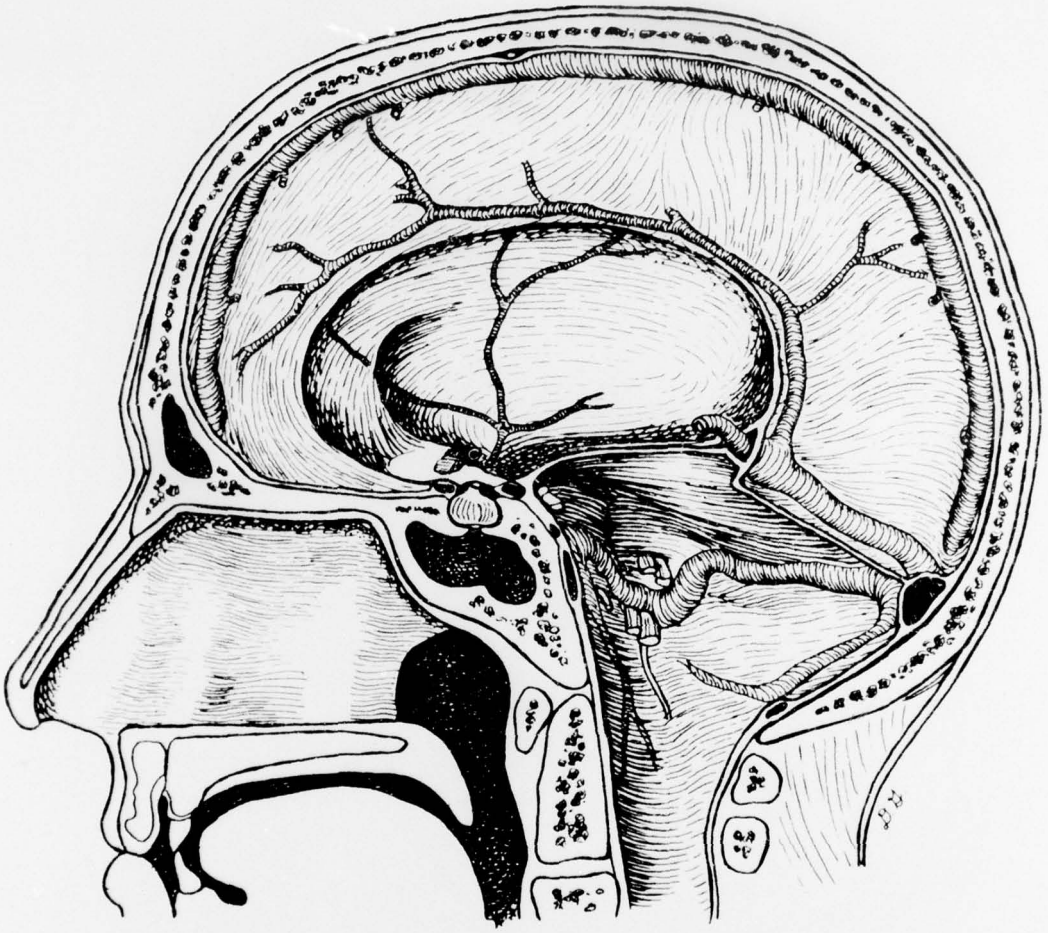

Figure A-4. The Meninges and Blood Vessels — the falx and major veins.

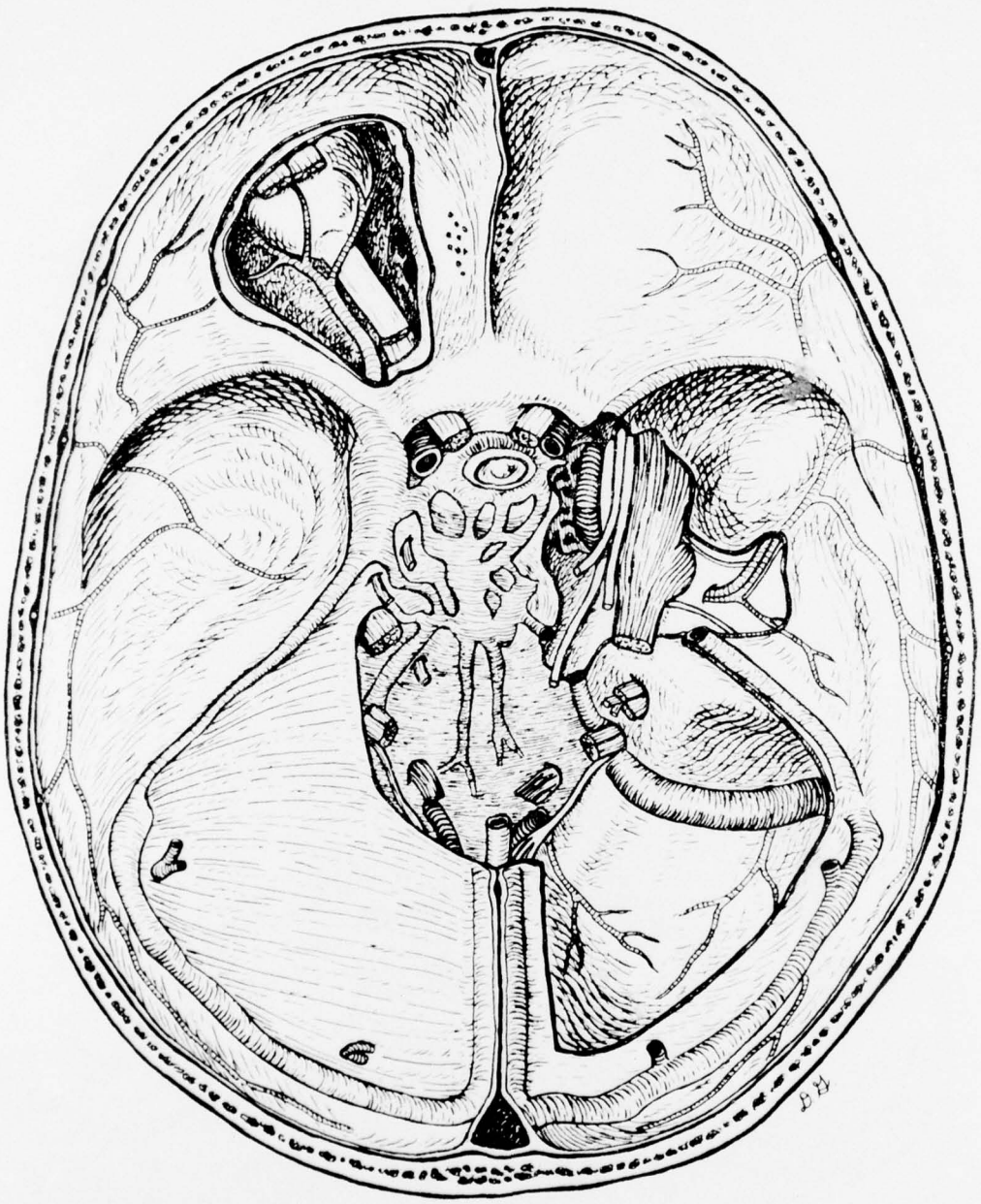

Figure A-5. The Meninges and Blood Vessels — the tentorium and teathering structures of the floor of the cranial cavity.

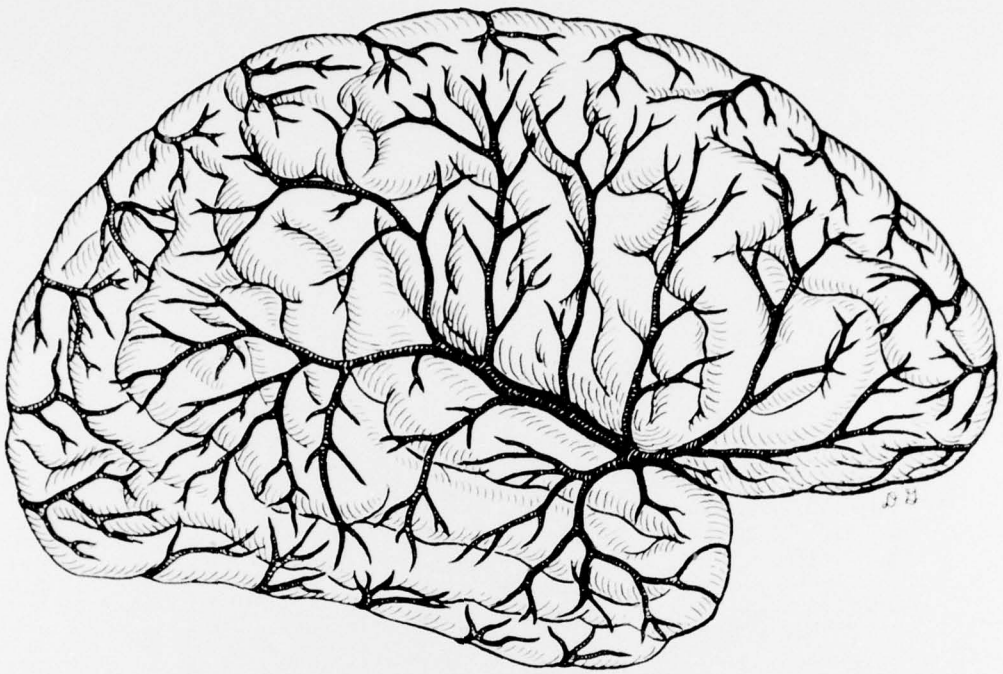

Figure A-6. The Meninges and Blood Vessels — the vessels over the lateral surface.

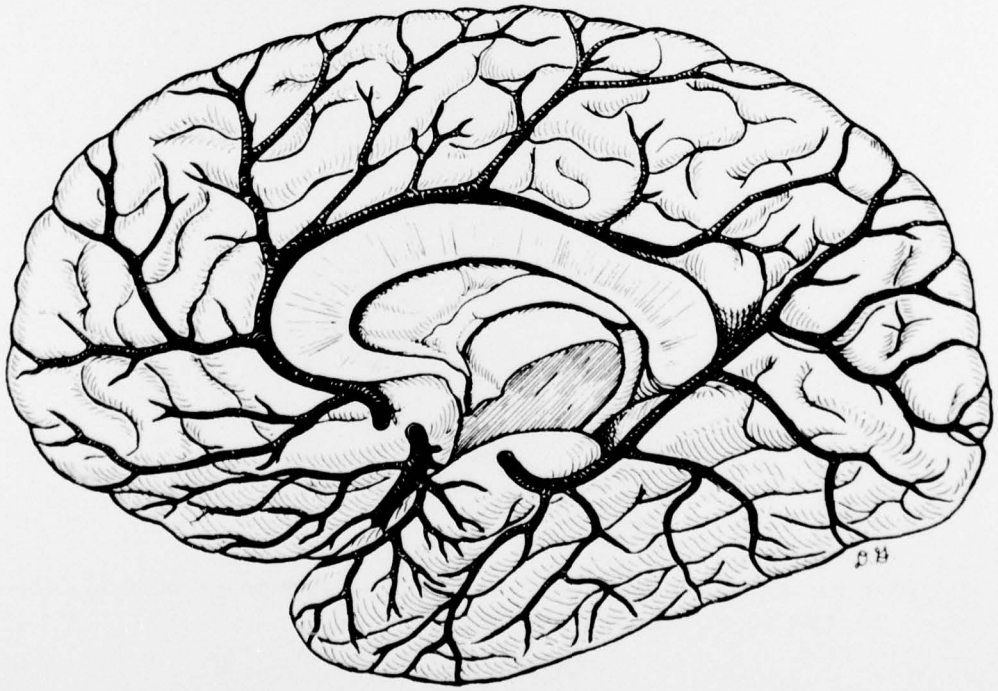

Figure A-7. The Meninges and Blood Vessels — the vessels over the medial surface.

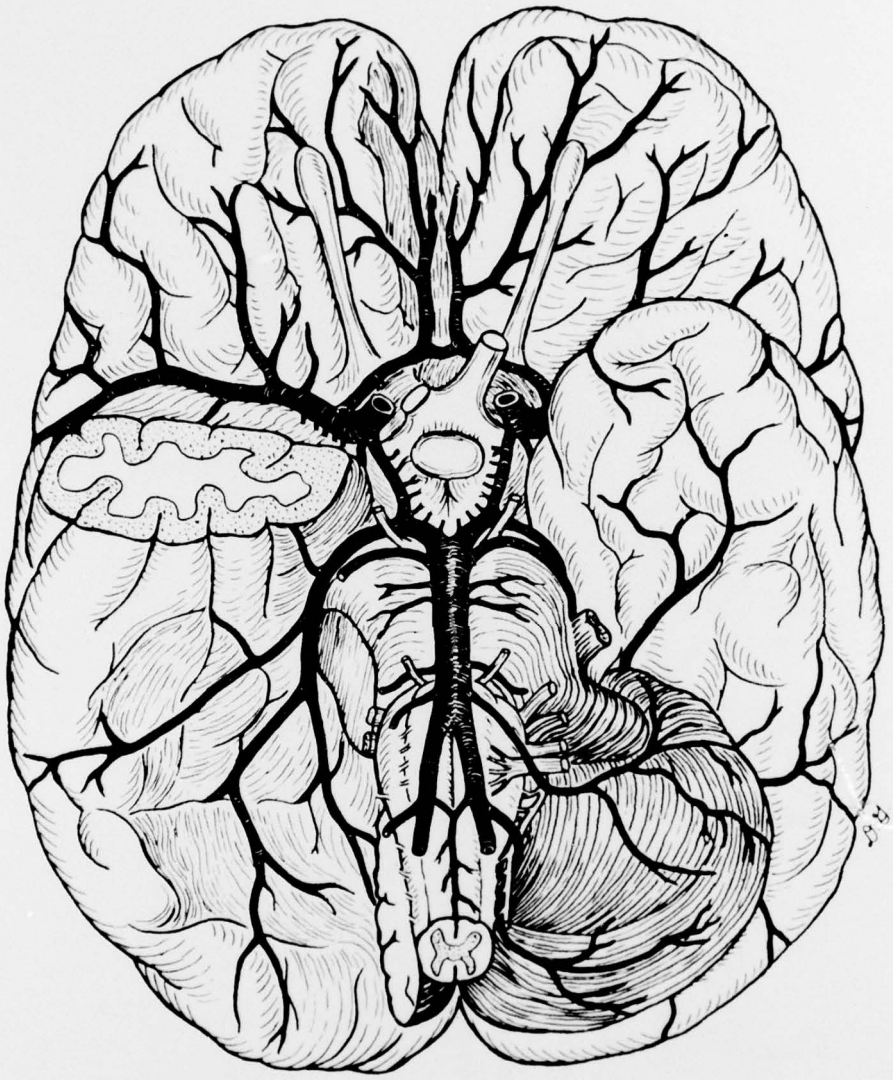

Figure A-8. The Meninges and Blood Vessels — the vessels of the base.

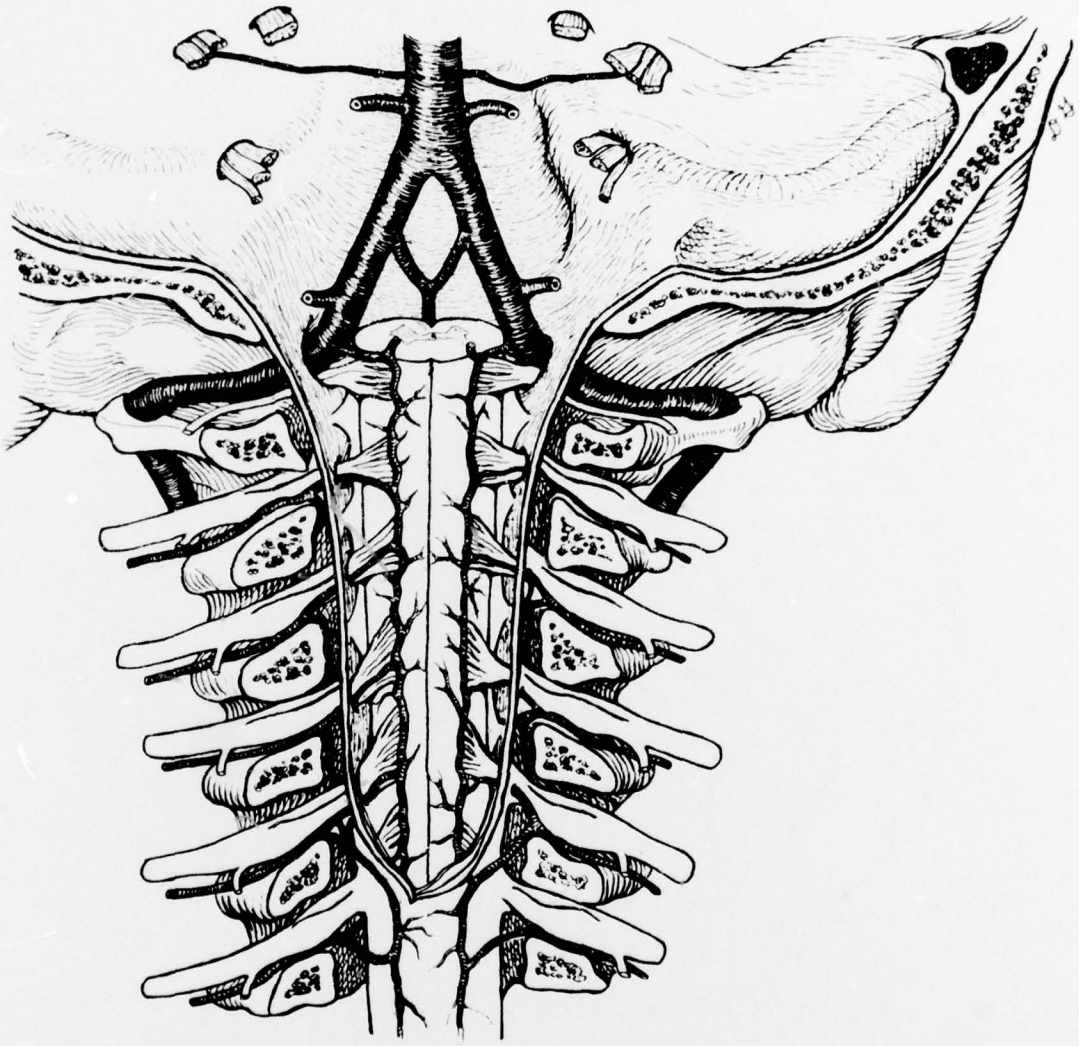

Figure A-9. The Meninges and Blood Vessels – the posterior fossa and cervical cord.

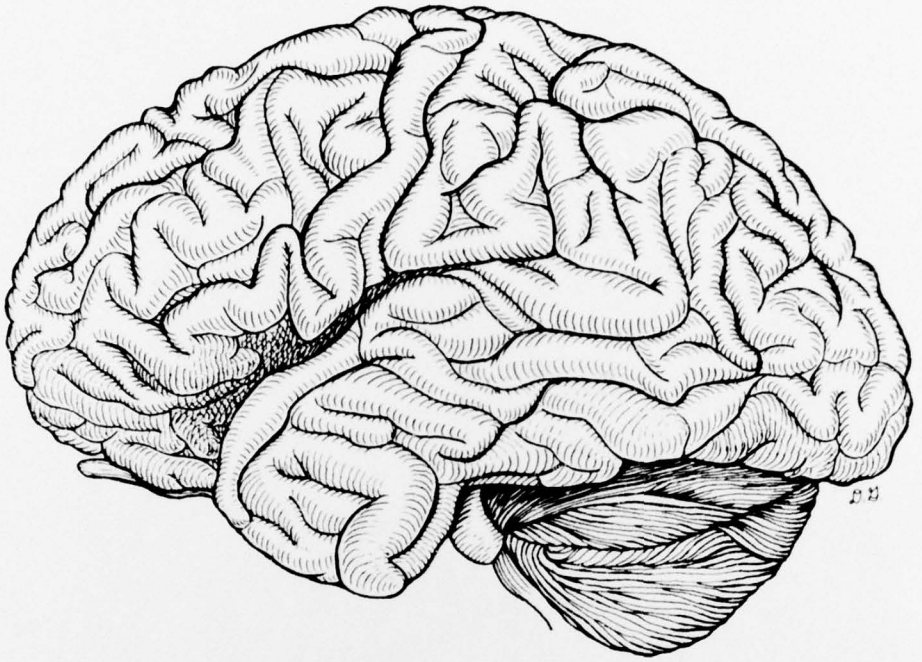

Figure A-10. The Brain – the lateral surface.

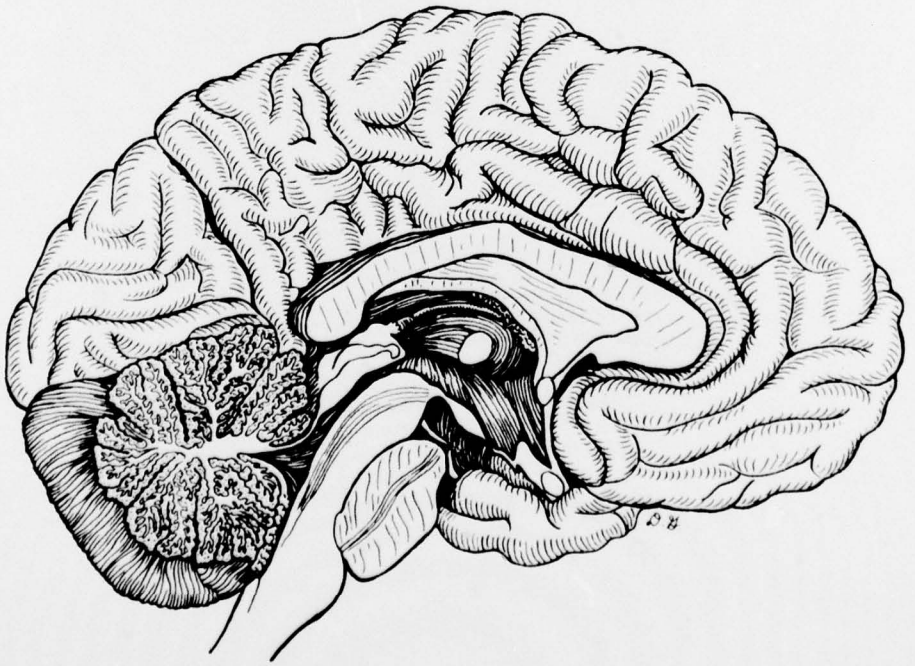

Figure A-11. The Brain – the medial surface.

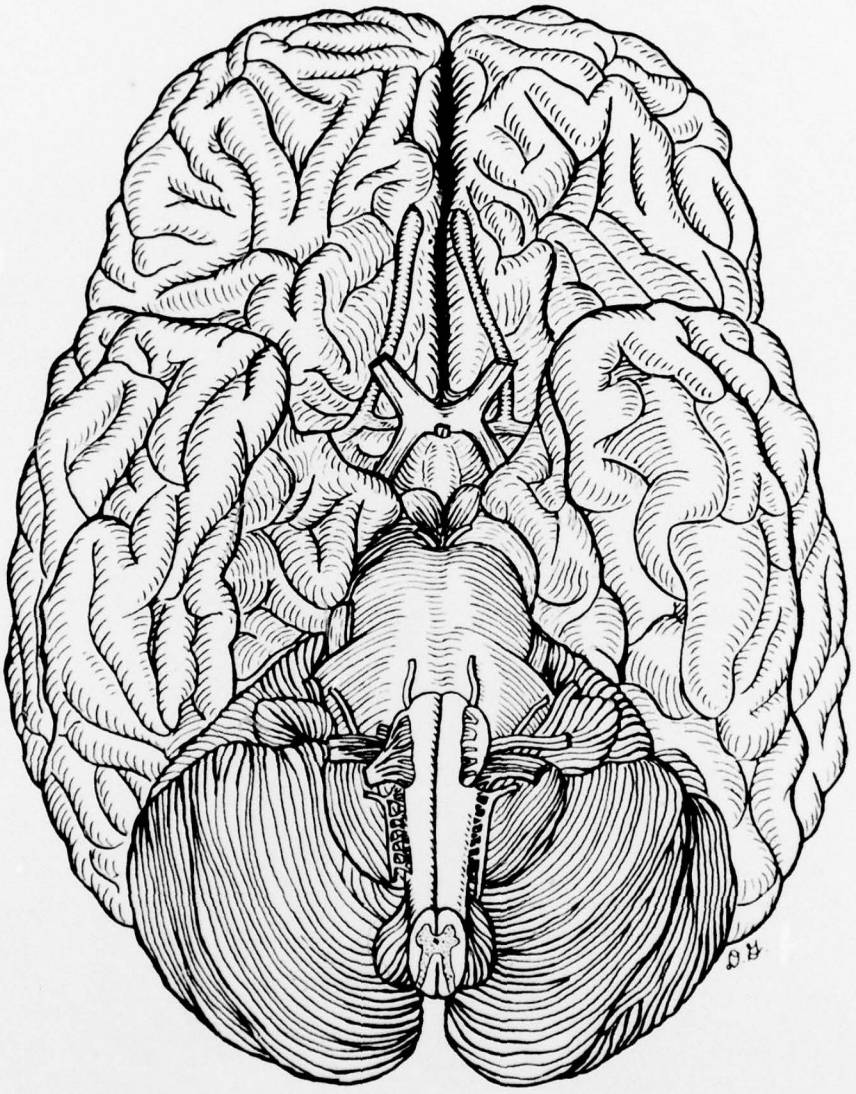

Figure A-12. The Brain — the base.

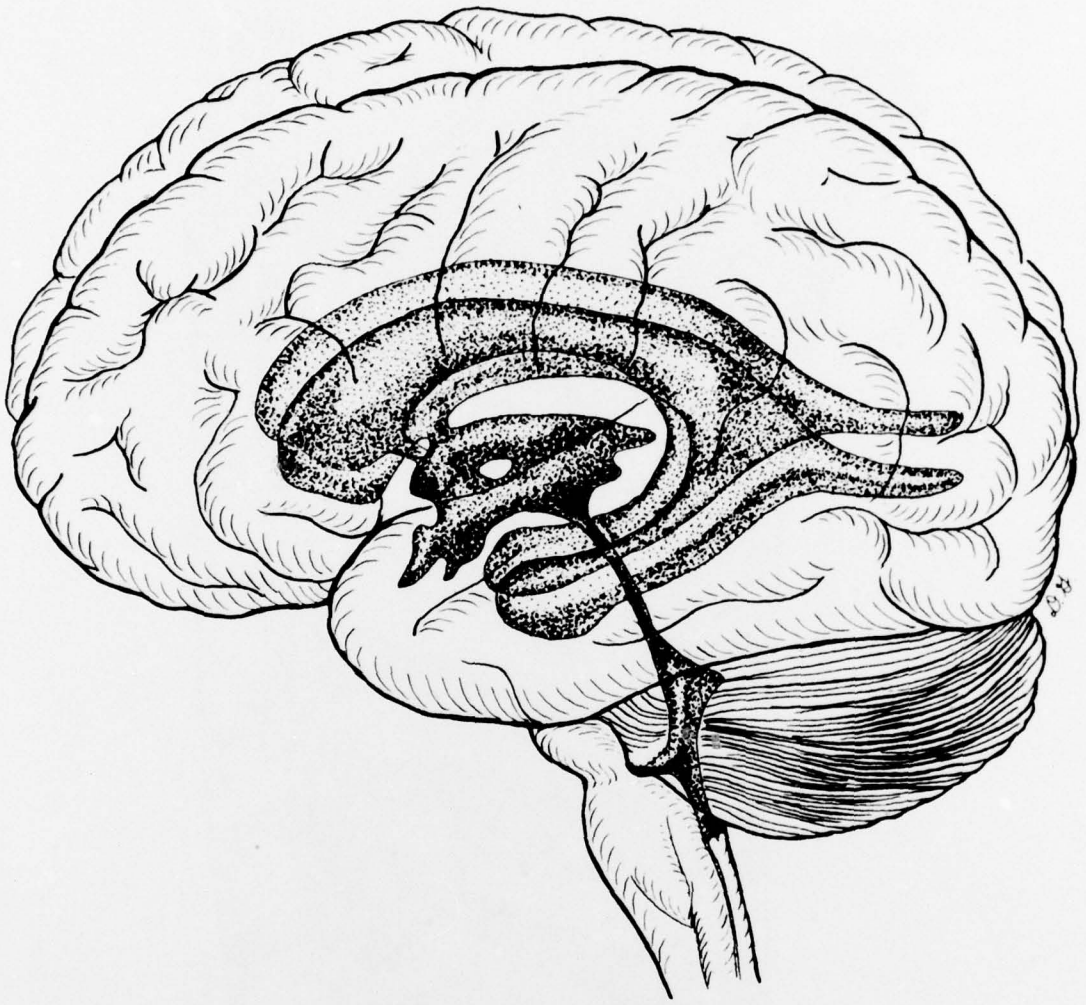

Figure A-13. The Ventricular System.

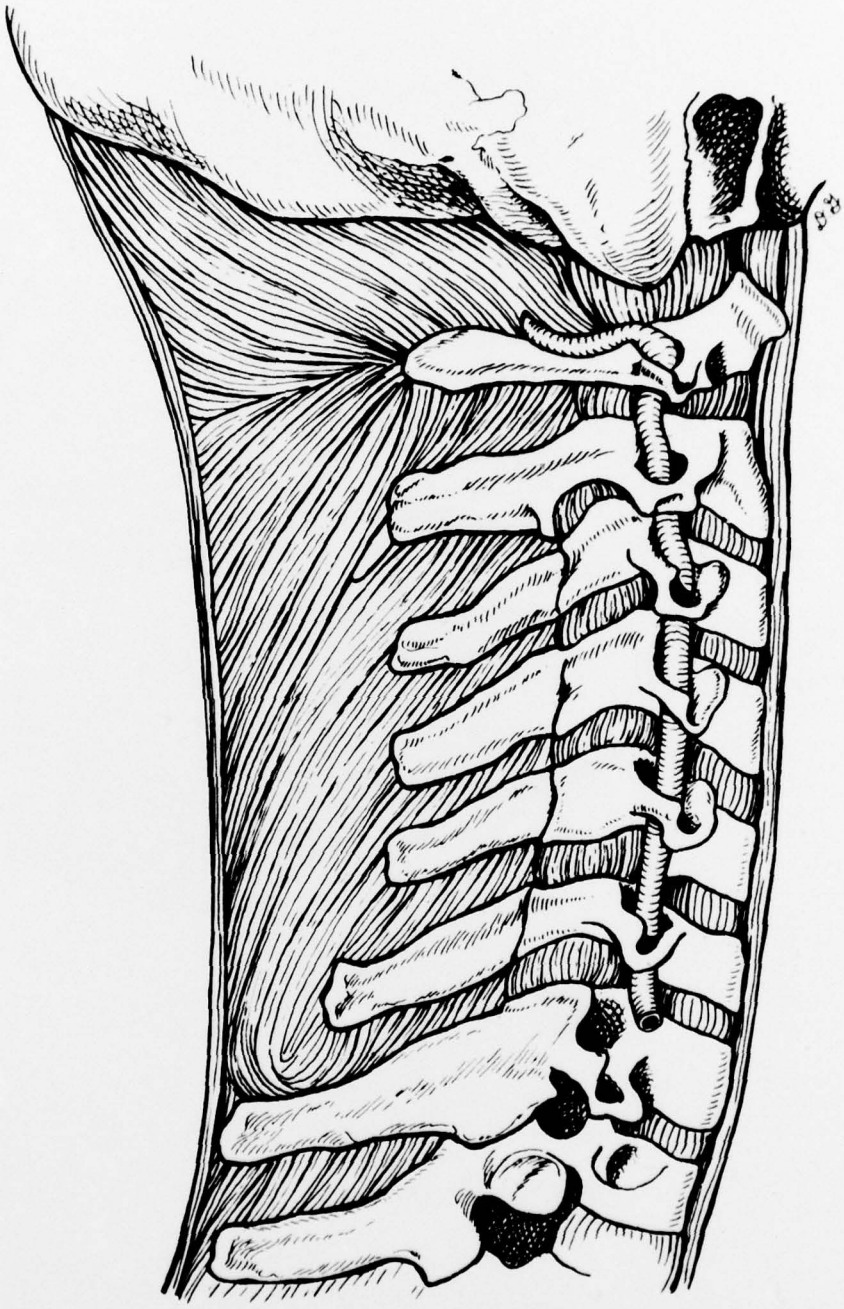

Figure A-14. The Neck — lateral view of the neck.

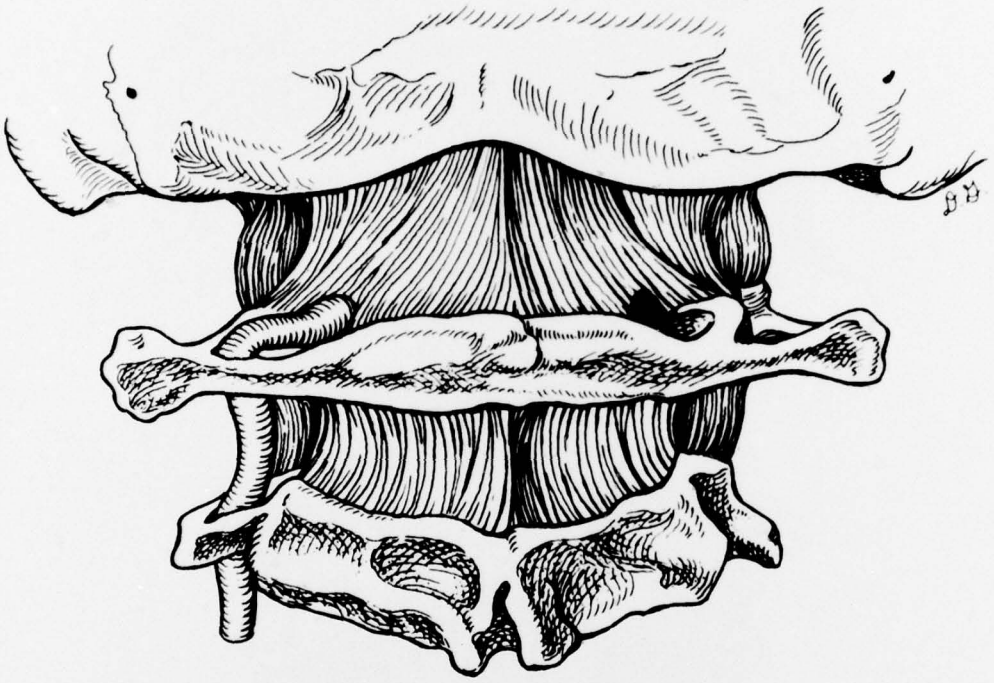

Figure A-15. The Neck – anterior view of the neck.

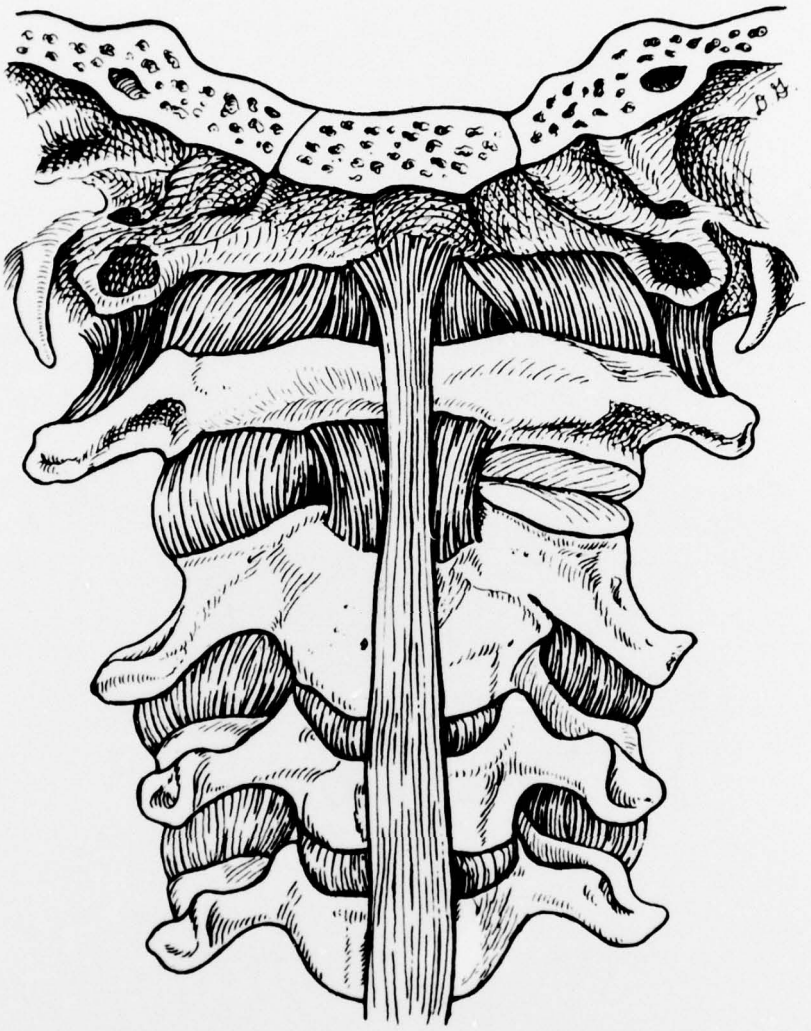

Figure A-16. The Neck – posterior view of upper neck.

BIBLIOGRAPHY

1. Blackwood, W., McMenemey, W. H., Meyer, H., Norman, R., and Russell, D. S.: Greenfield's Neuropathology, Arnold, London, 1963.

2. Brown, D. D. and Russell, W. R.: Experimental Cerebral Concussion, Brain 64, 93-164, 1941.

3. Carlsson, C. A., van Essen, C., and Lofgren, J.: Factors Affecting the Clinical Course of Patients with Severe Head Injuries. J. of Neurosurg. 29: 242-51, 1968.

4. Caveness, W. F. and Walker, A. E.: Head Injury: Conference Proceedings. Lippincott, Philadelphia, 1966.

5. Chason, J. L., Fernando, O. U., Hodgson, V. R., Thomas, L., and Gurdjian, E. S.: Experimental Brain Concussion: Morphologic Findings and a New Cytologic Hypothesis. J. Trauma 6: 767-79, 1966.

6. Courville, C. B.: Traumatic Alterations in the Neurons of the Human Brain Incident to Craniocerebral Injury. Bull. L. A. Neurol. Soc. 17, 71-93, 1952.

7. Courville, C. B.: Commotio Cerebri. San Lucas Press, Los Angeles, 1953.

8. Flamm, E. S.: The Dilated Pupil and Head Trauma. Med. Hist. 16, 194-199, 1972.

9. Gosch, H. H., Gooding, E., and Schneider, R. C.: The Lexan Calvarium for the Study of Cerebral Responses to Acute Trauma. J. of Trauma 10, 1970.

10. Greenfield, J. G.: Some Observations on Cerebral Injuries. Proc. Roy. Soc. Med. 32, 1938.

11. Groat, R. A. and Simmons, J. Q.: Loss of Nerve Cells in Experimental Cerebral Concussion. Journ. of Neuropath. Exp. Neurol. 9, 150-63, 1950.

12. Groat, R. A., Windle, W. F., and Magoun, H. W.: Functional and Structural Changes in the Monkey's Brain During and After Concussion. J. Neurosurg. 2, 26-35, 1945.

13. Gross, A. G.: A New Theory on the Dynamics of Brain Concussion and Brain Injury. J. Neurosurg. 15, 548-61, 1958.

14. Gurdjian, E. S., Thomas, L. M., Hodgson, V. R. and Patrick, L. M.: Impact Head Injury. GP (Kansas) 37/2: 78-87, 1968.

15. Holbourn, A. H. S.: Mechanics of Head Injuries. Lancet 2: 438-41, 1943.

16. Holbourn, A. H. S.: The Mechanics of Brain Injuries. Brit. Med. Bull. 3: 147-49, 1945.

17. Kopecky, J. A. and Rippenger, E. A.: Closed Brain Injury: An Engineering Analysis. J. Biomech. 2: 29-34, 1969.

18. Lampert, P. W.: A Comparative Electron Microscopic Study of Reactive, Degenerating, Regenerating, and Dystrophic Axons. J. Neuropath. Exp. Neurol. 26: 345-68, 1967.

19. Lindenberg, R. and Freytag, E.: Morphology of Cortical Contusions. Arch. Path. 63: 23-42, 1957.

20. Lindenberg, R. and Freytag, E.: The Mechanism of Cerebral Contusions. Arch. Path. 69: 440-69, 1960.

21. Nevin, N. C.: Neuropathological Changes in the White Matter Following Head Injury. J. Neuropath. Exp. Neurol. 26: 77-84, 1967.

22. Ommaya, A. K. and Sadowsky, D.: A System of Coding Medical Data for Punched-Card Machine Retrieval II. As Applied to Head Injuries. J. Trauma 6: 605-12, 1966.

23. Ommaya, A. K.: Mechanical Properties of Tissues of the Nervous System. J. Biomech. 1: 127-38, 1968.

24. Oppenheimer, D. R.: Microscopic Lesions in the Brain Following Head Injury. J. Neurol. Neurosurg. Psychiat. 31: 299-306, 1968.

25. Peerless, S. J. and Newcastle, N. B.: Shear Injuries of the Brain. Canad. Med. Assoc. J. 96: 577-82, 1967.

26. Pudenz, R. H. and Shelden, C. H.: The Lucite Calvarium—A Method for Direct Observation of the Brain. J. Neurosurg. 3: 487-505, 1946.

27. Strich, S. J.: Diffuse Degeneration of the Cerebral White Matter in Severe Dementia Following Head Injury. J. Neurol. Neurosurg. Psychiat. 19: 163-85, 1956.

28. Strich, S. J.: Shearing of Nerve Fibers as a Cause of Brain Damage Due to Head Injury. Lancet 2: 443-8, 1961.

29. Rose, F. C. and Symonds, C. P.: Persistent Memory Defect Following Encephalitis. Brain 83: 195-212, 1960.

30. Symonds, C. P.: Concussion and Its Sequelae. Lancet 1: 1-5, 1962.

31. Russell, W. R.: Cerebral Involvement in Head Injury. Brain 55: 549-603, 1932.

32. Unterharnscheidt, F. and Higgins, L. S.: Traumatic Lesions of Brain and Spinal Cord Due to Nondeforming Angular Acceleration of the Head. Tex. Rep. Biol. Med. 27: 127-53, 1969.

33. Windle, W. F., Groat, R. A. and Fox, C. A.: Experimental Structural Alterations in the Brain During and After Concussion. Surg. Gynec. Obstet. 79: 561-72, 1944.